UNIVERSITÀ
DEGLI STUDI
DI PADOVA

Head Office: Università degli Studi di Padova

Department
Industrial Engineering

Ph.D. COURSE IN: Industrial Enginneering
CURRICULUM: Electrical Engineering
SERIES XXXIV

PROCESSES FOR FOOD AND DRYING ASSISTED BY ELECTRO THERMAL SOURCES (RF, INDUCTION AND MW)

Thesis written with the financial contribution of inovaLab s.r.l.

Coordinator: Prof. Giulio Rosati
Supervisor: Prof. Fabrizio Dughiero

Ph.D. student : Antonio Marconi

Contents

List of Figures

List of Tables

Abstract

Abstract Nowadays dying process is one of the most energy intensive processes in food industry, plastic industry, textile industry and in many different industrial sectors. The most important and used way to eliminate the water from a material are processes based typical on the forced convection of hot air that can be dehumidified at a certain relative humidity that typically depends from the material that it is necessary to dry. In some special applications, for example in plastic industry it is necessary to use hot and dry air: not high temperature (up to 180[degC]) to guarantee the product integrity and low dew-point (up to -40[degC].) to guarantee extremely low material RH (up to 10[ppm]). In food industry, instead, and for example in coffee-roasting processes, air temperature may reach 300[degC] to guarantee high heating rates and Maillard reactions but they are characterized by high dew-point (also 10[degC]). Because of the request of producers in the last 30 years is to have higher and higher productivity of drying lines, industry and its R&D departments invested great resources (in terms of time and money) to obtain fastest processes. One of the first concept was to modify batch processes to obtain continuous processes with high convection-air temperature. Two of the main problems of modern hot-air processes are the global efficiency of drying and how the hot air is generated. Many drying process are nowadays characterized by process-air temperature as high as possible and that practically increases specific losses to the environment. It is clear that in 2022 it is no longer ecologically acceptable to burn hydrocarbons as methane, ethane or propane, but recent world events caused, for example, a large increase in natural gas (up to about +200[%]) and that questioned the economic convenience of gas compared to electric energy, also for heating. For that reason Radio-frequency (RF) and Microwave (MW) drying and heating processes are becoming nowadays more and more interesting. But why they are so interesting? It is clear that it is not physically possible to reduce the latent heat of vaporization of water, but because of microwaves and radio-frequency waves directly heat materials, and in many cases directly generate power sources inside the wet-material matrix they make possible in many applications to dry (at a certain drying rate) with lower temperatures: “cold dry”. In home-appliance applications, such as microwave ovens, new technologies: Solid State MW generators are becoming interesting to improve final product quality and to solve some famous problems, such as the non uniformity in food heating. Because of it is necessary to design system with

certain field distribution, to guarantee high efficiency and high quality product: metaphysical computer-aided methods (e.g. FEMs) make possible to design with high accuracy processes and devices. For that reason in my work the scientific approach follows, for every problem (and example) proposed the following line-up:

- Process analysis and State Of Art analysis: It is necessary to obtain a benchmark of the actual process (drying, heating, thawing, cooking). It is necessary to define process performances indicators (PPI), that can be for example: temperature profile, drying rate, temperature distribution, water vapor distribution in the material, efficiency, etc.
- Material characterization: Because of electromagnetic, temperature, mass flow problem are described by partial differential equations, if properties are not accurate, the design FEM based will not be accurate. For that reason the work proposed several techniques for example to measure the properties of materials (e.g. complex permittivity) with relative low cost
- Pre-design of the device: Analytical approaches, and the solutions of some particular cases make possible to get a preliminary draft of the prototype. That must be the starting point for the virtual prototype.
- Multi-physics analysis: FEM models and numerical optimization to model and the design the process and the device. RF-MW drying processes are complex process in which many physics occur: Maxwell equations, Thermal diffusion, convection and advection, Mass movement, moisture transfer, latent heat of vaporization, etc. For that reason simplified models are faster and easier to compute and make possible to get relatively accurate designs, but coupled approaches may be more suitable. For example in the work is proposed an analysis of the sealing of packaging material for food industry, and the analysis of dynamics of the sealing profile allowed us to design the so called “smart-matching-network”: because of dielectric permittivity is function of temperature, and because of the size of the phenomena is extremely small (also smaller than 1[mm]) for an RF sealing process, the Multi-physics model made possible to accurately predict the impedance value, to precisely design the matching network and to condition the matching algorithm.
- Mock-up, prototype and laboratory measures.

The structure of the present work follows the following structure for it chapters:

- Chapter (1) analyses main drying mechanism and parameters. Material properties influences drying performances and then drying technologies must be chosen in relation to them. A new induction-hot-roller is analysed and its design process is introduced. An energetic analysis of losses during the pre-heating is developed.

- Chapter (2) introduces a description of the electromagnetic problem and its main electromagnetic material properties. The numerical solution of the electromagnetic problem is the base of virtual-design of EPM devices and process for EPM devices.

- Chapter (3) studies the thermal problem of conduction and heat transport. The final part of the chapter introduces a synthesis of main food material properties for a particularly interesting process: thawing

- Chapter (4) deeply studies dielectrics materials and several techniques used to measure their dielectric properties. The chapter proposes complex dielectric permittivty measuring results on plastics, food and fabrics.

- Chapter (5) studies the engineering problem of how to design a radio-frequency heating device (RFH) and studies with particular attention the problem of load adaptation (Matching network).

- Chapter (6) presents a new Radio-Frequency dryer for plastic materials. The entire design process is introduce in the chapter

- Chapter (7) introduces a description of the electromagnetic problem for MW problems, where high frequencies cause propagation. The design of an entire system robust and with high process efficiency is still a technical challenge. The chapter analyses TE,TM,TEM waveguides and resonant cavities and chokes, that fully characterizes a MWH design (and process).

- Chapter (8) finally closes that work with a synthesis of main results.

The present work uses uses both analytical and numerical methods (primarily FE methods) to design, study and optimize specific technical problems, such as electromagnetic transmission, electromagnetic shielding and filtering, process efficiency, fast drying and high final quality and uniformity.

Chapter 1

Background and motivation

1.1 Electromagnetic Processing of Materials (EPM)

Electromagnetic processing of materials (EPM) is the technology of transforming electrical energy into heat. EPM has evolved over the past thirty years thanks to the development of power electronics, becoming a technology of great interest not only for industry but also for home appliances.

The variety of such applications has greatly contributed to industrial development since the forties. In fact, EPM began its development in the early decades of the century, first with arc furnaces and, subsequently, with induction furnaces. However, it has developed particularly well, both from an application point of view and of research, especially in the last thirty years. In particular, the increase in oil and labor costs - which occurred a starting from the 70s has increased the importance of hiring a fundamental role in the industrial activity of individual countries. The variety of applications has meant that in the past they have been concerned as particular aspects of different technical disciplines and that also in realizations they are often known only in the context of their respective sectors of use and therefore in a small circle of users. In reality, the characteristics of EPM applications in production processes derive mainly from the common origin, which consists in the transformation of electricity into heat, and it is therefore appropriate to treat the applications themselves as a homogeneous complex. This opportunity has emerged especially in recent years, as we take note of both the increasing diffusion of the techniques traditional EPM and the development of applications that use processes recently built technology. The heating methods that characterize EPM today include i so-called

traditional procedures, and specifying:

- arc heaters
- heating by resistance
- induction heating
- radiofrequency heating
- microwaves,
- plasma applicators
- electron beams
- lasers
- ion bombardment.

Drying of solids is one of the oldest and most common unit operations found in diverse processes such as those used in the agricultural, ceramic, chemical, food, pharmaceutical, pulp and paper, mineral, polymer, and textile industries. It is also one of the most complex and least understood operations because of the difficulties and deficiencies in mathematical descriptions of the phenomena of simultaneous—and often coupled and multi phase—transport of heat, mass, and momentum in solid media.

1.2 Drying in industry processes

Drying describes the process of thermally removing moisture from a solid product. Moisture may be present in the solid material as chemical bonds (liquid phase) or trapped in the micro structures of the solid (bound moisture). Mujumdar in its handbook of industrial drying offers a deep and complete analysis of drying mechanism and mainstream drying techniques [62]. Thermal drying is characterized by two main processes: transfer of energy from the surroundings to the material and transfer of internal moisture to the environment. It is clear that the rate at which drying is accomplished is governed by the rate at which the two processes proceed. Energy transfer as heat from the surrounding environment to the wet solid can occur as a result of:

- convection
- conduction
- radiation

and in many cases as a result of a combination of these effects. In State Of Art (SOA) classical industrial dryers the heat is transferred to the surface of the wet solid and then to the interior. However, in dielectric, radio frequency (RF), or microwave (MW) drying, thermal energy is generated directly internally within the solid and flows to the exterior surfaces. The removal of water as vapor from the material surface, depends on the external conditions of temperature, air humidity and flow, area of exposed surface, and pressure. The movement of moisture internally within the solid, is a function of the physical nature of the solid, the temperature, and its moisture content. In that work we will analyze only evaporation processes, that are characterized by the conversion of a liquid phase into a concentrated liquid phase. Phase change and production of a solid phase as end product are essential features of the drying process. Drying is an essential operation in the chemical, agricultural, biotechnology, food, polymer, ceramics, pharmaceutical, pulp and paper, mineral processing, and wood processing industries. Drying is perhaps the oldest, most common and most diverse of chemical engineering unit operations. Over 400 types of dryers have been reported whereas over 100 distinct types are commonly available. It competes with distillation as the most energy-intensive unit operation due to the high latent heat of vaporization and the inherent inefficiency of using hot air as the (most common) drying medium. Several studies report national energy consumption for industrial drying operations ranging from 10–15 % for United States, Canada, France, and U.K. to 20–25 % for Denmark and Germany. Before proceeding to the basic principles, it is useful to note the following unique features of drying, which make it a fascinating and challenging area for research and development (R&D):

- Product size may range from 1 $[\mu m]$ to 10 $[cm]$ (in thickness or depth)
- Product porosity may range from 0 to 99.9%
- Drying times range from 0.25 $[s]$ (drying of tissue paper) to 1 $[year]$ (for certain hardwood species)
- Production capacities may range from 0.10 $[kg/h]$ to 100 $[tons/h]$
- Product speeds range from 0 $[m/s]$ (stationary drying) to 1 $[m/s]$ (tissue paper)

- Drying temperatures range from below the triple point (T_t) to above the critical point of the liquid (T_c)
- Operating pressure may range from fraction of 1[$mbar$] to 25[bar]
- Heat may be transferred continuously or intermittently

Drying is a complex operation involving transient transfer of heat and mass along with several rate processes, such as physical or chemical transformations, which, in turn, may cause changes in product quality as well as the mechanisms of heat and mass transfer. Physical changes that may occur include shrinkage, puffing, crystallization, and glass transitions. Drying occurs by effecting vaporization of the liquid by supplying heat to the wet feed-stock. As noted earlier, heat may be supplied by convection (direct dryers), by conduction (contact or indirect dryers), radiation or volumetrically by placing the wet material in a microwave or RF electromagnetic field. Over 85% of industrial dryers are of the convective type with hot air or direct combustion gases as the drying medium. Over 99% of the applications involve removal of water. All modes except the dielectric (microwave and RF) supply heat at the boundaries of the drying object so that the heat must diffuse into the solid primarily by conduction. The liquid must travel to the boundary of the material before it is transported away by the carrier gas (or by application of vacuum for non convective dryers). Transport of moisture within the solid may occur by any one or more of the following mechanisms of mass transfer:

- Liquid diffusion, if the wet solid is at a temperature below the boiling point of the liquid [77]
- Vapor diffusion, if the liquid vaporizes within material [9]
- Knudsen diffusion, if drying takes place at very low temperatures and pressures, e.g., in freeze drying [11]
- Surface diffusion (possible although not proven) [72]
- Hydro-static pressure differences, when internal vaporization rates exceed the rate of vapor transport through the solid to the surroundings
- Combinations of the above mechanisms

Note that since the physical structure of the drying solid is subject to change during drying, the mechanisms of moisture transfer may also change with elapsed time of drying.

1.2.1 External conditions: removing water as vapor from the material surface

The main external variables are temperature, humidity, airflow distribution and the geometry of the solid that we want to dry and of the environment. External drying conditions are especially important during the initial stages of drying when unbound surface moisture is removed. Surface evaporation is influenced by the diffusion of vapor from the surface to the environment atmosphere through a thin film of air in contact with the surface and with a certain temperature. For that reason there is the necessity to know two main characteristics:

- the equilibrium characteristics of the wet solid
- the enthalpy characteristics

Vapor-Liquid equilibrium and enthalpy for a pure substance

When a liquid is exposed to a dry gas, the liquid naturally evaporates. Assuming the so called ideal gas behaviour for the vapor, after having defined the mass of vapor (m_W) in gas-phase [68]:

$$P_W V = \frac{m_W}{M_W} RT \tag{1.1}$$

where the maximum value of the pressure of the vapor that can be reached is the so called saturated vapor pressure (P_{W-0}). It is possible to obtain the Vapor-Pressure curve for a material and find three different zones: the solid zone, the liquid zone and the vapor zone. Vapor-Pressure curve introduces three main properties

- the critical temperature (T_c $[K]$): a substance with a temperature greater than the critical temperature is a gas
- the critical pressure (p_c $[Pa]$): at that pressure it is possible to define the critical point (C) at which distinction between the liquid and vapor phase disappears, and all properties of the liquid, such as density, viscosity, and refractive index, are identical with those of the vapor.

The Clausius-Clapeyron Equation

At a constant pressure, the Clausius–Clapeyron equation relates the slope of the vapor pressure–temperature curve to the latent heat of vaporization through the equation [43]:

$$\frac{\partial P_{W-0}}{\partial T} = \frac{\Delta H_W}{T\left(V_W - V_L\right)} \tag{1.2}$$

where the specific molar volume of saturated vapor (V_W), the saturated liquid (V_L) and the molar latent heat of vaporization (ΔH_W) are introduced.

Enthalpy and Heat Capacity

In any steady flow system there is an additional energy associated with forcing streams into a system against a pressure and in forcing streams out of the system. This work per unit mass is the product of pressure (p $[Pa]$) and specific volume V $[m^3]$) where The enthalpy (H $[J/kg]$) is a "composed" energy that takes into account the sum of the pressure work (pV $[J/kg]$) and the internal energy (u $[J/kg]$):

$$H = pV + u \tag{1.3}$$

Absolute values of enthalpy of a substance like the internal energy are not known. Relative values of enthalpy at other conditions may be calculated by arbitrarily setting the enthalpy to zero at a convenient reference state.

The heat capacity is defined as the heat required to raise the temperature of a unit mass of substance by a unit temperature. The so called constant-pressure heat capacity is:

$$C_p = \frac{\partial Q}{\partial T} = \frac{\partial H}{\partial T} \tag{1.4}$$

In drying process it is typically convenient to compute the mean value in a certain temperature range:

$$\bar{C}_p = \frac{1}{\Delta T}\int_{T_0}^{T_0+\Delta T} C_p dT \tag{1.5}$$

1.2.2 Vapor-Air mixtures

When a gas or gaseous mixture remains in contact with a liquid surface, it will acquire vapor from the liquid until the partial pressure of the vapor in the gas mixture equals the vapor

pressure of the liquid. In drying applications the typical gas is air and the liquid is water. Humid air is a mixture of water vapor and gas composed by a mass of water vapor (m_W) and a mass of air (m_A). It is then possible to define the absolute humidity (AH $[-]$) as the ratio of water vapor mass to air mass and because of the gas law for vapor and air fractions and the Dalton's law of partial pressures are every time valid:

$$AH = \frac{m_W}{m_A} = \frac{p_W}{p_A}\frac{M_W}{M_A} = \frac{p_W}{p - p_W}\frac{M_W}{M_A} \tag{1.6}$$

The relative humidity (RH $[-]$) of a water vapor-air mixtures is is defined as the ratio of the partial pressure of the vapor p_W to the saturated pressure P_{W-0} at the same temperature:

$$RH = \frac{P_W}{P_W^0} \tag{1.7}$$

and finally the absolute humidity is function of the relative humidity through the molar mass of its components. For air and water vapor:

Molar mass		
Material	M_i	Molar mass $[g/mol]$
Water vapor	M_W	18.01
Air	M_W	28.96

Table 1.1: Molar mass for air and water vapor.

Unsatured vapor-gas mixtures: psychrometry of drying

Two processes occur simultaneously during the thermal process of drying a wet solid:

- heat transfer to vary the temperature of the wet solid (sensible heat) and to evaporate its surface water vapor (latent heat)
- mass transfer of moisture from the surface of the material and its evaporation from the surface to the environment

Dry bulb temperature

The so called dry bulb temperature (T_{db} $[degC]$) is the temperature of a vapor–gas mixture determined by the immersion of a thermometer in the mixture.

Dew Point

The dew point (T_d $[degC]$) is temperature at which a vapor–gas mixture becomes saturated when cooled at a constant total pressure and it is not in contact with a liquid.

Humid volume

The humid volume (V_h $[m^3]$) of a vapor–air mixture is the volume taken by $1[kg]$ of dry air and by vapor at the a certain temperature and pressure. For a mixture (air + vapor) with an absolute humidity (AH $[-]$) at a certain condition of temperature (T $[degC]$) and pressure (P $[atm]$), the ideal gas law gives the humid volume (V_h $[m^3]$):

$$V_h = 0.082 \left[\frac{1}{M_A} + \frac{AH}{M_W} \right] \frac{T + 273.15}{P} \tag{1.8}$$

Enthalpy

The enthalpy of a humid gas (H_A $[kJ/kg]$) is the sum of the enthalpy of the dry gas (H_{DA} $[kJ/kg]$), of the the enthalpy of moisture (H_{AW} $[kJ/kg]$) multiplied with the absolute humidity of the mixture, and an additional terms to take into account mixing and other non reversible effects (ΔH_{AM} $[kJ/kg]$) [67]:

$$H_A = H_{AA} + (AH) \cdot H_{AW} + \Delta H_{AM} \tag{1.9}$$

in many practical cases may be interesting to describe the enthalpy as specific heat:

$$\begin{cases} H_A = C^*_{PH} T + \Delta H_{V0} \, (AH) \\ C^*_{PH} = C^*_{PA} + C_{PW} \, (AH) \end{cases} \tag{1.10}$$

where the mean heat capacitance of dry air (C^*_{PA} $[kJ/(kg \cdot K)]$), the mean heat capacitance of vapor moisture (C^*_{PW} $[kJ/(kg \cdot K)]$) and the mean humid heat (C^*_{PH} $[kJ/(kg \cdot K)]$) were defined in the previous equation. It is possible to define the path of enthalpy that from the liquid state to the vapor state:

$$T_0 \Rightarrow T_d \Rightarrow T_d, \Delta H_{vd} \Rightarrow T_{db} \tag{1.11}$$

and then the enthalpy of the global process is:

$$H_{AW} = C^*_{LW} \, (T_d - T_0) + \Delta H_{vd} + C^*_{PW} \, (T_{db} - T_d) \simeq C^*_{PW} \, (T_{db} - T_0) + \Delta H_{v0} \tag{1.12}$$

and finally the enthalpy of the humid gas can be rewritten as follows:

$$H_A = C^*_{PA} \, (T_{db} - T_0) + \Delta H_{v0} \, (AH) \tag{1.13}$$

where the latent heat of vaporization (ΔH_{v0} $[kJ/kg]$) is obtained at $0[degC]$

Adiabatic Saturation

Adiabatic saturation occurs when air enters in contact with a liquid phase and the result is a mass and heat transfer between the air and the liquid. At the end of the process the air leaves the system at conditions of humidity and temperature different from those at the inlet. The operation is adiabatic because no heat is exchanged with the surroundings. The mass and enthalpy balance then:

$$\begin{cases} m_v = m_A \left(AH_o - AH_{in}\right) \\ H_{A_{in}} - H_{A_{out}} = -\left(AH_{out} - AH_{in}\right) H_{LW} \end{cases} \tag{1.14}$$

solving the system of equations it is possible to get the adiabatic saturation relationship that relates the absolute humidity saturated (AH_{As} $[-]$) to the initial temperature air condition (T_{in} $[degC]$) and allow us to describe the so called adiabatic saturation temperature (T_{As} $[degC]$)

$$T_{As} = T_{in} + \left(AH_{in} - AH_{As}\right) \frac{\Delta H_{vs}}{C^*_{PA}} \tag{1.15}$$

Drying mechanism

The moisture content in the solid could be reduced further by exposing it to air of lower relative humidity. Solids can best be classified as listed in table 1.3. Moisture in a solid may be either unbound or bound as seen in table 1.3. There are two methods of removing unbound moisture: evaporation and vaporization.

Evaporation

Evaporation occurs when the vapor pressure of the moisture on the solid surface is equal to the atmospheric pressure.

$$\left[P_{W-0}\right]_{Evap} < P_{atm} \tag{1.16}$$

The temperature of the moisture is increased to the boiling point (T_b $[degC]$). That phenomenon occurs in hot roller for evaporation. The main mechanism is the conduction between the hot surface of the roller and the solid material that we want to dry. In that specific case the energy exchanged from the surface of the roller to the material is strictly related to the temperature difference between the material and the roller, in practice evaporation occurs at a constant temperature close to the boiling point of the material. Also in that case a convective heat flux may avoid condensation phenomena of the evaporated moisture that may exchange energy with colder surfaces of surroundings. In industry and are present many systems that use hot roller heated by diathermic oil or dry saturated steam. A good design of the roller topology, for example inserting ducts for the passage of hot oil may guarantee a fine control of the temperature

Moisture content of solids: a classification		
Type	Examples	Description
Non hygroscopic capillary-porous media	Sand Crushed minerals Non hygroscopic crystals Polymer particles Ceramics	Recognizable pore space The material is non hygroscopic The medium does not shrink
Hygroscopic porous media	Clay Sieves Wood Textiles	Recognizable pore space Bound liquid The medium shrinks
Colloidal nonporous media	Soap Glue Polymers Food	No pore space All bound liquid Only surface drying

Table 1.2: Classification of moisture content of solids: type, examples and description of phenomena.[54]

over the surface of the roller. One of the main problem of that technology is the pre-heating of the system. Because of these systems may characterized by big diameters ($D_r = 4[m]$) and long roller ($L_r = 3[m]$) to guarantee high production rate ($v_p \simeq 2000[m/min]$) there is the necessity of overheating the roller to guarantee full evaporation of water. The main problem of these systems are the high energy lost due to convective losses to the environment due to the high rotation speed of the roller.

Vaporization

In vaporization, drying is carried out by convection, that is, by passing warm air over the product. The air is cooled by the product, and moisture is transferred to the air by the product and carried away. In this case the saturation vapor pressure of the moisture over the solid is less than the atmospheric pressure:

$$[P_{W-0}]_{Vap} < P_{atm} \tag{1.17}$$

To properly design and optimize a drying process for a solid material it necessary to properly characterize the drying phenomenon of the specific product. The drying behavior of solids can be characterized by measuring the moisture content loss (δm_W) as a function of time. An hygroscopic material that is typical dried in these applications is characterized by a certain

drying rate behaviour:

- First drying stage: a constant drying rate phase, free moisture is extracted from the surface: vaporization
- Second drying stage: weak drying rate, capillarity from the hearth of the material to the surface
- Third drying stage: weak drying rate, heat conduction from the surface to the product

Moisture Diffusivity

Diffusion in solids during drying is a complex process that may involve:

- molecular diffusion
- capillary flow
- hydrodynamic flow diffusion

The effective diffusivity can be defined from Fick's second law 1.18 and summarizes all the previous phenomena:

$$\frac{\partial X}{\partial t} = D\nabla^2 X \tag{1.18}$$

where the effective diffusivity (D $[m^2/s]$) is function of the material and the material moisture content (X $[-]$) varies in time.

Effective Moisture Diffusivity in Some Materials			
Material	X $[-]$	T $[degC]$	D $[m^2/s]$
Apple	0.12	60	$6.5 \cdot 10^{-12} - 1.2 \cdot 10^{-10}$
Potato	0.60	54	$2.6 \cdot 10^{-10}$
Concrete	0.10-0.40	20	$5.0 \cdot 10^{-10} - 1.2 \cdot 10^{-8}$
Sand	0.05-0.10	45	$1.0 \cdot 10^{-7} - 1.0 \cdot 10^{-6}$
Wood	1.00	100-150	$1.0 \cdot 10^{-8} - 2.5 \cdot 10^{-8}$

Table 1.3: Effective Moisture Diffusivity in Some Materials

1.2.3 Drying in textile industry

Drying is necessary to eliminate ($RH \simeq 0$) or reduce the water content of the fibres, yarns and fabrics. Drying, in particular by water evaporation, is a high-energy-consuming step, because of the enthalpy of vaporization of water plays a main role in energy balance. Drying can be applied to the following textile materials:

- loose fibre
- hanks
- yarn packages
- fabric

Drying techniques are typically classified as mechanical or thermal: in mechanical processes the bound water is removed from the fiber 1.1 Thermal processes instead consist in heating the

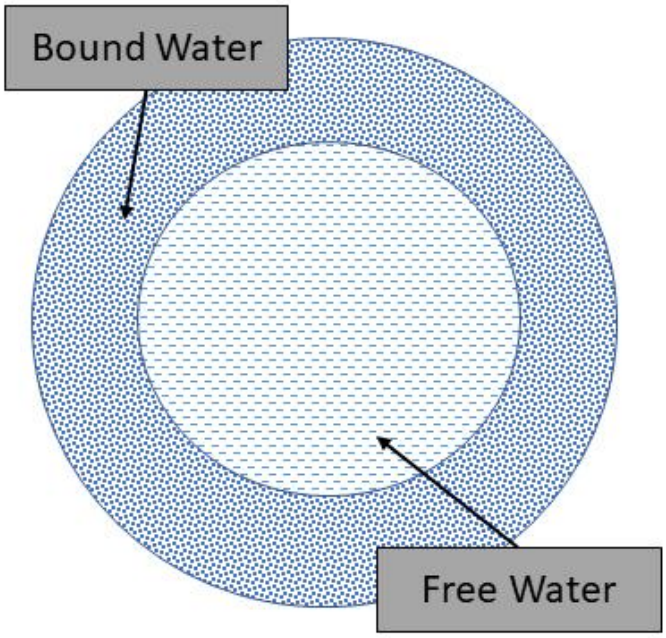

Figure 1.1: Bound water and free water in a wet material)

water and vaporizing it. Heat can be transferred by several mechanism:

- convection
- infrared radiation

- direct contact
- radio-frequency

In general drying involves at least two (or more) different techniques. It is easy to understand that it is possible to vaporize the water inside the material matrix, but we need a "vector" to extract it: convection (natural of forced) is probably the main and most used mechanism to "move" water vapor from the material to the environment.

Loose fibre drying

In loose fibre drying the water content of the fibre is initially reduced by centrifugal extraction or by mangling before the evaporative drying stage. Typical techniques for loose fibre drying are listed below.

Centrifugal extraction

Textile centrifugal extractors are an industrial type of the familiar tumble dryer that we can find in our homes, it mainly operates on a batch process. For wool drying, an extraction cycle of $3-5$ $[min]$ reduces residual moisture content to approximately $1.0[l/kg]$ dry fibre. **Mangling** They are used to reduce the water content. Mangling efficiency is typically lower than centrifugal extraction.

Evaporative drying

Evaporative dryers are based on hot air circulation through the product. Typically are present consecutive chambers to guarantee high performances and control the temperature during the process, and avoid overheating of textile products. Fibre are typically transported on a conveyor bel. High efficiency dryers with perforated steel converter belt have been developed which even out the air pressure drop across the fibre matt. This design results in more even drying and lower thermal requirements. The majority of hot-air dryers are steam heated or use methane burners to heat the process gas (hot air). Nowadays, several manufacturers developed radio frequency dryers, they are still vacuum tube technology based, but the development of Solid State should guarantee higher efficiencies in the next years. Radio frequency dryers are reported to be significantly more energy efficient than steam heated chamber dryers, and that work will analyse them deeply. Before the 2020 the higher efficiency was not always supported by lower operational cost due to the high cost of the primary energy needed (electrical energy for the power generators). But the last two years changed the European energy cost landscape: the cost

of the methane increased dramatically and the economical advantage of it must be reconsidered and reanalysed.

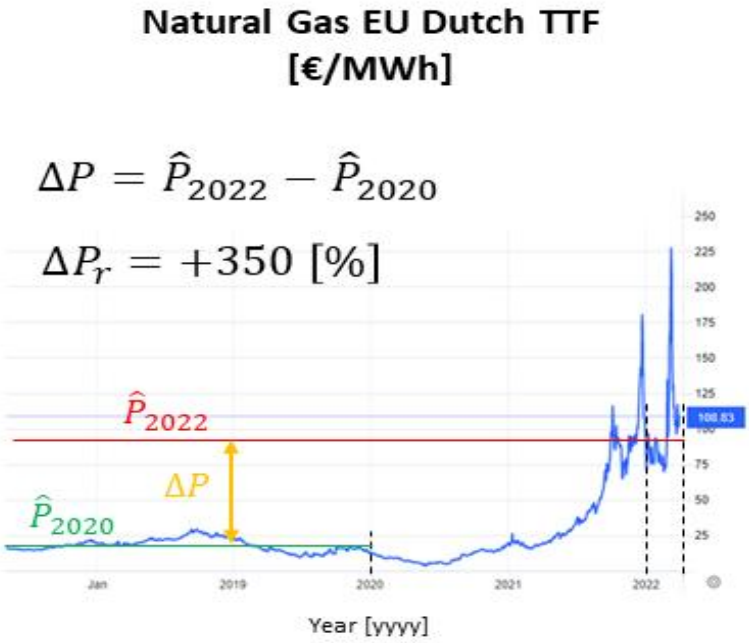

Figure 1.2: Natural Gas EU Dutch TTF (March 2022)

Fabric drying

The drying process for fabric usually involves two steps: the first one is aimed at removing water which is mechanically bound to fibres, while the second one is necessary to dry completely the fabric.

Squeezing Hydro-extraction and centrifugal hydro-extractor

The fabric is squeezed through two or three rollers covered with rubber in the first case, in the second case an horizontal axis machine may be used and exploits tangential component of velocity to extract mechanically water from the fabric: it demonstrated the best efficiency in mechanical water extraction. These processes cannot be applied to delicate fabric.

Stenter

This machine is used for full drying of the fabric. Hot air is blown across the fabric thereby producing evaporation of the water. It is characterized by high convection heating coefficients. The fabric undulates along the dryer to allow its shrinking. Most common stenter designs are horizontal and multi-layer.

Hot-flue dryer

This machine is composed of a large metallic box in which many rolls are applied to the fabric (in full width). The total distance the fabric travels may also reach 250$[m]$ inside the machine. The internal air is heated by means of heat exchangers and one or more impeller are used.

Contact dryer or heated cylinders

In this type of machinery the fabric is dried by direct contact with a hot surface. The fabric is longitudinally stretched on the surface of a set of metallic cylinders. The cylinders are heated internally by means of steam or direct flame.

Conveyor fabric dryer

The fabric transported within two blankets through a set of drying modules. Inside each module the fabric is dried by means of a hot air flow. This equipment is normally used for combined finishing operations on knitted and woven fabrics when, along with drying, a shrinking effect is also required in order to give the fabric a soft hand and good dimensional stability.

Air dryer-use in fabric processing

This machine can be used for washing, softening and drying operations on woven and knitted fabrics in. During the drying phase the fabric in rope form is re-circulated in the machine by means of a highly turbulent air flow. Water is thus partly mechanically extracted and partly evaporated.

1.2.4 Drying in paper industry

4em In paper industry hot roller are mainly used to guarantee high production rates. A rotating steel roller is heated by direct passage of hot fluid that may be dry saturated steam or diathermic oil. Hot fluid exchanges energy with conductive roller, and the hot roller exchanges energy with the paper that is in full contact with the surface. The production rate is related in that case to the tangential velocity of the roller. The system want to dry the material from its initial relative humidity (RH_{in} $[-]$) that may be in a range of $(30-40[\%])$ to the final product relative humidity (RH_{out} $[-]$) that may be in a range of $(10-5[\%])$. As seen before the main mechanism for that process is teh evaporation of water from the material matrix structure. That means the boiling temperature of vapor must reached (T_{boil} $[degC]$). An energetic analysis of power flows is necessary to understand the mechanism. If the system has a specific production rate (m_{prod} $[kg/s]$), the evaporated mass of water is net balance of the mass flow before and after the evaporation system, and the temperature of paper is increased during the process from T_{in}

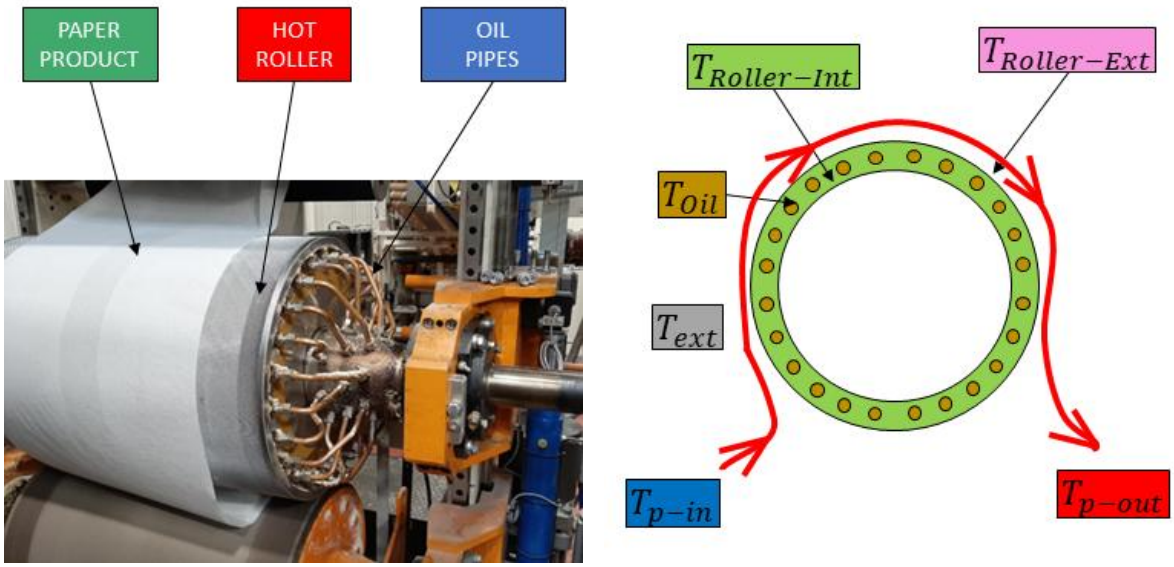

(a) (b)

Figure 1.3: Hot roller dryer for paper industry

$[degC]$ to T_{out} $[degC]$, that means:

$$\begin{cases} \dot{m}_{evap}(t) = \dot{m}_{in} - \dot{m}_{out} \\ \Delta T_p = T_{p-in} - T_{p-out} \end{cases} \tag{1.19}$$

The power balance is written in the next equation:

$$P_{heater} = P_l + P_{roller} + P_{paper} \tag{1.20}$$

where the heating power (P_{heater} $[W]$) is the energy given to the fluid (in that case diathermic oil) and the hot roller can be analysed as a simple exchanger where the energy is function of the temperature drop at the inlet (T_{o-in} $[degC]$) and at the outlet (T_{o-in} $[degC]$) of the roller and of the diathermic oil mass flow (m_{oil} $[kg/s]$):

$$P_{heater} = \dot{m}_{oil} Cp_{oil} (T_{oil-in} - T_{oil-out}) \tag{1.21}$$

The power accumulated in the roller is not negligible in non continuous applications. Nowadays the discontinuity of the production and the flexibility of production due to the high variability of the market of paper products is changing the typical production type that is every year more similar to batch processes than continuous processes. When the production is varied and there is the necessity of changing the material that we want to dry there is necessary to cool down the whole system because of the operator must directly work on the hot part of the system. The increasing of safety in the workplace also is asking every year lower safety temperatures. That

means a hot-roller system that during evaporation may also reach a steady-state temperature of 250[$degC$] must be cooled down to a safe temperature of also 60[$degC$].

$$P_{roller} = Ct_r^* \frac{\partial T_r^*}{\partial t} \tag{1.22}$$

A good design should minimize the global heat capacity of the roller (Ct_r $[J/K]$). A roller is typically a complex multi-layer system composed by several materials, and for that case we defined a mean heat capacity of it (Ct_r^* $[J/K]$) that relates the energy stores to its mean temperature (T_r^* $[degC]$). Losses are another important therm. They are practically related to tangential velocity. Because of we need surrounding air to extract vapor from the material, the roller can exchange energy with the surroundings by surface-convection phenomena. For a certain machine speed (or linear production velocity) (v_p $[m/s]$) the tangential speed is related to the rotational speed of the system (ω $[rpm]$) by the radius of the roller (R_r $[m]$)

$$v_{tan} = v_p = \frac{\omega}{R_r} \tag{1.23}$$

The Reynolds's Number (Re $[-]$) and the Prandtl's Number (Pr $[-]$) and the Raylegh's Number (Ra $[-]$) are then function of properties of the surrounding gas (air) and are necessary to estimate convective-exchange coefficient to estimate losses at the surface of the cylinder:

$$\begin{cases} Re = \frac{v_p R_r}{\mu_a \rho_a} \\ Pr = \frac{\mu_a Cp_a}{\lambda_a} \\ Ra = \frac{\rho^2 (g\beta\Delta T) L^3}{\mu^2} \end{cases} \tag{1.24}$$

and then the Nusselt's Number (Nu $[-]$) for a rotating cylinder

$$Nu = \left[0.6 + \frac{0.387 Ra^{0.2}}{\left[1 + \left(\frac{0.559}{Pr} \right)^{0.563} \right]^{0.444}} \right]^2 \tag{1.25}$$

and finally the convective coefficient (α_c $[W/(m^2K)]$) is:

$$\alpha_c = \frac{Nu \lambda_a}{L_d} \tag{1.26}$$

where the thermal conduction of air is estimated at the average temperature between the surface temperature and the environment temperature, and the total length of the roller is L_d $[m]$. In that work is considered a roller with $R_d = 350[mm] - 4000[mm]$ and $L_d = 500 - 3000[mm]$ with a linear production velocity $v_p = 100 - 2000[m/min]$ and that implies a wide range of convective coefficient to estimate losses to the environment: $\alpha_{conv} = 50200[W/(m^2K)] - 200[W/(m^2K)]$. Finally the energy exchanged with the paper is the net balance of all other power (heating and

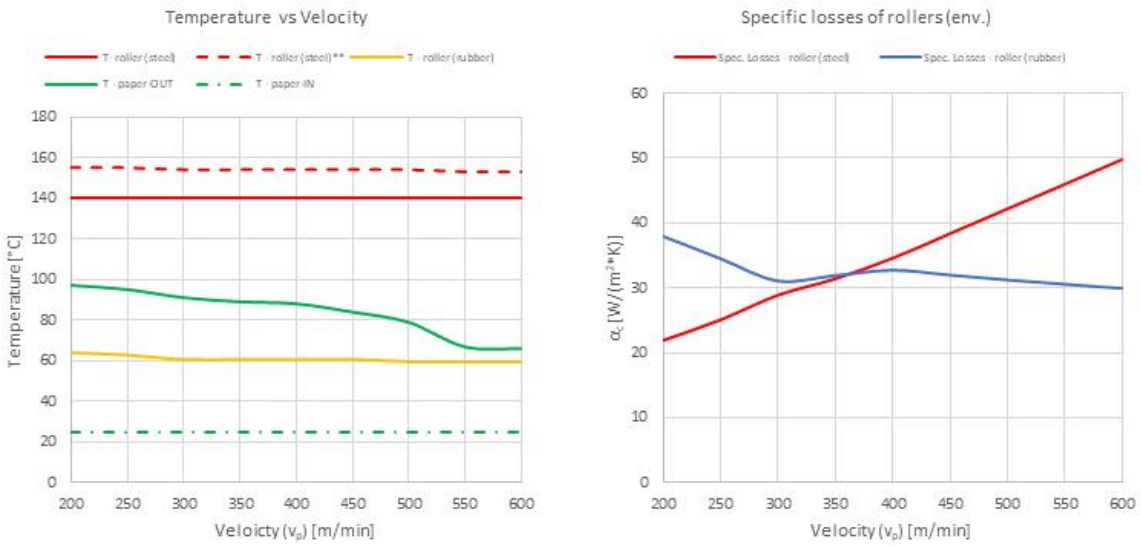

(a) **(b)**

Figure 1.4: Temperature and convective heat flux in a diathermic roller: Behaviours varying velocity (v_p $[m/min]$). (a) Temperatures; (b) Convective heat flux computed from the convection problem

losses) and is related to evaporation of water ($P_{evap} + P_{water}$) and accumulated energy in the paper-dry material (P_{dry}):

$$P_{paper} = P_{evap} + P_{water} + P_{dry} \tag{1.27}$$

where

$$P_{dry} = Cp_p \frac{T_{p-out} - T_{p-in}}{\Delta t} \tag{1.28}$$

and

$$\begin{cases} P_{water} = Cp_w \frac{T_b - T_{p-in}}{\Delta t} \\ P_{evap} = \Delta H_L \dot{m}_{evap} \end{cases} \tag{1.29}$$

where the process of evaporation takes place at the its boiling temperature (T_b $[degC]$). Figure **??** shows several roller-surface-temperature controlled behaviours. Increasing velocity (and so increasing production rate) losses dramatically increase for convective effects. At high velocities the phenomenon changes and vaporization occurs because of the turbulent-surface effects on the thin layer of the paper, that is experienced with a lower temperature of the paper at the outlet of the system. As seen before one of main problems of these systems is the time to pre-heat the system. Because of the exchange of power between the roller and the paper is due to thermal gradients, it is necessary to reach the surface temperature that may guarantee evaporation, in steady state condition, and in first approximation:

$$P_{paper} = K_{r-p} \left(T_{r-surf} - T_b^* \right) \tag{1.30}$$

where the conduction effect (roller-paper) is considered in the therm (K_{r-p}). Experimentally T_{r-surf} for that practically case may not overcome 160[$degC$] to guarantee the safety of the material (no superficial overheating). That means a certain time is required to reach the target temperature (T_{target} [$degC$]). Analyzing the transient problem, and that means, solving thermal-problem seen before, figure 1.5 highlights that 54[min] are require for the specific system to reach the working condition of 140[$degC$]. Induction heating is a new interesting

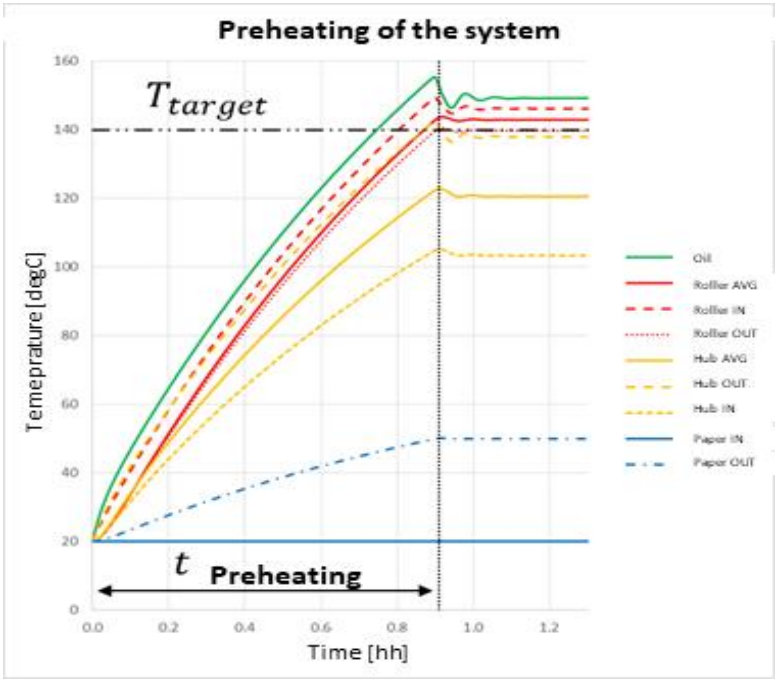

Figure 1.5: Temperature transient: Preheating of a diathermic oil roller.

technology because of can dramatically reduce the pre-heating time to reach the operational conditions for drying. We will see that it also may minimize energy necessary for that phase.

1.3 Drying with EPM

Electromagnetic Processing of materials, in accordance with the chosen frequency can heat conductive materials (induction heating), dielectrics (radio.frequency heating and microwave heating).Because of the main part of the work (5,6) will study the RF and MW technologies, now we will introduce a study a new application that we developed recently. Drying of paper with induction heating system.

1.3.1 Induction Heating heater form drying rollers

Induction heating of metals can guarantee high power densities directly to the material, and that means high heating rates. For that reason we tried to apply that technology to heat hot rollers used for drying of paper products (thin and wide). We design a custom

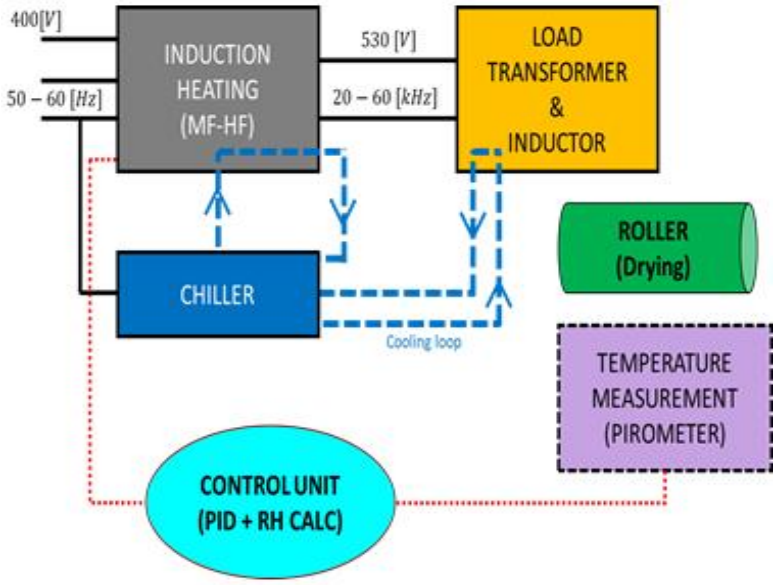

Figure 1.6: Induction heating system for hot roller for drying paper products.

inductor for the revamping of existing machines. Induction heating makes possibly to directly heat the surface of the roller and that meant we directly heated the interface between the paper and the steel roller. For that application we optimized a steel roller using a magnetic steel. The geometry of the roller is characterized by three dimensional structures to maximize the total surface and for the embossing phase. Using a frequency of $60[kHz]$ made possible to generate current densities directly on the profile of the teeth as is shown in figure **??** In figure **??** are highlighted the induction system and the surface of the roller: the power density sources, in accordance with the penetration depth of the steel are only on the surface at high frequencies (f $[Hz]$).

$$\delta_{pen} = \sqrt{\frac{2\rho_s}{2\pi f \mu_{r-s}\mu_0}} < 0.5[mm] \tag{1.31}$$

for typical magnetic materials and frequencies higher than $30[kHz]$. With the help of FEM analysis we designed and optimized an induction system to generate high density power sources an a small surface where the material enter in contact with the material. A n induction system must optimize the non uniformity due to the distribution of power sources along the length of

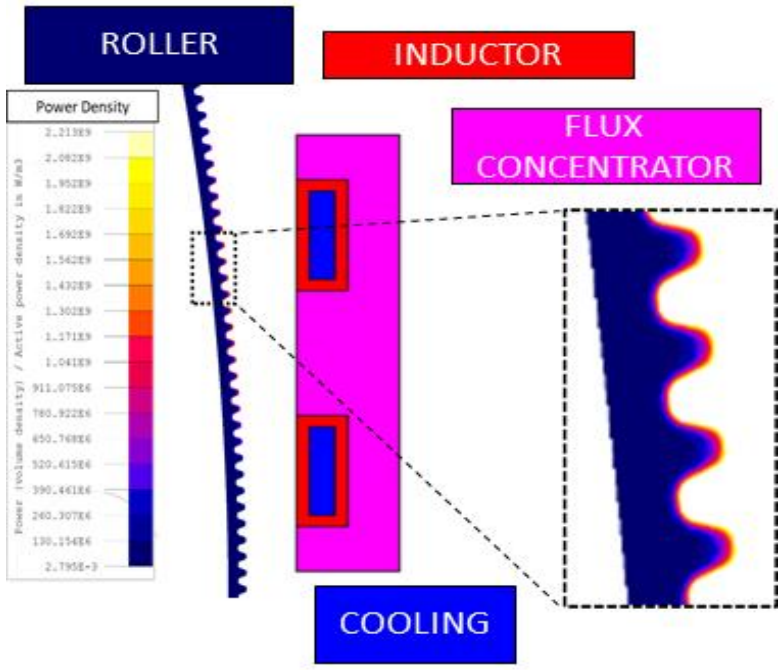

Figure 1.7: Roller profile with teeth and induction system.

the system. In figure 1.8 is shown the problem of edge effects due to the real three-dimensional distribution of current densities. A good design must optimise the edge effects to guarantee a good distribution of the temperature along length of the roller to obtain a constant evaporation in all the material width. An high power induction system consists of several parts as is highlighted in figure 1.6. An induction generation unit converts a three phase low frequency ($50[Hz] - 60[Hz]$), low voltage ($V_{net} = 400[V]$) input power through a resonant generator in an medium-high frequency ($20[kHz] - 60[kHz]$) low current output power. A matching-load transformer finally reduce voltage and increase current up to values of $100[A] - 10000[A]$. A typical global efficiency for that industrial system may reach an efficiency of 85[%]. For high power applications it is necessary to design and consider a chiller to cool down the induction system (generator, load transformer and inductor)

1.4 Heating and cooking with EPM

We saw in the previous section that one of the main problem of heating a roller using diathermic oil (or steam) is the pre-heating time, that may also need $1[h]$ to guarantee the good uniformity of the system. Induction heating, because of directly heat the surface solves dramatically that problem. Results of simulations are shown in figure 1.9: In therms of en-

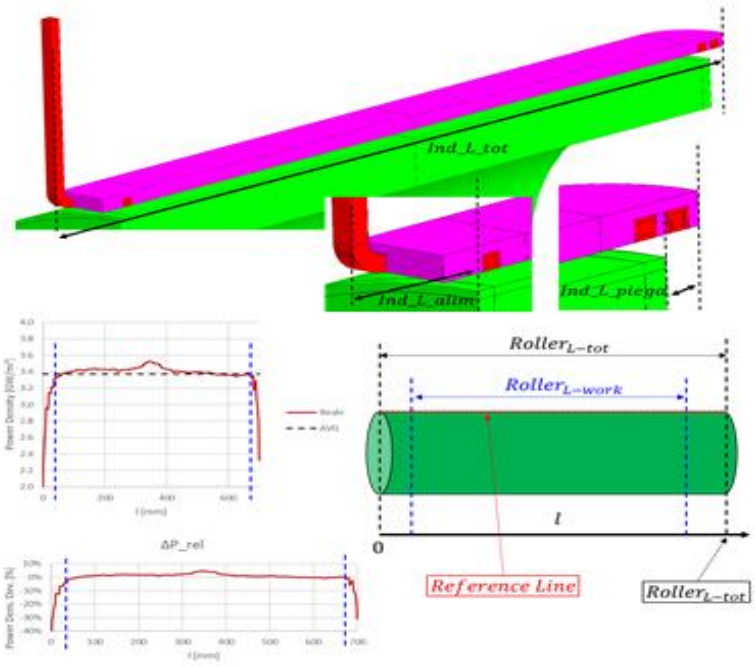

Figure 1.8: Induction system and roller. Distribution of heating power along the length of the system.

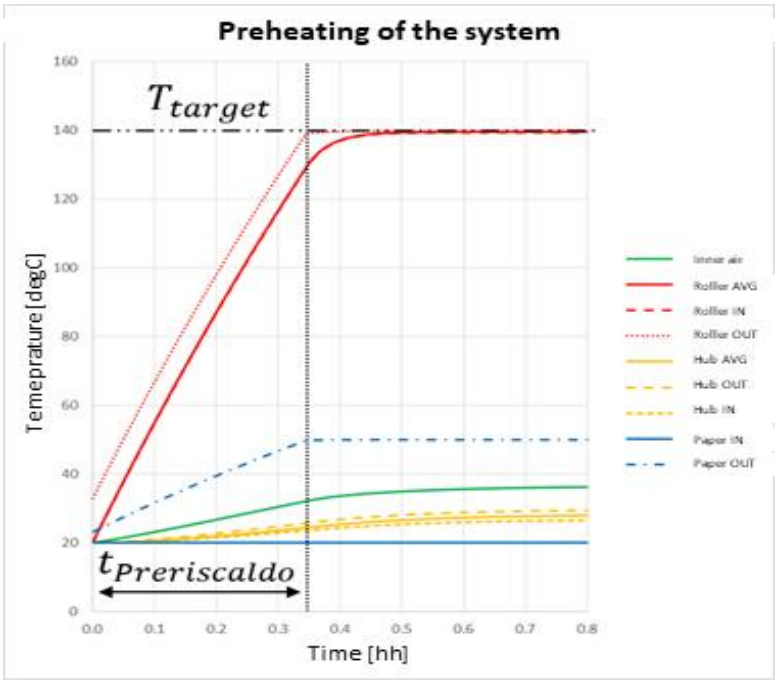

Figure 1.9: Pre-heating phase simulated for external induction system.

ergy cost induction heating can dramatically reduce energy consumption during the preheating phase. Because of many energy is spent in accumulated energy of the diathermic oil system and in circulating circuit for it the total energy for the preheating phase is reduce by also the 53[%] as is shown in figure 1.10 Cooking is the process that use heat to prepare (and modify) a certain food. The science of cooking is based on the concept of transformations. Food is

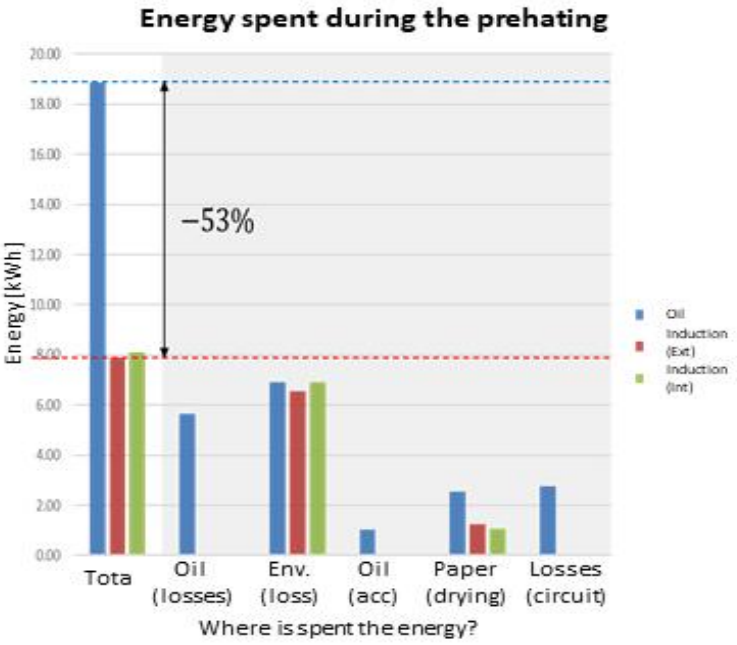

Figure 1.10: Pre-heating energy consumption analysis: induction heating (inner and outer) compared to classical diathermic oil heating.

mainly composed by carbohydrates, fats, protein and water. A cooking process consists primarily of transformations of these components to obtain a final product that is different from its ingredients. In cooking evaporation is one of the most important process and typically varies the modification of shape (density) and of consistency of the material (porosity). Flavour are one of the most important details of cooking. The chemicals responsible for flavor perception must be released from the food matrix and transported to the flavor receptors in the mouth and nose. The overall process is governed by the chemical properties of the flavor compounds, the nature of the food matrix and the physiological conditions of the mouth, nose and throat during food consumption. These factors combine to determine the concentrations and rate at which the flavor chemicals reach the receptors, thus creating the characteristic flavor profile of a food. Moreover, the temperature reached by food can improve or weak the flavors and taste of it. Overcooking can destroy flavor and nutrients. So it is crucial to cook to retain nutrients, flavor, color, texture and overall appeal. Cooking cannot improve poor-quality foods, but it can enhance the flavors of high-quality foods. More precisely some physical and chemical parameters can affect the taste and flavour of food. Among the others we can mention the following:

- Dilution effect: transfer of volatile compounds from mouth to nose involves dilution (from

10 to 100X lower concentrations in nose than in-mouth)

- Persistence, associated with the absorption of volatile flavors on the mouth/nose/throat lining, namely via interaction with mucus layer; to improve persistence, the final dish should be designed to contain different components (e.g., a duck + a sauce) so that the odorant and taste molecules are retained for different lengths of time before being released.
- Temperature (of food and tongue) – so-called "thermal tastes"
- Cooling/heating the tongue can arise the perception of tastes, even in the absence of food.
- The intensity of the sweet flavor, at the front of the tongue, increases as the temperature rises, and the sour taste caused by cooling becomes saltier as the temperature falls. In particular, the perception of thermal sweetness is greatest in the tip of the tongue while thermal sourness is most clearly perceived on the sides of the tongue

So Cooking, which is the art of preparing food for consumption with the use of heat, plays an important role in production of flavor on foods. Moreover, a perfect control of temperature during the cooking or reheating process of food can preserve not only the flavor(s) but also the texture, colors and nutrients in such a way to eat a perfect meal. Starting from these first ideas about the most important features affecting the quality and hence the flavor of food, we propose a specific research project dealing with the improving of flavor on food using a perfect control of temperature during cooking by using microwave heating. Microwave (MW) is a fast heating method using electromagnetic sources which are able to act directly inside the food. This is the reason why MW heating is so fast and so healthy. The heat sources inside the food have two different advantages: to put inside the food high values of power density and to increase the temperature by inside avoiding overheating and burning of food surface. Flavor release is the process through which specific molecules move out of a particular environment within a food into the air and/or the saliva or vapor phase [64]. In order to increase the flavor persistence, it is of paramount importance both to hamper their release when they are quite volatile species and to favor their emission when they are not volatile and/or embedded in some macro-molecular domains. A number of different strategies can be exploited to trap these molecules, namely by extraction, by playing with molecular interactions, by compartmentalization (micro- and macro-), by adding flavors and by designing chemical reactions in such a way that flavors are formed in the food itself. However, the "world" of flavors and flavor generation/release is quite troublesome due to the specific features of each food, its chemical components/nutrients, the

average taste of different people (e.g., Italian, Japanese, Chinese, Mexican etc), the individual taste including the physiological and genetic aspects (mouth volume, saliva flow rate and air flow rate through the mouth and nose). Another issue to consider is the typical mechanisms governing flavor release, such as partitioning, inter-facial mass transport and diffusion. Although the theory behind these factors is quite understood, applying them to the situation in-mouth during eating is difficult. This is because key parameters, such as surface area and flavor concentrations in the gas (i.e., air in the nose-mouth) and liquid (i.e., saliva) phases, change rapidly with time as a result of the physiological processes while eating. Furthermore, individuals vary in their rate of breathing, swallowing and salivation, which affects the transport of flavors from saliva to receptors on the tongue and in the nose. In this initial phase of the work, we will update in the field by exploring both scientific-technical papers and patent literature In home appliances, but also in industry, the main mechanism that allow to cook a certain food are the same seen before in the first part of that work:

- convection
- radiation heat transfer
- direct conduction
- air impingement
- microwave and radio-frequency heating

That work is focused on microwave heating and radio-frequency heating. Cooking is probably the most older process in food industry, and also its kernel, but nowadays the heating and thawing process are becoming two extremely important famous and innovative [87]. Preserve, store and regenerate cooked food is becoming an important concept in food sector. The main problem is the quality of the final product. In chapter 7 a thawing process is analysed. The main problem of using a general purpose domestic oven is the difficulty to reach high efficiencies and high final quality product in therms of uniformity and average temperature. Regeneration and thawing are a complex processes where many phenomena occur: heating, drying (evaporation and vaporization), defrosting (phase change of ice). We designed in chapter 7 a new cavity for a practical problem: regeneration of vegetable-ready meals.

Chapter 2

Electromagnetic problem

2.1 Electromagnetic waves

The main feature of EPM is the capability of directly heat materials, this is possible because the medium to which energy must be transferred is also the medium in which the electromagnetic field is generated.

2.2 Maxwell's Equations

The set of equations is the work of synthesis done by the Scottish mathematician and physicist James Clerk Maxwell (Edinburgh, 1831 - Cambridge, 1879) [60] [61], who published an early form of the equations that included the Lorentz force law ($\mathbf{F}_L$ $[\frac{N}{m^3}]$) as the combination of electric and magnetic force on a point charge due to electromagnetic fields. The modern form of the equations in their most common formulation is credited to the mathematician Oliver Heaviside (London, 1850 - Torquay, 1925) [65].
Maxwell's equations are a set of partial differential equations (PDEs) that, in completion of the definition of Lorentz Force, form the theoretical basis of classical electromagnetism.
The equations provide a mathematical model for all electromagnetic processing of materials. Maxwell's equations describe how electric and magnetic fields are generated by charge densities (ρ $[\frac{C}{m^3}]$), current densities ($\mathbf{J}$ $[\frac{A}{m^2}]$), and changes over time of electric field ($\frac{\partial \mathbf{E}}{\partial t}$ $[\frac{V}{ms}]$) and magnetic field ($\frac{\partial \mathbf{B}}{\partial t}$ $[\frac{T}{s}]$).

$$\nabla \cdot \mathbf{D} = \rho \tag{2.1}$$

$$\nabla \cdot \mathbf{B} = 0 \tag{2.2}$$

$$\nabla \times \mathbf{E} = -\frac{\partial \mathbf{B}}{\partial t} \tag{2.3}$$

$$\nabla \times \mathbf{H} = \mathbf{J} + \frac{\partial \mathbf{D}}{\partial t} \tag{2.4}$$

Equation 2.1 is the differential form of the Gauss's theorem for electric field ($\mathbf{E}$ $[\frac{V}{m}]$) and displacement field ($\mathbf{D}$ $[\frac{C}{m^2}]$). It claims that the divergence of the electric field is proportional to the volume charge density (ρ $[\frac{C}{m^3}]$) and at the same time inversely proportional to the permittivity (ϵ $[\frac{F}{m}]$) of the medium because there is a relationship between the electric field and the displacement field as in equation 2.8. It is important to remember that more generally permittivity of a certain medium can be expressed as the product of permittivity of free space (2.5) and relative permittivity of the medium.

$$\epsilon_0 = \frac{1}{\mu_0 c_0^2} \approx 8.854187 \left[\frac{F}{m}\right] \tag{2.5}$$

where the magnetic permeability of the vacuum can be expressed as in equation 2.6.

$$\mu_0 = 4\pi \cdot 10^{-7} \left[\frac{H}{m}\right] \tag{2.6}$$

and the speed of light in vacuum is

$$c_0 \approx 299792458 \left[\frac{m}{s}\right] \tag{2.7}$$

In electromagnetism, the relative permittivity ϵ_r is a measure of the electric polarizability of a dielectric material with respect to the ability to polarize of the vacuum. A material with high permittivity polarizes more in response to an applied electric field than a material with low permittivity.

$$\epsilon_r = \frac{1}{\epsilon_0} \cdot \frac{\mathbf{D}}{\mathbf{E}} \tag{2.8}$$

In addition to the differential form the integral form is often used to describe and better understand the Gauss's Law for the electric field. It affirms that the flux of the electric field through

an arbitrary closed surface $\partial\Omega$ is proportional to the electric charge (Q $[C]$) contained in the domain Ω which the closed surface is the support as shown in figure 2.1. The distribution of the charges does not influence the value of the flux of the electric field.

$$\Phi(\mathbf{E}) = \iint_{\partial\Omega} \mathbf{E} \cdot dS = \frac{Q}{\epsilon} \tag{2.9}$$

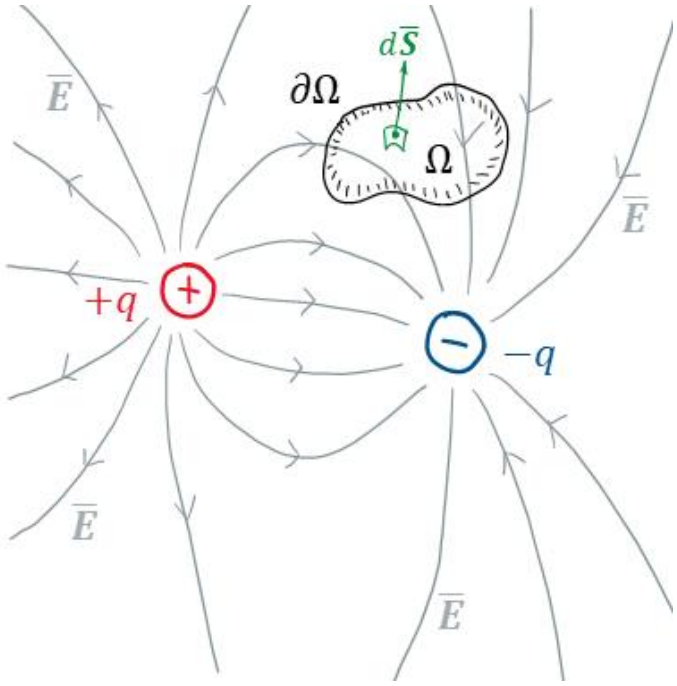

Figure 2.1: Gauss's theorem for electric field. Electric flux through an arbitrary surface $\partial\Omega$

Equation 2.2 is the differential form of the Gauss's theorem for magnetic field ($\mathbf{B}$ $[T]$). It states that divergence of a magnetic field is every time equal to zero, in other words that magnetic fields are solenoidal vector fields.

Helmholtz's theorem, [7] also known as the fundamental theorem of vector calculus, states that a three dimensional vector field $\mathbf{F}$ can be decomposed into the sum of an irrotational vector field and a solenoidal vector field:

$$\mathbf{F} = -\nabla\Phi + \nabla \times \mathbf{A} \tag{2.10}$$

If 2.10 and 2.2 are combined, than it possible to describe the Gauss's theorem also with the magnetic vector potential ($\mathbf{A}$ $[\frac{Vs}{m}]$). Magnetic vector potential is essential for the resolution of electromagnetic fields by numerical methods (computational electromagnetism). It is important

to highlight that $\mathbf{A}$ is generally a three-component vector if the magnetic field $\mathbf{B}$ (or $\mathbf{H}$) has three components.

$$\mathbf{B} = \nabla \times \mathbf{A} \tag{2.11}$$

Equation 2.2 can be also represented with its integral form:

$$\Phi(\mathbf{B}) = \iint_{\partial\Omega} \mathbf{B} \cdot dS = 0 \tag{2.12}$$

Equation 2.12 demonstrates the non existence of magnetic mono-poles. If we consider a simple magnet, made up by two poles, a north and a south, it is possible to generally define, as before done for the electric field, a close surface $\partial\Omega$ as shown in figure 2.2

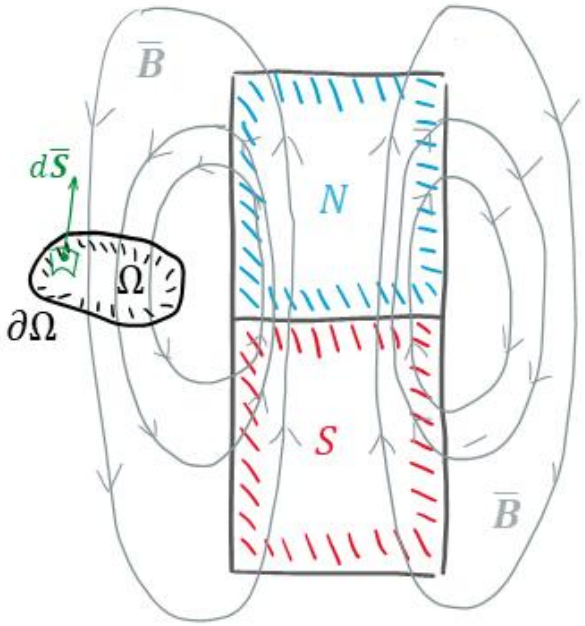

Figure 2.2: Gauss's theorem for magnetic field. Magnetic flux through an arbitrary surface $\partial\Omega$

In 1831 Faraday discovered electromagnetic induction phenomenon, simultaneously, but independently Joseph Henry published same results about interaction between magnetic field and electric circuits [23] and the generation of electromotive forces ($f.e.m.$ $[V]$).
The Maxwell–Faraday equation 2.3 describes the fact that a time-varying electric field always generates a time-varying magnetic field. At the same time, obviously, the equation can be read in the opposite verse: in other words that a time-varying magnetic field always generates a

time-varying electric field.

In electromagnetic processing of materials that equation is probably the most relevant to describe Induction Heating (IH) treatments and devices, where a time-varying magnetic field ($\frac{\partial \mathbf{B}}{\partial t}$) $[\frac{T}{s}]$ is used to generate an electric field into the surface of a conductor material, and therefore to transfer power directly to the work piece.

The Maxwell–Faraday equation can also be written in an integral form 2.15 by the Kelvin–Stokes theorem [29], that is made explicit in equation 2.13, where $\mathbf{A}$ is a general vector field:

$$\iint_{\Sigma} (\nabla \times \mathbf{A}) \cdot d\mathbf{S} = \oint_{\partial\Sigma} \mathbf{A} \cdot d\mathbf{l} \tag{2.13}$$

To better understand Faraday Law is useful define the Magnetic Flux Φ_B for any surface Σ whose boundary is the given loop $\partial\Sigma$ as shown in figure 2.3

$$\Phi_B = \iint_{\Sigma} \mathbf{B} \cdot d\mathbf{S} \tag{2.14}$$

And then it is possible to get the equation:

$$\oint_{\partial\Sigma} \mathbf{E} \cdot d\mathbf{l} = -\iint_{\Sigma} \frac{\partial \mathbf{B}}{\partial t} \cdot d\mathbf{S} \tag{2.15}$$

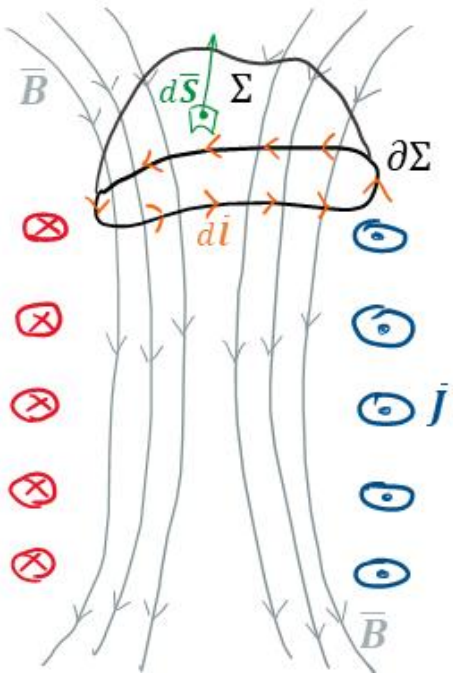

Figure 2.3: Faraday's theorem. Magnetic flux through an arbitrary surface Σ. The line integral around $\partial\Sigma$ is called circulation

In classical electromagnetism, Ampère's circuital law relates the integrated magnetic field around a closed loop to the electric current passing through the loop. In 1861 James Clerk

Maxwell [59] derived it using hydrodynamics analysis. After only four years he generalized the equation to with time-varying currents by adding the displacement current term ($\mathbf{J}_D$ $[\frac{A}{m^2}]$), resulting in the final form of the law, many times called the Ampère–Maxwell law, which is the fourth Maxwell's equation 2.4. The integral form of the original circuital law is a line integral of the magnetic field around an arbitrary closed loop $\partial\Sigma$. The closed loop is the bound of a surface Σ which the electric current concatenates.
In terms of total current, the line integral of the magnetic magnetic field ($\mathbf{B}$ $[T]$) around the close curve is proportional to the total current (I_{conc} $[A]$) passing through the surface Σ. The equivalent form of Ampère-Maxwell law is presented in equation 2.16

$$\oint_{\partial\Sigma} \mathbf{H} \cdot d\mathbf{l} = \iint_{\Sigma} \mathbf{J} \cdot d\mathbf{l} \tag{2.16}$$

If a displacement field is considered it is possible to extend the Ampère-Maxwell equation making explicit the displacement term. Equation 2.4 becomes:

$$\nabla \times \mathbf{H} = \mathbf{J}_c + \mathbf{J}_d = \mathbf{J}_c + \frac{\partial \mathbf{D}}{\partial t} \tag{2.17}$$

where $\mathbf{J}_c$ $[\frac{A}{m^2}]$ is the current density due to free charges and ($\mathbf{J}_D$ $[\frac{A}{m^2}]$) is the displacement density due to the presence of a dielectric material. At the same way it is possible to re-write equation 2.16 as equation 2.18. Figure 2.4 shows typical extended problem.

$$\oint_{\partial\Sigma} \mathbf{H} \cdot d\mathbf{l} = \iint_{\Sigma} \left(\mathbf{J}_c + \frac{\partial \mathbf{D}}{\partial t} \right) \cdot d\mathbf{l} \tag{2.18}$$

As already introduced in the previous pages the Lorentz Force completes Maxwell's equations and together with them forms the kernel of electromagnetic theory. Lorenz Force is the combination of electric force and magnetic force on a point charge due to electromagnetic fields. A particle of a certain charge (q $[C]$) moving with a certain velocity field ($\mathbf{v}$ $[\frac{m}{s}]$) in an electric field ($\mathbf{E}$ $[\frac{V}{m}]$) and a magnetic field ($\mathbf{B}$ $[T]$) experiences a force that is the effect of all three vector fields as shown in equation 2.19 and figure 2.5.

$$\mathbf{F} = q\left(\mathbf{E} + \mathbf{v} \times \mathbf{B}\right) \tag{2.19}$$

The four Maxwell's equations 2.12,2.9,2.15,2.16, along with Lorentz Force law 2.19, are enough to derive everything in classical electromagnetism [24]:

$$\frac{\partial \Phi_{\mathbf{B}}}{\partial t} = -\oint_{\partial\Sigma} (\mathbf{E} + \mathbf{v} \times \mathbf{B}) \cdot d\mathbf{l} \tag{2.20}$$

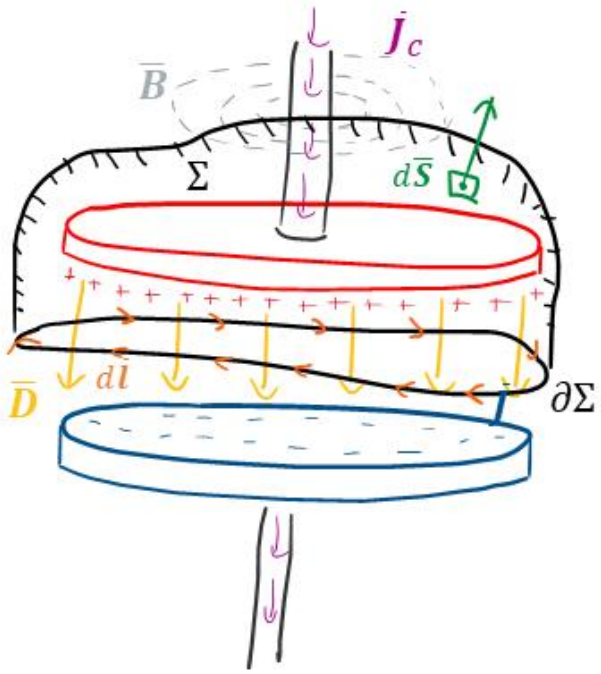

Figure 2.4: Ampère-Maxwell's law. Current flux through an arbitrary surface Σ. The line integral around $\partial\Sigma$ is called circulation of magnetic field

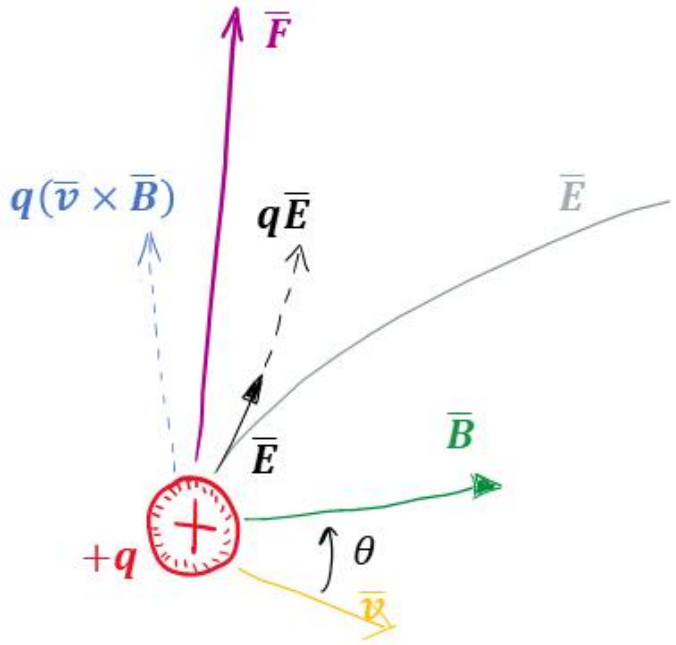

Figure 2.5: Lorentz Force. Sum of electric field and magnetic-velocity fields interaction

2.3 Solution of Maxwell's equations

Maxwell's equations are PDEs that relate the electric and magnetic fields to each other and to the electric charges and currents. Often, the charges and currents are themselves

dependent on the electric and magnetic fields via the Lorentz force equation and the constitutive relations as seen in the previous pages. These all form a set of coupled partial differential equations which are often very difficult to solve.

As for any differential equation, boundary conditions (BCs) and initial conditions (ICs) are necessary for a unique solution. In many cases that the present work want to deeply analyze, Maxwell's equations are solved in a finite region of space (1D,2D and/or 3D). In many real-life cases the most difficult part of the work is to define appropriate conditions on the boundaries of that region to represent the physics of the problem as correctly as possible.
Computational electromagnetic with its numerical methods for differential equations could be used to compute approximate solutions of Maxwell's equations. Nowadays the most import, and maybe most famous way to analyze and design devices and process for EPM is the so-called finite element method (FEM).

Before defining the approximate problem it is useful to try to solve simultaneously the four Maxwell's equations [24]. Starting from equations 2.2 and 2.3 it is possible to write:

$$\nabla \times \mathbf{E} = -\frac{\partial}{\partial t}\left(\nabla \times \mathbf{A}\right) \tag{2.21}$$

where $\mathbf{A}$ is the magnetic vector potential, and therefore after having defined a scalar potential ϕ and, as it is possible to do for electrostatic problems, where if $\nabla \times \mathbf{E} = 0$ than $\mathbf{E} = -\nabla V$ now it is possible to re-write the previous equation as:

$$\mathbf{E} = -\nabla\phi - \frac{\partial \mathbf{A}}{\partial t} \tag{2.22}$$

Solving two of Maxwell's equations, equation 2.22 suggests that to describe the electromagnetic fields $\mathbf{E}$ and $\mathbf{B}$, are necessary four degrees of freedom: a scalar potential (1D-vector) ϕ and a vector potential $\mathbf{A}$ (3D-vector).

Now it is possible to define a new vector potential and a new scalar potential without changing the behaviour of electromagnetic fields:

$$\mathbf{A}^{'} = \mathbf{A} + \nabla\psi, \quad \phi^{'} = \phi - \frac{\partial \psi}{\partial t} \tag{2.23}$$

Considering equations 2.1 and 2.22 it is possible to get the relation between potentials and electric sources:

$$-\nabla^2\phi - \frac{\partial}{\partial t}\nabla\cdot\mathbf{A} - \frac{\rho}{\epsilon} = 0 \tag{2.24}$$

Maxwell's fourth equation 2.4, remembering that $\mathbf{B} = \mu\mathbf{H}$ and that $c = \sqrt{\frac{1}{\mu\epsilon}}$, can be rewrote as:

$$c^2\nabla\times\mathbf{B} - \frac{\partial\mathbf{E}}{\partial t} - \frac{\mathbf{J}}{\epsilon} = 0 \tag{2.25}$$

and finally considering the potentials of electric and magnetic fields it is possible to get the final formulation for a general electromagnetic problem:

$$-c^2\nabla^2\mathbf{A} + c^2\nabla\left(\nabla\cdot\mathbf{A}\right) + \frac{\partial}{\partial t}\nabla\phi + \frac{\partial^2}{\partial t^2}\mathbf{A} - \frac{\mathbf{J}}{\epsilon} = 0 \tag{2.26}$$

Equation 2.26 is the complete form. It fully describes the electromagnetic field and for that reason it is many times called *Full Wave Formulation*. That equation is not easy to be solved and to be understood. It's possible at that point to choose a Gauge (*Gauge's Fixing*), or in other words to choose the value of $\nabla\cdot\mathbf{A}$. Considering now the so called Lorenz Gauge [53]:

$$\nabla\cdot\mathbf{A} = -\frac{1}{c^2}\frac{\partial\phi}{\partial t} \tag{2.27}$$

It possible to rewrite equation 2.26 as:

$$\nabla^2\mathbf{A} - \frac{1}{c^2}\frac{\partial^2\mathbf{A}}{\partial t^2} + \frac{1}{c^2}\frac{\mathbf{J}}{\epsilon} = 0 \tag{2.28}$$

and equation 2.24 as:

$$\nabla^2\phi - \frac{1}{c^2}\frac{\partial^2\phi}{\partial t^2} + \frac{\rho}{\epsilon} = 0 \tag{2.29}$$

2.4 Material Laws

As already introduced in the previous section, Maxwell's equations together with material laws and boundary conditions offer the capability of solving electromagnetic fields problems. That section will try to summarize main material laws, also introducing some models that try to describe non-linearities that characterize main EPM problems.

2.4.1 Magnetic Permeability

In electromagnetism, permeability is the measure of magnetization that a material obtains in response to an applied magnetic field. Heaviside in 1885 coined the term. There are important differences about the definition of magnetic field as function of the scale of the problem *Macroscopic vs Microscopic*.

In the macroscopic formulation of electromagnetism, there appears two different kinds of magnetic field:

- the magnetizing field ($\mathbf{H}$ $[\frac{A}{m}]$) which is for our applications generally generated by currents (conduction of free charges and displacement)
- the magnetic flux density ($\mathbf{B}$ $[T]$) which causes electromagnetic induction.

This work will not deeply analyze the magnetism problem and because of typical problems faced with accepts a simple proportional relationship between the magnetizing field and the magnetic flux density, than the magnetic permeability can be considered as:

$$\mu = \frac{\mathbf{B}}{\mathbf{H}} \tag{2.30}$$

and considering the magnetic permeability of the vacuum 2.6 it is possible to define the dimensionless relative magnetic permeability (μ_r $[-]$) as:

$$\mu_r = \frac{\mu}{\mu_0} = \frac{\mathbf{B}}{\mu_0 \mathbf{H}} \tag{2.31}$$

In the microscopic formulation of electromagnetism there is not the definition of a magnetizing field.
The vacuum permeability μ_0 directly relates total electric currents and time-varying electric fields to the magnetic flux density field they generate. In order to represent the magnetic response of a linear material with permeability μ, this instead appears as a magnetization $\mathbf{M}$ that arises in response to the $\mathbf{B}$ field:

$$\mathbf{M} = \left(\frac{1}{\mu_0} - \frac{1}{\mu}\right)\mathbf{B} = \left(\frac{\mu - \mu_0}{\mu\mu_0}\right)\mathbf{B} \tag{2.32}$$

Magnetic permeability is a property of materials in which time-varying magnetic field has a certain distribution in space. Radio-frequency heating and Microwave heating processes

are characterized by non-conductive and dia-magnetic materials, such as, water, wood, biological materials and fibers. Induction heating processes instead use conductive materials that may present para-magnetic behaviours such as steels or dia-magnetic materials such as copper, graphite and silver. A synthetic list of main materials and their relative permeability is presented in table 2.1. For

Relative magnetic permeability (constant)		
Material	Dia-magnetic	Para-magnetic
Water	0.999992	-
Copper	0.999994	-
Vacuum	1	-
Aluminium	-	1.000022
Steel AISI 312	-	1.001
Steel AISI 304	-	1.004
Steel AISI 403	-	< 900
Ferrite (3C90)	-	2100
Cotton fiber	~ 1	-
Wood	~ 1	-
Food (general)	~ 1	-

Table 2.1: Relative magnetic permeability (constant) for some typical dia-magnetic and para-magnetic materials used in EPM. Values measured at frequencies lower than 1 $[MHz]$ and magnetic fields lower than 1000 $[\frac{A}{m}]$. [35] [76] [75]

For many real life cases relative permeability varies with magnetic field amplitude as shown in figure 2.8.

$$\mu_r = f\left(\|\mathbf{H}\|\right) \tag{2.33}$$

When a non-linear behaviour of the magnetic permeability is considered, many times it is possible to define a mathematical model that helps to model saturation behaviour, for example for steels or ferrites that are commonly used in induction heating devices and processes as work-piece to be heated or as flux concentrators. A simple but extremely efficient model to take into account analytically magnetic non linearities is proposed in equation 2.34 and its main parameters are itemized in table 2.2.

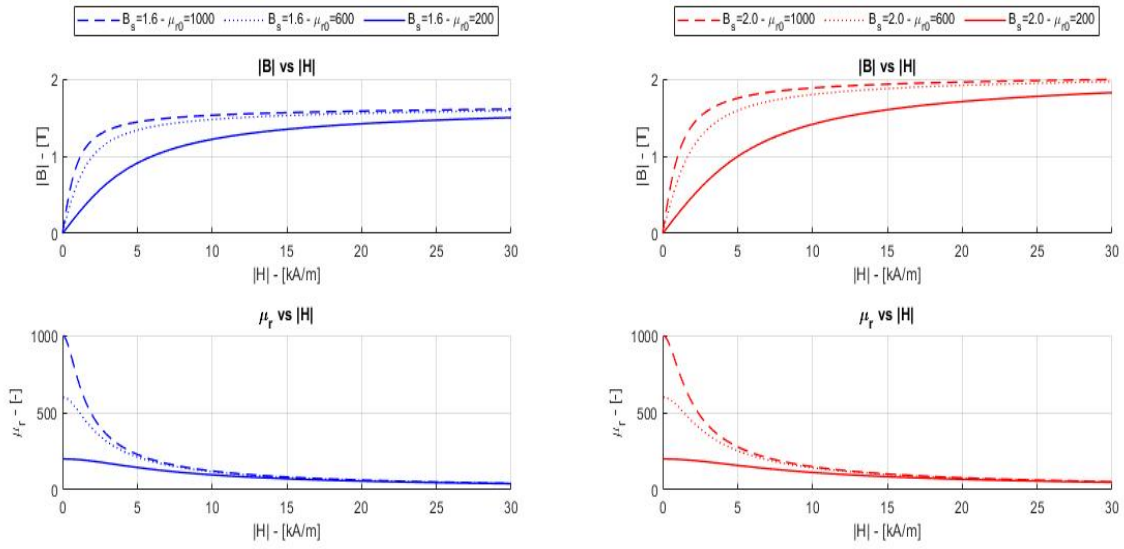

(a) **(b)**

Figure 2.6: Magnetic flux density ($|\mathbf{B}|$) and relative magnetic permeability (μ_r) as function of magnetic field ($|\mathbf{H}|$). (a) is a behaviour with a $B_s = 1.6$ $[T]$; (b) is a behaviour with a $B_s = 2.0$ $[T]$. The curves are obtained with a standard knee correction ($\alpha = 1$).

$$\|\mathbf{B}\| = \mu_0 \|\mathbf{H}\| + \frac{2B_s}{\pi} \tan^{-1}\left(\frac{\pi\left(\mu_{r0}-1\right)\mu_0\|\mathbf{H}\|}{2B_s}\right)^{\alpha} \tag{2.34}$$

Parameter	Symbol	Unit
Flux density Saturation	B_s	[T]
Initial relative permeability	μ_{r0}	[-]
Knee correction	α	[–]

Table 2.2: Saturation behaviour of magnetic field. Parameters for the analytical model presented in equation 2.34.

Equation 2.34 may be used to approximate a certain curve material with its closest analytical tangent-function, that for example minimize the residual between analytical function and measured data. In Figure 2.7 the red line curve is obtained with a simplex minimum search method. If a material is characterized by a *BH-Curve* is characterized by n samples of magnetic flux density (y_i $[T]$) for a certain limited magnetization field range ($x_n - x_1$ $[\frac{A}{m}]$) , it is possible to find the approximate function f that has the same form as in equation 2.34.

$$S = \sum_{i}^{n} \left(y_i - f\left(x_i\right)\right)^2 \tag{2.35}$$

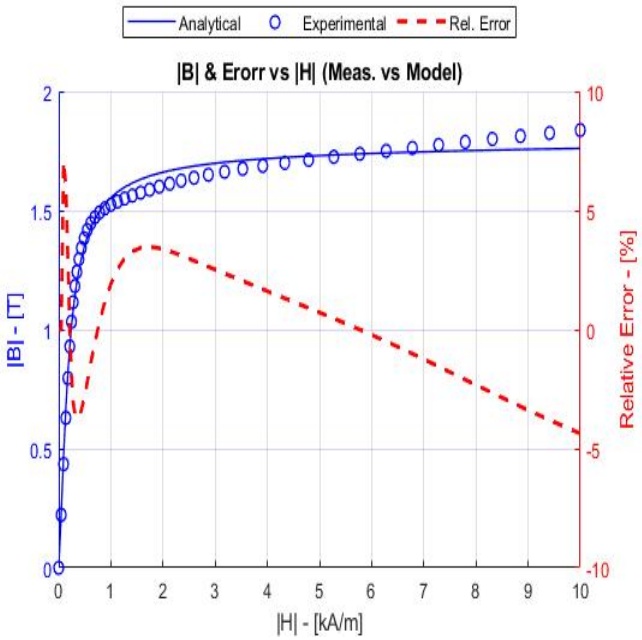

Figure 2.7: Ferrite 3C90 [36] measured BH Curve behaviour and Analytical behaviour 2.34 of magnetic saturation that minimize root mean square residual (RMR).

where

$$f = f\left(B_s, \mu_r 0, \alpha\right) \tag{2.36}$$

The problem consequently becomes to find B_s^*, μ_r^* and α^* that minimize the sum of square residuals. For that purpose it was used of Lagarias method, that is a direct search method that does not use numerical or analytic gradients [50].

$$\min S \Rightarrow \left(B_s^*, \mu_r^*, \alpha^*\right) \tag{2.37}$$

Some materials, for example Mn-Zn ferrites vary their permeability if the frequency varies as shown in figure 2.9.

$$\mu_r = f\left(\omega\right) = f\left(2\pi f\right) \tag{2.38}$$

When a non linear correlation between frequency and magnetic field exists, typically the permeability is modeled with its complex form, than μ is a complex operator:

$$\mu = \mu_0 \left(\mu_r^{'} - i\mu_r^{''}\right) \tag{2.39}$$

If a complex permeability is considered it is useful to understand the meaning of the argument of the complex permeability. While at low frequencies in a simple linear material (typically also at low field for conductive materials) the magnetic field (**H**) and the magnetic flux field

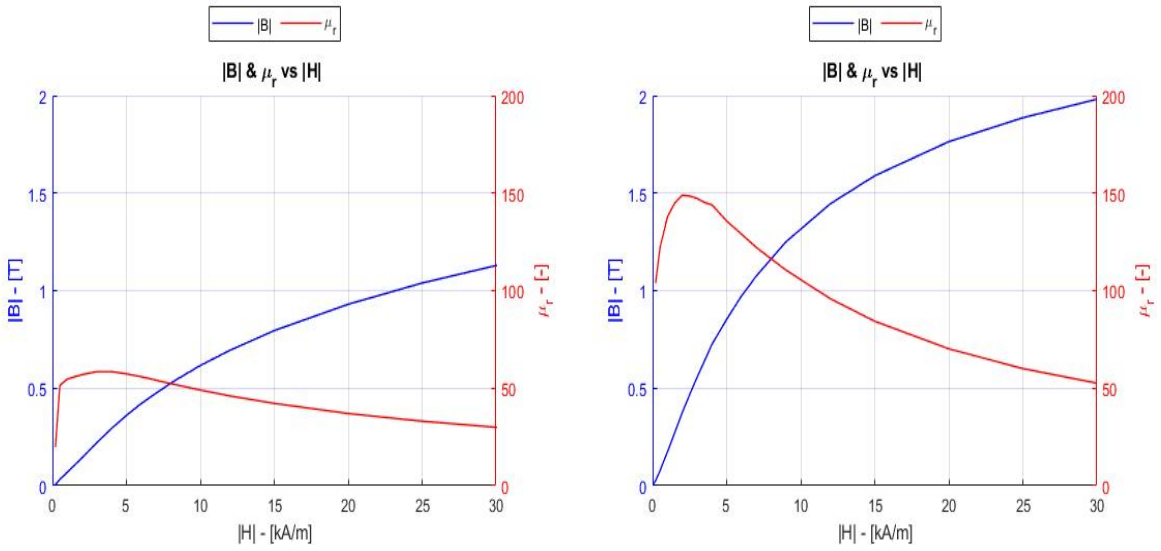

Figure 2.8: Magnetic flux density ($|\mathbf{B}|$) and Relative magnetic permeability (μ_r) as function of magnetic field ($|\mathbf{H}|$). (a) is the material Fluxtrol 50 ; (b) is the material Fluxtrol 100. [38] [37]

($\mathbf{B}$ are proportional to each other through the scalar permeability, at high frequencies these quantities will react to each other with some lag time. These fields can be written as phasors with a certain time-lag (δ $[s]$), such that:

$$\mu = \frac{\mathbf{B}}{\mathbf{H}} = \frac{\mathbf{B}_0}{\mathbf{H}_0} \cdot e^{-i\delta} \tag{2.40}$$

At the end the complex relative permeability by Euler's formula can be written as:

$$\mu_r = \frac{\mathbf{B}_0}{\mathbf{H}_0 \mu_0} \big(cos(\delta) - isin(\delta)\big) = \mu_r^{'} - i\mu_r^{''} \tag{2.41}$$

where

$$\delta = \tan^{-1}\left(\frac{\mu_r^{''}}{\mu_r^{'}}\right) \tag{2.42}$$

The ratio of the imaginary to the real part of the complex permeability is called the loss tangent $\tan(\delta)$ that provides a measure of how much power is lost in material compared to how much is stored in material. For that reason in the last years, especially for induction heating problems at high frequencies, ($f > 1$ $[MHz]$) modeling the permeability with its form is becoming extremely efficient and also affordable. The main problem remains the leakage of complex permeability at high frequencies

2.4.2 Dielectric Permittivity

The dielectric permittivity(ϵ $[F/m]$) is a measure of the electric polarizability of

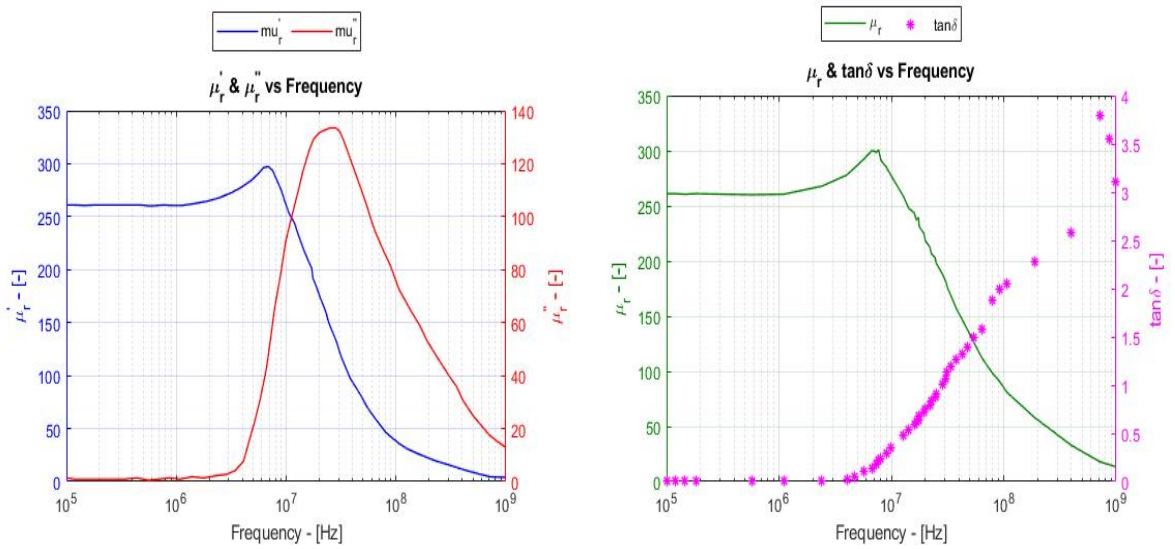

(a) **(b)**

Figure 2.9: Complex relative permeability as function of the frequency for Mn-Zn ferrite. (a) Real part ($\mu_r^{'}$) and imaginary part ($\mu_r^{'}$) of relative magnetic permeability as function of frequency (f) ; (b) Modulus ($\sqrt{\mu_r^{'2} + \mu_r^{''2}}$) and loss tangent ($\tan \frac{\mu_r^{''}}{\mu_r^{'}}$) of relative magnetic permeability as function of frequency (f). [69]

dielectrics and it will be analyzed deeply in Chapter 2. Higher is the permittivity more the material polarizes in response to an external electric field $\mathbf{E}$ and consequently more energy is stored in the material. In the simplest case, the electric displacement field $\mathbf{D}$ resulting from an applied electric field ($\mathbf{E}$) is

$$\mathbf{D} = \epsilon \mathbf{E} = \epsilon_r \epsilon_0 \mathbf{E} \tag{2.43}$$

More generally, the permittivity is a thermodynamic function of state [51]. It can depend on properties of electric field, such as: the frequency, magnitude, and direction The relative permittivity ϵ_r is the ratio of the absolute permittivity ϵ and the vacuum permittivity ϵ_0 and is directly related to the electric susceptibility:

$$\chi = \epsilon_r - 1 = \frac{\epsilon}{\epsilon 0} - 1 \tag{2.44}$$

The electric displacement field represents the distribution of electric charges in a given medium resulting from the presence of an electric field. This distribution includes charge migration and electric dipole reorientation. Generally a material cannot polarize instantaneously in response to an applied field, and so it is useful to define a more general formulation for the polarization field ($textbf{P}$) as function of time, and after Fourier transformation it can be expressed as function of frequency:

$$\mathbf{P}(\omega) = \epsilon_0 \chi(\omega) \mathbf{E}(\omega) = \epsilon_0 [1 - \epsilon_r(\omega)] \mathbf{E}(\omega) \tag{2.45}$$

At the high-frequency limit, the complex permittivity is commonly constant and limited (ϵ_∞ $[-]$). At lower frequencies instead dielectrics behave as conductors, and the permittivity can be approximated with the static permittivity (ϵ_s $[-]$):

$$\lim_{\omega \to \infty} \epsilon = \epsilon_\infty \tag{2.46}$$

$$\lim_{\omega \to 0} \epsilon = \epsilon_s \tag{2.47}$$

For intermediate frequencies instead, because of in frequency domain electric and displacement fields can be expressed by phasors, than the permittivity must bu a complex operator and that implies as the frequency increases a measurable phase difference (δ $[deg]$) emerges between $\mathbf{D}$ and $\mathbf{E}$:

$$D_0 e^{-i\omega t} = \epsilon(\omega) \cdot E_0 e^{-i\omega t + \delta} \tag{2.48}$$

and finally it possible to rewrite the permittivity as a complex operator:

$$\epsilon(\omega) = \frac{D_0}{E_0} e^{-i\delta} = |\epsilon| e^{-i\delta} = \epsilon^{'}(\omega) - i\epsilon^{''}(\omega) = |\epsilon| (\cos\delta - i \sin\delta) \tag{2.49}$$

where $\epsilon^{'}$ represents the real part of complex permittivity, $\epsilon^{''}$ represents the imaginary part of complex permittivity and $\tan\delta$ is the loss factor as defined in the next equation:

$$\tan\delta = \frac{\epsilon^{''}}{\epsilon^{'}} \tag{2.50}$$

Materials can be classified in first analysis according to their complex permittivity ($\epsilon(\omega)$ $[F/m]$), comparing of its real $\epsilon^{'}$ and imaginary $\epsilon^{''}$ parts. An ideal conductor has infinite conductivity,

$$\sigma_c = \infty \tag{2.51}$$

while a perfect dielectric is a material that has no conductivity at all adn for that case is a lossless media:

$$\sigma_d = 0 \tag{2.52}$$

Generally, if a simple lossy material is considered, it is possible to describe the total current density as the sum of conduction currents and displacement current, and taking advantage of Ampere's Law 2.4:

$$\nabla \times \mathbf{H} = \mathbf{J}_t = \sigma \mathbf{E} + \frac{\partial \mathbf{D}}{\partial t} = \mathbf{J}_c + \mathbf{J}_d \tag{2.53}$$

And considering the full complex form of the permittivity as proportional coefficient for the displacement field:

$$\mathbf{J}_t = \left[\sigma + i\omega\epsilon_0 \left(\epsilon_r^{'} - i\epsilon_r^{''}\right)\right] \mathbf{E} = i\omega\epsilon_0 \left[\left(\epsilon_r^{'} - i\epsilon_r^{''}\right) - i\frac{\sigma}{\omega\epsilon_0}\right] \mathbf{E} \tag{2.54}$$

Equation 2.54 can be modified again to highlights displacement dielectric effects and conductive effects:

$$\mathbf{J}_t = i\omega\epsilon_0\epsilon_r^{'}\mathbf{E}\left[1 - i\left(\frac{\sigma}{\omega\epsilon_0\epsilon_r^{'}} + \frac{\epsilon_r^{''}}{\epsilon_r^{''}}\right)\right] \tag{2.55}$$

And again, as we did for equation 2.50 it is possible to define another loss factor that takes into account the conduction of free charges and the displacement of charges:

$$\tan\gamma = \frac{\sigma}{\omega\epsilon_0\epsilon_r^{'}} + \tan\delta \tag{2.56}$$

And finally obtain the final law in a dielectric medium for the current density, that is also represented in the figure 2.10:

$$\mathbf{J}_t = i\omega\epsilon_0\epsilon_r^{'}\mathbf{E}\left[1 - i\left(\tan\gamma\right)\right] \tag{2.57}$$

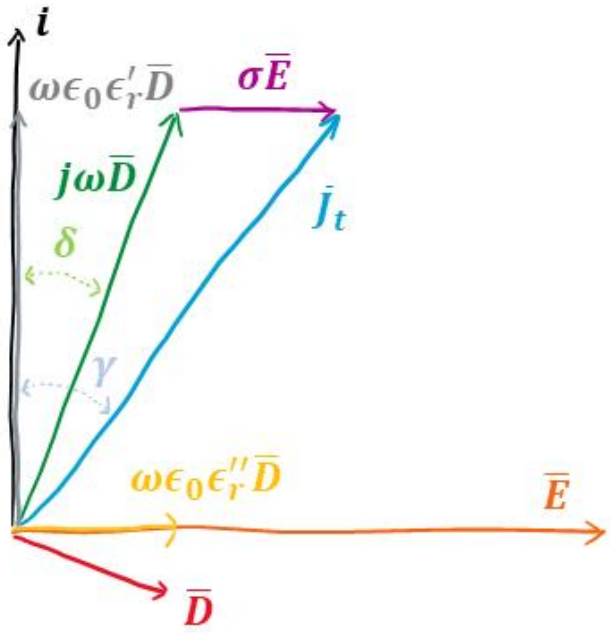

Figure 2.10: Phasor diagram of a dielectric material subjected to an alternative electric field.

A dielectric lossy material is characterized by $\tan\delta > 0$ and that, as the name suggests, causes losses inside its volume because, if an electric field $\mathbf{E}$ is applied to it:

$$s = \mathfrak{Re}(s) + i\mathfrak{Im}(s) = \mathbf{E}\cdot\mathbf{J}_t^* = \omega\epsilon_0\epsilon_r^{'}|\mathbf{E}|^2\left(\tan\gamma - i\right) \tag{2.58}$$

and therefore the active power is the real part of the complex power. The imaginary part of a dielectric material together with its conductivity expresses the total power losses density (w_h $[W/m^3]$ of it:

$$w_h = \omega\epsilon_0\epsilon_r^{'}|\mathbf{E}|^2\tan\gamma \tag{2.59}$$

A synthetic list of some relevant materials used in EPM and their relative permittivity is presented in list 2.3.

Relative permittivity (constant @20[$degC$])		
Material	$\epsilon_r^{'}$	$\tan\delta$
Vacuum	1	0
Water (distilled)	77	0.157
ABS	2.75 (2-3.5)	0.012 (0.00500-0.0190)
PTFE (Teflon)	2.1	0.00015
Pyrex (Glass)	4.7 (3.7-10)	0.0054
PE (Polyethylene)	2.25	0.00031
Mica	4.5 (3-6)	0.0003
PP (Polypropylene)	2.3 (2.2-2.36)	0.00033
Neoprene Rubber	4	0.034
Balsa Wood	1.22	0.1
BeO (Beryllium Oxide)	6.7	0.006
Ice (distilled)	3.2	0.0009
PEEK (Polyether-ether-ketone)	3.35	0.003
GaAs (Gallium Arsenide)	13.1	0.0016

Table 2.3: Relative dielectric permittivty (constant) for some typical materials used in EPM. Values measured at a frequency of 1 [GHz]. The table shows the relative permittivity and the loss factor.[47] [66] [25]

Figure 2.11 shows that different material responds differently at the same electric field. For example water is characterized by high dissipation factor (high dissipated energy density) and high relative permittivity (high stored energy) and for that reason is a goof material for RF and MW heating. Teflon conversely is characterized by low dissipation factor (low dissipated energy density) and low relative permittivity (low stored energy) and for that reason is a good insulator in RF and MW heating devices.

2.4.3 Electrical Conductivity

Volume resistivity (ρ [Ωm]) measures how strongly a material resists electric current. An ideal insulator is characterized by an infinite electrical resistivity, instead an ideal conductor by a electrical resistivity equal to zero.

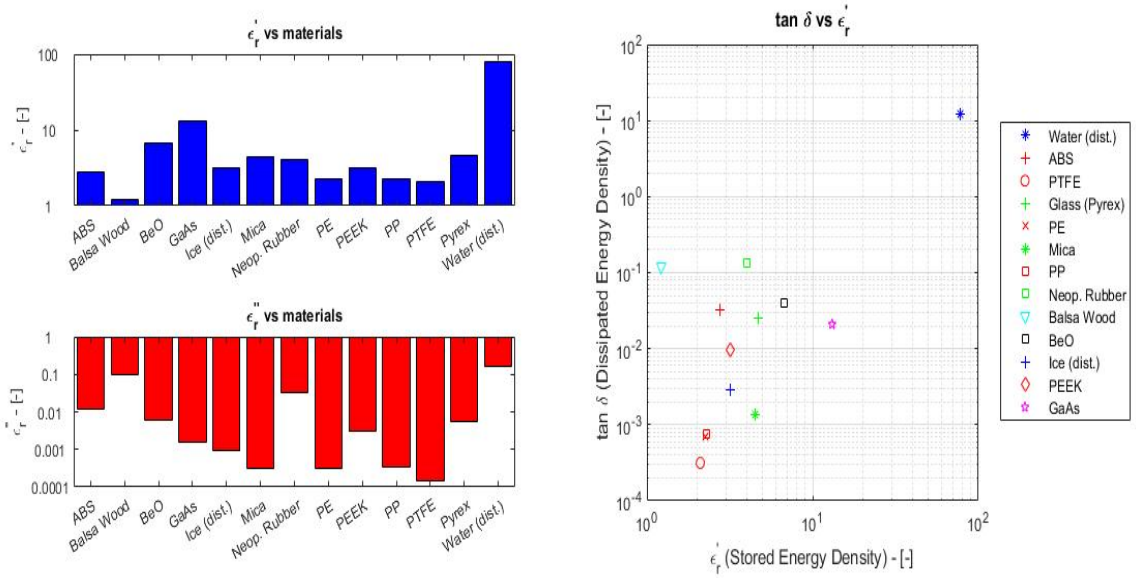

(a) **(b)**

Figure 2.11: Dielectric permittivity comparison of several materials 2.3 . (a) shows real part and imaginary part of dielectric permittivity. (b) shows relative permittivity and loss factor, or in other words, stored energy and dissipated energy if an electric field is applied ($|\mathbf{E}| = 1[V/m]$).

Electrical conductivity (σ $[\frac{S}{m}]$) is the reciprocal of electrical resistivity and it represents a material's ability to conduct electric current

$$\sigma = \frac{1}{\rho} \tag{2.60}$$

If an idealized piece of conductive material is considered (cross-section (Σ $[m^2]$) and physical composition of the examined material are uniform across the sample ($\rho = \rho^* = const$), and the electric field ($\mathbf{E}$) and current density ($\mathbf{J}$) are both parallel and constant everywhere the work-piece) it is easy to get a simple relation between the so called Electrical Resistance and conductivity of the piece:

$$\sigma = \frac{1}{R}\frac{l}{\Sigma} \tag{2.61}$$

where l is the length of the piece.

It is possible to generalize for less ideal cases: when the geometry is not constant or when the current density field and the electric field vary in different parts of the material:

$$\mathbf{J} = \sigma\mathbf{E} \tag{2.62}$$

Electric current is the ordered movement of electric charges. These charges are called current carriers. In metals and semiconductors, electrons are the current carriers; in electrolytes

Electrical conductivity(constant @20[$degC$])	
Material	σ [ωm]
Silver	$1.59 \cdot 10^{-8}$
Copper	$1.68 \cdot 10^{-8}$
Aluminum	$2.65 \cdot 10^{-8}$
Iron	$9.70 \cdot 10^{-8}$
Carbon steel	$1.43 \cdot 10^{-7}$
Titanium	$4.20 \cdot 10^{-7}$
Stainless steel	$6.90 \cdot 10^{-7}$
Graphite	$4.00 \cdot 10^{-6}$
GaAs (Gallium Arsenide)	$1.00 \cdot 10^{-3}$
Water (dist)	$1.80 \cdot 10^{+5}$
Glass (Pyrex)	$1.00 \cdot 10^{+11}$
Air (dry)	$1.00 \cdot 10^{+15}$
Wood (dry)	$1.00 \cdot 10^{+16}$
PET	$1.00 \cdot 10^{+21}$
PTFE (Teflon)	$1.00 \cdot 10^{+24}$

Table 2.4: Electrical resistivity (constant) for some typical materials used in EPM. Values measured at a frequency of 0 [Hz] and environment temperature. [73] [58] [18]

and ionized gases, positive and negative ions. In the general case, the current density of one carrier is determined by the average speed ($< \mathbf{v} >$ [m/s]) of a certain charge density (nq [C/m^3])

$$\mathbf{j} = qn < \mathbf{v} > \tag{2.63}$$

The band theory offers a good theoretical model to fully understand the conduction phenomenon [42]. According to elementary quantum mechanics, electrons can possess only certain discrete energy values, values between those quantized values are not permitted. Because of the number of atoms in a solid is a very large number, the number of orbitals is very large and thus they are very closely spaced in energy so the energy of the adjacent levels is so close together that they can be considered as a continuum, an energy band. A metal consists of a lattice of atoms, each with an outer cloud of electrons that can travel through the lattice. Metals can conduct electric currents: when an electrical potential difference ($\delta\Psi$ [V]) is applied across the metal structure, the resulting electric field ($\mathbf{E}$ [V/m] causes electrons to drift with

a low velocity. However, because of the number of electrons is very high it results in a large current density ($\mathbf{j}$ $[C/s]$).

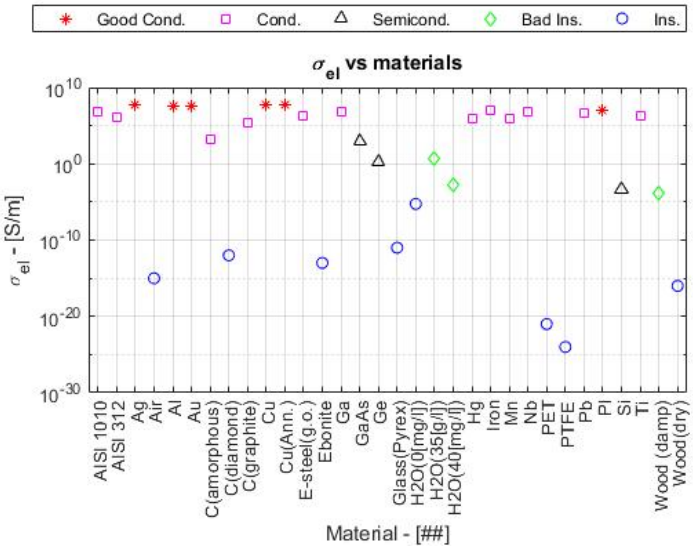

Figure 2.12: Electrical conductivity comparison of several materials. 2.4

Most metals have electrical resistance. In simple, non quantum mechanical models, electrical resistance can be explained by replacing electrons and the crystal lattice by a wave-like structure. When the electron wave travels through the lattice, the waves interfere, which causes resistance. The regularity of the crystal lattice is related to the resistance. The resistance is thus mainly caused by two factors:

1. by the temperature and thus amount of vibration of the crystal lattice. Higher temperatures cause bigger vibrations, which act as irregularities in the lattice.

2. by the purity of the metal is relevant as a mixture of different ions is also an irregularity.

In general, electrical resistivity of metals increases with temperature. Electron–phonon interactions can play a key role. At high temperatures, the resistance of a metal increases linearly with temperature. As the temperature of a metal is reduced, the temperature dependence of resistivity follows a power law function of temperature. Mathematically the temperature dependence of the resistivity (ρ) of a metal can be approximated through the Bloch–Grüneisen formula for transition metals [28]:

$$\rho\left(T\right)=\rho\left(0\right)+\gamma\left(\frac{T}{\theta_R}\right)^3\int_0^{\frac{\theta_R}{T}}\frac{x^3}{\left(e^x-1\right)\left(1-e^{-x}\right)}dx \tag{2.64}$$

The electrical resistivity of most materials changes with temperature. If the temperature (T $[K]$) does not vary too much, a linear approximation is typically used:

$$\rho(T) = \rho_0 [1 + \alpha (T - T_0)] \tag{2.65}$$

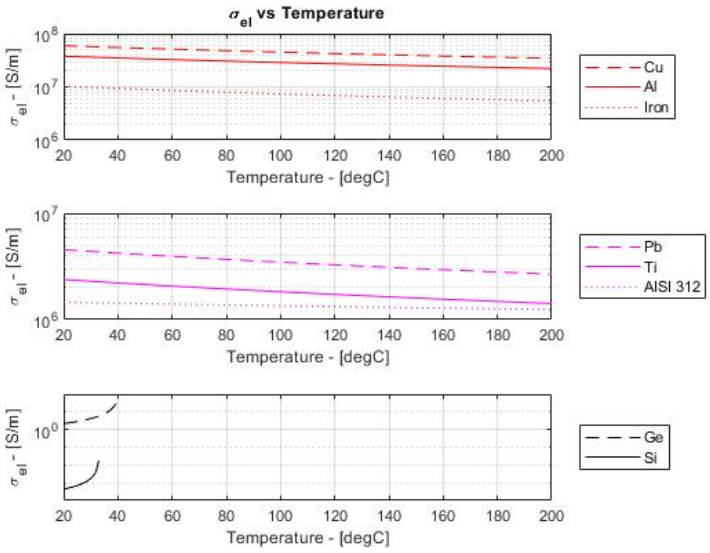

Figure 2.13: Electrical conductivity (σ_{el} $[S/m]$) as function of temperature (T $[degC]$) as in equation 2.65. Red lines are good conductors used as electrodes or inductors, magenta lines are typically induction heated conductors, black lines are semiconductors.

In metals, the Fermi level lies in the conduction band giving rise to free conduction electrons. However, in semiconductors the position of the Fermi level is within the band gap, about halfway between the conduction band minimum and the valence band maximum. In electric insulators electric current does not flow freely because its atoms have tightly bound electrons which cannot readily move. Most insulators have a large band gap. This occurs because the valence band containing the highest energy electrons is full, and a large energy gap separates two consecutive bands. There is always some voltage (called the breakdown voltage) that gives electrons enough energy to be excited into this band. Once this voltage is exceeded the material ceases being an insulator, and charge begins to pass through it.

Chapter 3

Thermal problem

3.1 Transfer of energy

In EPM processes another important phenomenon is the transfer of internal energy. Heat transfer, in engineering, concerns the generation, use, conversion, and exchange of heat between physical systems. Heat transfer is mainly classified into four mechanisms:

- conduction
- convection
- radiation
- phase change
- advection

In EPM thy often occur simultaneously in the same system: for example, in a drying process of porous media at least four of the above mechanisms are extremely relevant.

3.1.1 Heat conduction

Heat conduction, also called diffusion, is the direct microscopic exchange of kinetic energy of particles and lattice waves. In physics it is well know that heat spontaneously flows from a hotter to a colder body: When a first body is at a different temperature (T_1 $[K]$) from

second body (T_2 $[K]$) or its surrounding environment (T_{env} $[K]$), heat naturally flows so that the body and the surroundings reach a certain thermal-equilibrium temperature (T_{eq} $[K]$).

$$T_1^{'} = T_2^{'} = T_{env} \tag{3.1}$$

The second law of thermodynamics establishes the concept of entropy (S $[J/K]$). Entropy variation defines the direction of spontaneous processes, and determines if they are irreversible or impossible. The second law defines that the entropy of isolated systems cannot decrease because they converges to a state of thermodynamic equilibrium.

$$dS = \frac{\delta Q_{rev}}{T} \geq \frac{\delta Q}{T} \tag{3.2}$$

In conduction, the heat flow is within and through the body itself, that means that is directly

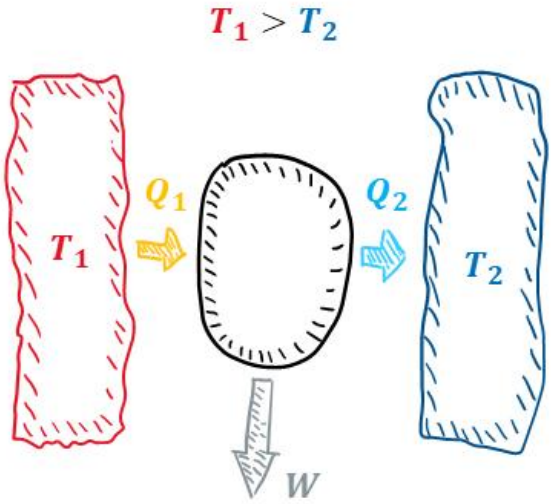

Figure 3.1: The second law of thermodynamics. The classical Carnot heat engine.

the medium that transports energy. On a microscopic scale, the internal energy diffuses due the interaction between atoms, molecules and adjacent particles. The kinetic and potential energies are transferred directly between particles. The mechanism of energy transfer can be distinguished according to the type of material and the mechanism as in table 3.1.

Fourier's Law

The law of heat conduction, also known as Fourier's law, states that heat flux ($\mathbf{q}$ $[W/m^2]$) is proportional to the temperature gradient in the space and to the thermal conduc-

Energy transfer (conduction)	
Material	Mechanism
Fluids	Elastic impact
Conductors	Free elecron diffusion
Insulators	Phonon vibration

Table 3.1: Energy transfer mechanism and material type

tivity (λ $[W/(m*K)]$), as written in equation 3.3:

$$\mathbf{q} = -\lambda \nabla T \tag{3.3}$$

Heat conduction equation ca be more generalized: the heat equation. It is a partial differential equation which solution is the so called caloric function. In 1822 Joseph Fourier modeled heat flux through a given region (Ω).

If a general point in the 3D-plane $\mathbf{P} = (x, y, z, t)$ is considered, it is clear that its function of 3 spatial variables ($\mathbf{s} = (x, y, z)$) and of the time (t). In that case it is possible in mathematics to define the so called Laplacian of a certain function (u):

$$\frac{\partial u}{\partial t} = \alpha \nabla^2 u = \alpha \left(\frac{\partial^2 u}{\partial x^2} + \frac{\partial^2 u}{\partial y^2} + \frac{\partial^2 u}{\partial z^2} \right) \tag{3.4}$$

It is clear that equation 3.3 is a particular form of eqaution 3.4, therefore:

$$\mathbf{q}\,(\mathbf{s}, t) = -\lambda \nabla T\,(\mathbf{s}, t) \tag{3.5}$$

and if we consider that internal heat energy ($Q\,(\mathbf{s}, t)$ $[W/m^3]$) is the expression of energy, than the time derivative of internal heat energy is proportional to the rate of temperature change of the material and the material properties:

$$\frac{\partial Q}{\partial t} = C_p \rho \frac{\partial T}{\partial t} \tag{3.6}$$

where C_p $[J/(kg*K)]$ is the specific heat capacity of a material at constant pressure and ρ $[kg/m^3]$ is the density. Considering a small domain as in figure 3.2 it is possible to apply the law of conservation of energy and it is possible to consider, more generally, an energy generation, or heat source (w $[W/m^3]$) in the domain:

$$\frac{\partial Q}{\partial t} = -\left(\frac{\partial \mathbf{q}}{\partial x} + \frac{\partial \mathbf{q}}{\partial y} + \frac{\partial \mathbf{q}}{\partial z} + \right) = w \tag{3.7}$$

$$\frac{\partial Q}{\partial t} = -\nabla \mathbf{q} = -\frac{1}{C_p \rho} \nabla \cdot (-\lambda \nabla T) = w \tag{3.8}$$

and finally obtain the final form of Fourier equation:

$$\rho C_p \frac{\partial T}{\partial t} - \nabla \cdot \nabla T - w = 0 \tag{3.9}$$

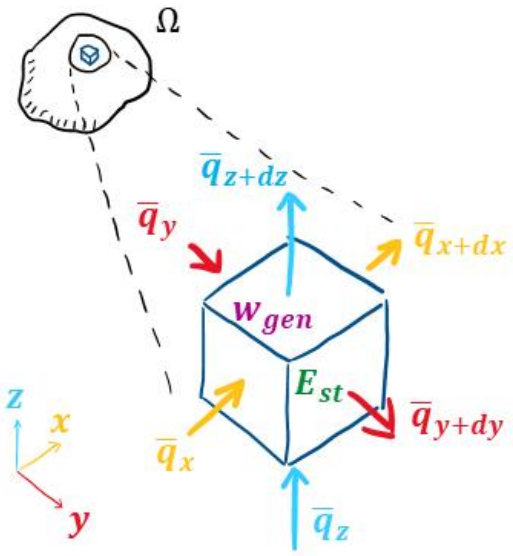

Figure 3.2: Fourier's law of heat conduction. Infinitesimal volume dx,dy,dz. In figure asre shown: the heat fluxes (**w** $[W/m^2]$) for the three tensors of the space. The energy generation term (w_g $[W/m^3]$) and the stored energy term (E_{st} $[W]$).

3.1.2 Heat convection

Convection is more generally the transfers of energy due to the bulk flow of a fluid, in liquid or gas phase and the heat diffusion. The former is called conduction, the latter advection. All convective processes also move heat partly by diffusion, as well. The flow of fluid may be forced by external processes, or sometimes by buoyancy forces caused by local variation of fluid density. For that specific case we can distinguish two main kinds of convection: natural and forced convection. In RF and MW process typically the body that we want to heat and (or) dry is placed in an environment in which air is typically in contact with the body surfaces. Natural convection is caused by buoyancy forces due to density differences caused by temperature variations in the fluid. At heating the density change in the boundary layer will cause the fluid to rise and be replaced by cooler fluid that also will heat and rise. This continues phenomena is called free or natural convection. Forced convection occurs when a fluid flow is induced by an external force, such as a pump, fan or a mixer. That is typical in hot air drying applications where air is forced on a material sample (for example wood, leather, textile fibers, etc.) because of air is the vector of the transport of energy and of the humidity

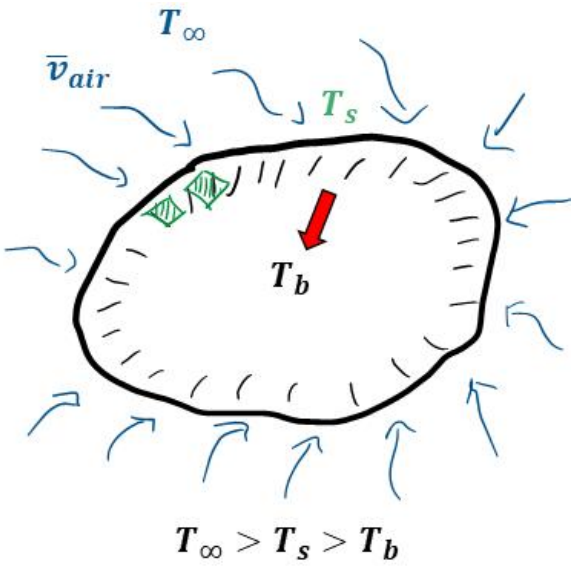

Figure 3.3: Convective Heat Transfer mechanism between a cold body and hot external fluid.

(water vapor). Boiling or condensing processes are also referred to as a convective heat transfer processes. The heat transfer per unit surface through convection was first described by Newton and the relation is known as the Newton's Law of Cooling. The equation for convection can be easily expressed as:

$$\mathbf{Q}_{conv} = \alpha_c \lambda T \tag{3.10}$$

Newton's law is a particular solution of the heat transfer problem. It makes possible to obtain a global relationship between energy exchange from an external fluid environment (in motion of fixed) and a fixed body. In table 3.3 are presented several value for the heat convection coefficient (α_c $[W/(m^2 * K)]$). Using equation 3.10 it is possible to get a synthetic solution for

Convective Heat Transfer Coefficients			
Type of convection	Fluid	$\min \alpha_c$ $[W/(m^2 * K)]$	$\max \alpha_c$ $[W/(m^2 * K)]$
Free	Air, Dry vapors	$5\dot{1}0^{-1}$	10^3
Free	Water	$5 \cdot 10^1$	$3 \cdot 10^3$
Forced	Water	10^1	10^3
Forced	Water	$5 \cdot 10^1$	10^4
Boiling	Water	$3 \cdot 10^3$	10^5
Condensating	Water and Vapor	$5 \cdot 10^3$	10^5

Table 3.2: Convective Heat Transfer Coefficients for several fluids and type of convection mechanism

a general body affected by convective heat transfer. The global power exchanged between the

external fluid, that has a certain temperature (T_∞ $[degC]$) and the body that has a certain average surface temperature (T_s $[degC]$) is proportional to the heat convection coefficient (α_c $[W/(m^2 * K)]$). If the surface of the body is well known (S $[m^2]$) the global power (P_{conv} $[W]$) is then:

$$P_{conv} = \alpha_c S \left(T_s - T_\infty\right) \tag{3.11}$$

In literature exist a good approximation for the convective heat transfer coefficient for air flow is:

$$\alpha_c = 12.12 - 1.16v + 11.6\sqrt{v} \tag{3.12}$$

Figure 3.4 represents a good approximation for the convection heat transfer coefficient of air as shown in equation 3.12. That equation is a good approximation in the range between $0[m/s]$ and $20[m/s]$. In chapter 5 equation 3.11 is used to estimate a global convective exchange

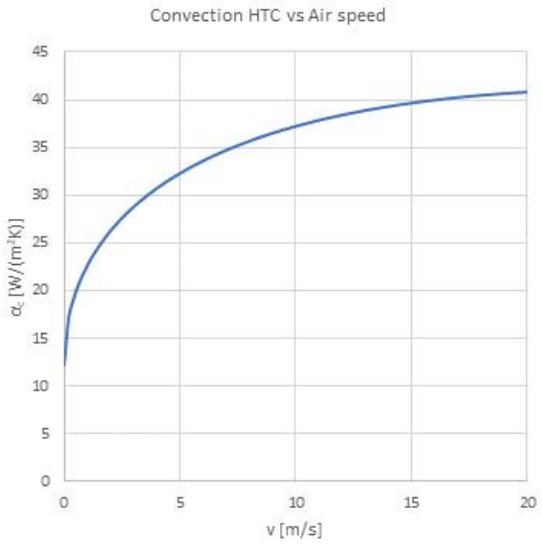

Figure 3.4: Convective Heat Transfer Coefficient (C-HTC) for air varying its speed (v).

coefficient ($\alpha_c^{'}$ $[W/K]$) between several systems:

$$\alpha_c^{'} = \frac{P_{conv}}{(T_s - T_\infty)} \tag{3.13}$$

To estimate global convective exchange coefficient it is necessary to have a good estimation of the average body temperature. In steady state condition it is easy to get a good estimation of convective coefficient, because of from equation 3.9 all transient therms go to zero (accumulated power in medium may be neglected) for thermal equilibrium condition. in figure 3.5 is presented a typical approach that may be used to estimate convection heat coefficient when hot air (or cold air) exchange energy with a system (that may be hotter or colder than air).

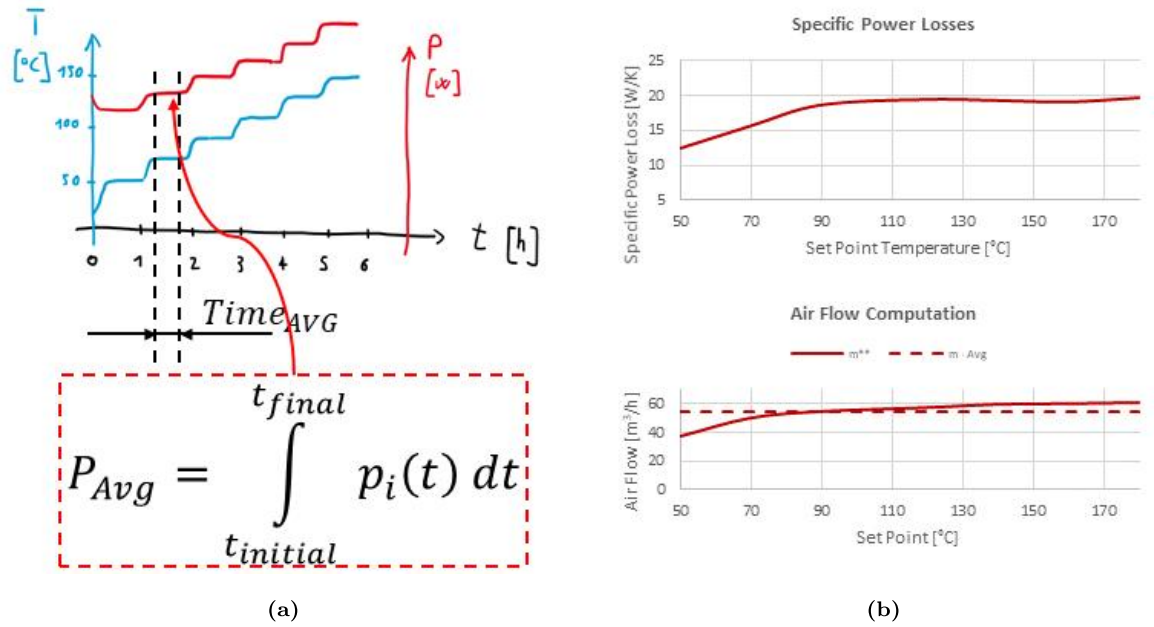

(a) (b)

Figure 3.5: Estimation of convection heat exchange process. (a) Algorithm for analysis; (b) Results of estimation of convection heat exchange coefficient and of air flow

3.1.3 Thermal radiation heat transfer

All heat transfer bodies constantly emit energy by a process of electromagnetic radiation. The intensity of such energy flux depends upon the temperature of the body and the nature of its surface. Most of the heat that reaches you when you sit in front of a fire is radiant energy. Objects that are cooler than the fire emit much less energy because the energy emission varies as the fourth power of absolute temperature. Usually, the radiant heat transfer, from cooler bodies to hotter bodies can be neglected in comparison with convection and conduction. But heat transfer processes that occur at high temperature, usually involve a significant fraction of radiation [33]. Thermal radiation occurs through a vacuum or any transparent medium (solid or fluid or gas). It is the transfer of energy by means of photons or electromagnetic waves governed by the same laws. The model for the perfect thermal radiator is a so all energy that reaches it and called black body. This is a body which absorbs reflects nothing. The term can be a little confusing, since such bodies emit energy. Thus, if we possessed infrared vision, a black body would glow with "color" appropriate to its temperature. of course, perfect all visible light (and all radiators are "black" in the sense that they absorb other radiation) that reaches them. Infrared radiation refers to a particular range of wavelengths, while heat refers to the whole range of radiant energy [10]. A fraction, (α), of the total incident energy (q_i $[W/m2]$), called the absorptance, is absorbed in the body; a fraction, called the reflectance (ρ), is reflected

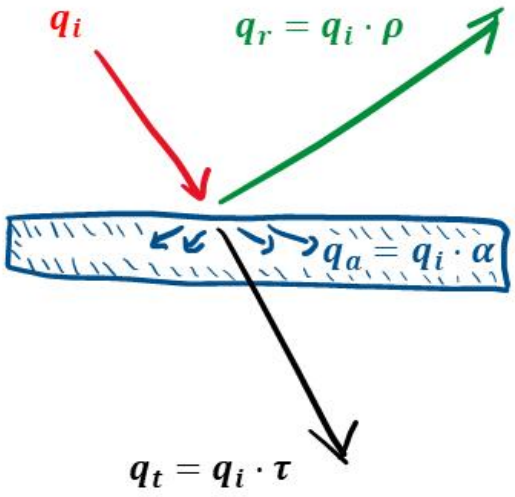

Figure 3.6: Distribution of energy on a traslucent slab. In figure are shown incident flux (q_i), reflected flux (q_r), transmitted flux (q_t) and absorbed flux (q_a) by the slab.

(q_r $[W/m2]$) from it; and a fraction, called the transmittance (τ), passes through (q_r $[W/m2]$). And then:

$$\alpha + \rho + \lambda = 1 \tag{3.14}$$

A black body is characterize, for definition that all radiant energy incident is absorbed, so that:

$$\alpha_{b-b} = 1 \Rightarrow \tau b - b = \rho_{b-b} = 0 \tag{3.15}$$

furthermore, the energy emitted from a black body reaches a theoretical maximum, which is given by the Stefan-Boltzmann law. The flux of energy radiating from a body ($e(\lambda, T)$ $[W/m^2]$) is for the Stefan-Boltzmann law:

$$e_\lambda(\lambda, T) = \frac{d}{d\lambda} e(\lambda, T) = \int_0^\lambda e(\lambda, T)\, d\lambda \tag{3.16}$$

where the distribution function of radiative flux in λ ($e_\lambda(\lambda, T)$ $[W/m^2]$), or the monochromatic emissive power, and then generalizing to a non limited spectrum:

$$e(\lambda, T) = \int_0^\infty e(\lambda, T)\, d\lambda \tag{3.17}$$

The dependence of the energy radiating from a body on with the temperature for a black body ($e_{b-b}(\lambda, T)$ $[W/m^2]$) was established experimentally by Stefan in 1879 and explained by Boltzmann on the basis of thermodynamics arguments in 1884. The Stefan-Boltzmann law relates temperature to the Stefan-Boltzmann constant ($\sigma = 5.6704 \cdot 10^{-8}$ $[W/(m^2K^4)]$):

$$e_{b-b} = \sigma T^4 \tag{3.18}$$

Radiant heat exchange

If we consider that a heated object 3.7 radiates to some other object and that both objects are thermally black. A portion of heat leaving object 1 arrives at object 2, and A portion of heat arriving at object 1 comes from object 2. Thus, the net heat transferred from object 1 to object 2, Q_{net}, is the difference between q_{12} and q_{21} and then:

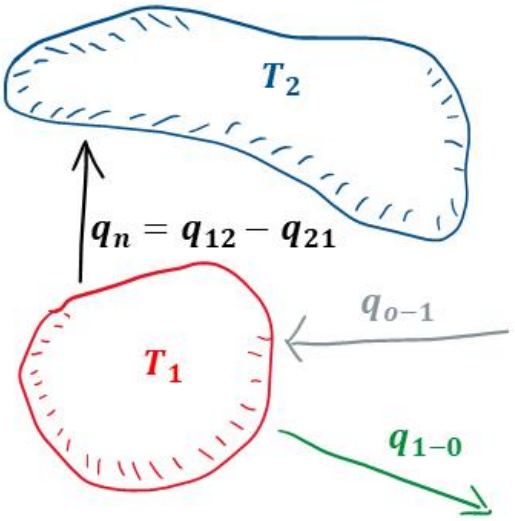

Figure 3.7: The net radiant heat transfer from one object to another and to the surroundings.

$$q_{net} = q_{12} - q_{21} = A_1 e_{b-b}(T_1) - A_1 e_{b-b}(T_2) = A_1 \sigma \left(T_1^2 - T_2^4\right) \tag{3.19}$$

Considering other surrounding objects that have a temperature not equal to object 1 and object 2 then a view factor (sometimes called a configuration factor or a shape factor) must be included (F_{12}):

$$q_{net} = A_1 F_{12} \sigma \left(T_1^4 - T_2^4\right) \tag{3.20}$$

A real body at a certain temperature (T $[K]$) does not emit with the black body emissive power equals to $e_{b-b} = \sigma T^4$ but rather with some fraction, ε, of e_{b-b}. The same is true of the monochromatic emissive power ($e_\lambda(T)$), which is always lower for a real body than the black body value given by Planck's law. Thus, we define either the monochromatic emittance as:

$$\varepsilon_\lambda = \frac{e_\lambda(T)}{e_{\lambda-b-b}(T)} \tag{3.21}$$

and finally the total emittance (ϵ) is:+

$$\varepsilon = \frac{e(T)}{e_{b-b}(T)} \tag{3.22}$$

For real bodies, both ε and ε_λ are greater than zero and less than one; for black bodies, $\varepsilon_{b-b} = 1$. The emittance is determined entirely by the properties of the surface of the particular body and its temperature. It is independent of the environment of the body. Table **??** lists typical values of the total emittance for a variety of substances. Notice that most metals have quite low emittances, unless they are oxidized. Most nonmetals have emittances that are quite high— approaching the black body limit of unity. Kirchhoff's law is a relationship between the

Emittance			
Material	Material type	Temperature range $[degC]$	emittance $[-]$
Aluminum (98% pure)	Metal	200-600	0.04-0.06
Aluminum (heavily oxidized)	Metal	90-540	0.30-0.33
Copper (polished)	Metal	90	0.02
Copper (heavily oxidized)	Metal	40	0.76
Gold (pure)	Metal	90-600	0.02-0.035
Steel (polished)	Metal	40-260	0.07-0.010
Steel (heavily oxidized)	Metal	40	0.80
Iron (cast)	Metal	40-260	0.57-0.66
Iron (wrought-oxidized)	Metal	20-360	0.94
Iron (stainless-polished)	Metal	40	0.07-0.17
Carbon (filament)	Non metal	1040-1430	0.53
Glass (Quartz)	Non metal	260-540	0.96-0.66
Glass (Pyrex)	Non metal	260-540	0.94-0.74
Ice	Non metal	0	0.97-0.98
Water	Non metal	20	0.96
Paper	Non metal	40	0.95-0.98

Table 3.3: Total emittances for a variety of surfaces (metals and non metals)

monochromatic, directional emittance and the monochromatic, directional absorptance for a surface that is in thermodynamic equilibrium with its surroundings. Kirchhoff's law states that a body in thermodynamic equilibrium emits as much energy as it absorbs in each direction and at each wavelength. If this were not so, for example, a body might absorb more energy than it emits in one direction, θ_1, and might also emit more than it absorbs in another direction, θ_2. The body would thus pump heat out of its surroundings from the first direction, θ_1, and into its surroundings in the second direction, θ_2. Since whatever matter lies in the first direction would

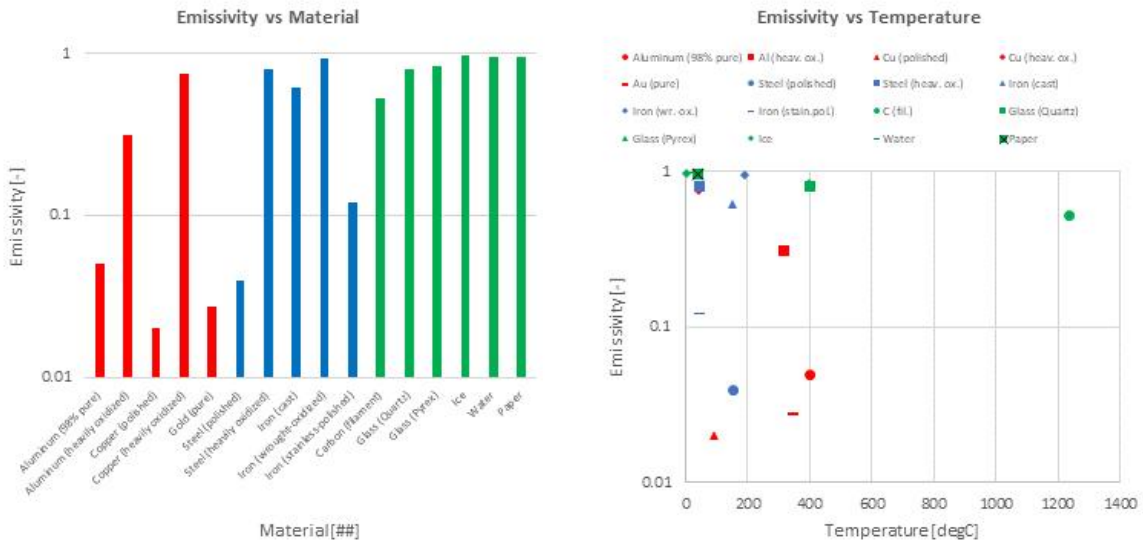

(a) (b)

Figure 3.8: Emittances comparison for a variety of surface materials (conductive vs not-conductive)

be refrigerated without any work input, the Second Law of Thermodynamics would be violated. Similar arguments can be built for the wavelength dependence. In essence, then, Kirchhoff's law is a consequence of the laws of thermodynamics. For a diffuse body, the emittance and absorptance do not depend on the angles, and Kirchhoff's law becomes for a grey body:

$$\varepsilon\left(T\right) = \alpha\left(T\right) \tag{3.23}$$

The gray body approximation can be expressed in first approximation with equation 3.23. When we consider two detached black bodies (in first approximation) it is necessary to calculate the black-body view factor. Considering two isothermal bodies and their infinitesimal surfaces (dA_1, dA_2) and considering angles between the normal of the surface and the direction of the heat (β_1, β_2) the heat fluxex between the two bodies:

$$\begin{cases} Q_{12} = \frac{\sigma T_1^4}{\pi}\left(\cos\beta_1 \cos\beta 2 dA_1 dA_2\right)\frac{1}{s^2} \\ Q_{12} = \frac{\sigma T_2^4}{\pi}\left(\cos\beta_1 \cos\beta 2 dA_1 dA_2\right)\frac{1}{s^2} \end{cases} \tag{3.24}$$

and then the net heat flux between the two bodies is:

$$\begin{cases} Q_{net_{12}} = Q_{12} - Q_{21} = \sigma\left(T_1^4 - T_2^4\right)\int_{A_1}\int_{A_2}\frac{\cos\beta_1\cos\beta_2}{\pi s^2} dA_1 dA_2 \\ Q_{net_{21}} = Q_{12} - Q_{21} = \sigma\left(T_1^4 - T_2^4\right)\int_{A_2}\int_{A_1}\frac{\cos\beta_1\cos\beta_2}{\pi s^2} dA_2 dA_1 \end{cases} \tag{3.25}$$

Considering equation 3.20 and the definition of the view factor (F) finally the two view factor

for the considered problem are:

$$\begin{cases} F_{12} = \frac{1}{A_1}\int_{A_1}\int_{A_2}\frac{\cos\beta_1\cos\beta_2}{\pi s^2}dA_1dA_2 \\ F_{21} = \frac{1}{A_2}\int_{A_2}\int_{A_1}\frac{\cos\beta_1\cos\beta_2}{\pi s^2}dA_2dA_1 \end{cases} \tag{3.26}$$

In many drying process radiant heaters are commonly used to heat products. They are particularly interesting when the material that we want to heat is thin ($< 300[\mu m]$) but the geometry of the radiative system and view factors are fundamental to properly exchange power. In many cases efficiency is strictly related to the geometry of the heating chamber. In literature exist many practical approaches to compute view factors for a preliminary heating system design. If we consider two separated linear system of length w facing each other at a certain distance h, that are shown in figure 3.11, the view factor is:

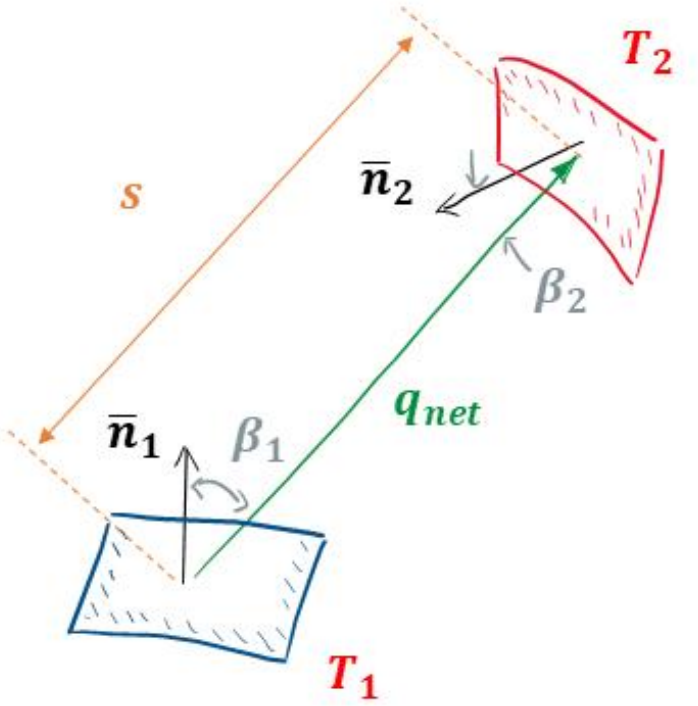

Figure 3.9: Radiant exchange between two black elements.

$$F_{12} = F_{21} = \sqrt{1 + \left(\frac{h}{w}\right)^2} - \frac{h}{w} \tag{3.27}$$

In many freeze-drying applications because of the system can't use convection mechanism to transfer thermal energy from an hot system to the load that it is necessary to heat and dry, a possibility is to use high temperature resistors ($T_{res} > 600[degC]$) as radiant bodies. Equation 3.27 highlights that because of the power density exchanged by two linear systems is

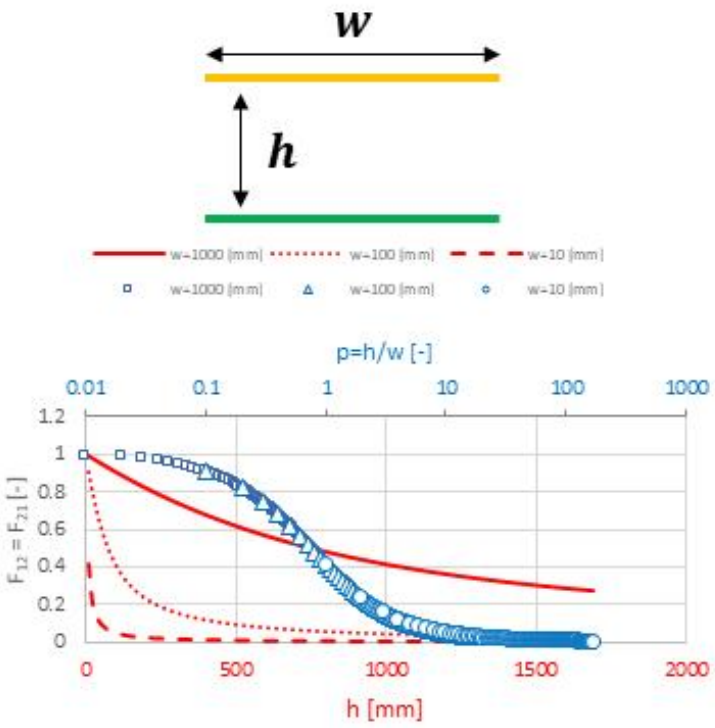

Figure 3.10: View factors for a typical of two-dimensional plane configuration (infinite in extent normal to the paper)

proportional to the view factor (F_{12}), if the yellow line of figure 3.11 is the hotter body (radiative resistor) and the green line is the colder body that we want to heat and dry (absorber) the maximum power exchanged between the two systems is obtained when the ration between the distance and the length of the elements ($p = \frac{h}{w}$) is equal to zero, in other words when the distance between resistor and sample is much lower than the length of the sample. That is typical for example in tobacco drying industry or textile drying industry. In many practical applications it is difficult to guarantee a narrow gap between the resistor and the load. Radio-frequency and Microwave technologies may solve that problem. A well design of electrodes can guarantee high efficiencies without the necessity of having the "power generator" extremely close to the sample that is necessary to heat and dry.

3.2 Thermal properties of food

Tto perform the various heat transfer calculations involved in designing storage and refrigeration equipment and estimating process times for refrigerating, freezing, heating, or drying of foods and beverages. Because the thermal properties of foods and beverages strongly

depend on chemical composition and temperature, and because many types of food are available, it is nearly impossible to experimentally determine and tabulate the thermal properties of foods and beverages for all possible conditions and compositions. However, composition data for foods and beverages are readily available from sources such as Holland et al. in 1991 [32] and USDA in 1975 [1]. These data consist of the mass fractions of the major components found in foods. Thermal properties of foods can be predicted by using these composition data in conjunction with temperature-dependent mathematical models of thermal properties of the individual food constituents. Thermo-physical properties often required for heat transfer calculations include density, specific heat, enthalpy, thermal conductivity, and thermal diffusivity. In addition, if the food is a living organism, such as a fresh fruit or vegetable, it generates heat through respiration and loses moisture through transpiration. Both of these processes should be included in heat transfer calculations. This chapter summarizes prediction methods for estimating these thermo-physical properties and includes examples on the use of these prediction methods. Tables of measured thermo-physical property data for various foods and beverages are also provided. Constituents commonly found in foods include water, protein, fat, carbohydrate, fiber, and ash. as highligted by Choi and Okos in 1986 [80]. They developed mathematical models for predicting the thermal properties of these components as functions of temperature in the range of –40 to 150°C 3.4; they also developed models for predicting the thermal properties of water and ice 3.5. In general, thermophysical properties of a food or beverage are well behaved when its temperature is above its initial freezing point. However, below the initial freezing point, the thermophysical properties vary greatly because of the complex processes involved during freezing. The initial freezing point of a food is somewhat lower than the freezing point of pure water because of dissolved substances in the moisture in the food. At the initial freezing point, some of the water in the food crystallizes, and the remaining solution becomes more concentrated. Thus, the freezing point of the unfrozen portion of the food is further reduced. The temperature continues to decrease as separation of ice crystals increases the concentration of solutes in solution and depresses the freezing point further. Thus, the ice and water fractions in the frozen food depend on temperature. Because the thermophysical properties of ice and water are quite different, thermophysical properties of frozen foods vary dramatically with temperature. In addition, the thermophysical properties of the food above and below the freezing point are drastically different. In spray drying there is the necessity for many food applications to fully characterize fat characteristics because of the use of powdered oils is grown in that area [31]

Thermal Property Models for Food Components ($-40 < T < 150[degC]$)			
$f = A_0 + A_1 \cdot T + A_2 \cdot T^2$			
Thermal Conductivity $[W/(mK)]$	A_0	A_1	A_2
Protein (λ_p)	$1.7881 \cdot 10^{-1}$	$1.1958 \cdot 10^{-3}$	$-2.7178 \cdot 10^{-6}$
Fat (λ_f)	$1.8071 \cdot 10^{-1}$	$-2.7604 \cdot 10^{-4}$	$-1.7749 \cdot 10^{-7}$
Carbohydrate (λ_c)	$2.0141 \cdot 10^{-1}$	$1.3874 \cdot 10^{-3}$	$-4.3312 \cdot 10^{-6}$
Fiber (λ_{fi})	$1.8331 \cdot 10^{-1}$	$1.2497 \cdot 10^{-3}$	$-3.1683 \cdot 10^{-6}$
Ash (λ_a)	$3.2962 \cdot 10^{-1}$	$1.4011 \cdot 10^{-3}$	$-2.9069 \cdot 10^{-6}$
Specific Heat $[kJ/(kgK)]$	A_0	A_1	A_2
Protein (Cp_p)	$2.0082 \cdot 10^{-1}$	$1.2089 \cdot 10^{-3}$	$-1.3129 \cdot 10^{-6}$
Fat (Cp_f)	$1.9842 \cdot 10^{-1}$	$1.4733 \cdot 10^{-4}$	$-4.8008 \cdot 10^{-6}$
Carbohydrate (Cp_c)	$1.5488 \cdot 10^{-1}$	$1.9625 \cdot 10^{-3}$	$-5.9399 \cdot 10^{-6}$
Fiber (Cp_{fi})	$1.8459 \cdot 10^{-1}$	$1.8306 \cdot 10^{-3}$	$-4.6509 \cdot 10^{-6}$
Ash (Cp_a)	$1.0926 \cdot 10^{-1}$	$1.8896 \cdot 10^{-3}$	$-3.6817 \cdot 10^{-6}$
Density $[kg/(m^3)]$	A_0	A_1	A_2
Protein (ρ_p)	$1.3299 \cdot 10^{3}$	$-5.1840 \cdot 10^{-1}$	0
Fat (ρ_f)	$9.2559 \cdot 10^{2}$	$-4.1757 \cdot 10^{-1}$	0
Carbohydrate (ρ_c)	$1.5991 \cdot 10^{3}$	$-3.1046 \cdot 10^{-1}$	0
Fiber (ρ_{fi})	$1.3115 \cdot 10^{3}$	$-3.6589 \cdot 10^{-1}$	0
Ash (ρ_a)	$2.4238 \cdot 10^{3}$	$-2.8063 \cdot 10^{-1}$	0

Table 3.4: Thermal properties models for food components.

3.2.1 Ice Fraction

To predict the thermophysical properties of frozen foods, which depend strongly on the fraction of ice in the food, the mass fraction of water that has crystallized must be determined. Below the initial freezing point, the mass fraction of water that has crystallized in a food is a function of temperature. In general, foods consist of water, dissolved solids, and undissolved solids. During freezing, as some of the liquid water crystallizes, the solids dissolved in the remaining liquid water become increasingly more concentrated, thus lowering the freezing temperature. This unfrozen solution can be assumed to obey the freezing point depression equation given by Raoult's law (Pham 1987). Thus, based on Raoult's law, Chen (1985) proposed the following model for predicting the mass fraction of ice (x_i) at a certain

Thermal Property Models for Water ($-40 < T < 150[degC]$)			
$f = A_0 + A_1 \cdot T + A_2 \cdot T^2$			
Thermal Property	A_0	A_1	A_2
Thermal conductivity λ_w $[W/(mK)]$	$5.7109 \cdot 10^{-1}$	$1.7625 \cdot 10^{-3}$	$-6.7036 \cdot 10^{-6}$
Specific heat, Cp_w $[kJ/(kgK)]$ $(-40 < T < 0)$	$4.1289 \cdot 10^{0}$	$-5.3062 \cdot 10^{-3}$	$+9.9516 \cdot 10^{-4}$
Specific heat, Cp_w $[kJ/(kgK)]$ $(0 < T < 150)$	$4.1289 \cdot 10^{0}$	$-9.0864 \cdot 10^{-5}$	$+5.4731 \cdot 10^{-6}$
Density ρ_w $[kg/m^3]$	$9.9718 \cdot 10^{2}$	$3.1439 \cdot 10^{-3}$	$-3.7574 \cdot 10^{-3}$
Thermal Property Models for Ice ($-40 < T < 150[degC]$)			
$f = A_0 + A_1 \cdot T + A_2 \cdot T^2$			
Thermal Property	A_0	A_1	A_2
Thermal conductivity λ_i $[W/(mK)]$	$2.2196 \cdot 10^{-1}$	$-6.2489 \cdot 10^{-3}$	$1.0154 \cdot 10^{-4}$
Specific heat, Cp_iw $[kJ/(kgK)]$	$2.0623 \cdot 10^{0}$	$6.0769 \cdot 10^{-3}$	0
Density ρ_i $[kg/m^3]$	$9.1689 \cdot 10^{2}$	$-1.3071 \cdot 10^{-1}$	0

Table 3.5: Thermal properties models for water and ice

food temperature (t $[K]$)

$$x_i = \frac{x_s R T_0^2 \left(t_f - t\right)}{M_s L_0 t_f t} \tag{3.28}$$

where x_s is the mass fraction of solids in food, Ms ($[kJ/mol]$) is relative molecular mass of soluble solids, $R = 8.314[kJ/(kg \cdot mol \cdot K)$ is the universal gas constant, $T_0 = 273.15[K]$ is the freezing point of water, $L_0 = 333.6[kJ/kg]$ is the latent heat of fusion of water and t_f is the initial freezing point of food that is its characteristic. The relative molecular mass of the soluble solids in the food may be estimated as:

$$M_s = \frac{x_s R T_0^2}{\left(x_b - x_{wo}\right) L_0 t_f} \tag{3.29}$$

where x_{wo} is the mass fraction of water in the unfrozen food and x_{wo} is the mass fraction of bound water in the food, that may be estimated with a stong relation with the mass fraction of the protein (x_p)

$$x_b = 0.4 \tag{3.30}$$

Considering the last three equations, it is possible to explicit with an empirical relationship for the ice mass fraction (x_{ice}):

$$x_{ice} = \left(x_{wo} - x_b\right) \left[\frac{t - t_f}{t}\right] \tag{3.31}$$

3.2.2 Density of food

To properly analyze a thermal load, of coarse in Fourier's equation the density is one of the coefficients or the PDEs. Because of food is a mixture of several species (water, protein, fat, carbohydrate, fiber and ash) it is possible to estimate the overall density of a certain food, but it is required the knowledge of the food porosity (ε $[-]$), as well as the mass fraction (x_i) and density(ρ_i) of the N food components. The density of foods and beverages (ρ $[kg/m^3]$) can be calculated as follows:

$$\rho = \frac{1-\varepsilon}{\sum_{i=1}^{N} \frac{x_i}{\rho_i}} \tag{3.32}$$

where it is important to remember that

$$\sum_{i=1}^{N} x_i = 1 \tag{3.33}$$

and the he porosity (ε $[-]$) is required to model the density of granular foods stored in bulk, but otherwise for other foods the porosity is approximately zero.

3.2.3 Specific heat capacity of food

Specific heat is a measure of the energy required to change the temperature of a food by one degree. Therefore, the specific heat of foods or beverages can be used to calculate the heat load imposed on the refrigeration equipment by the cooling or freezing of foods and beverages. In unfrozen foods, specific heat becomes slightly lower as the temperature rises from $0[degC]$ to $20[degC]$. For frozen foods, there is a large decrease in specific heat as the temperature decreases. The specific heat of a food, at temperatures above its initial freezing point, can be obtained from the mass average of the specific heats of the food components. Thus, the specific heat of an unfrozen food (Cp_u $[kJ/(kg \cdot K)]$) may be determined as follows if detailed information about the composition of the food are reported:

$$Cp_u = \sum_{i=1}^{N} Cp_i x_i \tag{3.34}$$

Below the food's freezing point, the sensible heat from temperature change and the latent heat from the fusion of water must be considered. Because latent heat is not released at a constant temperature, but rather over a range of temperatures, an apparent specific heat must be used to account for both the sensible and latent heat effects. A common method to predict the

apparent specific heat (Cp_a $[kJ/kg \cdot K]$) of foods is:

$$Cp_a = Cp_u + (x_b - x_{wo})(Cp_w - Cp_{ice}) + \frac{M_w}{M_s} x_s \left[\frac{RT_0^2}{M_w t^2} - 0.8 (Cp_w - Cp_{ice}) \right] \tag{3.35}$$

it is clear that equation 3.35 add to equation 3.34 the therm that is related to the frozen part of water and ice that is present in food at temperatures below the freezing point.

3.2.4 Thermal conductivity of food

Thermal conductivity relates the conduction heat transfer rate to the temperature gradient. A food's thermal conductivity depends on factors such as composition, structure, and temperature. Early work in the modeling of thermal conductivity of foods and beverages includes Eucken's adaption of Maxwell's equation [21]. This model is based on the thermal conductivity of dilute dispersion of small spheres (V_d) in a continuous phase (V_c):

$$\begin{cases} \lambda = \lambda_c \frac{1-\left(1-a\frac{\lambda_d}{\lambda_c}\right)b}{1+(a-1)b} \\ a = \frac{3\lambda_c}{2\lambda_c+\lambda_d} \\ b = \frac{V_d}{V_c+V_d} \end{cases} \tag{3.36}$$

where λ $[W/(mK)]$ is the thermal conductivity of the mixture, λ_c $[W/(mK)]$ is the thermal conductivity of the continuous phase, λ_d $[W/(mK)]$ is the thermal conductivity of the dispersed phase, V_d is the volume of dispersed phase and V_c is the volume of continuous phase. When foods consist of more than two distinct phases, the previously mentioned method for the prediction of thermal conductivity must be applied successively to obtain the thermal conductivity of the food product. The resulting thermal conductivity is then combined successively with the thermal conductivity of each remaining food constituent to determine the thermal conductivity of the food product:

$$\begin{cases} \lambda_{par} = \sum_{i=1}^{N} x_i^V k_i \\ \lambda_{per} = \frac{1}{\sum_{i=1}^{N} \frac{x_i^V}{k_i}} \\ x_i^V = \frac{\frac{x_i}{\rho_i}}{\sum_{i=1}^{N} \frac{x_i}{\rho_i}} \end{cases} \tag{3.37}$$

In that work, because of it is not easy to understand the model type of the conductivity we used an average model for the global conductivity (λ):

$$\lambda = \frac{1}{2}(\lambda_{par} + \lambda_{per}) \tag{3.38}$$

3.2.5 Enthalpy of food

The change in a food's enthalpy can be used to estimate the energy that must be added or removed to effect a temperature change. Above the freezing point, enthalpy consists of sensible energy; below the freezing point, enthalpy consists of both sensible and latent energy. Enthalpy (H $[kJ/kg]$) may be obtained from the definition of constant-pressure specific heat:

$$Cp = \left[\frac{\partial H}{\partial T}\right]_{p=const} \tag{3.39}$$

For foods at temperatures above their initial freezing point, enthalpy may be obtained by integrating the corresponding expression for specific heat above the freezing point. Thus, the enthalpy H of an unfrozen food may be determined by integrating equation 3.39 and it is the linear combination of the product where of the enthalpy of the individual food components (H_i) and their mass fractions (x_i):

$$H = \sum_{i=1}^{N} H_i x_i = \sum_{i=1}^{N} \int_{t'}^{t''} Cp_i x_i dT \tag{3.40}$$

and Chen in 1985obtained a good solution integrating the specific heat of unfrozen food:

$$H = H_f + (t - t_f)\left(4.19 - 2.30x_s - 0.628x_s^3\right) \tag{3.41}$$

where the initial freezing point (t_f $[degC]$), the enthalpy of food at initial freezing temperature (H_f $[kJ/kg]$) are required. For foods below the initial freezing point, mathematical expressions for enthalpy may be obtained by integrating the apparent specific heat models proposed in the previous sections:

$$H = (t - t_r)\left\{Cp_u + (x_b - x_{wo})(c_w - c_{ice}) + \frac{M_w}{M_s}x_s\left[\frac{RT_0^2}{18(T_0 - t_r)(T_0 - t)} - 0.8(c_w - c_{ice})\right]\right\} \tag{3.42}$$

where equation 3.42 is obtained with an integration between the reference temperature (t_r $[K]$) and the general food temperature (t $[K]$). In that work it is assumed that the reference temperature is constant and equal to:

$$T_r = -20[degC] = 253.15[K] \tag{3.43}$$

Chen in 1985 obtained the following expression for enthalpy below the initial freezing point:

$$H = (t - t_r)\left[1.55 + 1.26x_s + x_s\frac{RT_0^2}{M_s t t_r}\right] \tag{3.44}$$

that may be more simplified in:

$$H = (t - t_r)\left[1.55 + 1.26x_s + (x_b - x_{wo})\frac{L_0 t_f}{t t_r}\right] \tag{3.45}$$

Equation 3.45 may be used to calculate total energy necessary that is necessary to give to a certain mass (m_{food}) to change its temperature from $t^{''} = -20[degC]$ to the final temperature, assumed from be equal to $t^{'} = 60[degC]$. Because of a certain food is characterized by its components concentration as shown in table 3.6. It is possible to compute for a certain food item its main parameters: after having obtained the initial freezing point (t_f $[degC]$) of a certain

Unfrozen composition data of foods					
	Moisture	Protein	Fat	Carbohydrates	Ash
Food Item	x_{wo} [%]	x_p [%]	x_f [%]	x_c [%]	x_a [%]
Asparagus	92.40	2.28	0.20	4.54	0.57
Beans	90.27	1.82	0.12	7.14	0.66
Broccoli	90.69	2.98	0.35	5.24	0.92
Carrots	87.79	1.03	0.19	10.14	0.87
Lettuce	95.89	1.01	0.19	2.09	0.48
Mushrooms	91.81	2.09	0.42	4.65	0.89
Peas	78.86	5.42	0.40	14.46	0.87
Potatoes	78.96	2.07	0.10	17.98	0.89
Pumpkins	91.60	1.00	0.10	6.50	0.80
Spinach	91.58	2.86	0.35	3.50	1.72

Table 3.6: Unfrozen composition data for several vegetable-food items.

food, that is obviously function of concentration of its species, as seen in the first part of that section

$$\begin{cases} x_s = 1 - x_{wo} \\ x_b = 0.4 x_p \\ H_{t'} = \left(t^{'} - t_r\right)\left[1.55 + 1.26 x_s + (x_b - x_{wo})\frac{L_0 t_f}{t^{'} t_r}\right] \\ H_{t_f} = \left(t^{''} - t_r\right)\left[1.55 + 1.26 x_s + (x_b - x_{wo})\frac{L_0 t_f}{_f t_r}\right] \\ H_{t^{''}} = H_{t_f} + \left(t^{''} - t_f\right)\left(4.19 - 2.30 x_s - 0.628 x_s^3\right) \\ Q = m\Delta H = m\left(H_{t'} - H_{t^{''}}\right) \end{cases} \tag{3.46}$$

The set of equations 3.46 makes possible to estimate the energy required for a thawing process from an initial temperature $t^{''} = -20[degC]$ to the service temperature $t^{'} = -20[degC]$.

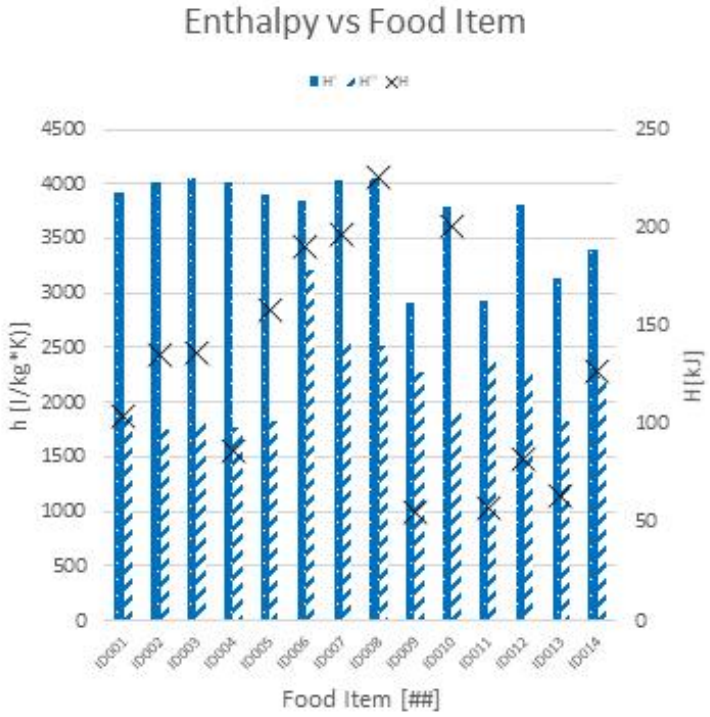

Figure 3.11: Enthalpy of food analysis for a regeneration process of several (14) frozen-ready-vegetable-meals. Initial temperature ($t^{''} = -20[degC]$) and final service temperature $t^{'} = -20[degC]$.

Chapter 4

Dielectrics

4.1 Dielectric Materials

Here we will discuss another of the peculiar properties of matter that is extremely important for Radio-frequency and Microwave heating problems. If an the electric field (**E**) is given in space, unlike in conductors, in which the charges move freely in response to the electric field to such points that there is no field left inside the conductor, insulators does not not conduct electricity and no conduction effect can be experienced. We will see instead that Electric Energy W_{es} $[J]$ will be stored in the medium. Faraday's experiments [39] discovered that that the capacitance (C $[F]$) of such a capacitor is increased when an insulator material is put between two conductive plates. If the insulator completely fills the space between the plates, the capacitance is increased by a factor ϵ_r $[-]$ which depends only on the nature of the insulating material: we will see that typically different materials show different dielectric properties. In electromagnetism insulating materials are typically called dielectrics. The dimensionless factor ϵ is then a property of the dielectric, and is called the relative dielectric constant. The vacuum is characterized by unity relative dielectric constant and its dielecric constant is ϵ_0 and its value its already been presented in 2.5. But why is there any electrical effect if the insulators do not conduct electricity? Faraday with its experimental observations offered a chance to understand that. As seen in previous if a dielectric is added the capacitance is increased. We will analyze a simple parallel-plate capacitor with some charges (Q $[C]$) on the surfaces of the conductors (negative charge on the top plate and positive charge on the bottom plate). The vacuum-gap

between the plates is d $[m]$ and the area of each plate is S $[m^2]$. The capacitance is then:

$$C = \epsilon_0 \frac{S}{d} \tag{4.1}$$

The electric charges:

$$Q = CV \tag{4.2}$$

If we put a piece of insulating material like glass between the plates, we measure a larger capacitance and then, for the same charge (Q) the voltage is lower. But the voltage difference between the electrodes is for its definition the integral of the electric field ($\mathbf{E}$ $[V/m]$) across the capacitor:

$$V = \int_0^d \mathbf{E} \cdot d\mathbf{l} \tag{4.3}$$

So we must conclude that inside the capacitor, the electric field is reduced even though the charges on the plates does not change. If the Gauss's Law for the electric field 2.9 is applied to a certain surface Σ, the total electric field flux Φ_E is proportional to the electric charge enclosed in the surface. Because of the electric field is reduced by the dielectric medium so the total net charge is reduced, too. This implies that must be positive charges on the surface of the dielectric as shown in figure 4.1. So the phenomena of electric field induction states that when a dielectric material (ϵ_r) is positioned in an electric field ($\mathbf{E}$) there is a positive charge induced ($+q$ $[C]$) on one surface and negative charge induced ($+q$ $[C]$) on the other surface. If the same experiment is made with a conductive material instead of the dielectric medium and the conductor has a certain thickness (d_2 $[m)$ the electric field induces a positive charge on the upper surface and a negative charge on the lower surface, so there is no field inside the conductor. The field in the rest of the space is the same as it was without the conductor, because it is the surface density of charge divided by the vacuum permittivity (ϵ_0) as shown in figure 4.2. If we integrate the electric field than:

$$V = \int_0^{d_0} \mathbf{E} \cdot d\mathbf{l} = \int_0^{\frac{d_0-d_1}{2}} \mathbf{E} \cdot d\mathbf{l} + \int_{\frac{d_0-+d_1}{2}}^{d_0} \mathbf{E} \cdot d\mathbf{l} = \frac{Q}{\epsilon_0}(d_0 - d_1) \tag{4.4}$$

and the total capacitance, using equation 4.1, if the surface of the conductive conductors is S and the non filled volume has a thickness of $d_0 - d_1$:

$$C = \epsilon_0 \frac{S}{d_0 - d_1} = \epsilon_0 \frac{S}{d_0}\left(\frac{1}{1 - \frac{d_1}{d_0}}\right) = C_0\left(\frac{1}{1 - \frac{d_1}{d_0}}\right) = C_0\gamma \tag{4.5}$$

where the capacitance of the empty capacitor C_0 $[F]$ is increased by a factor that is function of the ratio between the thickness of the inner conductor and the distance between the plates of the outer capacitor.

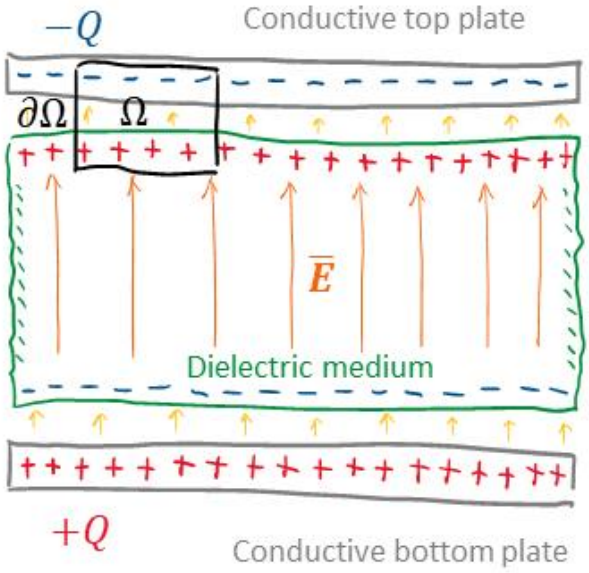

Figure 4.1: Parallel-plate capacitor filled with dielectric material In figure are highlighted conductive plates (grey), dielectric medium (green), positive (red) and negative (red) charges, electric field (orange) and Gaussian surface (black).

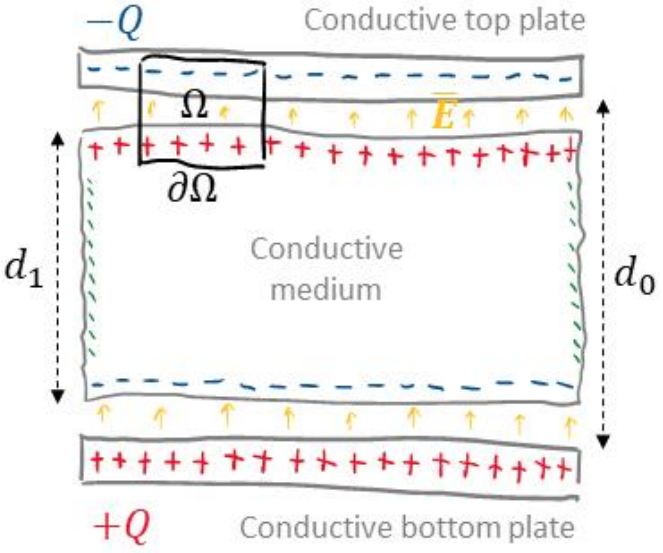

Figure 4.2: Parallel-plate capacitor filled with conductors. In figure are highlighted conductive plates (grey), positive (red) and negative (red) charges, electric field (orange) and Gaussian surface (black).

That short analysis offers us an obvious model for what happens with dielectrics: inside the material there are many infinitesimal conducting spheres separated from each other by

insulation, as shown in 4.3. The phenomenon of the dielectric constant is explained by the effect of the charges which would be induced on each sphere. This is one of the earliest physical models of dielectrics used to explain the phenomenon that Faraday observed. More specifically, it was assumed that each of the atoms of a material was a perfect conductor, but insulated from the others. The dielectric constant ϵ_r would depend on the proportion of space which was occupied by the conducting spheres. This is not, however, the model that is used today but it helps to understand the polarization phenomena [49].

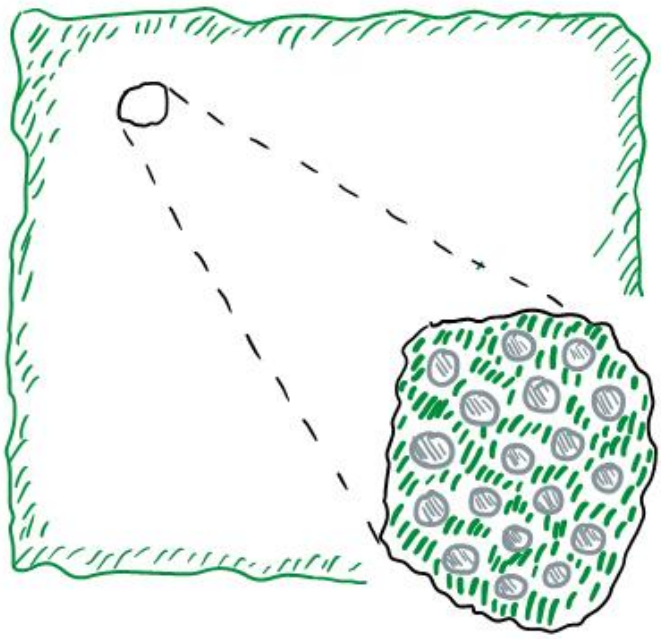

Figure 4.3: Idealized model for dielectric medium. In figure are highlighted conductive sphere (grey) and dielectric medium (green).

In the model proposed in figure 4.3 each of the small spheres acts like a dipole. The external electric field **E** induces a moment, the so called electrical dipole moment. The previous model that contemplates the existence of conductive spheres may be replaced with a new model that considers many little dipoles induced inside the material [41]. The nucleus of an atom has a positive charge $(+q)$. Electrons, that have a charge $(-q)$ orbit around the nucleus. If an external electric field is applied, the nucleus will be attracted in one direction and the electrons in the other. The wave patterns of the electrons will be distorted and will not longer be approximated with a perfect spherical surface but with a deformed one. The center of gravity of the negative charge will be displaced of a certain vector and will no longer coincide with the positive charge of the nucleus. If a far reference system is considered, that neutral configuration is equivalent to a little dipole. In a certain portion of space there are N atoms. If we assume that in each

atom there are charges q separated by a certain distance (δ $[m]$), so the specific dipole moment per volume unit ($\mathbf{P}$) is the vector:

$$\mathbf{P} = Nq\delta \cdot \mathbf{u}_\delta \tag{4.6}$$

where the vector has same components in space of the charge separation $\delta \cdot \mathbf{u}_{delta}$. Generally $\mathbf{P}$ varies inside the dielectric material but at any point in the material it is proportional to the electric field ($\mathbf{E}$). The constant of proportionality is a property of atoms that compose the material. If we consider a dielectric slab of material we can experience that if a constant electric field is applied at one surface the negative charges, the electrons, have effectively moved out and at the other surface they have moved in. As shown in 4.4 a surface density of charge *Surface Polarization Charge* exists at the surface of the dielectric. If an uniform polarization is considered: Because of the charge of a single electron is well known, it is possible to compute

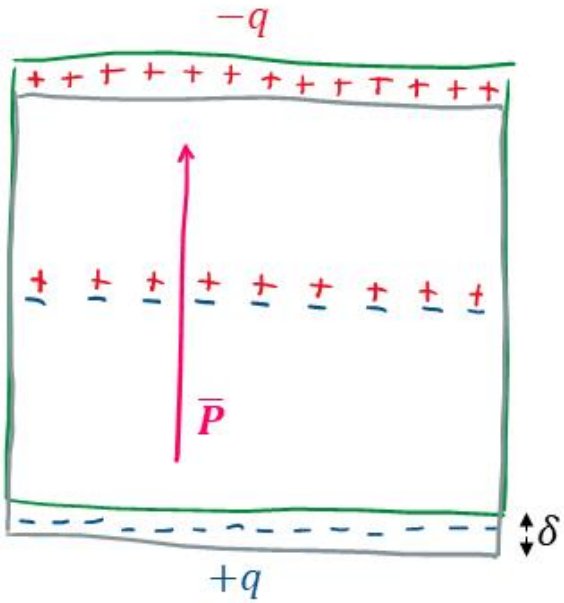

Figure 4.4: dielectric slab in a uniform field. The positive charges displaced the distance δ with respect to the negatives.

the surface charge density and observe that it is exactly equal to the right-hand side of the equation 4.6:

$$\sigma_p = N\delta_e q = P \tag{4.7}$$

If the complete capacitor shown in figure 4.2 and we consider the same Gaussian Surface, after have identified also the free-charge density of the conductive plates σ_f $[C]$, so it is possible to obtain the law that expresses the polarization field as a function of the electric field:

$$\mathbf{P} = \sigma_f - \mathbf{E}\epsilon_0 = \chi\epsilon_0\mathbf{E} \tag{4.8}$$

where χ is the dielectric susceptibility. Using the previous equation it is possible to describe the electric field in its modulus as:

$$E = \frac{\sigma_f}{\epsilon_0}\frac{1}{1+\chi} \tag{4.9}$$

and so, using equation 4.1 the total capacitance (C $[F]$) of the system shown in figure 4.2 is:

$$C = (1+\chi)\frac{\epsilon_0 S}{d} = \epsilon_r \frac{\epsilon_0 S}{d} \tag{4.10}$$

Equation 4.10 helps us to define the correlation between dielectric susceptibility and dielectric relative permittivity of a certain material. From previous equation it is clear that th susceptibility of the vacuum must be equal to zero. It is possible to generalize the model taking into account a not uniform polarization (P) and modify equation 4.7:

$$\sigma_p = \mathbf{P}\cdot\mathbf{n} \tag{4.11}$$

and observing that a non uniform polarization may result in a net charge in the arbitrary volume Ω:

$$\int_\Omega \rho_p dV = -\int_{\partial\Omega} \mathbf{P}\cdot\mathbf{n} dS \tag{4.12}$$

and finally the polarization charge density is:

$$\rho_p = -\nabla\cdot\mathbf{P} \tag{4.13}$$

Considering the first Maxwell's equation for the electric field 2.1:

$$\nabla\cdot\mathbf{E} = \frac{\rho}{\epsilon_0} = \frac{\rho_f+\rho_p}{\epsilon_0} = \frac{\rho_f}{\epsilon_0} - \frac{\nabla\cdot\mathbf{P}}{\epsilon_0} \tag{4.14}$$

Now it is possible to find equation of electrostatics when there are dielectrics:

$$\nabla\cdot\left(\mathbf{E}+\frac{\mathbf{P}}{\epsilon_0}\right) = \frac{\rho_f}{\epsilon_0} \tag{4.15}$$

$$\nabla\cdot\left[(1+\chi)\,\mathbf{E}\right] = \nabla\cdot\epsilon_r\mathbf{E} = \frac{\rho_f}{\epsilon_0} \tag{4.16}$$

The free charge is considered for our cases the global volume charge density. For that reason the displacement vector ($\mathbf{D}$) can be defined and used to rewrite Maxwell equations in a simple form:

$$\mathbf{D} = \epsilon_0\mathbf{E} + \mathbf{P} \tag{4.17}$$

and finally, considering what we did in equation 4.8 the displacement field is:

$$\mathbf{D} = (1+\chi)\,\epsilon_0\mathbf{E} = \epsilon_r\epsilon_0\mathbf{E} \tag{4.18}$$

From what highlighted in that part of the work it is obvious that the permittivity is extreamely important to describe with accuracy a phenomena where electric field exists, and particularly at high frequencies.

4.2 Dielectric permittivity measure

For radio-frequency heating (RFH) and microwave heating (MWH) processes design it is necessary to know material properties to properly predict global performances. Whether we decide to analyze the processes using analytical models or we choose an approximate approach, using finite element method (FEM), method of moment (MoM), or similar, it necessary, to know their dielectric permittivity (in their real and imaginary component). That part of the work proposes what, for dielectric heating processes, are the best way to measure dielectric properties. Over the years, several experimental techniques aimed at extracting the dielectric properties of a materials have been investigated [12]. The choice of the EM characterisation method depends on several parameters such as:

- the frequency band
- the accuracy
- physical state (solid, liquid)
- geometry shape
- size

In literature it is possible to find many works that analyze the accuracy of several method [**icolson1970measurement**], for example as function of loss factor: resonant methods provide reliable results for dielectric materials with low losses. These methods, employing resonant structures (cavity resonators), are based on the measure of the Q-factor and the resonance frequency of the cavity (f_{res} $[Hz]$). Alternatively, non-resonant methods, which employ transmission lines, rely on the measure of the signal reflected and transmitted by the specimen under test. The main difference between the two methods is typically the accuracy in the frequency range of the measure: resonant method is able to accurately characterise the material over a discrete number of frequencies, instead non-resonant methods inherently provide broadband results.The best feature of the non-resonant methods is the fact that they can be applied to different measuring setups and geometries. One of the most famous transmission line method is the so called Coaxial-line method that typically requires a very accurate shaping of the sample (3D-printing is a good way) but it can measure electromagnetic properties of the material over a very wide band and, in theory, at low frequencies. Wave-guide methods are usually more

popular since circular or rectangular samples are easier to produce than coaxial ones. However, wave-guide-based estimations are only valid over a limited frequency range, we will see in that section a good way to measure dielectric permittivity for example at a central-frequency of 2.45 $[GHz]$. On the other hand, free-space techniques not only circumvent the problem of the sample fit precision but also preserve the integrity of the sample (non-destructive). A major disadvantage of the free-space method is that, in order to avoid diffraction effects due to sample edges, the wireless measurement of the scattering parameters through antennas requires a sample of several wavelengths, and for example can't be applied for example for thin sample (compared with the EM-field wavelength).

4.2.1 NRW Method

One of the most popular procedures for the EM characterisation of materials is the Nicolson–Ross–Weir (NRW) method, based on Transmission-Reflection measurements (T/R) of the specimen under test. The properties of materials are retrieved from their impedance and the wave velocities in the material, that we know it is a fundamental function of its properties. It is well known that the main drawback of this method is related to the electrical thickness of the analysed material [3]. In particular, when the thickness of the specimen is an integer multiple of half wavelength in the material, the method produces ambiguous results due to the 2π-periodicity of the phase of the incident electromagnetic wave. In principle, from a priori information regarding the specimen, it is possible to achieve unambiguous results. In addition, as will be presented in this section, because of the inversion procedure adopted for the extraction of the EM parameters, the NRW method is not accurate in the case of low reflecting materials or thin samples. In NRW method typically a sample under test with a certain thickness (d $[mm]$) is located inside a two-port microwave device such as a coaxial cable or a rectangular waveguide. The sample of thickness d generates a certain phase delay T $[rad]$, and then the phase factor (T) is:

$$T = e^{-ikd} = e^{-\gamma d} = |T|e^{-i\Phi} \tag{4.19}$$

And if we define the transmission line's characteristic impedances in absence (Z_0 Ω) and in the presence of the sample (Z_1 Ω) it is possible to define the reflection coefficient (Γ $[-]$) as:

$$\Gamma = \frac{Z_1 - Z_0}{Z_1 - Z_0} \tag{4.20}$$

It is possible to write the scattering parameters as function of the reflection coefficient:

$$S_{11} = \Gamma_{IN} = \frac{\Gamma\left(1 - T^2\right)}{1 - \Gamma T^2} \tag{4.21}$$

$$S_{21} = \frac{\left(1 - \Gamma^2\right) T}{1 - \Gamma^2 T^2} \tag{4.22}$$

and explicit the reflection coefficient and the phase factor with scattering parameter, and if we solve simultaneously equations

$$\begin{cases} \Gamma = K \pm \sqrt{K^2 - 1} \\ T = \frac{S_{11} + S_{21} - \Gamma}{1 - (S_{11} + S_{21})\Gamma} \end{cases} \tag{4.23}$$

where

$$K = \frac{S_{11}^2 - S_{21}^2 + 1}{2S_{11}} \tag{4.24}$$

Starting from equation 4.19 it is possible to rewrite the phase factor as:

$$\gamma = \frac{1}{d}\left[-\ln|T| - i\Phi + i2\pi n\right] \quad \text{and} \quad n = ... - 3, -2, -1, 0, 1, 2, 3, ..., \tag{4.25}$$

Equation 4.25 contains an intrinsic ambiguity due to the term $2\pi n$ that is called branching and it cause infinite possible solution of the problem. To solve that problem it is possible to produce and measure samples with a certain defined thickness. If $d = \lambda/4$ then $n = 0$ and that close the problem because of if we are able to measure the γ-factor then we are able to evaluate complex permittivity and complex permeability (if $n = 0$) as:

$$\begin{cases} \epsilon = \frac{\gamma}{\gamma_0}\left(\frac{1-\Gamma}{1+\Gamma}\right) \\ \mu = \frac{\gamma}{\gamma_0}\left(\frac{1+\Gamma}{1-\Gamma}\right) \end{cases} \tag{4.26}$$

In a wave-guide environment (TE hypothesis) the two main parameters that describe and synthesize the propagation are the propagation constant (k) and the cut-off wave.number of the wave-guide (k_t), and after having defined the propagation constant in free space (k_0) as:

$$k_0 = \frac{2\pi}{\lambda_0} \tag{4.27}$$

and the more general propagation constant as:

$$k = \sqrt{k_0 \epsilon_r \mu_r - k_t^2} \tag{4.28}$$

it is possible to easily describe the magnetic permeability by analyzing the transmission parameters of the line (in a certain frequency range that validates the TE hypothesis):

$$\mu = \frac{\gamma}{\gamma_0}\frac{Z}{Z_0}|_{TE} = \mu_r \tag{4.29}$$

and finally it is possible to compute also the permittivity of the material as:

$$\epsilon_r = \frac{k^2 + k_t^2}{k_0^2}\mu_r = \frac{k^2 + k_t^2}{k_0^2}\frac{\gamma}{\gamma_0}\frac{Z}{Z_0}|_{TE} \tag{4.30}$$

With this formulation of the NRW method the user needs to choose the valid results depending on the different values of n. In order to overcome the limitations of the branch point selection, a step-wise scheme of the NRW method has been proposed [38]. The procedure is based on the fact that the measured sample is thinner than half-guided wavelength at the lowest frequency [55]. It is important to highlight that if the sample is not thinner than a half-guided wavelength at the lowest frequency, nonphysical solutions are also obtained using the step-wise method. The NRW direct inversion procedure is sensitive to the inaccuracies of the S-parameters at the $N\lambda_g/2$ resonances, with N an entire number. Indeed, at that frequency, the sample becomes a half-wavelength window and the reflection coefficient tends to zero. Consequently, it is not possible to apply the direct inversion procedure. Moreover, in the case of noisy measurements, this method will induce a high uncertainty in the extracted parameters of the material and may cause problems in finding the correct branch in the vicinity of these frequencies.

4.2.2 Iterative non-ambiguous method from T/R measurements

The extraction of the dielectric constants from T/R measurements can be ambiguous when the S-parameter inversion is performed frequency-by-frequency. The reason is the impossibility of determining the correct branch of the solution with any initial guess of the material properties. High values of permittivity or permeability might lead to a sample with an electrical thickness of several multiples of half-wavelengths, even at the lowest measurement frequency. Consequently, the choice of the ambiguity integer n is not straightforward. One of the main problems of the NRW direct inversion procedure is that it admits nonphysical non-causal solutions. Baker Jarvis proposed an alternative approach that exploits the correlation among contiguous frequency points, thus circumventing the ambiguity and discontinuity problems that plague the NRW method [5]. The best estimation of the dielectric permittivity can be obtained with an iterative fitting of an objective function, which minimises the quadratic errors on the magnitude and phase of S-parameters among the predicted and measured data. The method does not require any initial guess on the permittivity and may search the best estimation on the whole complex permittivity domain. Moreover, the algorithm can be successfully employed both with T/R measurements. The idea of the iterative method is to search only physical solutions analysing the scattering parameter over all the available frequency points at the same time. In this way, it

is possible to exploit the correlation among frequency points, which is instead neglected by the NRW method. Therefore, the unknown permittivity and permeability profiles can be estimated by computing the discrepancy between the measured scattering parameters and the analytically estimated ones based on physical permittivity models. The discrepancy can be estimated by using the following cost function:

$$F_C(\epsilon) = \sum_n |S_{11,M}(f_n) - S_{11}^*(f_n)|^2 + \sum_n |S_{21,M}(f_n) - S_{21}^*(f_n)|^2 \tag{4.31}$$

if the permittivity ($\epsilon = \epsilon^{'} - i\epsilon^{''}$) is a complex operator, and $S_{xy,M}$ are the measured scattering parameters and S_{xy}^* are the scattering parameters estimated by an ideal transmission model. An iterative line-search gradient algorithm (LS) makes possible to refine the permittivity from an initial value ϵ_0 and ensure fast-convergence:

$$\epsilon_{m+1} = \epsilon_m - \alpha_{m-1} \nabla F_C(\epsilon_m \tag{4.32}$$

4.2.3 FSS Waveguide Resonant Methods

Resonant methods usually exhibit lower inaccuracies and higher sensitivities than non-resonant methods, and they are more suitable for low-loss samples [17]. Resonant methods are based on the fact that their main two parameters: resonant frequency (f_{res} $[Hz]$) and quality factor (Q $[-]$) of a resonant cavity filled with a certain dielectric are determined by its permittivity ($\epsilon_[r]$) and permeability ($\mu_[r]$) . These methods are usually employed for the characterisation of low-loss dielectrics with permeability equal to μ_0. There are a large number of resonant methods for the estimation of the dielectric properties of materials but they usually require ad hoc cavities and a direct etching of the resonator on the unknown sample. The preparation of the sample under test can be a difficult task in cavity perturbation techniques, as the sample requires a regular geometry. In resonant methods, the sample permittivity is evaluated from the shift of the resonant frequency. All the resonant methods are limited to either a specific frequency range, some kinds of materials, or specific applications.

4.2.4 Rectangular Wave-guide Method (TE)

If we consider a simple geometry, practically a rectangular wave-guide, it is possible to measure with good accuracy relative permittivity, loss factor and relative magnetic permeability (also in its real and imaginary part). That technique is particularly interesting if we

are interested in measuring complex permittivity (or complex permeability) in the microwave range[63]. Considering chapter 7 it is possible to solve the EM problem for a rectangular geometry (TE Waveguide) and get an easy relationship between material properties ($\dot{\epsilon}_r$,$\dot{\mu}_r$) and reflection-transmission (T/R) parameters. That method makes to possible to measure with good accuracy complex dielectric permittivity of thin material. One important step when we approach that technique is the necessity of preparing the sample geometry that must fit the rectangular waveguide. That means practically to produce a material sample with specific dimensions in accordance of the frequency range at which we need to measure material properties. In table 4.1 are presented several rectangular waveguide dimensions for measuring complex permittivity. A simple setup for a $80[mm] \times 40[mm]$ waveguide transmission line is shown in figure

Rectangular waveguide dimensions for measuring complex permittivity				
f_{min} $[GHz]$	f_{max} $[GHz]$	f_{c-10} $[GHz]$	a $[mm]$	b $[mm]$
2	3	1.874	80	40
3	4	2.499	60	30
4	5	3.332	45	22.5
10	12	8.568	17.5	8.75

Table 4.1: Rectangular waveguide dimensions for measuring complex permittivity.

4.5. Considering a slab material of a certain thickness (t $[m]$), smaller than the characteristic wavelength, that is inserted in the waveguide (filled with air) as shown in figure 4.5, it is possible to explicit the electric potentials in the three regions: after Port 1 (1), the sample (s), before Port 2 (2):

$$\begin{cases} \Psi_1 = \cos\left(\frac{\pi x}{a}\right)\left(C_1 e^{ik_z z} + C_2 e^{-ik_z z}\right) \\ \Psi_s = \cos\left(\frac{\pi x}{a}\right)\left(C_3 e^{ik_{z-s} z} + C_4 e^{-ik_{z-s} z}\right) \\ \Psi_2 = \cos\left(\frac{\pi x}{a}\right)\left(C_5 e^{ik_z z}\right) \end{cases} \tag{4.33}$$

where the phase constant are different in air

$$k_z = \frac{\pi}{\lambda a}\sqrt{4a^2 - \lambda^2} \tag{4.34}$$

and in the sample is function of the complex permittivity ($\dot{\epsilon} = \epsilon^{'} - i\epsilon^{''}$):

$$k_{z-s} = \frac{\pi}{\lambda a}\sqrt{4\dot{\epsilon}a^2 - \lambda^2} \tag{4.35}$$

Because of Maxwell's curl equations for electric field and magnetic field are valid and the continuity condition for the tangential components of the electric field and of the magnetic field

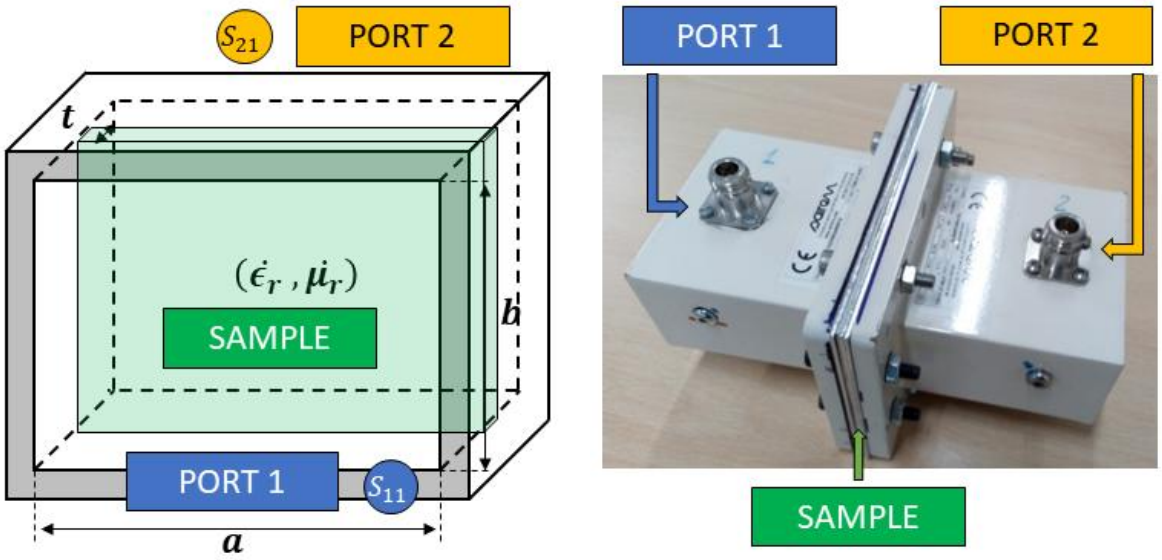

(a) (b)

Figure 4.5: A $80[mm] \times 40[mm]$ waveguide transmission line for measuring complex permittivity. (a) shows the theoretical problem of a two-port transmission line. (b) shows a real setup used in that work to measure material properties at $2.45[GHz]$.

at Port 1 and at the discontinuity between air and sample ($z = t$) the transmission coefficient (T) may be computed:

$$\begin{cases} T_a = 2\frac{k_{z-s}}{k_z} \\ T_b = \cos\left(k_{z-s}t\right) \\ T_c = \sin\left(k_{z-s}t\right) \\ T = \frac{C_5}{C_1} = \frac{T_a}{T_a T_b + i(T_a^2+1)T_c} \end{cases} \tag{4.36}$$

and it is possible to approximate the transmission coefficient to compute the relative dielectric permittivity. One of the main problem when we want to use a rectangular wave-guide method is the difficulty to ensure the sample is placed exactly at the waveguide flange [13]. Form small (thin) materials the term $k_{z-s}t$ is low and then:

$$\dot{\epsilon} = \frac{1 + \frac{(kt)^2}{8}\left(\frac{\lambda}{a}\right)^2 + i\frac{(k_z t)^2}{2(k_z t)\left[1-\frac{1}{2}\left(\frac{\lambda}{a}\right)^2\right]} - \frac{1}{T}}{\frac{(kt)^2}{2} - i\frac{(kt)^2}{2(k_z t)}} \tag{4.37}$$

Equation **??** approximate very well the material permittivity, but more important that approach is not affected by sample position. A vector network analyzer can be used for accurate measurement of $S-$parameters of the waveguide. Two-port calibration is performed without the thin slab using a standard Thru-Reflect-Line (TRL) method. That work also used a new different method to measure material properties: Transmission Phase Shift (TPS) method. It,

if compare with NRW method may cover a wider range of material permittivity. [79].

Transmission Phase Shift method (TPS)

TPS method by measuring scattering parameters and particularly the phase shift

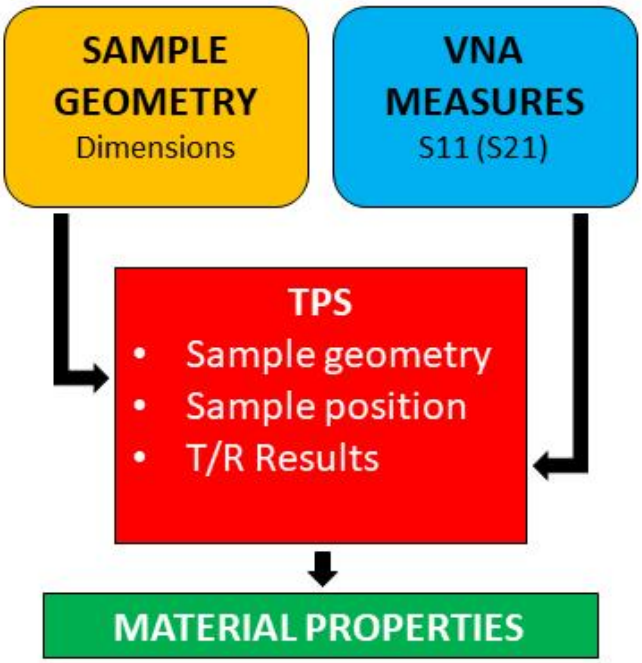

Figure 4.6: TPS algorithm for a complex permittivity measurement process.

between the no-load and the loaded waveguide scattering matrix may reconstruct the complex permittivity of the sample [19]. Many works in the last years analysed the method accuracy, and one work particularly highlighted the importance of good calibration of the system [46]. In typical MW applications dielectric materials are used and, if the relative permeability is a real number and may be approximated to the unity TPS method easily solves the permittivity measurement problem. Considering the same system shown in figure 4.5 by measuring with a Virtual Network Analyser (VNA) at port 1 and at port 2 the scattering complex parameters (S_{11} and (S_{21}) the complex permittivity ($\dot{\epsilon}_r = \epsilon_r^{'} - i\epsilon_r^{''}$) of the "rectangular" sample of thickness t $[mm]$ is:

$$\begin{cases} \epsilon_r^{'} = \frac{1}{k^2}\left[\beta + \frac{\Psi_{21}^{a} - \Psi 21^{s}}{1e^{-3}t} + \left(\frac{\pi}{a}\right)^2 - \alpha_c^2\right] \\ \epsilon_r^{''} = \frac{2\alpha_c}{k^2}\left[\beta + \frac{\Psi_{21}^{a} - \Psi 21^{s}}{1e^{-3}t}\right] \end{cases} \tag{4.38}$$

where the wave-number(k) is defined, as we will see in chapter 7, for a certain frequency (f $[Hz]$) as:

$$k = \frac{2\pi f}{c} \tag{4.39}$$

the propagation constant (β) is:

$$\beta = \sqrt{k^2 - k_c^2} = \sqrt{k^2 - \left(\frac{\pi}{b}\right)^2} \tag{4.40}$$

and the attenuation due to the presence of the sample is:

$$\alpha_c \simeq -1.15129 \left[\log_{10}\left(|S_{11}^s|^2 + |S_{21}^s|^2\right) - \log_{10}\left(|S_{11}^a|^2 + |S_{21}^a|^2\right)\right] \tag{4.41}$$

In that work we used that technique to measure practically complex permittivity for materials both with high loss tangent factor and low loss tangent factor. We found not acceptable complex permittivity (extreamely low accuracy and variability in results) only for materials with permittivity very high (greater than 10^2). Figure 4.7 shows several plastic-material permittivity measurements. The sample analysed are Teflon, Barex, PLA and some special derived materials with the inclusions of high dielectric permittivity particles inside the material matrix. Grey and black markers represents three well known material. Every-time we apply TPS method to measure complex permittivity we perform the calibration of the system with PTFE controlled sample. The dot lines represents the class of the material: A1,A2,A3 are modified EVA matrix; B1,B2,B3 are modified BAREX and finally C1,C2,C3,C4 are modified TEFLON (PTFE). All measures are performed in the range $2.4[GHz] - 2.6[GHz]$ but in figure 4.7 is highlighted the average value at $2.465[GHz]$ that in many application is the nominal frequency (f_{nom}) of many commercial microwave Magnetrons That method is extremely interesting also for high lossy

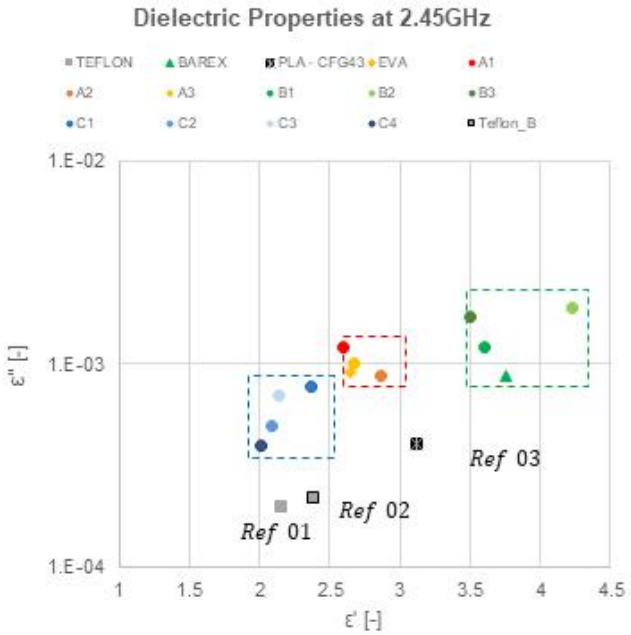

Figure 4.7: Results of TPS method applied to real sample of thickness $7[mm]$.

materials. One of the main problem is when there is necessity to characterize for example a food

meal, that is very complex because of it is a mixture of several ingredients, and particularly it is a complex structure of proteins, fats, carbohydrates, ash and water. In chapter 7 is presented a MW thawing system for vegan dishes. We performed many measures on several ready-meals to fully characterize the complex permittivity (and also the geometry that is finally one of the most important parameters) of 14 typical loads. The work flow for measuring dielectric material properties is shown in figure 4.6. One of the most important step is the preparation of samples that must properly fit the waveguide geometry. In that specific application the resonance cavity considered is designed for a typical Magnetron frequency ($2.465[GHz] \pm 15[MHz]$). Figure 4.8 shows a typical permittivity measure for a frozen pumpkin-cabbage based meal. We performed

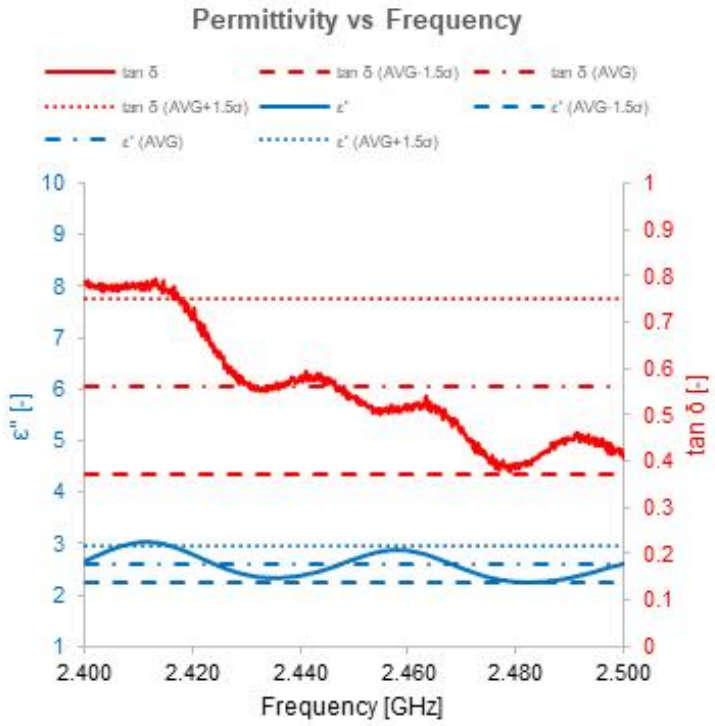

Figure 4.8: Relative permittivity (blue line) and loss-tangent (blue line) measured for a frozen pumpkin-cabbage based meal. The reference temperature for measurement is $-20[degC]$.

several measurements (21 samples for each meal type) for fourteen typical frozen meal (from $ID001$ to $ID014$). Results are presented in figure 4.9. The properties analyse highlighted that the real part of the permittivity is much lower than water permittivity. Typical microwave cavities are designed and optimised for "canonical" water loads with initial temperature close to $20[degC]$.Because of in a MW heating process the efficiency of the heating is strictly related to the transmission-reflection problem we wanted to deeply analyse material properties. It is clear, that for thawing applications of frozen vegetable meals it is necessary to design a tailored

resonant cavity. Measures highlighted that the imaginary part of the fourteen meals is still big compared to the real part. That is due to the high salts concentration and to the high water content. A next work will also deeply analyse the effect of the water vs ice volume fraction on the complex permittivity. A comparative analysis on frozen-vegetables food meals is presented in

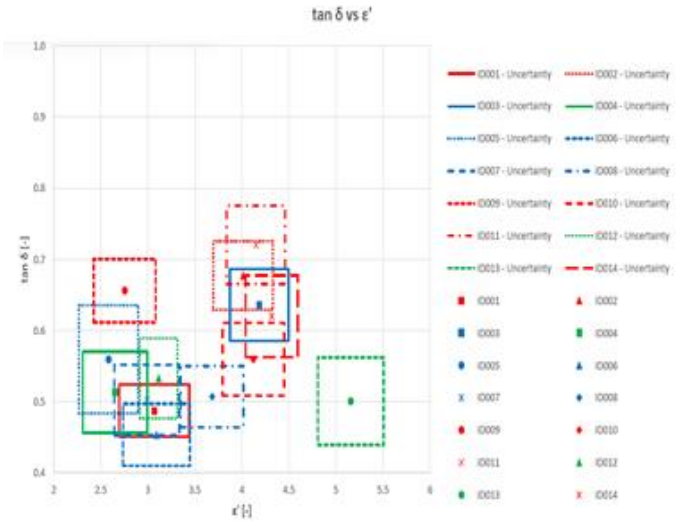

Figure 4.9: Loss tangent vs relative permittivity for food meals.The reference temperature for measurement is $T_{ref} = -20[degC]$.

figures 4.9 and 4.10. Red lines and markers represents foods that failed the standard thawing process with a standard commercial resonant cavity) and were characterized by low average temperatures and still frozen areas after the standard heating time. Blue lines and markers represents instead meals that passed the standard thawing process but demonstrated high non uniformity in the temperature distribution. Green lines instead demonstrated best results in therms of temperature and temperature uniformity. In figure 4.10 is highlighted the mean complex permittivity that is taken into account as reference value for the tailored resonant cavity.

4.2.5 Effective medium approximations

Many materials are not isotropic as ones seen in the previous chapter. It is then necessary to define a new mathematical permittivity that take into account the presence of two or more species in the medium. If we consider for example a mixture of sand and air it is

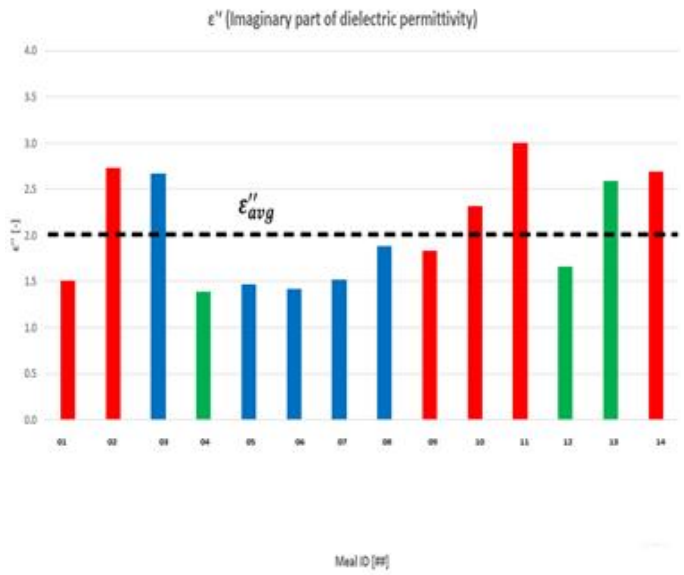

Figure 4.10: Imaginary part of the relative permittivity for food meals.The reference temperature for measurement is $T_{ref} = -20[degC]$. In figure is highlighted the average value considered for the MW design presented in chapter 7

clear that the presence of air interstices in the material changes the electric field distribution and then if we use the previous techniques a variation in the global impedance or scattering parameter [78]. Effective medium approximations (EMA) or effective medium theory (EMT) pertain to analytical or theoretical modeling that describes the macroscopic properties of composite materials. $EMAs$ or $EMTs$ are developed from averaging the multiple values of the constituents that directly make up the composite material. At the constituent level, the values of the materials vary and are in-homogeneous. Precise calculation of the many constituent values is nearly impossible. However, theories have been developed that can produce acceptable approximations which in turn describe useful parameters including the effective permittivity and permeability of the materials as a whole. In this sense, effective medium approximations are descriptions of a medium (composite material) based on the properties and the relative fractions of its components and are derived from calculations,[84] [82] and effective medium theory. Effective permittivity and permeability are averaged dielectric and magnetic characteristics of a micro-in-homogeneous medium. They both were derived in quasi-static approximation when electric field inside a mixture particle may be considered as homogeneous. So, these formulae can not describe the particle size effect.

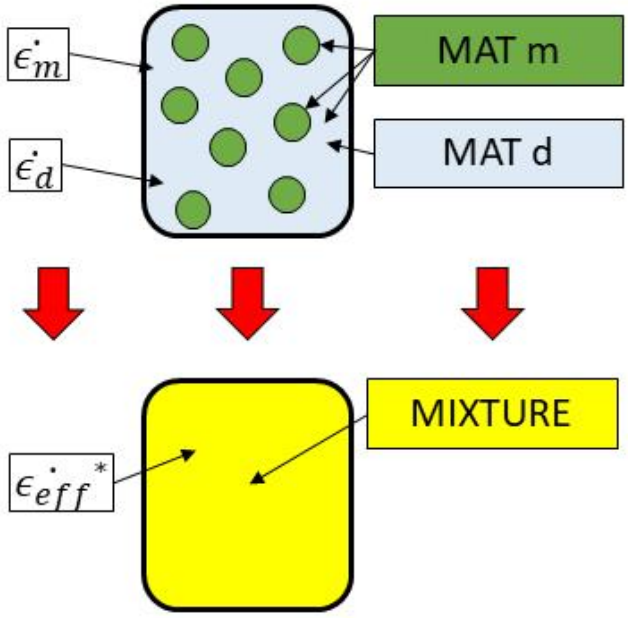

Figure 4.11: In-homogeneous dielectric material model: Dielectric material (ϵ_d with inclusions ϵ_m.

Bruggeman's model

Bruggeman found a a reasonable resonant curve for plasmon excitation in metal nanoparticles if their size is smaller than $10[nm]$[8] . But it is unable to describe the size dependence for the resonant frequency of plasmon excitations that are observed in experiments:

$$\epsilon_{eff} = \frac{1}{4}\left(H_b + \sqrt{H_b^2 + 8\epsilon_c\epsilon_d}\right) \tag{4.42}$$

where

$$H_b = (2 - 3c_c)\,\epsilon_d - (1 - 3c_c)\,\epsilon_c \tag{4.43}$$

where the medium is a mixture of dielectric particles and conductive particles and then it is possibly to define their relative complex permittivity: inside the picked conductive (ϵ_c) and inside the picked dielectric particle (ϵ_d) and finally the value of relative complex permittivty outside the picked particle (ϵ_{eff}) and the interaction with all the other particles is taken into account only in mean field approximation.

Maxwell Garnett equation

In the Maxwell Garnett approximation, the effective medium consists of a matrix medium with ϵ_m and inclusions with ϵ_i. He proposed his formula to explain colored pictures that

are observed in glasses doped with metal nanoparticles [26]. It describes the effective relative complex permittivity of the mixture (ϵ_{eff}) as function of the relative complex permittivity of the background medium (ϵ_d) and of the complex relative permittivity of small spherical inclusions (ϵ_m): The main hypothesis is that the volume fraction of inclusion is much lower then unity:

$$\begin{cases} \epsilon_{eff} = \epsilon_d \left[1 + 3\frac{c_m \Delta\epsilon}{\Delta\epsilon(1-c_m)+3\epsilon_d}\right] \\ \Delta\epsilon = \epsilon_m - \epsilon_d \end{cases} \tag{4.44}$$

where the volume fraction of inclusions (c_m) must be lower than the unity. In figure 4.12 are shown the dielectric effective loss tangent and the effective relative dielectric permittivity for two materials, varying the inclusions concentration. The red lines represent a dielectric lossy material in which are included lose-less low dielectric materials. The figure highlights that the effective dielectric permittivity decrease if the concentration of the low dielectric material (c_m) is increased. The effective loss tangent instead is not affected practically by the presence of a lossless material. Blu lines instead represent a low dielectric constant material with small losses (HDPE) in which are included high dielectric constant particles. The figure highlights the capability of dramatically increasing the loss tangent also by a ten factor. In figure arrows describe the effect of the concentration on the complex permittivity in the range 10^{-5} - 10^{-1}.

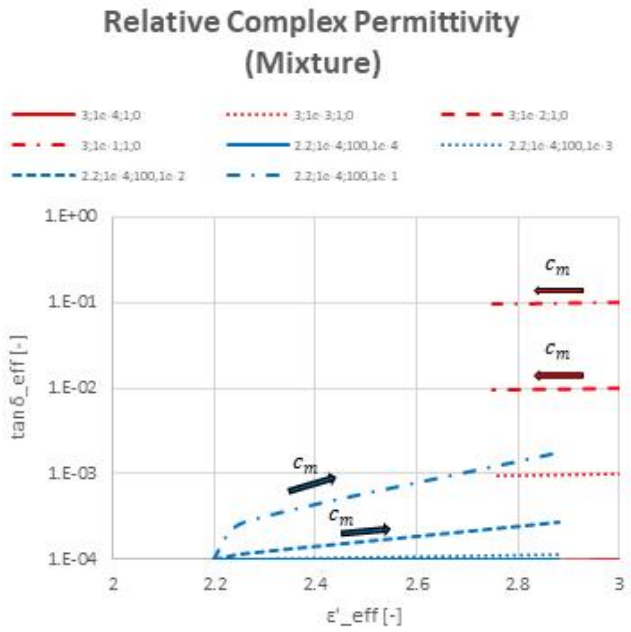

Figure 4.12: In-homogeneous dielectric material model: Dielectric material (ϵ_d with inclusions ϵ_m. Each analysed material is described as a vector: $[\epsilon_d^{'}; \tan\delta_d; \epsilon_m^{'}; \tan\delta_m]$. In figure are presented results varying the volume fraction from 10^{-5} to 10^{-1}.

Chapter 5

Radio-frequency (RF) Design

5.1 Radio-Frequency Heating systems

5.2 Impedance equivalent model

Generally it is useful to study an RF heater device as impedances. Because Maxwell's equations makes possible to solve the radio-frequency electromagnetic problem in a geometrical domain (Ω) in terms of electric field ($\mathbf{E}$ $[V/m]$) it is every-time possible to obtain a simple lumped-elements model transforming distributed variables of the main problem in space. Two main variables are electrostatic energy stored in the system and energy dissipated in the system for the effect of lossy materials, that typically are the materials that we want to heat. Electric potential energy (W_e $[J]$), is the potential energy that results from conservative Coulomb forces and is associated with electric charges and relative position of electric charges. In our case electric field are in any case time-varying fields. Many authors studied how to design electrodes and coils for RF application, and that field has grown, particularly thanks to magnetic resonance design [27] and radar design [22]. The electric potential energy (W_e) of the single charge (q $[C]$) in its position ($\mathbf{s}_i$ $[m]$) if an electric field ($\mathbf{E}$ $[V/m]$) is applied is defined by:

$$W_{e,i}(\mathbf{s}) = -\int_{\mathbf{s}_0}^{\mathbf{s}_i} q\mathbf{E}(\mathbf{s}) \cdot d\mathbf{s} = qV(\mathbf{s}) \tag{5.1}$$

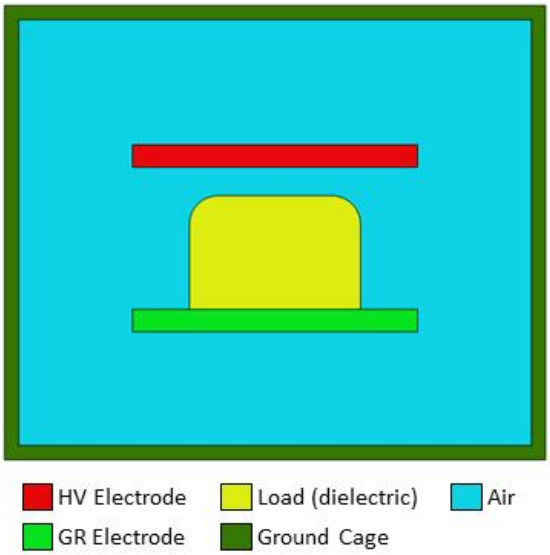

Figure 5.1: Radio-frequency heater: parallel-plate type. A rms voltage ($V_{rfh} = 1000[V]$ is applied between the two electrodes. GR (ground) Electrode is characterized by $V_{GR} = 0[V]$, HV (high-voltage) Electrode is characterized by $V_{GR} = 1000[V]$. The distance between the two electrodes is $d_{el} = 50[mm]$ and they have a width $w_{el} = 100[mm]$.

In other words, the electrostatic potential energy, is defined as the product of the charge and the electric potential ($V\ [V]$). If a system of N charges is considered, then it is possible to extend equation in a more general form, where each point-charge has a certain electric potential ($V_j\ [V]$):

$$W_e = \frac{1}{2}\sum_{j=1}^{N} q_j V(\mathbf{s}_j) = \frac{1}{4\pi\epsilon_0}\frac{1}{2}\sum_{j=1}^{N} q_j \left(\sum_{k=1,k\neq j}^{N} q_k \frac{1}{\mathbf{s}_{jk}}\right) \tag{5.2}$$

Starting from the definition shown in equation 5.2 it is possible to extend the concept to a more general continuous charge distribution, where an electric field distribution ($\mathbf{E}$) is applied (or an electric potential distribution (V)). Observing that Gauss's law for electric field 2.1 is still valid:

$$W_e = \frac{1}{2}\int_{\Omega} \rho(\mathbf{s})\, V(\mathbf{s}))\, d\Omega = \frac{1}{2}\int_{\Omega} \epsilon \|\mathbf{E}\|^2 d\Omega \tag{5.3}$$

and finally for a general point of the space it is possible to obtain the electric potential energy density per unit volume ($u_e\ [J/m^3]$) as:

$$w_e = \frac{1}{2}\epsilon\|\mathbf{E}\|^2 = \frac{1}{2}\epsilon_r\epsilon_0\|\mathbf{E}\|^2 \tag{5.4}$$

In a typical radio-frequency heating (RFH) device a certain sinusoidal voltage ($v_{RFH}(\omega t)\ [V]$) is applied between two electrodes that surround a dielectric material to be heated. In radio-frequency applications sources are time-varying greatness, typically characterized by fun-

damental frequencies greater than $1[MHz]$. All greatness will be computed with the root mean square (RMS) of the voltage (V_{RFH} $[V]$). If we consider a simple heater device consisting of a parallel-plate capacitor as in figure 5.1 (but what we'll say may be generalize for a more complex geometry as in the next chapters) and if a single source exists, it easy to compute the global capacitance of the radio-frequency heater, so the total energy accumulated in the capacitor (C_{RFH} $[F]$) is:

$$W_e = \frac{1}{2} C_{RFH} V_{RFH}^2 = \frac{1}{2} \int_\Omega \epsilon \|\mathbf{E}\|^2 d\Omega \tag{5.5}$$

and that means that if is possible to compute the distribution of the electric field for a certain domain, and the distribution of the permittivity is well known (and that is typical for radio-frequency heating applications), so it is possible to compute the total capacitance of the system (C_{RFH}), and this is a parallel-type capacitance (it is in parallel to the resistance that we'll compute soon from the total dissipated energy):

$$C_{RFH} = \frac{2W_e}{V_{RFH}^2} = \left(\int_\Omega \epsilon \|\mathbf{E}\|^2 d\Omega \right) \frac{1}{V_{RFH}^2} \tag{5.6}$$

Because of the system is characterized by time-varying (sinusoidal in a linearity condition) voltage so if we consider the fundamental frequency of the voltage (f $[Hz]$) it is possible also to compute the global parallel reactance (pure capacitor) of the system (X_p $[\Omega]$) as:

$$X_p = -\frac{1}{2\pi f C_{RFH}} = -\frac{V_{RFH}^2}{2\pi\epsilon_0} \frac{1}{2f} \left(\int_\Omega \epsilon_r \|\mathbf{E}\|^2 d\Omega \right)^{-1} \tag{5.7}$$

Considering equations 2.58 and 2.59 it is possible to prove that if a complex value of the permittivity is considered ($\epsilon = \epsilon_r (1 - i \tan\delta)$ $[-]$) equation does not change, instead it is possible to compute the total dissipated energy (power losses) in the domain as:

$$W_r = \int_\Omega w_r d\Omega = 2\pi f \epsilon_0 \int_\Omega \epsilon_r'' \|\mathbf{E}\|^2 d\Omega = 2\pi f \epsilon_0 \int_\Omega \epsilon_r \tan\delta \|\mathbf{E}\|^2 d\Omega \tag{5.8}$$

Now if a simple resistive electrical model is considered, the total dissipated energy can be modeled with a resistance in parallel to the previous purely capacitve impedance, and then the parallel resistance (R_p $[\Omega]$) is equal to:

$$R_p = \frac{V_{RFH}^2}{W_r} = \frac{V_{RFH}^2}{2\pi\epsilon_0} \frac{1}{f} \left(\int_\Omega \epsilon_r \tan\delta \|\mathbf{E}\|^2 d\Omega \right)^{-1} \tag{5.9}$$

Considering equations 5.7 and 5.9 it is finally possible to compute global series impedance in real part (R_s $[\Omega]$) and imaginary part (X_s $[\Omega]$) as:

$$R_s = X_p \left(\frac{R_p X_p}{R_p^2 + X_p^2} \right) \tag{5.10}$$

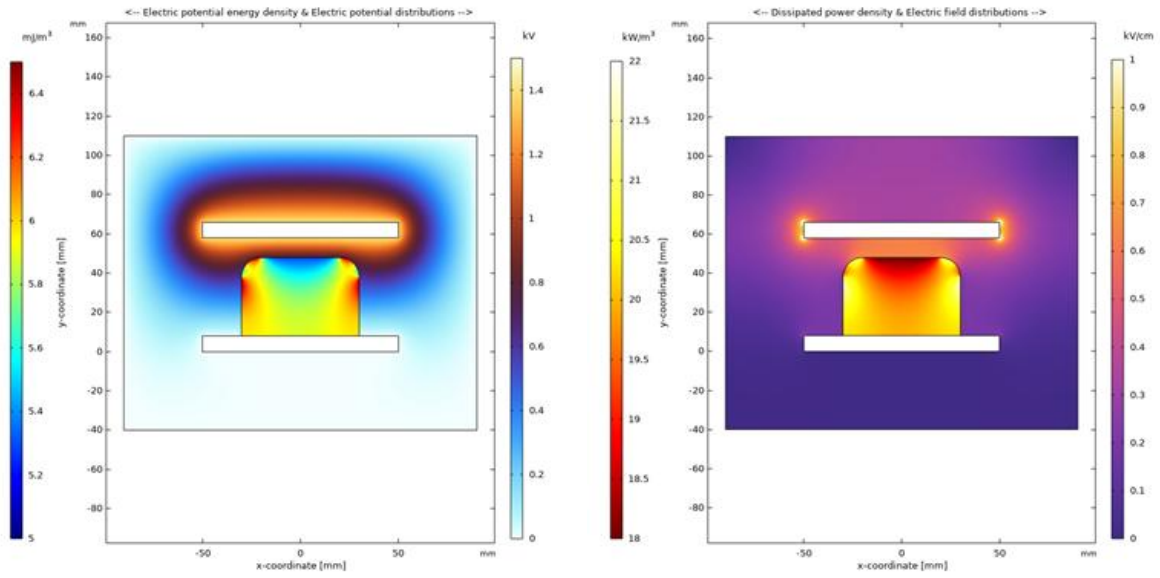

(a) **(b)**

Figure 5.2: Radio-frequency heater: parallel-plate type. (a) Electric potential density energy distribution in the dielectric load and electric potential distribution in the surrounding air. (b) Dissipated power density distribution in the dielectric load and electric field distribution in the surrounding air.

$$X_s = R_p \left(\frac{R_p X_p}{R_p^2 + X_p^2} \right) \tag{5.11}$$

and finally it is possible to obtain a synthetic form for the two components, in real part and imaginary part of the series impedance:

$$R_s = \frac{V_{RFH}^2}{2\pi\epsilon_0} \frac{2}{f} \frac{\int_\Omega \epsilon_r \tan\delta \|\mathbf{E}\|^2 d\Omega}{\left(\int_\Omega 2\epsilon_r \|\mathbf{E}\|^2 d\Omega\right)^2 + \left(\int_\Omega \epsilon_r \tan\delta \|\mathbf{E}\|^2 d\Omega\right)^2} \tag{5.12}$$

$$X_s = -\frac{V_{RFH}^2}{2\pi\epsilon_0} \frac{4}{f} \frac{\int_\Omega \epsilon_r \|\mathbf{E}\|^2 d\Omega}{\left(\int_\Omega 2\epsilon_r \|\mathbf{E}\|^2 d\Omega\right)^2 + \left(\int_\Omega \epsilon_r \tan\delta \|\mathbf{E}\|^2 d\Omega\right)^2} \tag{5.13}$$

In physics and engineering, the quality factor (Q [−]) is a dimensionless parameter that describes how under-damped an oscillator or resonator is. It is approximately defined as the ratio of the initial energy stored in the resonator to the energy lost in one full cycle of oscillation at a certain frequency. The quality factor is alternatively defined as the ratio of a resonator's centre frequency to its bandwidth when subject to an oscillating driving force. These two definitions give numerically similar, but not identical, results. Resonators with high quality factors have low damping, so that they ring or vibrate longer. The Q-factor (Q_{RFH} [−]) of a capacitor with a series loss resistance, that are defined in equations 5.12 and 5.13 is:

$$Q_{RFH} = -\frac{X_c}{R_c} = 2 \frac{\int_\Omega \epsilon_r \|\mathbf{E}\|^2 d\Omega}{\int_\Omega \epsilon_r \tan\delta \|\mathbf{E}\|^2 d\Omega} \tag{5.14}$$

Now we can try to deeper analyze electric resistance, reactance and quality factor. For a typical radio-frequency heating device we can easily distinguish several sub regions, that are function of their materials:

- dielectric regions (Ω_h) characterized by lossy materials where the lossy factor is greater than zero and relative permittivity not equal to the unity ($\epsilon_r > 1$ and $\tan\delta > 0$)
- dielectric regions (Ω_i) characterized by lossless materials and relative permittivity not equal to the unity ($\epsilon_r > 1$ and $\tan\delta = 0$)
- air (or vacuum) regions (Ω_a) characterized by lossless materials and relative permittivity equal to the unity ($\epsilon_r = 1$ and $\tan\delta = 0$)

It is clear that the union of the all regions defines the electromagnetic domain (Ω):

$$\Omega = \Omega_h \cup \Omega_l \cup \Omega_a \tag{5.15}$$

And so it possible to modify equations 5.12, 5.13 and 5.18 in:

$$R_s = \frac{V_{RFH}^2}{2\pi\epsilon_0}\frac{2}{f}\frac{\int_{\Omega_h}\epsilon_r \tan\delta \|\mathbf{E}\|^2 d\Omega}{\left(\int_\Omega 2\epsilon_r\|\mathbf{E}\|^2 d\Omega\right)^2 + \left(\int_{\Omega_h}\epsilon_r\tan\delta\|\mathbf{E}\|^2 d\Omega\right)^2} \tag{5.16}$$

$$X_s = -\frac{V_{RFH}^2}{2\pi\epsilon_0}\frac{4}{f}\frac{\int_{\Omega}\epsilon_r \|\mathbf{E}\|^2 d\Omega}{\left(\int_\Omega 2\epsilon_r\|\mathbf{E}\|^2 d\Omega\right)^2 + \left(\int_{\Omega_h}\epsilon_r\tan\delta\|\mathbf{E}\|^2 d\Omega\right)^2} \tag{5.17}$$

$$Q_{RFH} = -\frac{X_c}{R_c} = 2\frac{\int_\Omega \epsilon_r\|\mathbf{E}\|^2 d\Omega}{\int_{\Omega_h}\epsilon_r\tan\delta\|\mathbf{E}\|^2 d\Omega} \tag{5.18}$$

and finally it possible to define the global series impedance of the radio-frequency applicator (Z_s $[Ohm]$) as:

$$\dot{Z}_s = R_s + iX_s \tag{5.19}$$

5.3 Series impedance study

Equations 5.16, 5.17 and 5.18 are not so easy to be analyzed. If we try to explicit in a different form the terms it is possible to obtain a more understandable mathematical model. Starting from equations 5.7 and 5.9 it is possible to find the series resistance and the series reactance in a different way. But before we explicit the term $\frac{R_pX_p}{R_p^2+X_p^2}$ as:

$$\frac{R_pX_p}{R_p^2+X_p^2} = \frac{2\omega W_r W_e}{(W_r^2 - 2\omega W_e)^2} \tag{5.20}$$

and finally the series resistance and the series reactance are:

$$R_s = V_{RFH}^2 \frac{1}{\left[1 + \left(2\omega \frac{W_e}{W_r}\right)\right]\left[1 - \left(2\omega \frac{W_e}{W_r}\right)\right]} \tag{5.21}$$

$$X_s = V_{RFH}^2 \frac{-1}{\left[1 + \left(2\omega \frac{W_e}{W_r}\right)^{-1}\right]\left[1 - \left(2\omega \frac{W_e}{W_r}\right)^{-1}\right]} \tag{5.22}$$

Now, to make our life easier it is possible to define the dimensionless variable Ψ as:

$$\Psi = 2\omega \frac{W_e}{W_r} \tag{5.23}$$

and obtain:

$$R_s = V_{RFH}^2 \frac{1}{(\Psi + 1)(\Psi - 1)} \tag{5.24}$$

$$X_s = V_{RFH}^2 \frac{-\Psi}{(\Psi + 1)(\Psi - 1)} \tag{5.25}$$

and if we use equations 5.24 and 5.24 in the definition of the quality factor we obtain an extremely interesting form of it!

$$Q_{RFH} = -\frac{X_s}{R_s} = \Psi = 2\omega \frac{W_e}{W_r} = 4\pi f \frac{W_e}{W_r} \tag{5.26}$$

Remembering now that it is possible to explicit also the electric energy and the dissipated energy with equations 5.5 and 5.8 we'll study Ψ:

$$\Psi = \frac{\int_\Omega \epsilon_r \|\mathbf{E}\|^2 d\Omega}{\int_\Omega \epsilon_r \tan\delta \|\mathbf{E}\|^2 d\Omega} \tag{5.27}$$

Now we remember that we can partition the domain in function of its properties and because $\Omega = \Omega_h + \Omega_i + \Omega a$:

$$\Psi = \frac{\Psi_1 + \Psi_2 + \Psi 3}{\Psi_4} \tag{5.28}$$

Now first of all we study the denominator of Ψ:

$$\Psi_4 = \int_{\Omega_h} \epsilon_{r,h} \tan\delta_h \|\mathbf{E}\|^2 d\Omega + \int_{\Omega_i} \epsilon_{r,i} \tan\delta_i \|\mathbf{E}\|^2 d\Omega + \int_{\Omega_a} \epsilon_{r,i} \tan\delta_a \|\mathbf{E}\|^2 d\Omega \tag{5.29}$$

and remembering that for lossless materials (Ω_i and Ω_a) the loss factor must be equal to zero:

$$\Psi_4 = \epsilon_{r,h} \tan\delta_h \int_{\Omega_h} \|\mathbf{E}\|^2 d\Omega \tag{5.30}$$

We can do the same thing for the nominator of Ψ:

$$\Psi_1 = \int_{\Omega_h} \epsilon_{r,h} \|\mathbf{E}\|^2 d\Omega = \epsilon_{r,h} \int_{\Omega_h} \|\mathbf{E}\|^2 d\Omega \tag{5.31}$$

for the term Ψ_2 if we have N different materials in the electromagnetic problem so:

$$\Psi_2 = \int_{\Omega_i} \epsilon_{r,i} \|\mathbf{E}\|^2 d\Omega = \sum_{i=1}^{N} \left(\epsilon_{r,i} \int_{\Omega_i} \|\mathbf{E}\|^2 d\Omega \right) \tag{5.32}$$

and finally the term Ψ_3, because it's materials can only be air or vacuum, with a relative permittivity equal to one:

$$\Psi_3 = \int_{\Omega_a} \epsilon_{r,a} \|\mathbf{E}\|^2 d\Omega = \int_{\Omega_a} \|\mathbf{E}\|^2 d\Omega \tag{5.33}$$

Now considering equations 5.28,5.31, 5.32, 5.33, and 5.30 it possible to obtain a more complex form of Ψ:

$$\Psi = \frac{1}{\tan \delta_{r,h}} + \frac{1}{\epsilon_{r,h} \tan \delta_{r,h}} \left(A_0 + \sum_{i=1}^{N} \epsilon_{r,i} B_i \right) \frac{1}{\gamma} \tag{5.34}$$

where the new variable gamma (γ $[Vm]$) is is the volume integral of the square of the electric field in the material that we want to heat:

$$\gamma = \int_{\Omega_h} \|\mathbf{E}_h\|^2 d\Omega \tag{5.35}$$

the term A_0 ($[Vm]$) is the volume integral of the square of the electric field in air:

$$A_0 = \int_{\Omega_a} \|\mathbf{E}_a\|^2 d\Omega \tag{5.36}$$

and the term B_i ($[Vm]$) is the volume integral of the square of the electric field inside a dielectric material multiplied for its relative permittivity:

$$B_i = \epsilon_{r,i} \int_{\Omega_i} \|\mathbf{E}_i\|^2 d\Omega \tag{5.37}$$

and it is possible to define also a term that takes into account all dielectrics materials B_{i0} ($[Vm]$):

$$B_0 = \sum_{i=1}^{N} B_i \tag{5.38}$$

At that point it possible to easily study Ψ:

$$\Psi = \frac{1}{\tan \delta_{r,h}} + \frac{1}{\epsilon_{r,h} \tan \delta_{r,h}} (A_0 + B_0) \frac{1}{\gamma} \tag{5.39}$$

Because of the model is analyzing a circuit in which we can only have resistors and capacitors, the quality factor must be greater or equal to zero. That involves

$$\Psi \geq 0 \tag{5.40}$$

the second constraint derives from equation 5.24. The model can only admit positive resistances, so:

$$R_s \geq 0 \Rightarrow \Psi \leq -1 \ \ \& \ \ \Psi \geq 1 \tag{5.41}$$

the third constraint derives from equation 5.25. The model can only admit positive resistances, so:

$$X_s \leq 0 \Rightarrow \Psi \geq -1 \;\; \& \;\; \Psi \leq 0 \Psi \geq 1 \tag{5.42}$$

and finally combining the tree existence conditions, ($\Psi \geq 1$) it is possible to move the constraint to gamma, but knowing that gamma may only be positive (because of it is the integral of the square of the electric field in the medium that we want to heat) and finally we obtain the existence range for the solution:

$$\gamma \geq -\frac{A_0 + B_0}{\epsilon_{r,h}\,(1 - \tan\delta_h)} \Rightarrow \gamma \geq 0 \tag{5.43}$$

In a RF-heating process typically we want to transfer a certain power ($W_m\ [W]$) directly to the load. Therefore it is possible to define:

$$\widetilde{W}_m = \omega \epsilon_0 \epsilon_{r,h} \tan\delta_{r,h} \int_{\Omega_h} \|\widetilde{\mathbf{E}}_h\|^2 d\Omega \tag{5.44}$$

and now we observe that the integral term in the right-hand side of the previous equation must be constant (but not the electric field distribution, it may vary) and then:

$$\widetilde{\gamma} = \frac{\widetilde{W}_m}{\omega \epsilon_0 \epsilon_{r,h} \tan\delta_{r,h}} \tag{5.45}$$

And considering the final solution of the problem the equation 5.45 highlights that the general term gamma that we defined previously is fixed for a certain frequency and for a certain material that we want the heat! Finally we obtain an extremely nice formulation of the problem:

$$\Psi = \frac{1}{\tan\delta_{r,h}} + \frac{\epsilon_0 \omega}{\widetilde{W}_m} A_0^* + \frac{2\epsilon_0 \omega^2}{\widetilde{W}_m} B_0^* \tag{5.46}$$

$$\Psi = \frac{1}{\tan\delta_{r,h}} + \frac{\epsilon_0 \omega}{\widetilde{W}_m} A_0^* + \frac{\epsilon_0 \omega}{\widetilde{W}_m} B_0^* \tag{5.47}$$

where the two terms A_0^* and B_0^* are the integral of the square of electric fields that solve the problem.

5.4 Matching network design

We discussed in previous paragraph 5.2 that a radio-frequency heating device can be modeled with its impedance and summarized as an electrical circuit. We know that transmission lines have a characteristic impedance and we know that this impedance is an important factor

in RF circuitry, because impedances must be matched to prevent standing waves and to ensure efficient transfer of power from source to load. In figure 5.3 are shown voltage sources and load impedances that need to be adapted with a specific matching network.

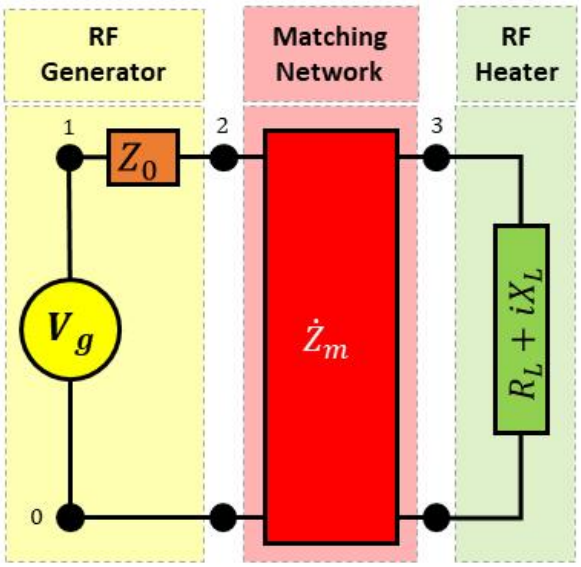

Figure 5.3: Electrical circuit diagram of Radio-frequency heating device. In figure are shown high frequency voltage generator (yellow), RF heater (green) and matching network (red). The electrical ground ($V = 0[V]$) is the node 0.

5.4.1 Matching Network Characterization

Matching networks for radio frequency heating are characterized by high currents and high voltages, because of we want to transfer power to dielectric loads. As seen in the previous section we know that to total power in the medium that we want to load is proportional to the square of the average electric field applied to it. The electric field is also proportional to the voltage difference between the two RF-electrodes. In figure 5.4 the voltage applied to the electrodes is the potential difference between nodes 3 and 0 ($V_{RFH} = V_3 - V_0$ $[V]$). Because of the power that we want to transfer in a typical RF-heater device may vary a lot, from a few tenths of watts to thousands of watts, it is necessary to define different matching networks and different components with which it is possible to design them.

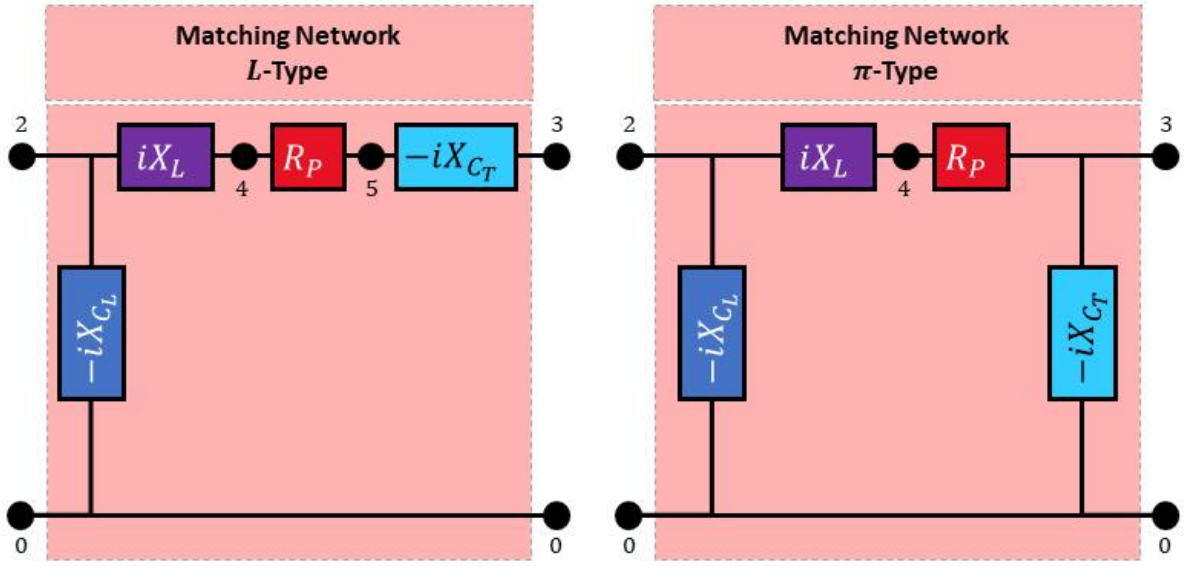

(a) **(b)**

Figure 5.4: Electrical circuit diagram of two typical matching networks for RF-heating process: (a) L-type matching network, (b) π-type matching network. In figure are shown load capacitance (C_T) (blue), tune capacitance (C_T) (turquoise) and series inductance (violet) and series resistance (R_P) (red). The electrical ground ($V = 0[V]$) is the node 0. RF-Generator is connected between nodes 2 and 0, instead the RF-heater device is connected between nodes 3 and 0.

5.4.2 Maximum power transfer theorem

If a load is connected to a generator and we want to transfer the highest possible power to the load we know that we need to solve the so called maximum power transfer problem. In an RF heating process we want to transfer the total power from the generator to the load, and in other words we want to cancel the reflected power. It is well known that the condition that makes possible to transfer the maximum power is:

$$Z_{\dot{L}OAD} = \dot{Z}_0 \Rightarrow (R_{LOAD} + iX_{LOAD}) = (R_0 + iX_0) \tag{5.48}$$

In our RF and MW cases the impedance of the generator is purely resistive: $\dot{Z}_0 = Z_0 + i0$ and that finally define the two equations that is necessary to solve every time to guarantee zero-reflections in the network:

$$Re\left(\dot{Z}_{LOAD}\right) = R_{LOAD} = Z_0 \tag{5.49}$$

$$Im\left(\dot{Z}_{LOAD}\right) = X_{LOAD} = 0 \tag{5.50}$$

Because, as seen in previous paragraphs, the global impedance of the system is only function of the topology of the device and of the material properties, it is every time necessary

for an RF-heating process to properly design and include a matching network between the load and the RF-heater device that has the function of transforming the load impedance to a "good" impedance that satisfies equations 5.49 and 5.50

5.4.3 L-Network

Now we consider a typical matching network composed of a parallel capacitance (C_L $[F]$) (in parallel with respect to the generator), of a series capacitance (C_T $[F]$) and an inductance (L $[H]$) (in series with respect to the tune capacitance) as shown in figure 5.9. Because of in a real matching network components are real it is necessary to model also resistive components that generate losses inside the matching network. In practice, the most important element that dissipates power is the series inductance (R_P $[\Omega]$). Typical RFH L-networks match well to systems with an average resistance region (around $5[\Omega]$), and they are able to cope with varying load capacitance: They also are a suitable choice for plastics welding with a good loss factor (ϵ'') where their ability to adapt also to fast capacitance variations. The main weakness of L-networks is that the load resistance (or resistive part of a series impedance) must generally below $50[\Omega]$. A low load resistance may involve to typically increase the load capacitance, and typically another matching type network (T-type) can be more suitable.

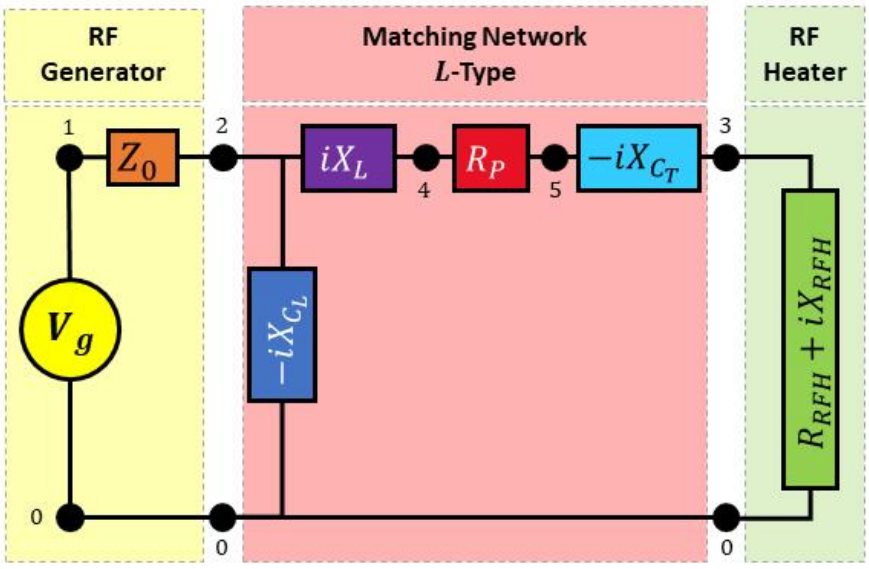

Figure 5.5: Electrical circuit diagram of a π-type matching network for Radio-frequency heating devices. In figure are shown load capacitance (C_T) (blue), tune capacitance (C_T) (turquoise) and series inductance (violet) and series resistance (R_P) (red). The electrical ground ($V = 0[V]$) is the node 0. RF-Generator is connected between nodes 2 and 0, instead the RF-heater device is connected between nodes 3 and 0.

First of all it is necessary to compute the equivalent impedance of the network at the generator nodes, or in other words to analyze the impedance seen from the RF-generator (Z_{eq} [Ω]), after having defined electrical reactances at the given working frequency (f_{nom} [MHz]). In the present work instead of the frequency, we'll use the angular frequency ($\omega = 2\pi f_{nom}$ [rad/s]). The impedances of capacitors and inductance are then:

$$\dot{Z}_{CT} = -iX_{CT} = -i\frac{1}{\omega C_T} \ , \ \dot{Z}_{CL} = -iX_{CL} = -i\frac{1}{\omega C_L} \ , \ \dot{Z}_L = iX_L = \omega L \tag{5.51}$$

The equivalent impedance for the L-network is the parallel of the load capacitance with the series of the RF-heating device load with the tune capacitance and real inductance:

$$\dot{Z}_{eq} = R_{eq} + iX_{eq} = \frac{\left(\dot{Z}_{RFH} + \dot{Z}_{CT} + \dot{Z}_L + R_P\right)\dot{Z}_{CL}}{\dot{Z}_{RFH} + \dot{Z}_{CT} + \dot{Z}_L + R_P + \dot{Z}_{CL}} \tag{5.52}$$

And then dividing 5.52 in its real and imaginary parts as in the two following equations it is possible to deeper analyze the matching condition and its equations:

$$R_{eq} = \frac{\left(R_{RFH} + R_P\right)X_{CL}.^2 + \left(X_{RFH} + X_L\right)X_{CT}X_{CL}}{\left(R_{RFH} + R_P\right)^2 + \left(X_{RFH} + X_L - X_{CT} - X_{CL}\right)^2} \tag{5.53}$$

$$X_{eq} = -\frac{X_{CL}\left[\left(R_{RFH} + R_P\right)^2 + \left(X_{RFH} + X_L - X_{CT}\right)^2 - \left(X_{RFH} + X_L - X_{CT}\right)X_{CL}\right]}{\left(R_{RFH} + R_P\right)^2 + \left(X_{RFH} + X_L - X_{CT} - X_{CL}\right)^2} \tag{5.54}$$

In first analysis in a typical RF heating device, but more generally for a certain transmission problem with a L-network topology it is necessary to design the value of the tune capacitance (C_T) and of the load capacitance C_L with a certain inductance that makes sense. Normally, with a an iterative method it is possible to find a good value for the series inductance L that guarantee the matching condition. Figure 5.7 shows a practical case of matching where the out-of-matching parameter ($\dot{\Delta}_m$ [Ω]) is the complex operator:

$$\dot{\Delta}_m = |\ R_{eq} - Z_0| + i|\ R_{eq}| \tag{5.55}$$

The figure results of the figure are obtained varying the tune capacitance and the load capacitance, searching a matching condition. It is clear that if Δ_m is equal to zero it means we found the matching condition, and we solved the matching problem. It is useful to better understand the function that we want to solve. To do that we may, use two new variables (α,β) that takes into account the resistive effects of the system and the reactances of the inductance and of the load. For the moment they are not unknowns because we impose them (parameters).

$$\alpha = R_{RFH} + R_P \tag{5.56}$$

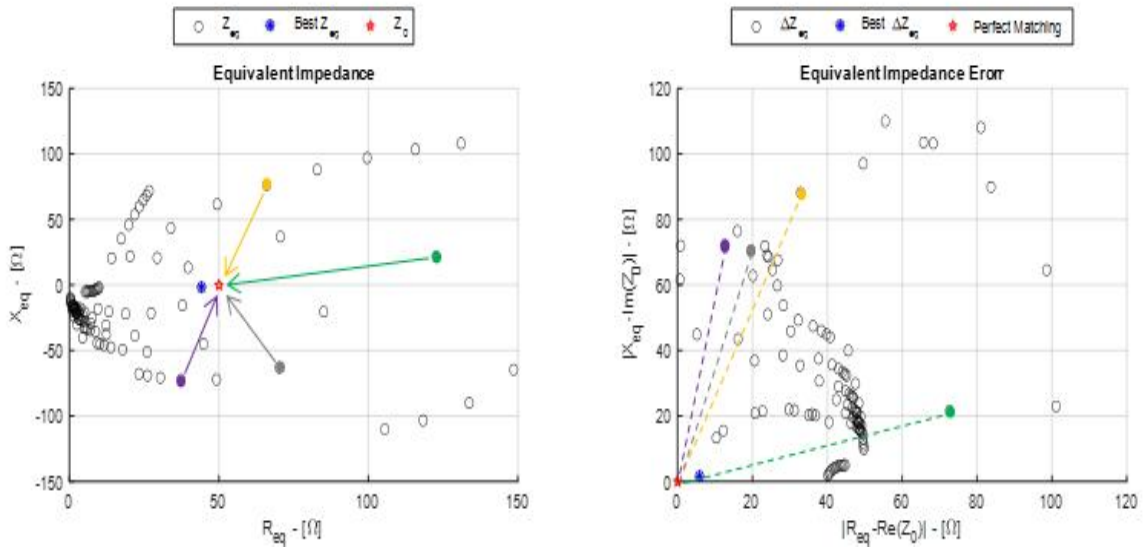

(a) (b)

Figure 5.6: Practical RF network case at $f_{nom} = 27.125[MHz]$ with $\dot{Z}_{RFH} = 10(1-i)[\Omega]$ and $L = 400[nH]$. (a) represents the representation in the real-imaginary plane of the equivalent impedance of the system. (b) represents the out-of-matching parameter in term of impedance, in real part and imaginary part.

$$\beta = X_{RFH} + X_L \tag{5.57}$$

and it is possible to use equations 5.53 and 5.54 written in 5.49 and 5.50 to write two functions F_r and F_i that must be zero.

$$F_r = \alpha^2 + \beta^2 + X_{CT}.^2 + X_{CL}^2 \left(1 - \frac{\alpha}{Z_0}\right) - 2\beta\left(X_{CT} + X_{CL}\right) + 2X_{CT}X_{CL} = 0 \tag{5.58}$$

$$F_i = \alpha^2 + \beta^2 + x_{CT}^2 - \beta\left(2X_{CT} + X_{CL}\right) + X_{CT}X_{CL} = 0 \tag{5.59}$$

It is possible to solve these two second order equations and for example to constraints the tune reactance value (C_T) to the load reactance (C_L):

$$X_{CT} = \frac{Z_0\beta - X_{CL}\left(Z_0 - \alpha\right)}{Z_0} \tag{5.60}$$

Because of, for definition, the tune capacitance is defined before as a positive value (the negative sign is inside the impedance), the equation 5.60 must be a real and positive value, and that add to the matching system a new necessary constraint:

$$X_{CL} \leq \frac{Z_0 - \beta}{Z_0 - \alpha} \tag{5.61}$$

Combining equation 5.60 and 5.59 it is possible finally to obtain the analytical solution for the considered *L*-network topology that guarantee the matching condition only knowing the

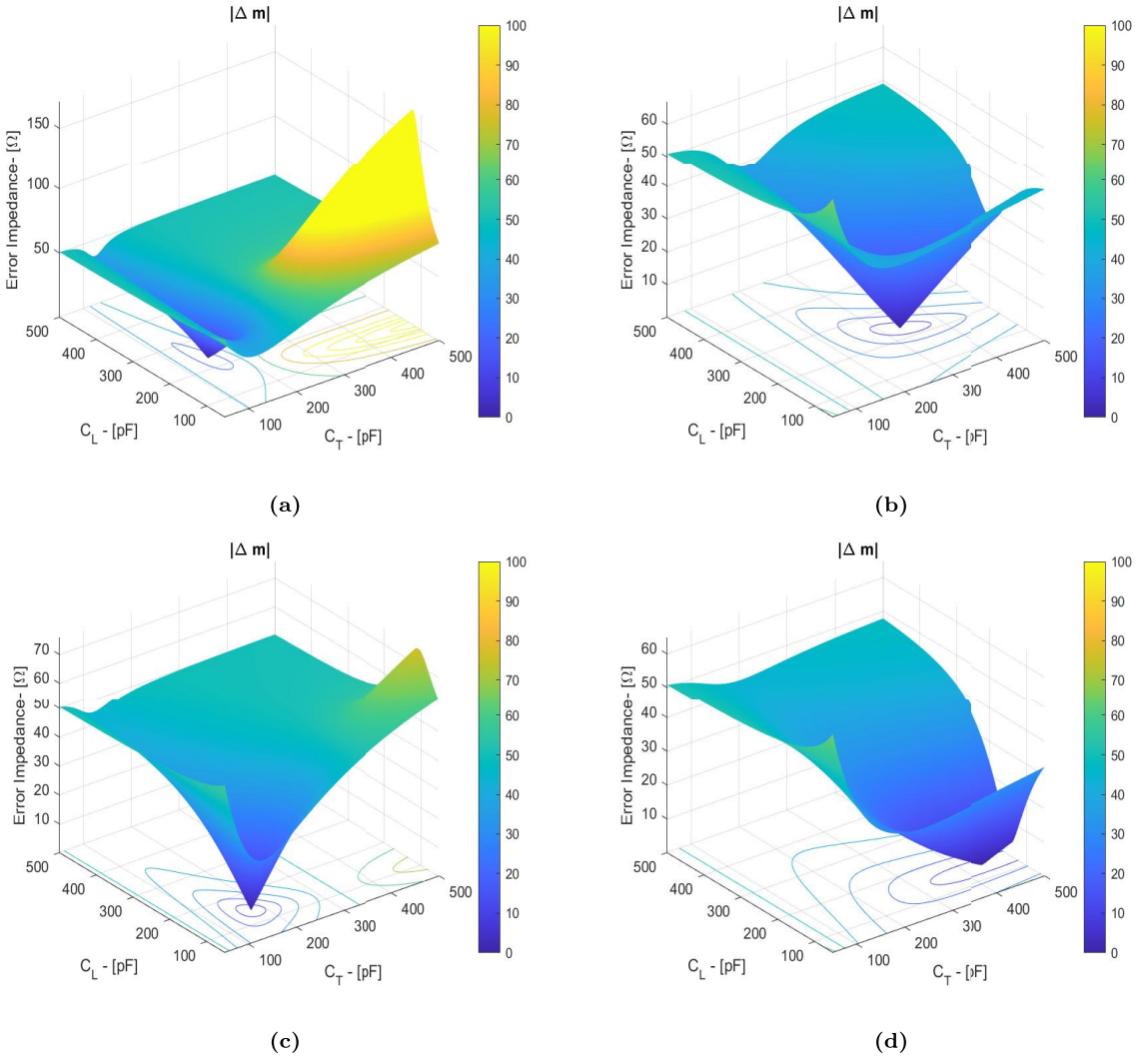

Figure 5.7: Out-of-matching parameter in modulus as function of tune matching (C_T) and load matching (C_L). (a) $Z_{RFH} = 10(1-i)$, (b) $Z_{RFH} = 10(1-i3)$, (c) $Z_{RFH} = 20(1-0.5i)$, (b) $Z_{RFH} = 20(1-1.5i)$

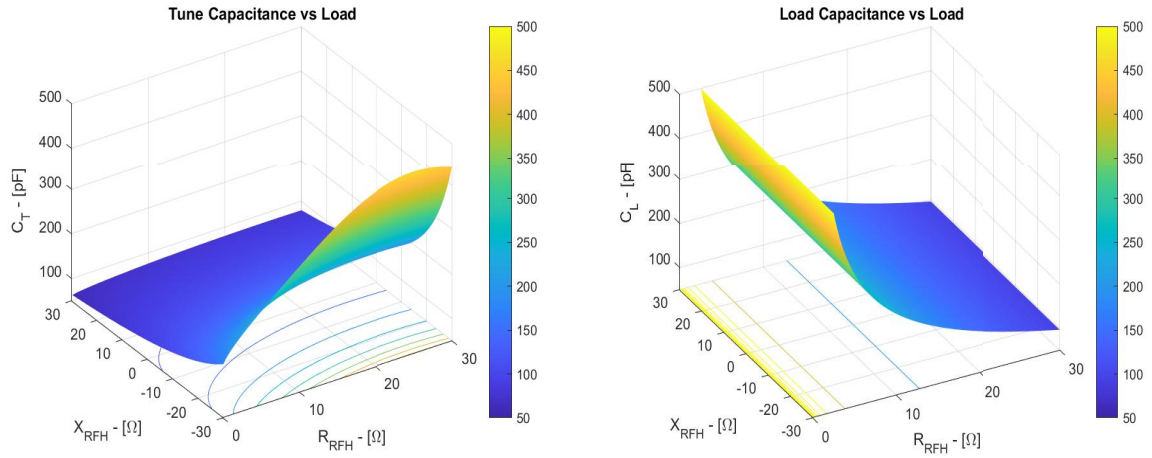

(a) **(b)**

Figure 5.8: Analysis of a matching response surface. The figure is obtained computing the matching parameters (tune capacitance and load capacitance) for a wide range of load impedance ($\dot{Z}_{eq} = R_{eq} + iX_{eq}$ [Ω]). The considered system is a specific matching network designed for RF-heating process. (a) Variable tune capacitance C_T $[pF]$, (b) Variable load capacitance (C_L $[pF]$).

RF-device impedance and (at the moment) the constant matching inductance (L $[H]$):

$$C_L = \frac{1}{\omega}\left(\alpha\frac{Z_0}{\sqrt{\alpha\left(Z_0-\alpha\right)}}\right)^{-1} \tag{5.62}$$

$$C_T = \frac{1}{\omega}\left(\beta-\sqrt{\alpha\left(Z_0-\alpha\right)}\right)^{-1} \tag{5.63}$$

Figure 5.8 highlights that if the load varies it is necessary to adapt the matching network to the load. In an RF typical process that every time happens because of three main phenomena: temperature variation, phase change and variation of the humidity. Each dielectric material has different properties, and then different variations with temperature and humidity. For a drying process for example the variation can be extremely high and fast, because of the system, and we can say the electric field, is "measuring" dielectric properties variations ($\epsilon_r^{'}$ and $\epsilon_r^{''}$). A practical result of that is that the components of the matching network (typically capacitors) must vary their values, and sometimes also in an high range, if the load varies a lot. The figure shows that when the response surface goes to zero the perfect matching condition is achieved, and four different load impedance ($\dot{Z}_{RFH}$) are considered.

5.4.4 π-Network

Now we consider a typical matching network composed of a parallel capacitance (C_L

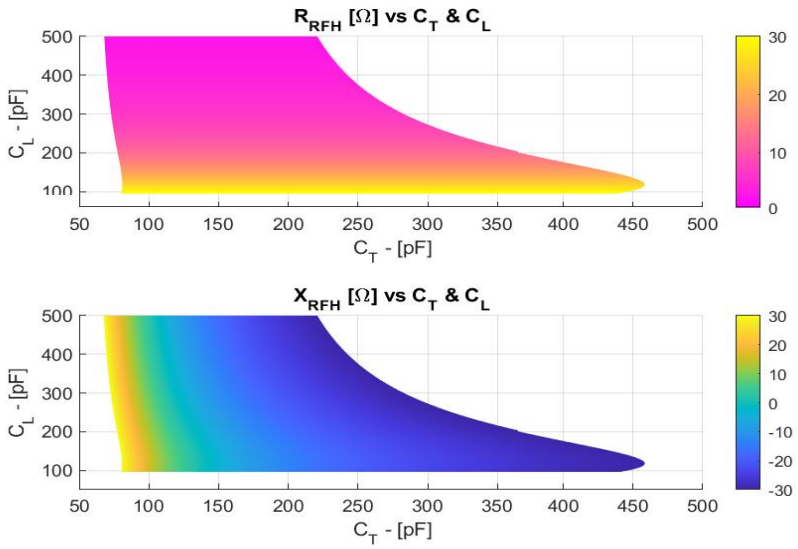

Figure 5.9: Matching area for a matching network with $L = 400$ $[nH]$ in a wide range of loads.

$[F]$) (in parallel with respect to the generator), of a parallel capacitance to the load (C_T $[F]$) and a "central" inductance (L $[H]$) (in series with respect to the parallel of the load and the tune capacitance) as shown in figure **??**. Because of in a real matching network components are real it is necessary to model also resistive components that generate losses inside the matching network. In practice, the most important element that dissipates power is the series inductance (R_P $[\Omega]$).

5.4.5 T-Network

Now we consider a typical matching network composed of a parallel capacitance (C_L $[F]$) (in parallel with respect to series of the load and the series inductance), of a series capacitance (C_T $[F]$) with the generator and finally an inductance (L $[H]$) (in series with the load) as shown in figure 5.11. Because of in a real matching network components are real it is necessary to model also resistive components that generate losses inside the matching network. In practice, the most important element that dissipates power is the series inductance (R_P $[\Omega]$). T-network finds use where the load resistance is extremely low, even below 1$[\Omega]$. This can be a typical value of the load for dielectric heating process with load characterized by extremely low dielectric permittivity or low loss factor, and also it can occur in applications where there is a poor coupling between the load material and the electric field generated by the system.The T-net is able to cope with large variations in the load capacitance only if it is possible to vary the inductance. One of the main benefit it is that the bulk of the load current

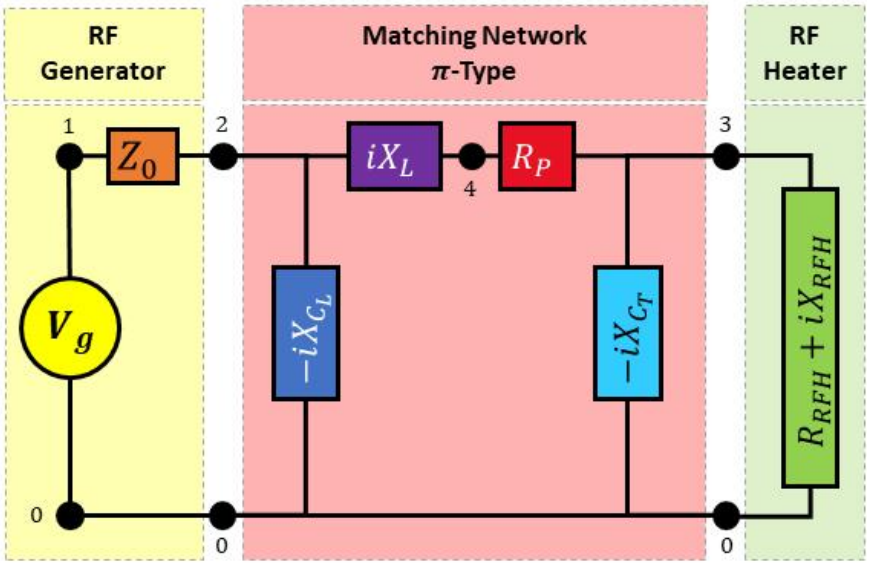

Figure 5.10: Electrical circuit diagram of a π-type matching network for Radio-frequency heating devices. In figure are shown load capacitance (C_T) (blue), tune capacitance (C_T) (turquoise) and series inductance (violet) and series resistance (R_P) (red). The electrical ground ($V = 0[V]$) is the node 0. RF-Generator is connected between nodes 2 and 0, instead the RF-heater device is connected between nodes 3 and 0.

passes through the series inductor and the load capacitor but not through the tune capacitor. T-networks can achieve the so called auto-matching (matching into it's own circuit) risking also high overheating of its components: for that reason in many industrial applications may be necessary to use water-cooling systems for its components.

5.4.6 Matching Network components design

When we design a matching network we know that we have two different approaches: the first one is to design a complete customized matching network, and that means to design and realize capacitors and inductors with specific values (and may be extremely expensive), the second is to choose components offered by the high voltage, high current and high frequency components manufacturers market. Because of the problem at the end is to design or choose the capacitors, because of it is extremely easy to properly design and realize a specific inductance as shown in the next rows.

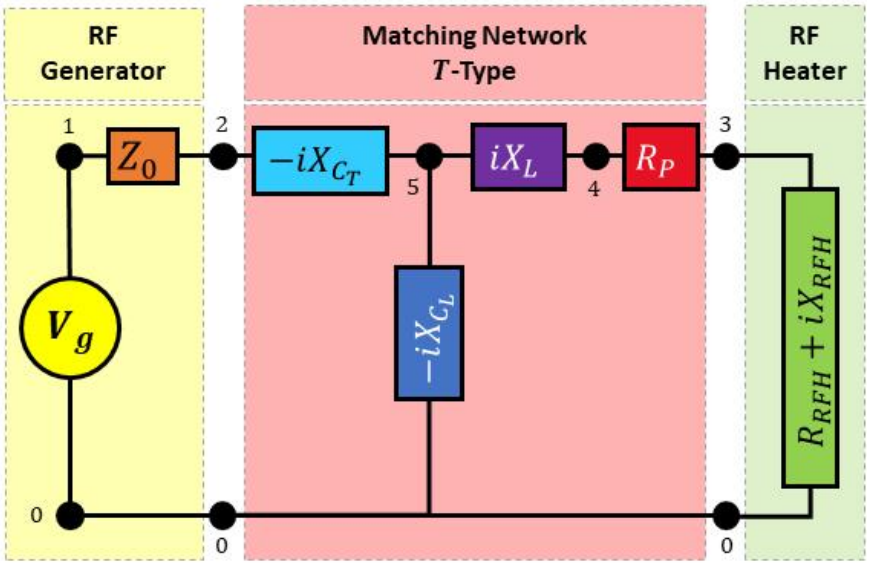

Figure 5.11: Electrical circuit diagram of a T-type matching network for Radio-frequency heating devices. In figure are shown load capacitance (C_T) (blue), tune capacitance (C_T) (turquoise) and series inductance (violet) and series resistance (R_P) (red). The electrical ground ($V = 0[V]$) is the node 0. RF-Generator is connected between nodes 2 and 0, instead the RF-heater device is connected between nodes 3 and 0.

Inductance design

I highlights that if someone want to design it in a in a more precise way it is possible to design it, for example with a FEM method, and design the the most correct geometry, also taking into account non-linear problems. If we consider a simple solenoid inductor, with a certain number of coils (N $[-]$), a certain inner radius (R $[m]$), a certain total length (L $[m]$), a certain conductive thickness (t $[mm]$) and filled with a material with a certain relative permeability (μ_r $[-]$) it is easy to compute the inductance with a simple analytical approach:

$$L = \frac{\Phi_B}{I} = \pi \mu_0 \mu_r \frac{N^2 R^2}{L} \tag{5.64}$$

for a real component it is known that also a resistive component must exist, because of the conductive material of the inductor it is not ideal. And if we consider a certain electrical resistivity for the conduction material (ρ_{el} $[\Omega m]$) and we know the working frequency of that component, assuming that the current density distribution does not "cover" the whole thickness of the conductor, but it distributes in a penetration depth (δ_P $[m]$):

$$R_P = \frac{\rho_{el} C}{\Sigma} \tag{5.65}$$

where C $[m]$ is the total length of the solenoid, and Σ is the surface where the current density "flows":

$$C = 2\pi N \sqrt{R^2 + \left(\frac{L}{2\pi N}\right)^2} \tag{5.66}$$

$$\Sigma = \pi \left[t^2 - (t - \delta_P)^2\right] \tag{5.67}$$

and finally the total resistance of the inductor is:

$$R_P = 2\rho_{el} N \frac{\sqrt{R^2 + \left(\frac{L}{2\pi N}\right)^2}}{\delta_P \left(2t - \delta_P\right)} \tag{5.68}$$

where the penetration depth is:

$$\delta_P = \sqrt{\frac{2\rho_{el}}{\omega \mu_0 \mu_r}} \tag{5.69}$$

Capacitor design

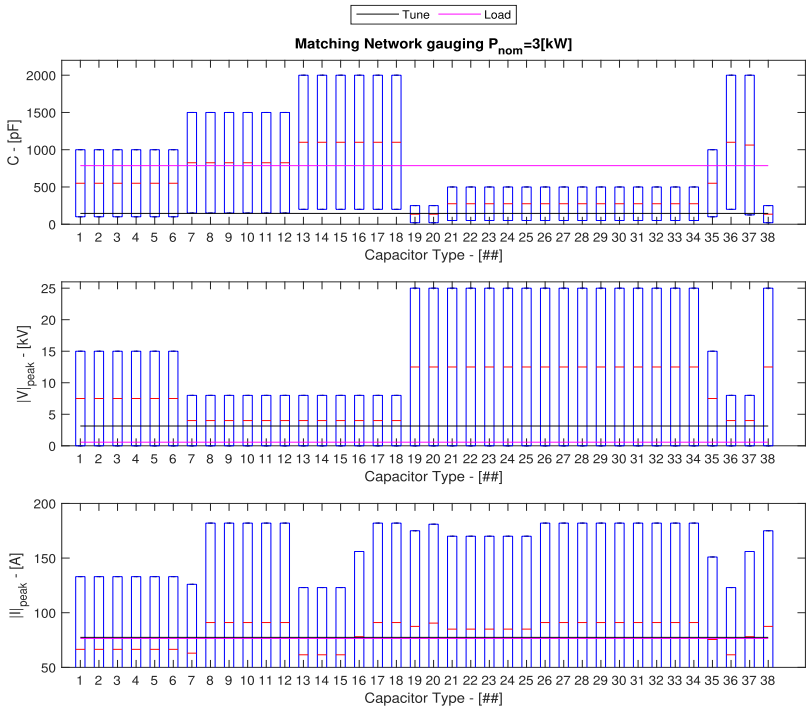

Figure 5.12: Choose of the capacitors for the L-network layout for a specific load.

5.4.7 Smart Matching Network

Working again with matching transfer function it is possible to obtain the load impedance during the process, and for example measure the temperature of the known load or the humidity.

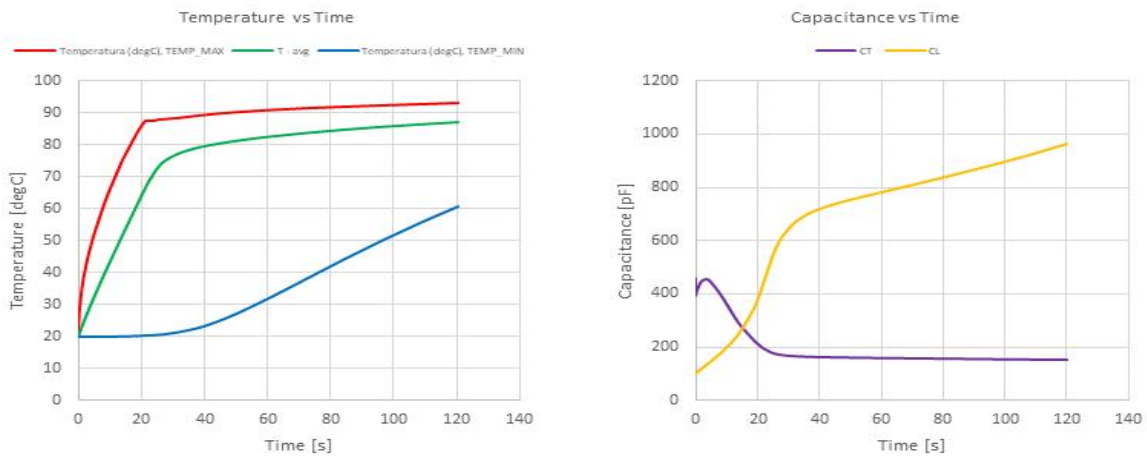

(a) **(b)**

Figure 5.13: Temperature evolution and matching components variation during the process for the RF drying device. (a) Temperature, (b) Tune capacitance and Load capacitance

Starting from equations 5.63 and 5.62 that express the matching capacitance in function of the load parameters it is possible to transform the equation, and in perfect-matching conditions it is possible at each instant, for example to compute the total load impedance and have a fast evaluation of its main parameters:

$$R_{RFH} = \alpha - R_P = \frac{Z_0 X_{CL}^2}{Z_0.^2 + X_{CL}.^2} - R_P \tag{5.70}$$

$$X_{RFH} = \beta - X_L = X_{CT} + \frac{Z_0.^2 X_{CL}}{Z_0.^2 + X_{CL}^2} - X_L \tag{5.71}$$

Equations 5.70 and 5.71 highlight that if tune reactance and load reactance are function of time it is possible to analytically find the value of the impedance during time as shown in figure **??**. That means it is possible to analyze load properties variation during a radio-frequency heating process. It is easy to understand that it is possible to relate load properties, such as temperature, humidity and physical state to the matching network variations. We analysed an evaporation process , where a infrequency system heat and dry a high-hygroscopic materials. In the next figures are reported the main results: A π.network is considered. The solution of the mathematical model seen before makes possible to relate average temperature, that is related to the permittivity relationship of the material with the temperature and the phase change condition. In figure 5.14 are shown load Solving the transfer problem we can obtain an instantaneous value of the impedance. Because of the global impedance of the system is a qualitative-quantitative measure of the electromagnetic problem, the reconstruction of the load impedance is an indirect "image" of the thermal phenomena: we know that complex permittivity varies its real and its imaginary part during the heating. New Solid State RF generators (SSRF)

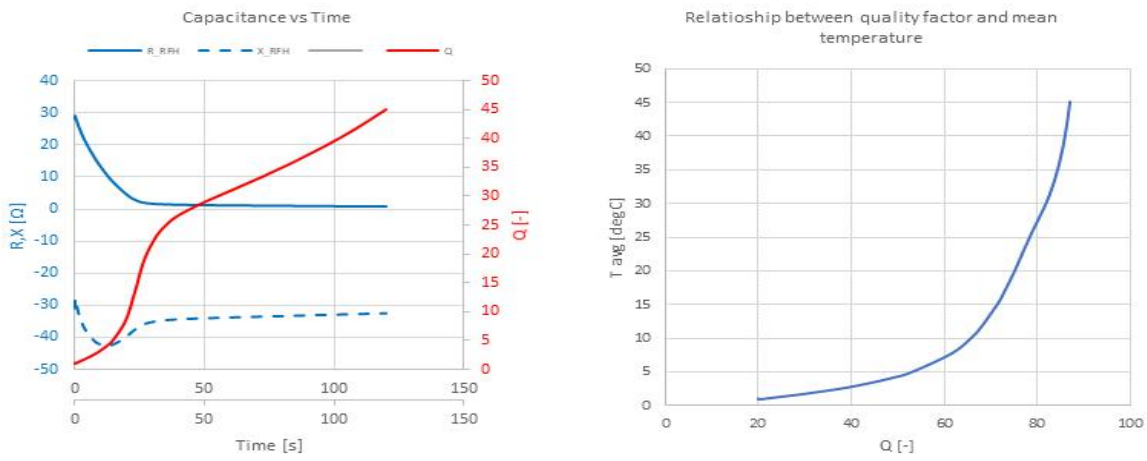

(a) **(b)**

Figure 5.14: Impedance evolution and relationship temperature-matching of the load. (a) Load impedance and quality factor during the process; (b) Relationship between temperature (sensible energy) and matching solution (quality factor)

makes then possible to directly evaluate processes and its main parameters. That unique feature is not achievable with standard resonant-tube technologies. New more sophisticated and precise applications will surely take advantages of these "smart" capabilities.

Chapter 6

Radio-frequency (RF) Drying

6.1 Radio-Frequency Drying

Radio-frequency technologies are particularly suitable for materials that present water inside them because of dielectric properties are significantly enhanced if water is present in its porous matrix. It is clear that a drying process need to extract water from the material. Nowadays RF drying is typically applied to specific sectors: wood drying, fabric drying, leather drying, vegetables drying in food industry [86]. It is useful to understand that it is possible to generalize the drying process for food industry. That part of the work presents an interesting process for plastic drying. PET-extruded-products production plants are characterized by the necessity of drying PET before printing. These processes are characterized by extremely low final material relative humidity and final material temperature also lower than 10 [ppm]. It is possible to dry plastic materials at RH close to 500[ppm] using environment air as process gas. In that case of coarse the drying performances, and particularly the final relative humidity of the material is function of environment conditions, such as absolute humidity (AH) of environment air that is used as gas process. In figure 6.1 is shown a typical layout of drying hopper with hot air generation. It is possible to easily write a power balance, knowing the power flows of the system:

$$P_H = P_L + P_{PET} + P_W \tag{6.1}$$

The total absorbed power is the sum of the power lost to the environment (P_L $[W]$) and the power exchanged with the raw material (P_{PET} $[W]$) and the power yielded to the water (P_W $[W]$). As seen in chapter 1 we want to vaporize water from the material, and then the total

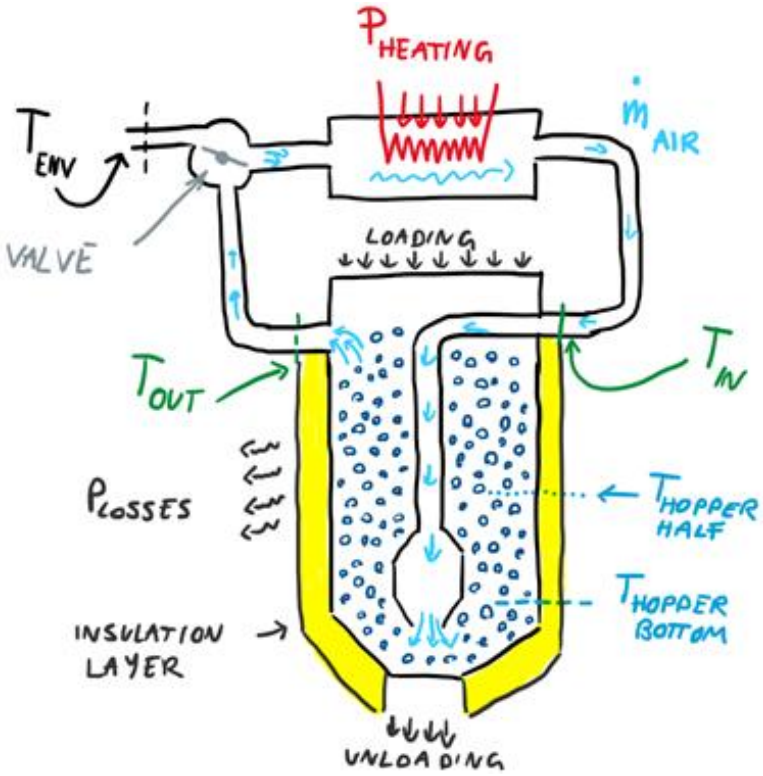

Figure 6.1: Drying hopper for plastic material.

power exchanged with water is the sum of sensible and latent powers:

$$P_W = P_{W-Latent} + P_{W-Sensible} \tag{6.2}$$

A batch process analyzed in that work as SOA initial condition is shown in figure 6.11: it shows temperatures-vs-time behaviour during a 6[h] batch process with a set point temperature $T_{REF} = 160[degC]$ of an initial wet-mass $m_0 = 50[kg]$ with a relative humidity $RH_0 = 2000[ppm]$. Blue line represents the average temperature of the PET (T_{PET}) computed with 32 temperature sensors (PT_{1000}) along the hopper drying chamber height ($h = 0.8[m]$). Green lines represent the temperature of process hot air at the inlet (T_{IN}) and at the outlet of the drying chamber (T_{OUT}). Black line represents the average outer temperature of the hopper ($T_{Hopper-Ext}$) and it is useful to describe losses to the environment (that is controlled at 20[degC]). Analyzing temperature behaviour and drying rates (for example drawing off small portion of material during the process) it is possible to obtain power-vs-time behaviours that fully describe the drying process and are useful to compute drying efficiency and estimate true drying time. Because of the dry material is characterized by its thermal properties: heat capacity (C_{p-PET} $[J/(kg * K)]$) it is possible to relate the heating rate to the sensible power. The energy stored in the material is proportional to the temperature difference between two

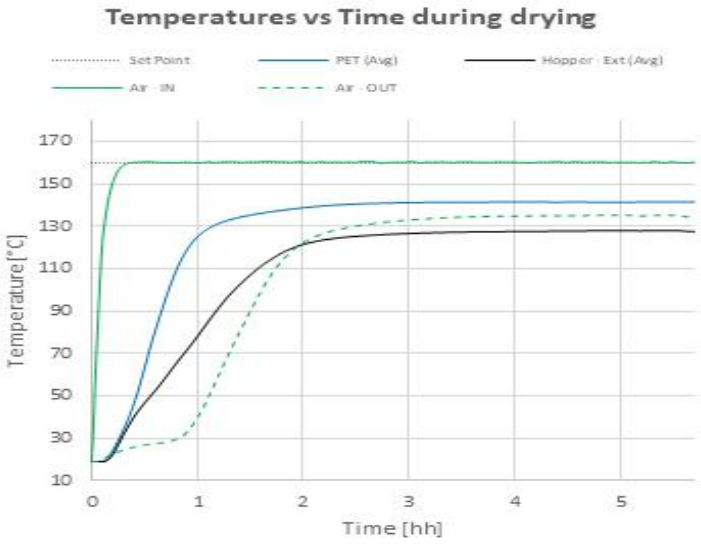

Figure 6.2: Drying process for plastic material. The system for the analysis is represented in figure 6.1. Figure shows temperatures-vs-time behaviour during a 6[h] batch process.

different states (different times: $t^{'}$ and $t^{''}$) during the drying:

$$\Delta H_{PET} = C_p \rho V \Delta T = C_p m \left(T^{''} - T^{'} \right) \tag{6.3}$$

and then the sensible power exchanged to the dry material is:

$$P_{PET} = \frac{\Delta H_{PET}}{t^{''} - t^{''}} = C_p \rho V \frac{\Delta T}{\Delta t} = C_p m \frac{T^{''} - T^{'}}{t^{''} - t^{'}} \tag{6.4}$$

The hopper is an heat exchanger and then knowing temperature differences between inlet and outlet of the hopper and the process-gas (air) mass flow (m_a $[m^3/h]$ the power yielded to the hopper (P_H $[W]$) is: related to the power absorbed by the resistor that is used to heat air in the heating chamber, positioned at the inlet of the hopper-dryer:

$$P_H = \dot{m}_a Cpa \rho_a \left(T_{OUT} - T_{IN} \right) \tag{6.5}$$

where the heat capacity of the air (Cpa $[J/(kg * K)]$) and its density (ρ_a $[kg/m^3]$) are function of the temperature. A good approaximated assumption is to compute it at the average temperature (T_{a-AVG} $[degC]$)

$$T_{AVG} = \frac{T_{OUT} + T_{IN}}{2} \tag{6.6}$$

The target of drying of coarse is to extract water from the material, it is so significant to be able to compute or estimate mass that evaporates from the wet material. The evaporated

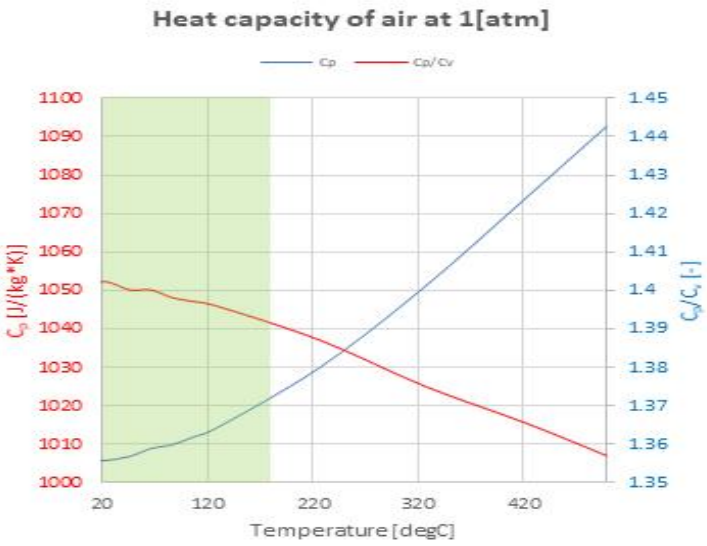

Figure 6.3: Heat capacity of air at 1[atm].[44]

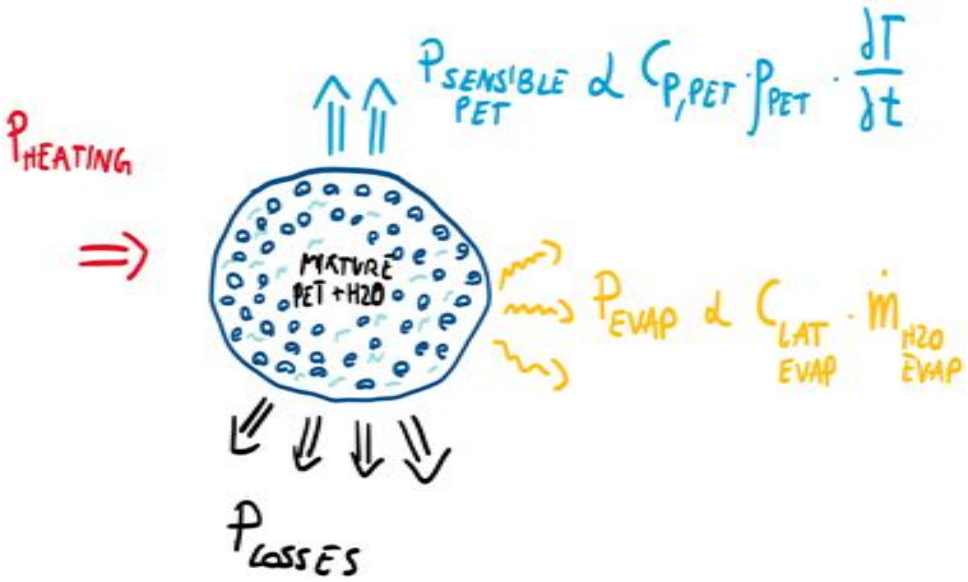

Figure 6.4: Drying process for plastic material: power flows analysis for a discrete volume portion of material dV. The red arrow is the heating power exchange by hot air with the material mixture of PET, water (and air). The yellow rows represent the evaporation power, light-blue arrows represent the sensible heat, proportional to the heat capacity of the material, black arrows represent losses.

mass of water ($\dot{m}_{W-evap}$ $[mg/s]$) is related to the latent heat of vaporization (C_{W-lat} $[J/mg]$).

$$E_{W-evap} \simeq E_{W-Latent} = C_{W-lat} m_{W-evap} \tag{6.7}$$

and then it is easily possible to get power of vaporization:

$$P_{W-Latent} = \frac{E_{W-Latent}}{\Delta t} = C_{W-lat} \frac{m_{W-evap}}{t'' - t'} = C_{W-lat} \dot{m}_{W-evap} \tag{6.8}$$

and then

$$\dot{m}_{W-evap} = \frac{P_{W-Latent}}{C_{W-lat}} \tag{6.9}$$

To compute the power necessary to evaporate e certain quantity of water from the material it is necessary to calculate with a certain accuracy all the powers that occurs in the process. Losses are proportional to:

- the temperature difference between the system and the environment at a constant controlled temperature (T_{env} $[degC]$)
- the insulation of the system
- the environment condition

The energy exchanged between a fluid and a solid component can be easily described with a convection relation:

$$P_{conv} = \alpha_{conv} S \left(T_{solid} - T_{\infty}\right) \tag{6.10}$$

where the undisturbed fluid temperature (T_{∞} $[degC]$) is assumed equal to the environment controlled temperature (T_{env} $[degC]$), the convection coefficient (α_{conv} $[W/(m^2K)]$) can be in first analysis approximated, to a constant value under the condition of environment fix air (no ventilation in the test area) and the total exchange surface of the solid body (S $[m^2]$) is the interface between the body end the external air. Equation 6.10 presents three practical problems: the difficulty of calculating the exchange surface of the real body (the hopper), the difficulty of computing its average external surface temperature (T_{solid}) and the difficulty of choosing a correct external convection coefficient. To solve that problem it is possible to perform a steady state analysis of heat fluxes of equation 6.1. In steady state condition the Fourier equation presented in chapter 3 lost its derivative terms:

$$Q_{sources} = -\lambda \nabla T + C_p \rho \frac{\partial T}{\partial t} \Rightarrow Q_{sources} = -\lambda \nabla T \tag{6.11}$$

Considering equation 6.11 it is easy to rewrite equation 6.10 in its steady state condition: that condition is assumed when the system is in an energetic, and then thermal equilibrium with the environment: in other words all the energy given to the system is lost with the external air:

$$P_H = P_L = \alpha_{conv} S \left(T_{solid} - T_{\infty}\right) \tag{6.12}$$

assuming now that the average temperature of the load (T_{PET}) describes well the energy of the system and considering a controlled environment temperature, in steady state condition it is

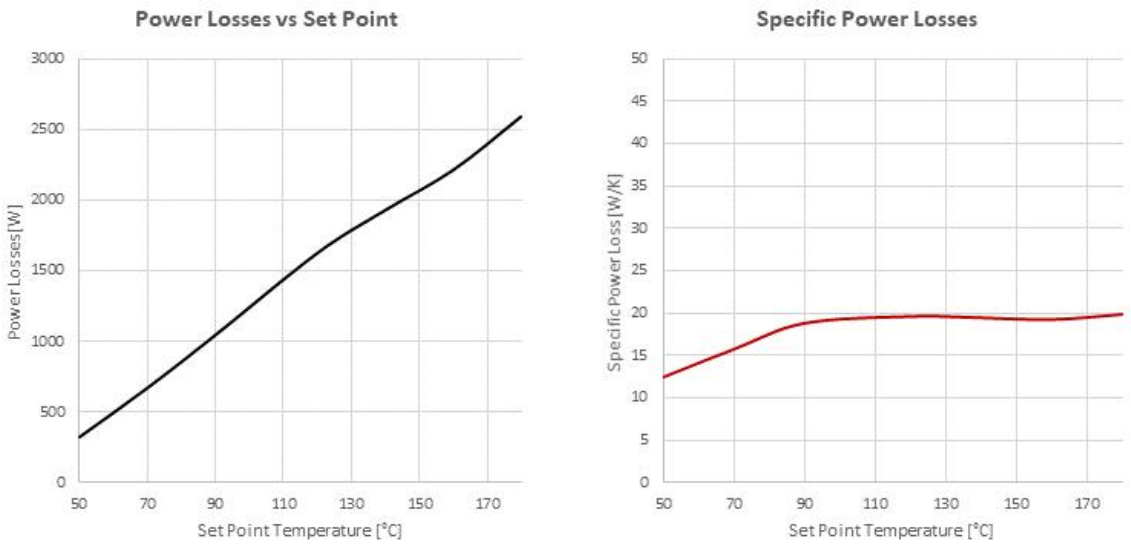

(a) **(b)**

Figure 6.5: Steady state analysis for a drying hopper. (a) Measured losses in steady state condition; (b) Convection specific coefficient for losses ($\alpha_L^{'}$ $[W/K]$).

possible to obtain a specific losses coefficient ($\alpha_L^{'}$ $[W/K]$) that relates the energy given to the gas process by the heater and the energy stored in the plastic material:

$$\alpha_L^{'} = \frac{P_H}{T_{PET} - T_{env}} \tag{6.13}$$

Figure 6.5b shows the relationship between the set-point average material temperature (T_{SET}) and the specific loss coefficient. To fully characterize a drying system for drying it is necessary to calculate the mass flow of the process gas that flows through the hopper. In steady state condition the heating power is related to the environment-losses (as seen in equation 6.12) and also to the energy yielded to the process-gas as accumulated energy in the air flow:

$$P_H = P_L = \rho_a\left(T\right) C_{pa}\left(T\right) \dot{m}_a \left(T_{OUT} - T_{IN}\right) \tag{6.14}$$

And finally it is possible to obtain the mass flow of the process gas:

$$\dot{m}_a = \frac{P_H}{\rho_a\left(T_{AVG}\right) C_{pa}\left(T_{AVG}\right)\left(T_{OUT} - T_{IN}\right)} \tag{6.15}$$

Finally it is possible to write the power conservation law as seen in equation and solve the

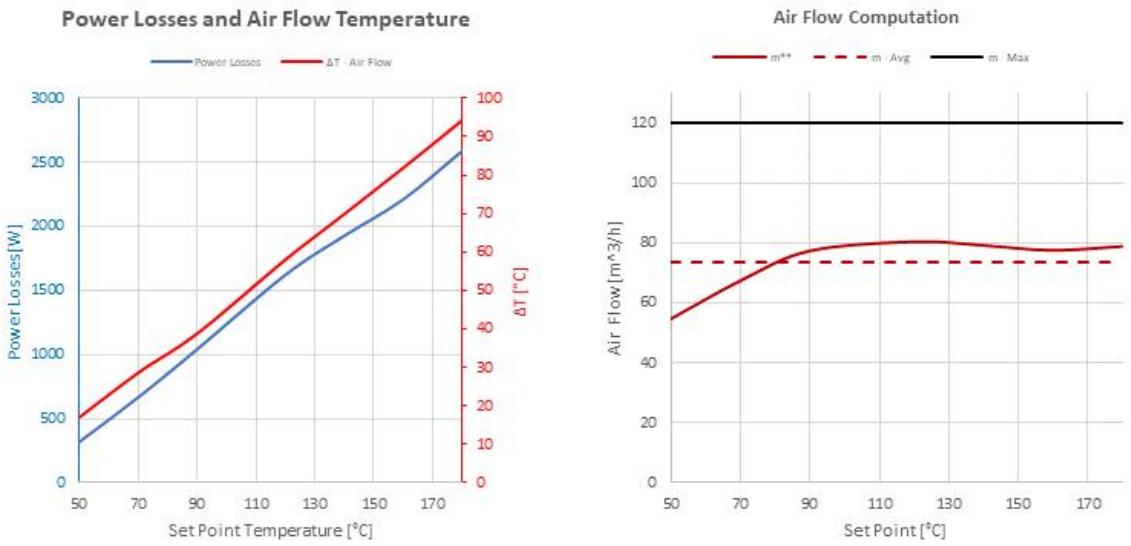

(a) **(b)**

Figure 6.6: Steady state analysis for a drying hopper. (a) Measured losses in steady state condition and air temperature drop; (b) Gas process flow ($\cdot m_a$ $[m^3/h]$).

equation system dynamically:

$$\begin{cases} T_{th} = kT_{el} \\ P_H = \frac{1}{T_{el}} \int_{t_0}^{t_0+kT_{el}} p_H(t)\, dt \\ P_L = -\alpha_L^{'}\left(T_{PET}(t)\right)\left[T_{PET}(t) - T_{ENV}(t)\right] \\ P_{PET} = \left(C_{pPET} m_{PET}\right)\left[\frac{T_{PET}(t_0) - T_{PET}(t_0+T_{th})}{T_{th}}\right] \\ P_H = P_W + P_{PET} + P_L \end{cases} \tag{6.16}$$

where the thermal discretization time (T_{th} $[s]$) is much bigger than the electrical period (T_{el} $[s]$). Finally it is possible to get an approximate calculation of the power given to the water (sensible and latent) and of the evaporation rate ($m_{W.evap}$ $[mg/s]$). If we consider a RFH process it is clear that the electric field generated inside the system directly heat the material that we want to dry. That means it is necessary to modify the power balance taking into account also the dielectric power density (w_{RF} $[W/m^3]$) generated by the electromagnetic field:

$$w_{RF} = \omega \epsilon'' |\mathbf{E}|^2 = \epsilon_r \tan\delta |\mathbf{E}|^2 \tag{6.17}$$

where the electric field ($\mathbf{E}$ $[V/m]$) is characterized by an oscillating frequency (f $[Hz]$) that for the specific system is $27.125[MHz]$. It is clear that the electric field has a specific space distribution that is function of the design of the radio-frequency system (geometry of electrodes) and of the dielectric materials properties inside the system. The global radio-frequency heating

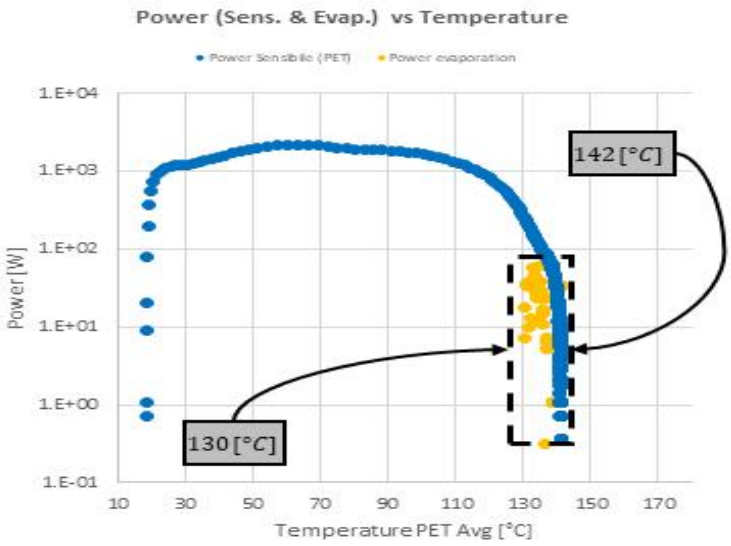

Figure 6.7: Drying process for plastic material. The system for the analysis is represented in figure 6.1. Figure shows power-vs-time behaviour during a 6[h] batch process.

power is the integral of the radio-frequency power distribution that may vary also considerably inside the volume (Ω $[m^3]$):

$$P_{RF} = \int_{\Omega} w_{RF} dV = \omega \int_{\Omega} \epsilon_r \tan\delta |\mathbf{E}|^2 dV \text{??} \tag{6.18}$$

In a RF-assisted process that terms practically increases drying rate because of it can directly provides power to the wet material and finally it increases the evaporation rate (m_{W-evap} $[mg/s]$). The equations system 6.16 may be completed taking into account 6.1:

$$\begin{cases} T_{th} = kT_{el} \\ P_H = \frac{1}{T_{el}} \int_{t_0}^{t_0+kT_{el}} p_H(t)\, dt \\ P_L = -\alpha_L^{'}\left(T_{PET}(t)\right)\left[T_{PET}(t) - T_{ENV}(t)\right] \\ P_{PET} = \left(C_{pPET} m_{PET}\right)\left[\frac{T_{PET}(t_0) - T_{PET}(t_0+T_{th})}{T_{th}}\right] \\ P_H + P_{RF} = P_W + P_{PET} + P_L \\ P_{RF} = \int_{\Omega} w_{RF} dV \end{cases} \tag{6.19}$$

To properly analyze and understand the capability of a radio-frequency drying process for plastic materials we designed and made a first prototype to heat and dry. The system consist of two metallic electrodes. The material was inserted between them and hot air was blown between the material (convection term). We did several analysis varying the RF applied power and the hot-air-process temperature. Figure 6.8 shows the geometry of the first prototype and figure 6.10 shows instead temperate-vs-time behaviour varying RF power and process air temperature

that is necessary to exchange humidity between the material and the environment. The process was done without dehumidify the process gas. The air was taken by the environment, controlled at a 20[$degC$] temperature. Generating power directly in the wet material it is possible to more

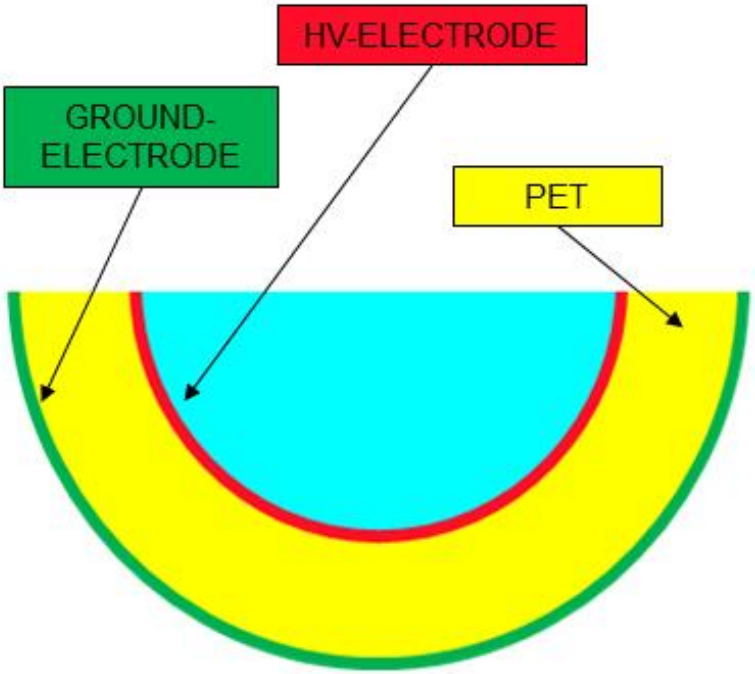

Figure 6.8: Drying process feasibility prototype for plastic materials. Figure represented a mock-up system for the analysis of RF drying of PET. The total loaded mass is 2[kg].

rapidly dry the plastic material because of the evaporation phenomena id driven by the RF heat sources. That increase in drying performances is emphasized by the capability to increase the heating power without increasing the temperature. Standard convection processes need hotter process gas temperature to increase drying rate because of energy released to a solid body is proportional to the temperature difference between the fluid and the solid wet body:

$$P_{body} = \alpha^{'} \left(T_{fluid} - T_{solid}\right) \tag{6.20}$$

and it is clear that in any case the power flux is a vectorial field directed from the surface to the heart of the material: a surface hating characterized by the maximum temperature assumed at the surface of the material. Because of plastic materials are characterized by low thermal conductivity (λ $[W/(m * K)]$) there is the risk to overheat the surface material if it is necessary to increase the drying rate. Plastic materials are characterized by maximum working temperature of 180[$degC$] and this is practically the maximum reachable process-gas temperature. A Radio-frequency device, instead generates inner power sources and it makes

possible to generate relatively uniform heating inside the material matrix without increasing the process gas temperature and that minimizes the risk of overheating. Figure 6.10 highlights

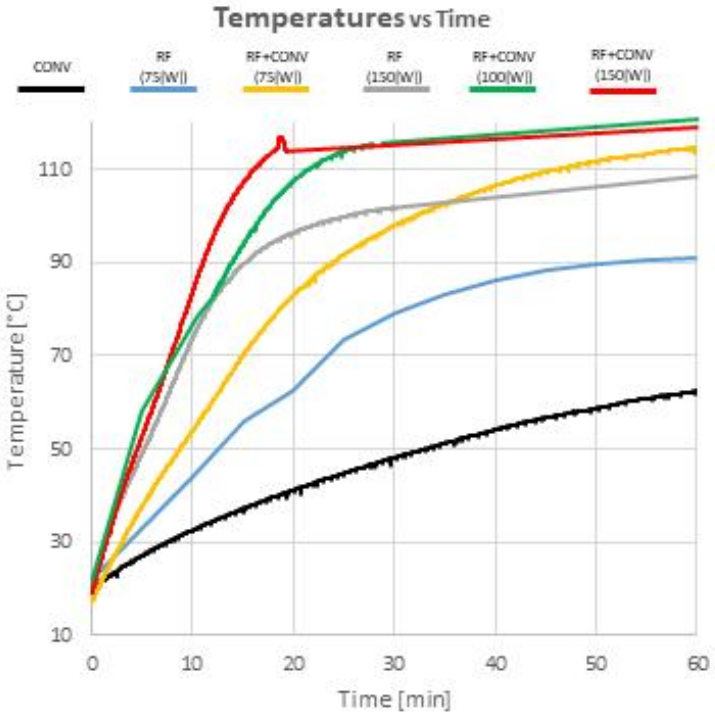

Figure 6.9: Drying process comparison for plastic material. The system for the analysis is represented in figure 6.8. Figure shows PET average temperature-vs-time behaviour during a 60[min] batch process.

that generating radio-frequency heating directly inside the material matrix makes possible to dramatically improve the drying rate of the process. Best results in term of drying performances were obtained with the combination of radio-frequency heating (125[W/kg]) and hot air at a controlled temperature of 120[degC]. The final product didn't show temperature surface defects in terms of color because of the drying process is low compared with the material critical temperature of 180[degC]. Considering now equations 6.19 it is possible to estimate main process characteristics as function of time. We used twelve 6[h] batch process, to estimate main drying process parameters that are necessary to solve the problem and that are listed in table 6.1. Heating and radio-frequency powers are measured with the help of power analysers. As seen before several PT100 measures were used to estimate average load temperature. Finally, solving equations 6.19 it is possible to obtain during the process most relevant power flows as shown in figure 6.11. To properly design an RF system it is necessary to evaluate load permittivity. One of the main process of that particular case is to estimate the complex permittivity as mixture of lossy and lossless materials. Figure 6.12 represents a mixture of air and PET. For

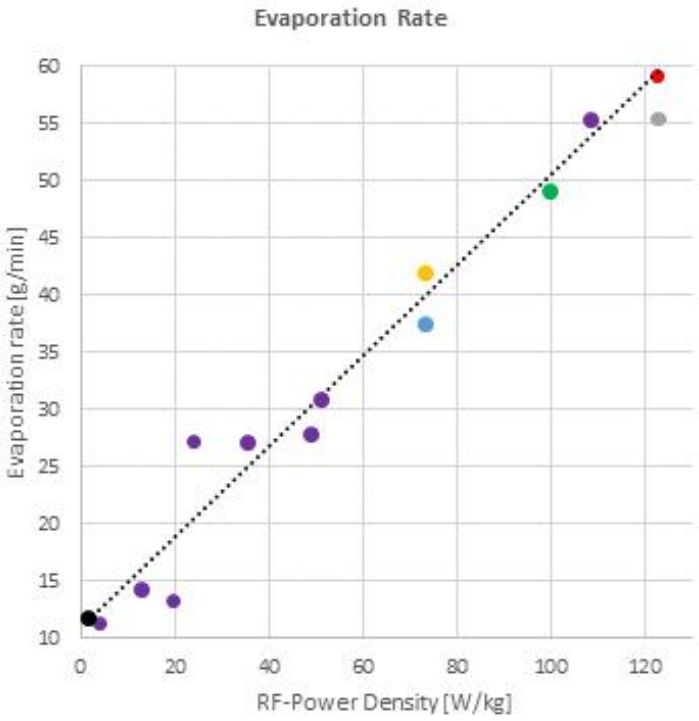

Figure 6.10: Drying process comparison for plastic material. The system for the analysis is shown in figure 6.8. Figure shows drying rate-vs-RF power behaviour during a 60[min] batch process.

PET drying process parameters @20[$degC$]		
Parameter	Unit	Value
External convection coefficient	$[\frac{W}{m^2}]$	20
PET heat capacity	$[\frac{kJ}{kgK}]$	1.25
Water heat capacity	$[\frac{kJ}{kgK}]$	4.186
Water heat of vaporization	$[\frac{kJ}{kg}]$	2453.6
Reference material wet mass	$[kg]$	42
Initial relative humidity	$[ppm]$	2000

Table 6.1: Process parameters to estimate power flows and relative humidity during the batch process.

that particular case a Maxwell-Garnet equation for two species non mixable materials is used.

If we want to dry at extra low RH (lower than 100[ppm]) there is the necessity to dehumidify hot air that exchange energy with the material, in that case it is necessary to dehumidify gas process. In figure 6.14 is shown a typical layout of drying hopper with dehumidification unit. The system consists of a drying chamber, (hopper) and a dryer with air dehumidification. The elimination of water vapor is done with the use of molecular sieve. Two sieves are used. During

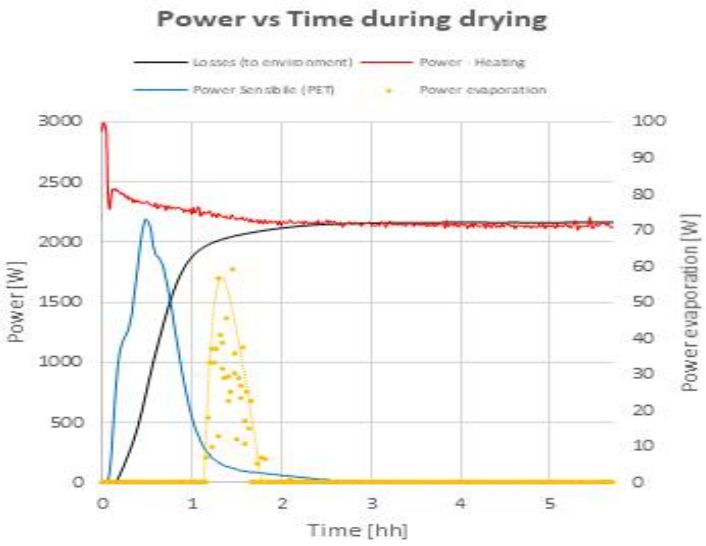

Figure 6.11: Drying process for plastic material. The system for the analysis is shown in figure 6.1. Figure shows power-vs-time behaviour during a 6[h] batch process.

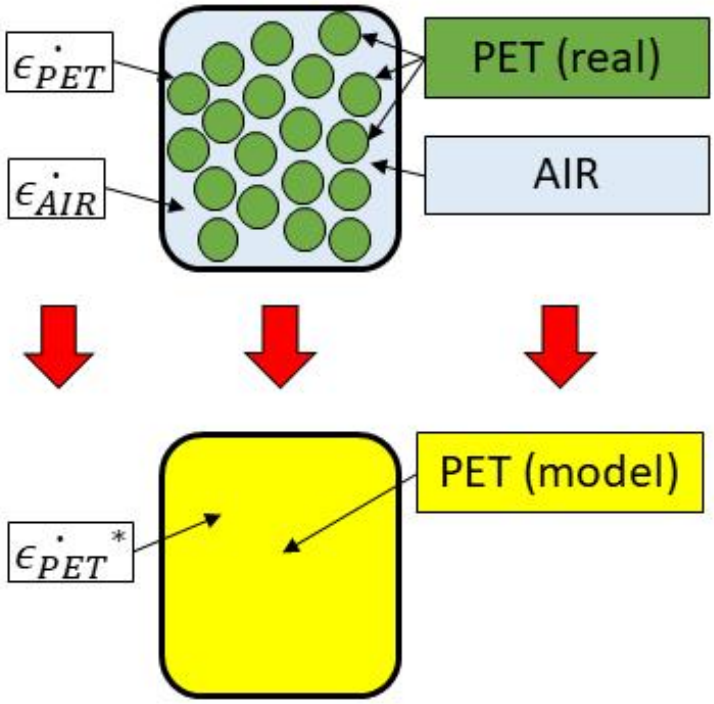

Figure 6.12: Model for permittivity for mixture of a lossy and lossless material.

the process the system automatically changes the sieve: one is regeneration and one in process, and practically dehumidify the process gas. Dew point as seen in chapter 1 is measured during the process. To guarantee high quality of the final product (low humidity also behind 100[ppm]) a ultra-low dew point is controlled in the system. Inf figure 6.13 are shown the power analysis

obtained using equations seen in the first part of that work. Measuring Dew Point during of the process, energy consumed by the heating systems (regeneration-towers heaters and hot air heaters) and temperatures in several points is possible to compute the drying performances of the system. It is evident from figure 6.13 , if compared with results of classical dryer without de-humidification of air that drying is a more enhanced vaporization process.

$$T_d \simeq -40[degC] \tag{6.21}$$

The industrial-scale first prototype was developed using the theoretical scheme of figure 6.14

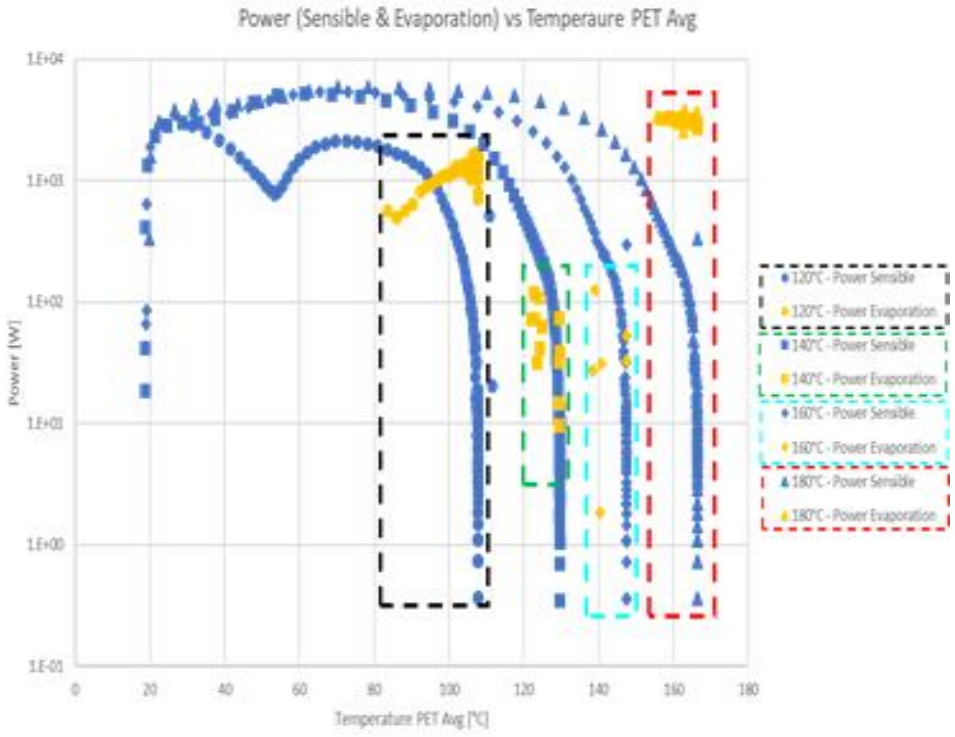

Figure 6.13: Drying power analysis for humidification process.

but adding three main components: a Solid State generator, a Matching Network and optimized electrodes to generate heating sources directly inside the material. The design phase of electrode needed a FEM analysis of the electromagnetic problem. To goal of the design and optimization was to:

- maximize heating uniformity in the cross section
- minimize the risk of discharge, and that means we can accept only electric field that avoid critical breakdown of air in the drying chamber

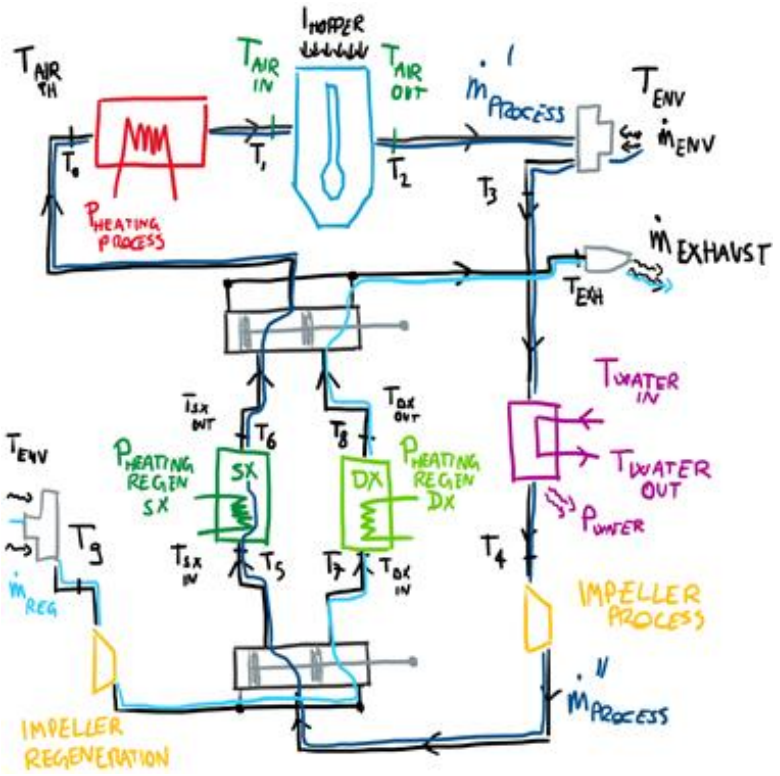

Figure 6.14: Drying hopper for plastic material with air dehumidification.

- optimize the impedance of the heater (what is seen after the matching network) to obtain reasonable value of matching-network parameters (C_T,C_L,L_L)
- maximize the filling factor of the hopper: because of we add cylindrical electrodes, we decrease the loading capacity of the system: Because of in a batch process the specific cost of the process is inversely proportional to system size (load capacity).

The final optimization function that we want to minimize takes into account all these concepts, opportunely weighted: it is more important obviously optimize RF load impedance ($\dot{Z}_{RFH}$ [Ω]) instead of minimize the maximum electric field in the chamber. An hopper with a load capacity of 42[kg] was considered. The permittivity of the PET was modeled as seen before. In figure 6.15 are shown the main design parameters for the hopper, for a first concept of having only high voltage electrodes inside the drying chamber:

- turquoise surface: in the inner part of the hopper is shown the central diffusion pipe: it is a steel conductor that is in contact with the material, the interface surface is a steel region and it represents the ground electrode ($V_G = 0[V]$)
- yellow surface: cross section of the hopper; in figure is shown the PET region. The

external surface is a metallic steel conductor that is bound to the ground (Faraday Cage).

- red surface: copper cylindrical high-voltage electrodes. An electric voltage is applied between the ground and electrode (V_{HV} $[V]$).

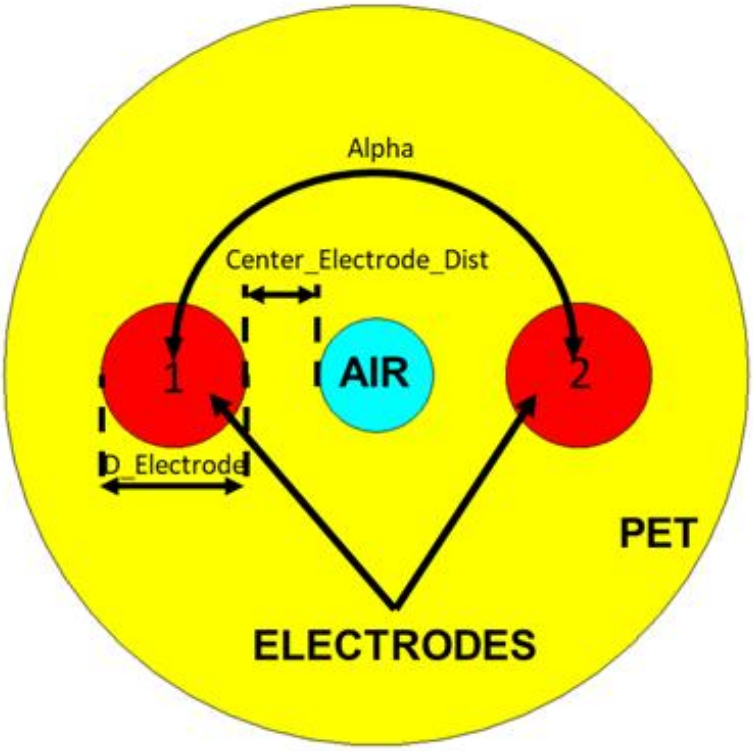

Figure 6.15: Drying electrodes design: Cross section of the hopper.

It is possible to more generally have an RF heater where we can use tubular electrodes with fix high potential (H_{HV} $[V]$) as is shown in figure **??** that highlights the difficult to maximize heating uniformity with an only electrode. We performed an optimization of the system defining the optimization function that we want to minimize (F_{obj}) that is the weighted sum of impedance matching function, uniformity function, filling factor function and risk of discharge function:

$$F_{obj} = F_z + F_u + F_{ff} + F_d \tag{6.22}$$

Results of electric field ($\mathbf{E}$ $[V/m]$) are reported in figure **??** and highlights the difficulty of heating the cross section of the hopper with a low losses only electrode, increasing the number of electrodes may increase uniformity (until a maximum) but dramatically gets worse the impedance condition. In figure **??** is shown the electrical field distribution inside the heating chamber that presents a greater uniformity if compared with the case of one only electrode. To estimate the uniformity it is necessary to define several probes in the computational domain. Because of the considered geometry does not present shapes with sharp corners (to minimize

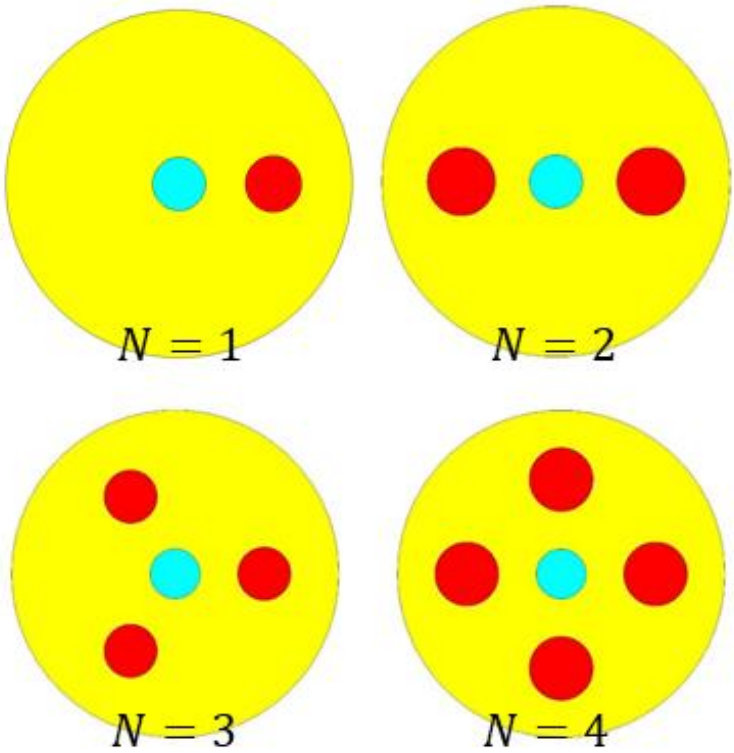

Figure 6.16: Drying electrodes design: electrode with fix potentials. Four different configurations with a different number of electrodes (N [−]).

the risk of discharge), the famous "divergence-problem" does not occur on sharp corners, and it makes sense to consider the maximum value of the power density ($w_{RFH-max}$ $[W/m^3]$). In the same way it is possible to define the minimum value of the the power density ($w_{RFH-min}$ $[W/m^3]$) and the mean value of the the power density ($w_{RFH-avg}$ $[W/m^3]$ and the final estimator for the uniformity is the function:

$$F_u = \frac{\Delta w}{w_{RFH-min}} = \frac{w_{RFH-max} - w_{RFH-min}}{w_{RFH-avg}} \tag{6.23}$$

the impedance matching function instead takes into account the difficulty of a matching system and in an analysis with a constant feeding potential:

$$\begin{cases} R_{RFH} = f\left(W_{es}, P_{RFH}\right) \\ X_{RFH} = g\left(W_{es}, P_{RFH}\right) \\ C_{L,m} = h\left(R_{RFH}, X_{RFH}, L_n, C_{T,m}\right) \\ C_{T,m} = i\left(R_{RFH}, X_{RFH}, L_n, C_{L,m}\right) \end{cases} \tag{6.24}$$

A certain configuration of the electrodes will be characterized by a certain value of complex impedance $\dot{Z}_{RFH}$ and then, the matching network (a certain topology) will be defined by

capacitances and inductance that solve the maximum power transfer condition as written in the equation 6.24. The solution of that problem will define currents and voltages on the system as seen in chapter 5. There are strict condition on the maximum voltage of the capacitors and inductances of the matching network:

$$\begin{cases} |V_{CT}| = |\dot{Z}_{CT}\dot{I}_{RFH}| < V_{CT,max} \\ |V_{CL}| = |\dot{Z}_{CT}\dot{I}_{CT}| < V_{CT,max} \end{cases} \tag{6.25}$$

and finally the impedance matching function (f_z) takes into account all these conditions. Practically, for a π-network topology of the matching network we want to solve the following problem for a certain fixed power heating

$$\begin{cases} opt^* \Rightarrow \max R_{RFH} \\ opt^* \Rightarrow \min X_{RFH} \\ opt^* \Rightarrow \dot{Z}_{LOAD}\left(opt^*\right) - Z0 = 0 \\ opt^* \Rightarrow V_{CT}\left(opt^*\right) < C_{CT-max} \\ opt^* \Rightarrow V_{CL}\left(opt^*\right) < C_{CL-max} \\ opt^* \Rightarrow \min P_{LN}\left(opt^*\right) \\ op^* \Rightarrow \max|\mathbf{E}| < 0.1 \cdot E_{cb} \end{cases} \tag{6.26}$$

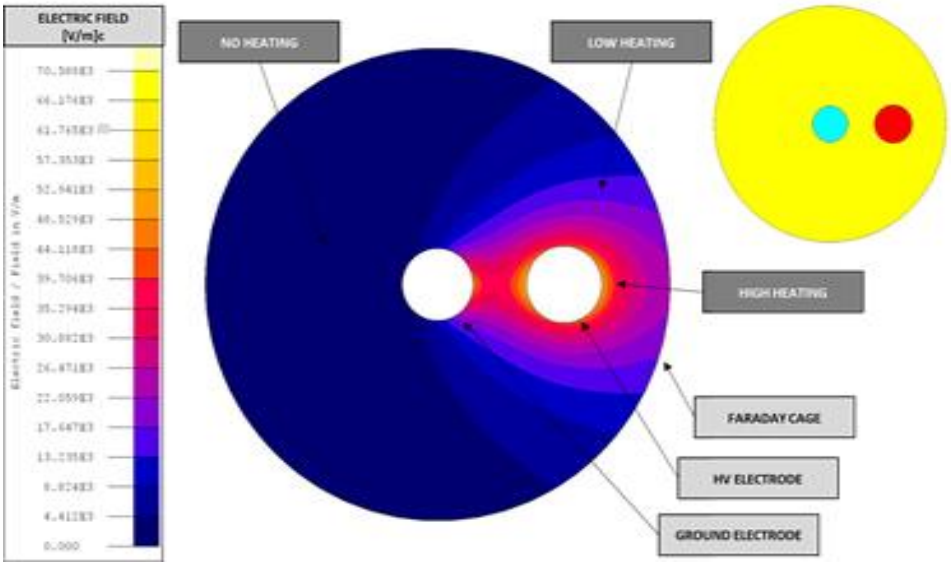

Figure 6.17: Results of the first considered geometry: one only cylindrical copper electrode ($N = 1$). Electrical field inside the cavity

In figure 6.19 is shown the final optimized geometry for a RF drying problem. The system is designed to transfer a maximum heating power of $5[kW]$ to a plastic load. The

electrodes (red) are connected with the use of short-circuited rings on the top and bottom part. The direction of the material during the process is from the top to the bottom. The air is in blown by the bottom part of the diffusion cone (turquoise).

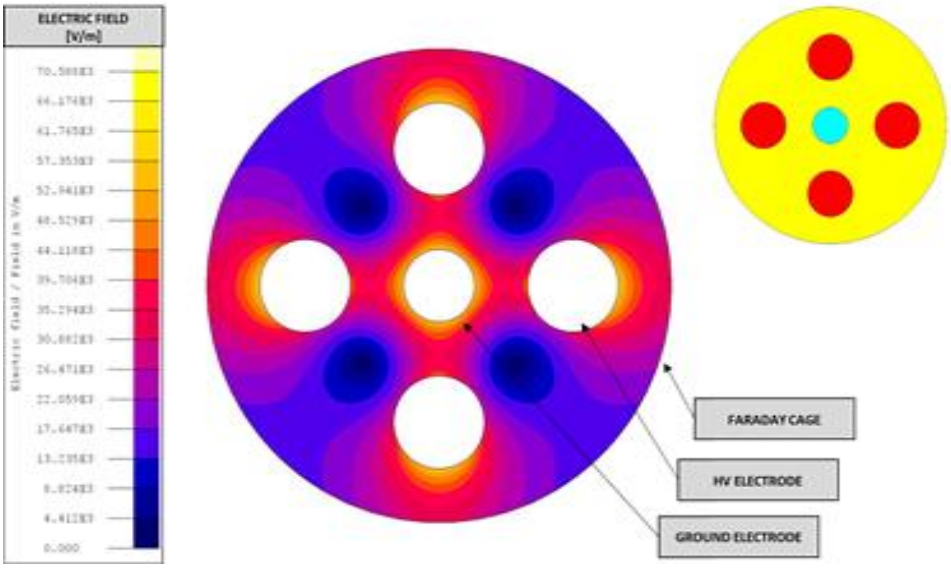

Figure 6.18: Results of the first considered geoemtry: one only cylindrical copper electrode ($N = 2$). Electrical field inside the cavity

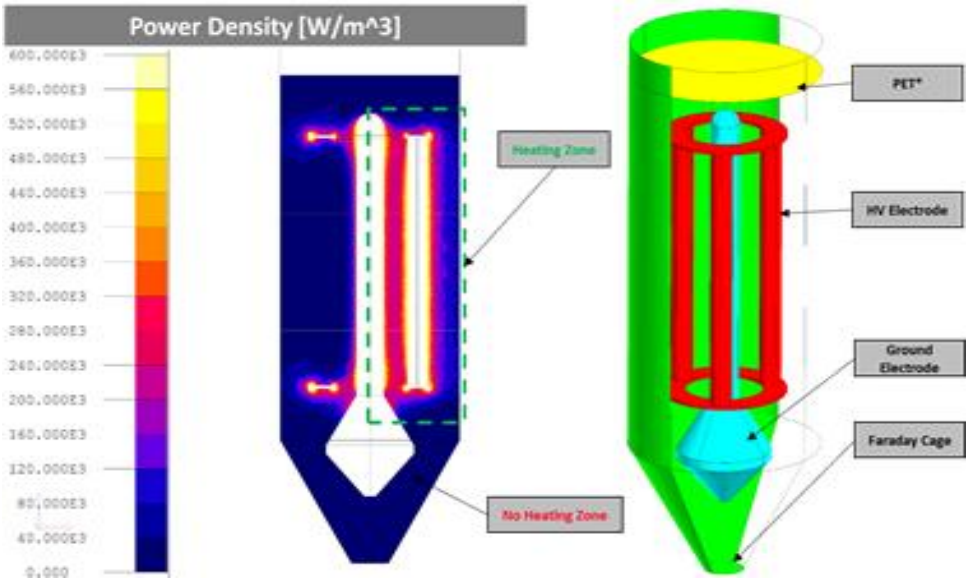

Figure 6.19: Final optimized RF hopper design that solve the complete RF problem.

Chapter 7

Microwave (MWH) Heating

7.1 Microwave Theory

The field of radio frequency (RF) microwave engineering (MW) generally covers the behavior of alternating current signals with frequencies in the range of $100[MHz]$ to $1[THz]$. It is possible to summarize different ranges:

- VHF range: $30 - 300[MHz]$
- UHF range: $30 - 3000[MHz]$
- MW range: $3 - 3000[GHz]$

to ultra high frequency (UHF) (300–3000 MHz), Of course, in air and free space the frequency of the electromagnetic wave is related to its wavelength, and for that MW are characterized by a typical wavelength in the order of millimeters. Because of the high frequencies (and short wavelengths), standard circuit theory often cannot be used directly to solve microwave network problems. In a sense, standard circuit theory is an approximation, or special case, of the broader theory of electromagnetism as described by Maxwell's equations. This is due to the fact that, in general, the lumped circuit element approximations of circuit theory may not be valid at high RF and microwave frequencies.

7.2 Microwave Electromagnetic problem

Remembering Maxwell's equations that we saw in chapter 2 it is possible to consider not a general form of the electric field ($\mathbf{E}$ $[V/m]$) and of the magnetic field ($\mathbf{H}$ $[A/m]$), but considering a sinusoidal, or harmonic, time dependence, it is possible to take advantage of the phasor notation and write all fields as complex vectors. For that reason an electric field ($\mathbf{E}$ $[V/m]$), polarized in a general direction ($\mathbf{x}$) can be expressed as:

$$\mathbf{E}^{'}(x,y,z,t) = \mathbf{x}A(x,y,z,t)\cos(\omega t + \phi) = Re\left[\mathbf{E}(x,y,z,t)\,e^{i\omega t}\right] \tag{7.1}$$

where we defined the real amplitude (A), the radian frequency ($\omega = 2\pi f$) and finally the phase reference of the wave (ϕ). For time harmonic fields, it is useful to deeper analyze the time-average of quadratic quantities, such as power and energy. If we consider more general three-dimensional electric field:

$$\mathbf{E}^{'} = \mathbf{x}E_x\cos(\omega t + \phi_x) + \mathbf{y}E_y\cos(\omega t + \phi_y) + \mathbf{z}E_3\cos(\omega t + \phi_z) \tag{7.2}$$

it easily has the phasor form:

$$\mathbf{E} = \mathbf{x}E_x e^{i\phi_x} + \mathbf{y}E_y e^{i\phi_y} + \mathbf{z}E_z e^{i\phi_z} \tag{7.3}$$

And finally the average of the square of the magnitude of the electric field has the form:

$$|\mathbf{E}^{'}|^2_{avg} = \frac{1}{T}\int_0^T \mathbf{E}^{'}\cdot\mathbf{E}^{'}dt = \frac{1}{2}\left(E_x^2 + E_y^2 + E_z^2+\right) = \frac{1}{2}\mathbf{E}\cdot\mathbf{E}^{*} \tag{7.4}$$

Considering the time dependence of the fields as only described by the operator $e^{i\omega t}$ it is possible to rewrite Maxwell's equations 2.1 2.2 2.4 2.3 as:

$$\nabla\cdot\mathbf{D} = \rho \tag{7.5}$$

$$\nabla\times\mathbf{B} = 0 \tag{7.6}$$

$$\nabla\times\mathbf{E} = -i\omega\mathbf{B} - \mathbf{M} \tag{7.7}$$

$$\nabla\times\mathbf{H} = i\omega\mathbf{D} + \mathbf{J} \tag{7.8}$$

The electric current source ($\mathbf{J}$ $[A/m^2]$) and the magnetic current source ($\mathbf{M}$ $[V/m^2]$) are, volume current densities, but typically for MW problems the current densities are int he form of current sheet or line current. As already seen in chapter 2 material bodies are always present in MW heating problems. For that reason it is necessary to define material properties that make possible to relate different electromagnetic fields. For a dielectric material, if an electric field ($\mathbf{E}$ $[V/m]$)

is applied to it, atoms or molecules polarize, creating dipole moments that increase the total displacement field ($\mathbf{D}$ $[C/m^2]$. The augment of the displacement is defined as the electric polarization ($\mathbf{P}_e$ $[C/m^2]$) as seen in chapter 4 and we know that in a liberalized material it is linearly related to the electric field through the electric susceptibility (χ):

$$\mathbf{D} = \epsilon_0 \mathbf{E} + \mathbf{P}_e = \epsilon_0 \left(1 + \chi_e\right) \mathbf{E} = \epsilon_r \epsilon_0 \mathbf{E} \tag{7.9}$$

where the relative dielectric constant of the material can be more generally a complex operator, where the real part describes the accumulated energy inside the medium and the imaginary part the energy dissipated into it:

$$\dot{\epsilon}_r = \epsilon_r^{'} - i\epsilon_r^{''} = \epsilon_r \left(1 - i \tan \delta\right) \tag{7.10}$$

The loss of a dielectric can also be modeled, as it is usual, whit an equivalent electric conductor loss. In a general conductive region with a non-zero electrical conductivity (σ $[S/m]$), the current density ($\mathbf{J}$ $[A/m^2]$) is defined by the Ohm's law, as seen in chapter 2,

$$\mathbf{J} = \sigma \mathbf{E} \tag{7.11}$$

Considering Maxwell-Ampere's equation in the frequency domain 7.8 it is possible to explicit the curl of the magnetic field:

$$\nabla \times \mathbf{H} = i\omega\epsilon_0 \dot{\epsilon}_r \mathbf{E} + \sigma \mathbf{E} = i\omega\epsilon_0 \left(\epsilon_r^{'} - i\epsilon_r^{''} - i\frac{\sigma}{\omega\epsilon_0}\right) \mathbf{E} \tag{7.12}$$

The real part of equation 7.12 can be considered as the total "effective" conductivity and makes possible to finally define the loss tangent ($\tan \delta$ $[-]$) as seen in chapter 4:

$$\tan \delta = \frac{\epsilon_r^{''}}{\epsilon_r^{'}} + \frac{\sigma}{\omega \epsilon_r^{'}} \tag{7.13}$$

Microwave materials in MWH processes are usually characterized their relative permittivity and their loss factor at a certain frequency. In many applications, materials are an-isotropic, and that implies that the polarization vector does not have the same direction of the electric field. Crystal structures and ionized gases show an-isotropic behaviours. For that reason the relative permittivity can be defined as a complex tensor:

$$\begin{bmatrix} D_x \\ D_y \\ D_z \end{bmatrix} = \begin{bmatrix} \dot{\epsilon}_{xx} & \dot{\epsilon}_{xy} & \dot{\epsilon}_{xz} \\ \dot{\epsilon}_{yx} & \dot{\epsilon}_{yy} & \dot{\epsilon}_{yz} \\ \dot{\epsilon}_{zx} & \dot{\epsilon}_{zy} & \dot{\epsilon}_{zz} \end{bmatrix} \cdot \begin{bmatrix} E_x \\ E_y \\ E_z \end{bmatrix} = \begin{bmatrix} \dot{\epsilon} \end{bmatrix} \cdot \begin{bmatrix} E_x \\ E_y \\ E_z \end{bmatrix} \tag{7.14}$$

As we did for electric field it is possible to define material properties also for magnetic materials. An applied magnetic field may align magnetic dipole moments in a magnetic material to produce a magnetic polarization ($\mathbf{P}_m$ $[A/m]$):

$$\mathbf{B} = \mu_0\mathbf{H} + \mu_0\mathbf{P}_m = \mu_0\left(1 + \chi_m\right)\mathbf{H} = \mu_0\mu_r\mathbf{H} \tag{7.15}$$

and also in that case, for example for ferrites the relative magnetic permeability may be expressed with a complex tensor operator:

$$\begin{bmatrix} B_x \\ B_y \\ B_z \end{bmatrix} = \begin{bmatrix} \dot{\mu}_{xx} & \dot{\mu}_{xy} & \dot{\mu}_{xz} \\ \dot{\mu}_{yx} & \dot{\mu}_{yy} & \dot{\mu}_{yz} \\ \dot{\mu}_{zx} & \dot{\mu}_{zy} & \dot{\mu}_{zz} \end{bmatrix} \cdot \begin{bmatrix} H_x \\ H_y \\ H_z \end{bmatrix} = \begin{bmatrix} \dot{\mu} \end{bmatrix} \cdot \begin{bmatrix} H_x \\ H_y \\ H_z \end{bmatrix} \tag{7.16}$$

If linear material are considered, it is possible re-write Maxwell's equations, taking into account material properties:

$$\nabla \cdot \mathbf{E} = \frac{\rho}{\dot{\epsilon}_r\epsilon_0} \tag{7.17}$$

$$\nabla\mathbf{H} = 0 \tag{7.18}$$

$$\nabla \times \mathbf{E} = -i\omega\dot{\mu}_r\mu_0\mathbf{H} - \mathbf{M} \tag{7.19}$$

$$\nabla \times \mathbf{H} = i\omega\dot{\epsilon}_r\epsilon_0\mathbf{E} + \mathbf{J} \tag{7.20}$$

To mathematically solve Maxwell's equations it is necessary to impose boundary values.

7.2.1 Fields at a General Material Interface

Considering an interface between two different media, as shown in figure 7.1 it is possible to obtain relations between normal and tangential fields. Boundary conditions makes possible to close the mathematical problem and solve the electromagnetic waves in the space and in the time. Considering the divergence of the displacement field in it's integral form, for a time harmonic field and applying it to a closed cylindrical volume region Σ, which closed surface is $\partial\Omega$:

$$\oint_{\partial\Omega} \mathbf{D} \cdot d\mathbf{s} = \int_{\Omega} \rho dV \tag{7.21}$$

If the cylinder has volume $\Omega = hS$ where $S = \pi R^2$ is the base surface integral and we consider the infinitesimal value of the volume as shown in figure 7.2

$$\lim_{h\to 0} \mathbf{D} \cdot d\mathbf{s} = \lim_{h\to 0} \begin{bmatrix} D_t \\ D_n \end{bmatrix} = \begin{bmatrix} 0 \\ D_n \end{bmatrix} \tag{7.22}$$

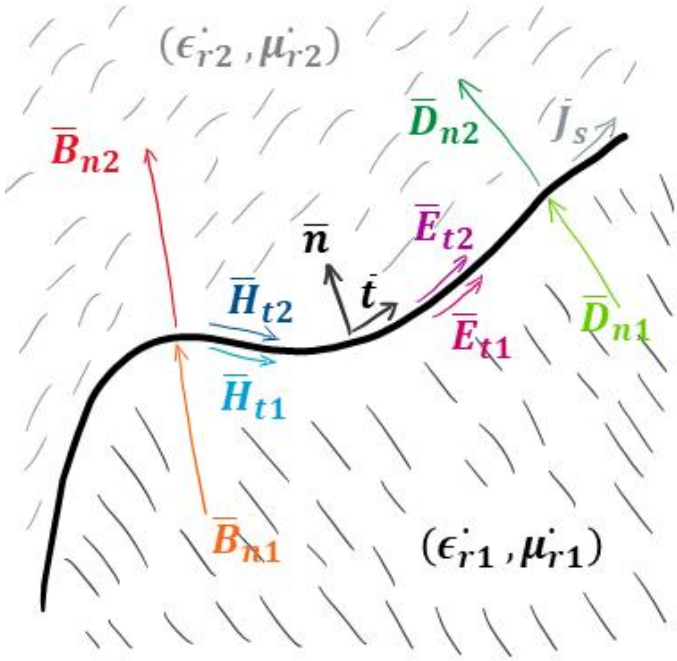

Figure 7.1: Electric field (**E**), current density (**J**), magnetic field and surface charge density at a general interface between two media (1 and 2)

and that means it is possible to obtain the vectorial form for the displacement field, where the surface charge density is defined by ρ_s:

$$\mathbf{n} \cdot (\mathbf{D}_2 - \mathbf{D}_1) = \rho_s \tag{7.23}$$

A similar approach may be done for magnetic field and get the final conservation law for it:

$$\mathbf{n} \cdot \mathbf{B}_1 = \mathbf{n} \cdot \mathbf{B}_2 \tag{7.24}$$

It is useful to use the integral for of Faraday-Maxwell's law 2.15 for the electric field (**E**) in the frequency domain for a general surface Σ bounded by the close loop $\partial\Sigma$:

$$\oint_{\partial\Sigma} \mathbf{E} \cdot d\mathbf{l} = -i\omega \int_{\Sigma} \mathbf{B} \cdot d\mathbf{s} - \int_{\Sigma} \mathbf{M} \cdot d\mathbf{s} \tag{7.25}$$

And as already did for the displacement field it is possible to compute the infinitesimal quantity $d\partial\Sigma = dh \cdot dl$ and if h go to zero we get the vector form of the conservation law for the electric field through an interface that relates the electric fields in the two media to the magnetic surface current density ($\mathbf{M}_s$ $[A/m^2]$):

$$(\mathbf{E}_2 - \mathbf{E}_1) \times \mathbf{n} = \mathbf{M}_s \tag{7.26}$$

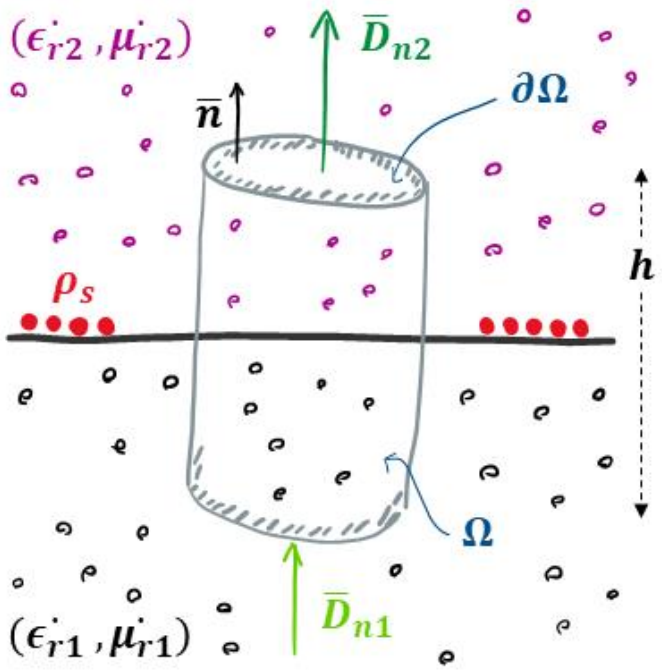

Figure 7.2: Normal components of displacement field ($\mathbf{D}_n$), and surface charge density (ρ_s) at a general interface (black line) between two media (1 and 2), respectively highlighted with purple dots and black dots. The grey curve is the infinitesimal cylinder of height h

and finally after defining the electric surface current density ($\mathbf{J}_s$ $[A/m^2]$):

$$\mathbf{n} \times (\mathbf{H}_2 - \mathbf{H}_1) = \mathbf{J}_s \tag{7.27}$$

Fields at a dielectric interface

In a domain with two dielectric ideal materials ($\tan\delta = 0$) can't exist a surface current and previous equations state that the normal components of the displacement field ($\mathbf{B}$) and of the magnetic flux density ($\mathbf{B}$) and the tangential component of the electric field ($\mathbf{E}$) and of the magnetizing field ($\mathbf{H}$) must conserve:

$$\begin{cases} \mathbf{n} \cdot \mathbf{D}_1 = \mathbf{n} \cdot \mathbf{D}_2 \\ \mathbf{n} \cdot \mathbf{B}_1 = \mathbf{n} \cdot \mathbf{B}_2 \\ \mathbf{n} \times \mathbf{E}_1 = \mathbf{n} \times \mathbf{E}_2 \\ \mathbf{n} \times \mathbf{H}_1 = \mathbf{n} \times \mathbf{H}_2 \end{cases} \tag{7.28}$$

These equations are not linearly independent and they impose continuity of fields across interfaces of dielectric material.

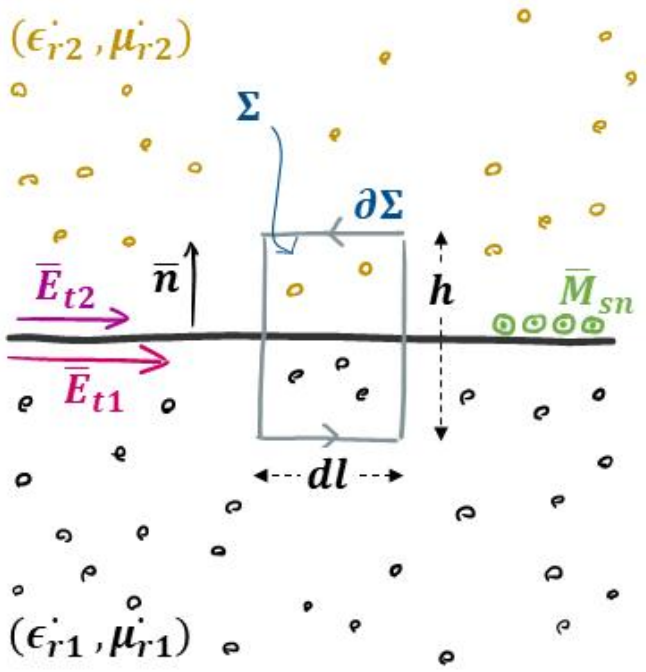

Figure 7.3: Tangential components of electric field ($\mathbf{E}_t$), and magnetic surface current density ($\mathbf{M}_s$) at a general interface (black line) between two media (1 and 2), respectively highlighted with brown dots and black dots. The grey curve is the infinitesimal path of h and width dl

Fields at the interface with a perfect conductor (PEC)

Lossless conductive boundaries ($\sigma = \infty$) are often used to describe for example external shielding for RF systems or boundaries conductive for resonant cavities if extremely good conductor are taken into account (for example copper, aluminum or gold). In this case of a perfect conductor, all field components must be zero inside the conducting region. As seen in chapter 1 in alternating electric field the skin depth describes the attitude of the current to distribute only in thin layers. Ideal materials are characterized by skin depth equal to zero, and in that case the superficial magnetic current density must be zero too, and it is possible to obtain the BCs for perfect electric conductors (PECs) that demonstrate how perfect electric conductors short the electric field: that's typically what happens in a microwave cavity.

$$\begin{cases} \mathbf{n} \cdot \mathbf{D} = \rho_s \\ \mathbf{n} \cdot \mathbf{B} = 0 \\ \mathbf{n} \times \mathbf{E} = 0 \\ \mathbf{n} \times \mathbf{H} = \mathbf{J}_s \end{cases} \tag{7.29}$$

Fields at the interface with a perfect magnet (PM)

Dual to the preceding boundary condition is the magnetic wall boundary condition, where the tangential components of **H** must vanish. Such a boundary does not really exist in practice but may be approximated by a corrugated surface or in certain planar transmission line problems. We will also see that the magnetic wall boundary condition is analogous to the relations between the voltage and current at the end of an open-circuited transmission line, while the electric wall boundary condition is analogous to the voltage and current at the end of a short-circuited transmission line.

$$\begin{cases} \mathbf{n} \cdot \mathbf{D} = 0 \\ \mathbf{n} \cdot \mathbf{B} = 0 \\ \mathbf{n} \times \mathbf{E} = -\mathbf{M}_s \\ \mathbf{n} \times \mathbf{H} = 0 \end{cases} \tag{7.30}$$

7.2.2 The wave equation

Taking into account equations 7.7, 7.8 it is possible to obtain the so called Helmholtz's equation for the electric field for a source-free, linear, isotropic, homogeneous region:

$$\nabla^2 \mathbf{E} + \left(\frac{\omega}{c}\right)^2 \mu_r \epsilon_r \mathbf{E} = 0 \tag{7.31}$$

and at the same way, the Helmholtz's equation for the magnetic field:

$$\nabla^2 \mathbf{H} + \left(\frac{\omega}{c}\right)^2 \mu_r \epsilon_r \mathbf{H} = 0 \tag{7.32}$$

In all high frequency electromagnetic problems it is suitable to define the propagation constant (k $[1/m]$):

$$k = \omega\sqrt{\mu\epsilon} = \frac{\omega}{c}\sqrt{\mu_r \epsilon_r} \tag{7.33}$$

and finally re-write the previous equations as:

$$\nabla^2 \mathbf{E} + k^2 \mathbf{E} = 0 \tag{7.34}$$

and at the same way, the Helmholtz's equation for the magnetic field:

$$\nabla^2 \mathbf{H} + k^2 \mathbf{H} = 0 \tag{7.35}$$

If a plane wave is considered it is possible to easily get the wavelength (λ $[m]$) of a plane wave, the phase velocity (v_p $[m/s]$) and more important the so called intrinsic impedance of a medium (Z_c $[\Omega]$):

$$\begin{cases} \lambda = \frac{2\pi}{k} = \frac{2\pi v_p}{\omega} \\ v_p = \left(\frac{1}{\sqrt{\epsilon_0 \mu_0}}\right)(\mu_r \epsilon_r)^{-\frac{1}{2}} = c\,(\mu_r \epsilon_r)^{-\frac{1}{2}} \\ Z_c = \left(\sqrt{\frac{\mu_0}{\epsilon_0}}\right)\left(\sqrt{\frac{\mu_r}{\epsilon_r}}\right) = Z_0\left(\sqrt{\frac{\mu_r}{\epsilon_r}}\right) \end{cases} \tag{7.36}$$

where Z_0 is the intrinsic impedance of the vacuum-free space and it is equal to 377$[\Omega]$.

It is possible to consider now a real lossy material and take into account the equations:

$$\begin{cases} \nabla \times \mathbf{E} = -i\omega\mu_r\mu_0\mathbf{H} \\ \nabla \times \mathbf{H} = i\omega\epsilon_r\epsilon_0\mathbf{E} + \sigma\mathbf{E} \end{cases} \tag{7.37}$$

and we can obtain the wave equation for the electric field for a lossy material:

$$\nabla^2\mathbf{E} + \gamma^2\mathbf{E} = 0 \tag{7.38}$$

where it is defined the complex propagation constant (γ) that takes into account the attenuation effects due to the presence of a real material.

$$\gamma = i\omega\sqrt{\mu_r\epsilon_r}\left(\frac{1}{c}\right)\sqrt{1 - i\frac{\sigma}{\omega\epsilon_r\epsilon_0}} = \alpha + i\beta \tag{7.39}$$

where equation 7.39 introduces the attenuation constant (γ) and the phase constant (β).

If a good conductor is considered it is possible to properly compute the complex propagation constant, considering that the conductive current is several order greater than the displacement current ($\sigma \gg \omega\epsilon_r\epsilon_0$, and then:

$$\gamma = \alpha + i\beta \simeq (1+i)\sqrt{\frac{\omega\mu\sigma}{2}} \tag{7.40}$$

From equation 7.40 it is possible to define the penetration depth (δ_s $[m]$) defined as the distance after which the amplitude of the fields in the conductor decays by the 36.8[%]:

$$\delta_s = \frac{1}{\alpha} = \sqrt{\frac{2}{\omega\mu_r\mu_0\sigma}} \tag{7.41}$$

7.2.3 General plane wave solution

That section looks at plane waves from a more general point of view and solves the wave equation by the method of separation of variables. [15] In free-vacuum space the Helmholtz

equation for the electric field 7.34

$$\nabla^2\mathbf{E} + k_0^2\mathbf{E} = \frac{\partial^2\mathbf{E}}{\partial x^2} + \frac{\partial^2\mathbf{E}}{\partial y^2} + \frac{\partial^2\mathbf{E}}{\partial z^2} + k_0^2\mathbf{E} = 0 \tag{7.42}$$

may be rewritten as a product of three functions for each components of the space and for each of the three components of the space, considering $\mathbf{E} = (E_x, E_y, E_z)$ and E_x, E_y, E_z as a function of the space:

$$\frac{\partial^2 E_i}{\partial x^2} + \frac{\partial^2 E_i}{\partial y^2} + \frac{\partial^2 E_i}{\partial z^2} + k_0^2 E_i \quad \text{with } i = x, y, z \tag{7.43}$$

$$E_x(x, y, z) = f(x)\, g(y)\, h(z) \tag{7.44}$$

This equation can be solved by the method of separation of variables, a standard technique for treating such partial differential equations. It is possible easily, considering equation and 7.44 to obtain a more compact form of 7.43:

$$\frac{f''(x)}{f(x)} + \frac{g''(y)}{g(y)} + \frac{h''(z)}{h(z)} + k_0^2 = k_x^2 + k_y^2 + k_z^2 + k_0^2 = 0 \tag{7.45}$$

Considering a simple plane wave traveling in the positive direction, it is possible for each coordinate to write the complete solution of the electric field. It is possible to define the wave number ($\mathbf{k}$) as the resultant vector that has the same direction of the direction of the propagation of the wave:

$$\mathbf{k} = k_x\mathbf{x} + k_y\mathbf{y} + k_z\mathbf{z} = k_0\mathbf{n} \tag{7.46}$$

and the module of the wave number is:

$$k_0 = \sqrt{k_x^2 + k_y^2 + k_z^2} \tag{7.47}$$

Considering the position vector ($\mathbf{r} = x\mathbf{x} + y\mathbf{y} + z\mathbf{z}$) the electric field can be expressed in its components:

$$\begin{cases} E_x(x, y, z) = |E_x^*| e^{-i\mathbf{k}\cdot\mathbf{r}} \\ E_y(x, y, z) = |E_y^*| e^{-i\mathbf{k}\cdot\mathbf{r}} \\ E_z(x, y, z) = |E_z^*| e^{-i\mathbf{k}\cdot\mathbf{r}} \end{cases} \tag{7.48}$$

The electric field is the combination of its three components vectorial components:

$$\begin{cases} \mathbf{E}_0 = |E_x^*|\mathbf{x} + |E_y^*|\mathbf{t} + |E_z^*|\mathbf{z} \\ \mathbf{E} = \mathbf{E}_0 e^{-i\mathbf{k}\cdot\mathbf{r}} \end{cases} \tag{7.49}$$

and finally the divergence theorem of the electric field imposes the condition of perpendicularity between the electric field and the wave number vector:

$$\mathbf{k} \cdot \mathbf{E}_0 = 0 \tag{7.50}$$

Now it is possible to consider the curl equation of the Magnetic Field in the frequency domain 7.7 and re-write it to obtain a new relation between magnetic field and electric field that relates the magnetic field is in a plane normal to the wave number (propagation direction) and also perpendicular to the electric field as shown in figure 7.4.

$$\mathbf{H} = i\frac{1}{\omega\mu_0}\nabla \times \mathbf{E} = \frac{1}{Z_0}\mathbf{n} \times \mathbf{E} \tag{7.51}$$

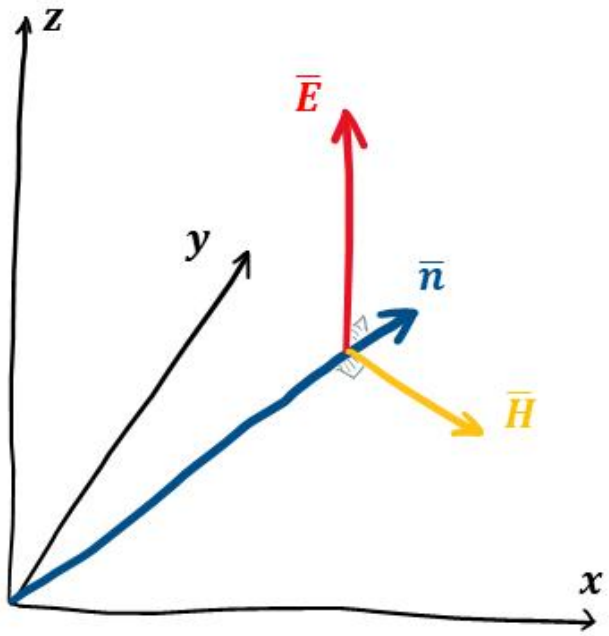

Figure 7.4: Electric field (**E**), magnetic field (**H**) and propagation vector (**n**) in the space for a general plane wave solution.

7.2.4 Energy and Power of an Electromagnetic Wave

A source of electromagnetic energy sets up fields that store electric and magnetic energy and carry power that may be transmitted or dissipated as loss. In the sinusoidal steady-state case, the time-average stored electric energy in a volume region (Ω) is given by:

$$W_e = \frac{1}{4}Re\left(\int_\Omega \mathbf{E} \cdot \mathbf{D}^* dV\right) \tag{7.52}$$

and the stored magnetic energy is

$$W_m = \frac{1}{4}Re\left(\int_\Omega \mathbf{H} \cdot \mathbf{B}^* dV\right) \tag{7.53}$$

As seen in chapter 2 the Poynting vector is:

$$\mathbf{S} = \mathbf{E} \times \mathbf{H}^* \tag{7.54}$$

and the Poynting's theorem states the complex power balance equation between the power delivered by the source (P_s), the power transmitted through the surface (P_0), the power dissipated in the volume region (P_l) and the sum of the "reactive" energy stored in the area multiplied by a factor 2ω.

$$P_s = P_0 + P_l + i2\omega \left(W_m - W_e\right) \tag{7.55}$$

where the power dissipated in the volume region is due to to conductivity, dielectric, and magnetic losses:

$$P_l = \frac{1}{2}\sigma \int_\Omega |\mathbf{E}|^2 dV + \frac{1}{2}\omega \int_\Omega \epsilon_r'' \epsilon_0 |\mathbf{E}|^2 dV + \frac{1}{2}\omega \int_\Omega \mu_r'' \mu_0 |\mathbf{H}|^2 dV \tag{7.56}$$

and the power transmitted through the surface ($\partial\Omega$) is described by the flux of the poynting vector:

$$P_0 = \frac{1}{2} \oint_{\partial\Omega} \mathbf{S} \cdot d\mathbf{s} \tag{7.57}$$

7.2.5 Plane wave reflection from a media interface

It is fundamental to introduce and study reflection coefficient that well describes the transmission problem for a RF and MW problem. To do that it is possible to analyze the the behavior of electromagnetic fields at the interface of various types of media, including lossless media, lossy media, good conductors, or a perfect conductors. With no loss of generality we can assume that the incident plane wave has an electric field vector oriented along the x-axis and is propagating along the positive z-axis. Electromagnetic fields may be studied for $z < 0$ and it is possible to define two different kind of EM fields: reflected ($\mathbf{E}_r$ and $\mathbf{H}_r$) and incident ($\mathbf{E}_i$ and $\mathbf{H}_i$). The incident fields to a certain boundary interface are:

$$\begin{cases} \mathbf{E}_i = \mathbf{x} E_0 e^{-ik_0 z} \\ \mathbf{H}_i = \mathbf{y} \frac{1}{Z_0} E_0 e^{-ik_0 z} \end{cases} \tag{7.58}$$

The reflected fields to a certain boundary interface are instead:

$$\begin{cases} \mathbf{E}_r = \Gamma \left(\mathbf{x} E_0 e^{+ik_0 z}\right) \\ \mathbf{H}_r = \Gamma \left(-\mathbf{y} \frac{1}{Z_0} E_0 e^{+ik_0 z}\right) \end{cases} \tag{7.59}$$

and equations system 7.59 introduces the reflection coefficient (Γ) of the reflected electric field. It is possible at the same way define the transmission coefficient (T) of the transmitted electric field and the characteristic impedance of the region (Z_c):

$$\begin{cases} \mathbf{E}_t = T\left(\mathbf{x}E_0 e^{-\gamma z}\right) \\ \mathbf{H}_t = T\left(\mathbf{y}\frac{1}{Z_c}E_0 e^{-\gamma z}\right) \end{cases} \tag{7.60}$$

Taking into account equations 7.59,7.60,7.58 it is possible to obtain the equation system:

$$\begin{cases} 1+\Gamma = T \\ \frac{1-\Gamma}{Z_0} = \frac{T}{Z_c} \end{cases} \tag{7.61}$$

and find a nice relation between the intrinsic impedances and the reflection coefficient:

$$\Gamma = \frac{Z_c - Z_0}{Z_c + Z_0} \tag{7.62}$$

and also to explicit the transmission coefficient:

$$T = 1 + \Gamma = \frac{2Z_c}{Z_c + Z_0} \tag{7.63}$$

7.3 Transmission Line Theory

Transmission line theory bridges the gap between field analysis and basic circuit theory and therefore is of significant importance in the analysis of microwave circuits and devices. As we will see, the phenomenon of wave propagation on transmission lines can be approached from an extension of circuit theory or from a specialization of Maxwell's equations. In RFH and MWH process it is necessary to design the system to guarantee for example the good matching condition and the process robustness. Many times it is useful to consider the system or only small parts of it (cables, connections) as TR-lines: The key difference between circuit theory and transmission line theory is electrical size. Circuit analysis assumes that the physical dimensions of the network are much smaller than the electrical wavelength, while transmission lines may be a considerable fraction of a wavelength, or many wavelengths, in size. Thus a transmission line is a distributed parameter network, where voltages and currents can vary in magnitude and phase over its length, while ordinary circuit analysis deals with lumped elements, where voltage and current do not vary appreciably over the physical dimension of the elements. It is possible to model the line shown in figure **??** with lumped elements per unit length: the series resistance (R $[\Omega/m]$), the series inductance (L $[H/m]$), the parallel conductance (G $[S/m]$)

and the parallel capacitance (C $[F/m]$). Considering Kirchhoff's voltage law and Kirchhoff's current law it is possible to the infinitesimal line for the sinusoidal condition:

$$\begin{cases} \frac{\partial V(z)}{\partial z} = -\left(R + i\omega L\right) I\left(z\right) \\ \frac{\partial I(z)}{\partial z} = -\left(G + i\omega C\right) V\left(z\right) \end{cases} \tag{7.64}$$

It is possible to solve simultaneously equations 7.64 to give wave equations for voltage and current, defining again the complex propagation constant as already done in the previous section and obtain the traveling wave solution for electric voltage:

$$V\left(z\right) = V_0^+ e^{-\gamma z} + V_0^- e^{+\gamma z} \tag{7.65}$$

and for electrical current:

$$I\left(z\right) = I_0^+ e^{-\gamma z} + I_0^- e^{+\gamma z} \tag{7.66}$$

and the propagation constant is function of the electric network parameters:

$$\gamma = \alpha + i\beta = \sqrt{\left(R + i\omega L\right)\left(G + i\omega C\right)} \tag{7.67}$$

From previous equations it is possible to get the characteristic impedance of the system:

$$Z_0 = \frac{V_0^+}{I_0^+} = \frac{-V_0^-}{I_0^-} = \sqrt{\frac{R + i\omega L}{G + i\omega C}} \tag{7.68}$$

Transmission Line: Coaxial Line

In MW and RF heating processes some of most important component are connection cables. Coaxial line makes possible to connect different components with simplicity and without the necessity to properly design wave-guides (e.g. TE-air wave-guides). Coaxial lines must guarantee low losses through the line and robustness of the system. Because of currents and voltage may be extremely high there is the necessity anyway to pay attention in the cable choosing. The electric and magnetic fields of a traveling TEM wave inside the coaxial line can be describe with:

$$\mathbf{E} = V_0 \frac{\mathbf{r}}{r \ln \frac{b}{a}} e^{-\gamma z} \tag{7.69}$$

$$\mathbf{H} = I_0 \frac{\theta}{2\pi r} e^{-\gamma z} \tag{7.70}$$

where the propagation constant (γ) of the line is expressed by 7.67 . The conductors are assumed to have a surface resistivity (Rs) , and the material filling the space between the conductors is assumed to have a complex permittivity ($\epsilon = \epsilon^{'} - i\epsilon^{''}$) and a real permeability ($\mu = \mu_r \mu_0$). The

coaxial line is defined by a inner radius (a $[m]$) and an outer radius (b $[m]$). It is possible to obtain the parameters of the coaxial line:

$$L = \frac{\mu}{2\pi} \ln \frac{b}{a} \tag{7.71}$$

$$C = \frac{2\pi\epsilon^{'}}{\ln \frac{b}{a}} \tag{7.72}$$

$$R = \frac{R_s}{2\pi} \frac{b+a}{ab} \tag{7.73}$$

$$G = \frac{2\pi\omega\epsilon^{''}}{\ln ba} \tag{7.74}$$

Starting from a coaxial line it is possible to derive the telegrapher equations 7.64 only using circuit theory or Maxwell's equations. A TEM wave on the coaxial line will be characterized by $E_z = H_z = 0$; furthermore, due to its symmetry, the fields will have no θ variation, and then $\frac{\partial}{\partial\theta} = 0$. The fields inside the coaxial line will satisfy Maxwell's curl equations:

$$\begin{cases} \nabla \times \mathbf{E} = -i\omega\dot{\mu}\mathbf{H} \\ \nabla \times \mathbf{H} = i\omega\dot{\epsilon}\mathbf{E} \\ \frac{\partial E_r}{\partial z} = -i\omega\dot{\mu}H_\theta \\ \frac{\partial H_\theta}{\partial z} = -i\omega\dot{\epsilon}E_r \end{cases} \tag{7.75}$$

and considering the TEM hypothesis:

$$\begin{cases} E_\theta = \frac{f(z)}{r} \\ H_\theta = \frac{g(z)}{r} \\ E_r = \frac{h(z)}{r} \end{cases} \tag{7.76}$$

Voltage drop between the the conductors (inner and outer conductive layer) can be computed as the line-integral of the electric field and the current that flows through the system as the surface integral of the magnetic flux. Finally, it is possible to obtain telegrapher equations:

$$\begin{cases} \frac{\partial V(z)}{\partial z} = -i\omega L I\,(z) \\ \frac{\partial I(z)}{\partial z} = -\left(G + i\omega C\right) V\,(z) \end{cases} \tag{7.77}$$

For a coaxial line it is easy to derive its main transmission parameters. The propagation constant:

$$\gamma = i\omega\sqrt{\dot{\mu}\dot{\epsilon}} \tag{7.78}$$

The characteristic impedance (Z_0 [Ω]) of a TEM coaxial-line is instead:

$$Z_0 = \frac{V_0}{I_0} = \sqrt{\frac{\dot{\mu}}{\dot{\epsilon}}} \frac{1}{2\pi} \ln \frac{b}{a} \tag{7.79}$$

One of most relevant problems of transmission lines is when they are terminated to a general load. It is easy to understand that in RF-MW heating process that is normal. If we consider for example that our heating device (cavity or electrodes) can be modeled with a synthetic impedance (Z_{MWH} [Ω]) that describes its electromagnetic behaviour, the coaxial line that connects the wave generator to the load is terminated to the impedance of the heating device. This problem will illustrate wave reflection on transmission lines, a fundamental property of distributed systems. Considering as already done in the previous section that an incident wave ($V_0^+ e^{-i\beta z}$ is generated from a field source for negative z-coordinates, it is possible to obtain the voltage-reflection-coefficient (Γ):

$$\Gamma = \frac{V_0^-}{V_0^+} = \frac{Z_{MWH} - Z_0}{Z_{MWH} - Z_0} \tag{7.80}$$

And finally the total voltage and current waves on the line can then be written as

$$\begin{cases} V(z) = V_0^+ \left(e^{-i\beta z} + \Gamma e^{i\beta z}\right) \\ I(z) = \frac{V_0^+}{Z_0} \left(e^{-i\beta z} - \Gamma e^{i\beta z}\right) \end{cases} \tag{7.81}$$

From these equations it is seen that the voltage and current on the line consist of a superposition of an incident and a reflected wave; such waves are called standing waves. Only when $\Gamma = 0$ is there no reflected wave. Equation 7.80 states that to don't have reflection, the total impedance of the heating device (RF or MW) must be equal to the characteristic impedance of the transmission line, as seen from. That condition was already introduced in chapter 5 for the so called perfect-matching condition in radio frequency matching design. If we now consider the time-average power flow along the line it easy to see that the average power flow is constant at any point on the line and that the total power delivered to the load is equal to the incident power minus the reflected power.

$$P_{avg} = \frac{1}{2} \frac{|V_0^+|^2}{Z_0} \left(1 - |\Gamma|^2\right) \tag{7.82}$$

When the load is mismatched a certain amount of power is not delivered to the load, and practically can only return to the generator (and that can also destroy it) and it is useful to define the so-called return loss (RL [dB]):

$$RL = -20 \log |\Gamma| \tag{7.83}$$

When the load is mismatched another the presence of a reflected wave leads to standing waves, and the magnitude of the voltage on the line is not constant but instead oscillates between a minimum and a maximum value. As the voltage-reflection-coefficient increases, the ratio of V_{max} to V_{min} increases, so a measure of the mismatch of a line, called the standing wave ratio (SWR [–]):

$$SWR = \frac{V_{max}}{V_{min}} = \frac{1 + |\Gamma|}{1 - |\Gamma|} \tag{7.84}$$

An automatic matching network solves the transmission problem varying its components in a certain way to make zero the standing wave ratio.

7.3.1 The Smith Chart

The Smith chart represented in figure **??** is probably the best known and most widely used way to analyze and solve the transmission line problems. It was developed in 1939 by P. Smith. It is based on a polar plot of the voltage reflection coefficient [74]. The real utility of the Smith chart, however, lies in the fact that it can be used to convert from reflection coefficients to normalized impedances. The reflection coefficient may be expressed in magnitude and phase:

$$\dot{\Gamma} = |\Gamma| e^{i\theta} = \frac{\dot{Z}_L - 1}{Z_L + 1} \tag{7.85}$$

where the load impedance ($\dot{Z}_L$ [Ω]) may be normalized with a complex number defined by a real part and an imaginary part:

$$\dot{z}_L = \frac{\dot{Z}_L}{Z_0} = \frac{1 + |\Gamma| e^{i\theta}}{1 - |\Gamma| e^{i\theta}} = r_L + i x_L \tag{7.86}$$

that approach makes possible to obtain the total resistance of the load and the total reactance of the laod:

$$\begin{cases} R_L = Z_0 \frac{1 - Re(\Gamma)^2 - Im(\Gamma)^2}{(1 - Re(\Gamma))^2 + Im(\Gamma)^2} \\ X_L = Z_0 \frac{2 Im(\Gamma)}{(1 - Re(\Gamma))^2 + Im(\Gamma)^2} \end{cases} \tag{7.87}$$

The Smith chart can also be used to graphically solve the transmission line impedance equation to minimize the reflected power since this can be written in terms of the generalized reflection coefficient.

7.3.2 Lossy transmission lines

In practice, transmission lines have losses due to finite conductivity and/or lossy dielectric, but these losses are usually small. In many practical problems loss may be neglected, but at

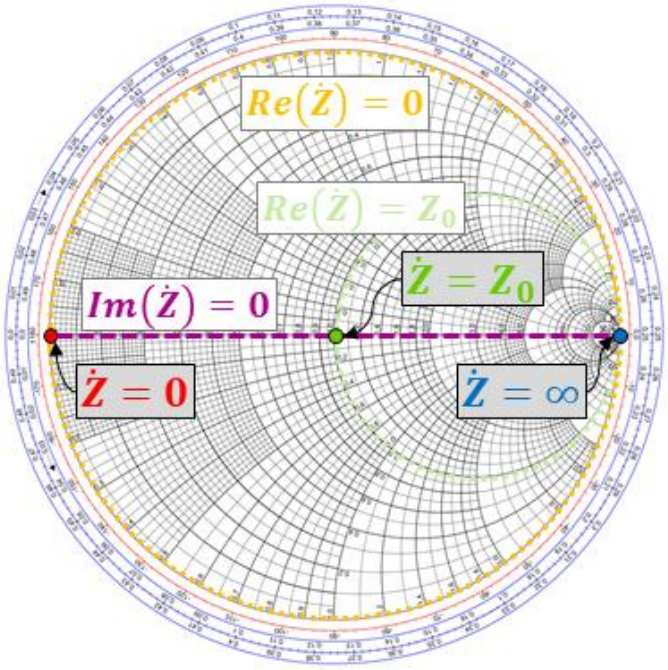

Figure 7.5: Smith Chart. In figure are presented several well known impedances ($\dot{Z}_L = \dot{z}_L Z_0$). The blue point represents the open load condition, the green point represents the perfect matched condition and the red dot represents the short-circuit condition.

other times the effect of loss may be very important, as when dealing with the attenuation of a transmission line, noise introduced by a lossy line, or the quality factor Q $[-]$ of a resonator. In this section we will study the effects of loss on transmission line behavior and show how the attenuation constant can be computed as:

$$\gamma = i\omega\left(\sqrt{LC}\right)\sqrt{1 - i\left(\frac{R}{\omega L} + \frac{G}{\omega C} - \frac{RG}{\omega^2 LC}\right)} \tag{7.88}$$

In most practical microwave and radio-frequency heating transmission lines the losses in the line are small compared to power dissipated in the heating device. In that case it is possible to simplify the propagation constant and the characteristic impedance of the line. The two main hypothesis for those systems are:

$$\begin{cases} \frac{R}{\omega L} \ll 1 \\ \frac{G}{\omega C} \ll 1 \end{cases} \tag{7.89}$$

and then the propagation constant and the characteristic impedance can be approximated to:

$$\begin{cases} \gamma = \alpha + i\beta \simeq \left[\frac{1}{2}\left(\frac{R}{Z_0} + GZ_0\right)\right] + i\left[\omega\sqrt{LC}\right] \\ Z_0 \simeq \sqrt{\frac{L}{C}} \end{cases} \tag{7.90}$$

7.4 Waveguides

Heaviside considered the possibility of propagation of electromagnetic waves inside a closed hollow tube in 1893, but he rejected the idea because he believed that two electrical conductive materials were necessary for the transfer of electromagnetic energy [30]. In 1897, Lord Rayleigh (John William Strutt) mathematically proved that wave propagation in waveguides was possible for both circular and rectangular cross sections [70]. Rayleigh also noted the infinite set of waveguide modes of the TE and TM type that were possible and the mathematical existence of a cutoff frequency. Waveguides have the advantage of high power-handling capability and low losses on them. In this section the properties of several types of waveguide typically used int MW systems are presented and analyzed. First of all it is necessary to understand the different types of wave propagation and modes that can exist on general waveguide geometries. Transmission lines that consist of two or more conductors may support transverse electromagnetic (TEM) waves. TEM lines are characterized by:

- a uniquely defined voltage,
- a uniquely defined current,
- a uniquely defined characteristic impedance,

Waveguides taht consist of a single conductor, support insted transverse electric waves (TE) and transverse magnetic waves (TM). Such waves can't admit an unique definition of characteristic impedance.

7.4.1 TEM, TE and TM waves and their solution

Considering only general two-conductor transmission lines and closed waveguides it is possible to assume time-harmonic electric field (**E**) and magnetic field **H** and rewriting curl-Maxwell's equations it is possible to obtain a relation of x-component and y-component as function of z-compo net. In figure 7.6:

$$H_x = i\frac{1}{k_c^2}\left(\omega\epsilon\frac{\partial E_z}{\partial y} - \beta\frac{\partial H_z}{\partial x}\right) \tag{7.91}$$

$$H_y = -i\frac{1}{k_c^2}\left(\omega\epsilon\frac{\partial E_z}{\partial x} + \beta\frac{\partial H_z}{\partial y}\right) \tag{7.92}$$

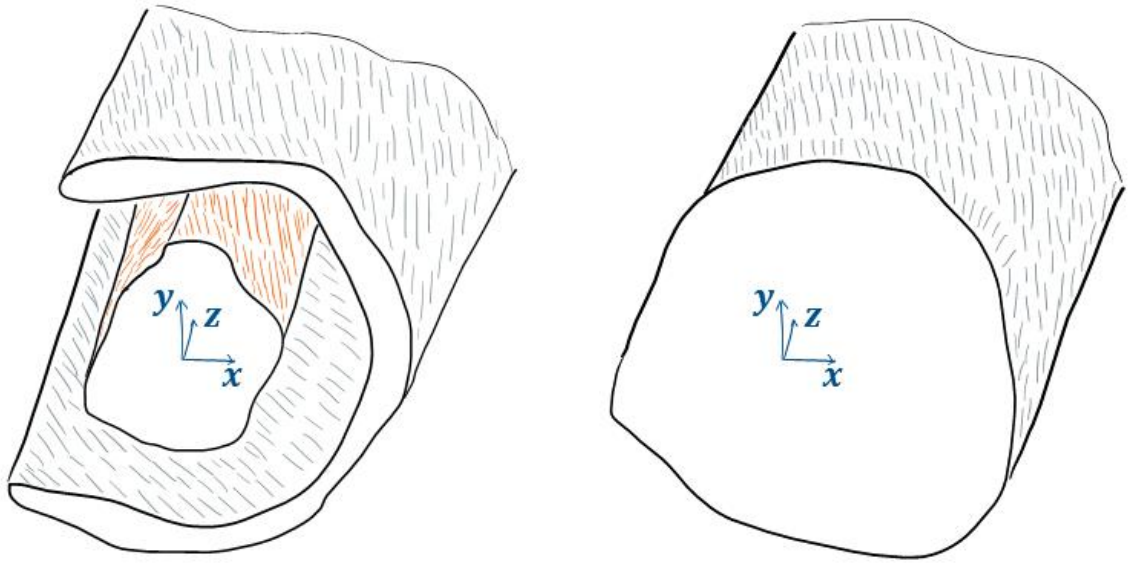

(a) (b)

Figure 7.6: Transmission Lines. (a) General two-conductor transmission line and (b) closed waveguide.

$$E_x = -i\frac{1}{k_c^2}\left(\beta\frac{\partial E_z}{\partial x} + \omega\mu\frac{\partial H_z}{\partial y}\right) \tag{7.93}$$

$$E_y = i\frac{1}{k_c^2}\left(-\beta\frac{\partial E_z}{\partial y} + \omega\mu\frac{\partial H_z}{\partial x}\right) \tag{7.94}$$

where the cut-off wave number (k_c):

$$k_c = k^2 - \beta^2 \tag{7.95}$$

and the wave number (k) of the material filling the transmission line or waveguide region can be more generally a complex operator, if the dielectric material is lossy:

$$k = \omega\sqrt{\dot{\mu}\dot{\epsilon}} \tag{7.96}$$

Attenuation in a transmission line or waveguide can be caused by either dielectric loss (due to the oscillating electric field) or conductor loss (due to the effect of low conductivity and electric current density). The total attenuation constant (α) can be considered as the sum of the two previous effects:

$$\alpha = \alpha_d + \alpha_c \tag{7.97}$$

the complex propagation constant in first analysis may take into account only dielectric losses, and if the dielectric fills the waveguide (or transmission line):

$$\gamma = \alpha_d + i\beta = \sqrt{k_c^2 - \omega^2\mu_0\epsilon_0\epsilon_r\left(1 - i\tan\delta\right)} \tag{7.98}$$

TEM waves

The transverse fields of a TEM wave are thus the same as the static fields that can exist between the conductors. They are characterized by z-components equal to zero. The cutoff wave number must be zero for a TEM wave:

$$k_{c-TEM} = 0 \tag{7.99}$$

That means the propagation constant must be equal to the wave number:

$$\beta = k \tag{7.100}$$

The wave impedance of a TEM mode can be found as the ratio of the transverse electric and magnetic fields and it must be equal to the characteristic impedance of the vacuum:

$$Z_{TEM} = \frac{E_x}{H_y} = \frac{-E_y}{H_x} = \sqrt{\frac{\mu}{\epsilon}} = Z_0 \tag{7.101}$$

and the attenuation constant:

$$\alpha_d \simeq \frac{k}{2} \tan\delta + i\beta \tag{7.102}$$

TE waves

Transverse electric (TE) waves are characterized by z-component of the electric field equals to zero. The propagation constant (β) is generally a function of the frequency and of the geometry because of the cut-off wave number can't be zero.

$$\beta = \sqrt{k^2 - k_c^2} \tag{7.103}$$

The TE wave impedance is instead:

$$Z_{TE} = \frac{E_x}{H_y} = \frac{-E_y}{H_x} = \omega\frac{\mu}{\beta} = Z_0\frac{k}{\beta} \tag{7.104}$$

and the attenuation constant:

$$\alpha_d \simeq \frac{k^2}{2\beta} \tan\delta + i\beta \tag{7.105}$$

TM waves

Transverse electric (TE) waves are characterized by z-component of the magentic field equals to zero. The propagation constant (β) is generally a function of the frequency and of

the geometry because of the cut-off wave number can't be zero.

$$\beta = \sqrt{k^2 - k_c^2} \tag{7.106}$$

The TM wave impedance is instead:

$$Z_{TM} = \frac{E_x}{H_y} = \frac{-E_y}{H_x} = \frac{1}{\omega}\frac{\beta}{\epsilon} = Z_0\frac{\beta}{k} \tag{7.107}$$

and the attenuation constant:

$$\alpha_d \simeq \frac{k^2}{2\beta}\tan\delta + i\beta \tag{7.108}$$

7.4.2 Rectangular Waveguides

Rectangular waveguides are one of the most used type of transmission lines used to transport microwave signals in MW applications. In the applications proposed in that work they are typically the geometry used to transfer power from the MW generator (Magnetron or Solid State MW generator) to the resonant cavity. Nowadays micro-strips and strip-lines are becoming extremely interesting alternative to rectangular waveguides but for high power applications ($P_{MW} > 1[kW]$) rectangular waveguides still represent the best choice. The hollow rectangular waveguide can propagate TM and TE modes but not TEM. waves since only one conductor is present (and it is external). We will see that the TM and TE modes of a rectangular waveguide have cutoff frequencies ($f_c\ [Hz]$) below which propagation is not possible: evanescent modes. In that section only TE modes analysis is presented because of for MWH process typically rectangular waveguides that admit only TE modes are used and designed [16].

TE Modes for a rectangular waveguide

The geometry of a rectangular waveguide is extremely simple: the cross section (xy-plane) is a rectangle (characterized by its width ($a\ [m]$) and its height ($b\ [m]$)) and the z-component of the electric field must be zero as seen in the previous section [20]. A canonical rectangular waveguide is presented in figure 7.7. With these hypothesis the wave equation can be reduced as:

$$\left(\frac{\partial^2}{\partial x^2} + \frac{\partial^2}{\partial y^2} + k_c^2\right) H_z e^{i\beta z} = 0 \tag{7.109}$$

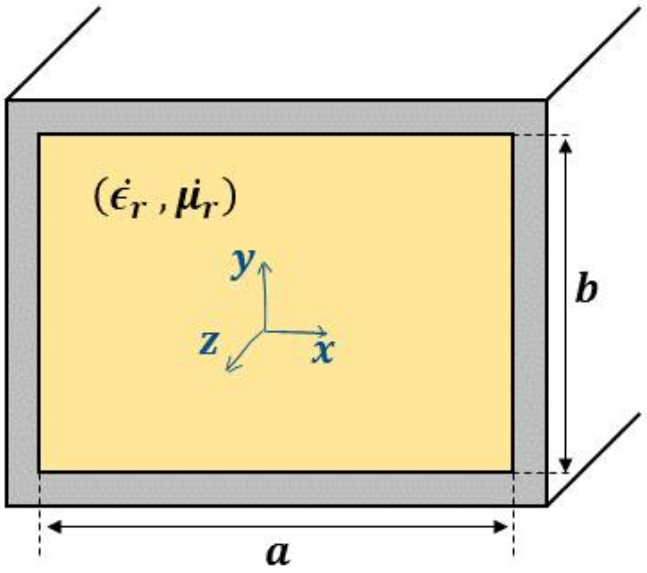

Figure 7.7: Rectangular waveguide. The propagation direction for the geometry is the z-coordinate. The rectangular waveguide is characterized uniquely by its width (a $[m]$) and by its height (b $[m]$).

where the cutoff wave number is:

$$k_c^2 = k^2 - \beta^2 = k_x^2 + k_y^2 \tag{7.110}$$

If we solve the wave equation at the end we can find the transverse field components of the so called TE_{mn} mode, where $m = 0, 1, 2, ...$ and $n = 0, 1, 2, ...$ and each mode is characterized by a combination of m and n. The cutoff wave number can be rewritten as function of m and n:

$$k_c = \sqrt{\left(\frac{m\pi}{a}\right)^2 + \left(\frac{n\pi}{b}\right)^2} \tag{7.111}$$

The propagation constant highlights that propagation may occur only if its value is real and that imposes a constraint on the wave number: it must be greater than the cutoff wave number:

$$Im\,(\beta) = 0 \Rightarrow k > k_c \tag{7.112}$$

Anyway each mode (has a cutoff frequency f_{c-mn} given by:

$$f_{c-mn} = \frac{k_c}{2\pi\sqrt{\mu\epsilon}} = \frac{1}{2\pi}\,(\mu\epsilon)^{-\frac{1}{2}}\left[\left(\frac{m\pi}{a}\right)^2 + \left(\frac{n\pi}{b}\right)^2\right]^{\frac{1}{2}} \tag{7.113}$$

The mode with the lowest cutoff frequency is called the dominant mode and in that case (if $a > b$) the dominant mode is the TE_{10}:

$$f_{c-10} = \frac{1}{2a\sqrt{\mu\epsilon}} \tag{7.114}$$

Finally it is possible to calculate also characteristic impedance of a rectangular waveguide for the dominant mode and remembering that the propagation constant is $k = \omega\sqrt{\epsilon\mu}$:

$$Z_{TE} = Z_0\frac{k}{\beta} = Z_0\frac{k}{\sqrt{k^2 - \left(\frac{\pi}{a}\right)^2}} = Z_0\frac{k}{\beta} = Z_0\frac{1}{\sqrt{1 - \left(\frac{\pi}{ak}\right)^2}} \tag{7.115}$$

In many applications can be interesting to know also the wavelength of the waveguide. For example if we want to solve numerically (e.g. FEM model) it is necessary to mesh the volume or surface regions. To obtain a good discretizationn of the geometry is necessary to know a characteristic dimension of the electromagnetic wave: the waveguide-wavelength (λ_g $[m]$) and for a rectangular waveguide with only TE_{mn} and it is the distance between two maximum in the waveguide:

$$\lambda_g = \frac{2\pi}{\beta} = \frac{2\pi}{\sqrt{k^2 - \left(\frac{\pi}{a}\right)^2}} = \frac{2\pi}{k}\frac{1}{\sqrt{1 - \left(\frac{\pi}{ak}\right)^2}} = \lambda\frac{1}{\sqrt{1 - \left(\frac{\pi}{ak}\right)^2}} > \lambda \tag{7.116}$$

At a given operating frequency (f_w $[Hz]$) only modes having $f_w > f_c$ will propagate. Modes with $f_w > f_c$ will decay exponentially away from the source of excitation, such modes are called evanescent modes. If more than one mode is propagating, the waveguide is said to be overmoded. In a MWH design typically waveguide dimensions are chosen so that only the dominant TE_{10} mode will propagate. In that case we are not interested in other modes and it is possible to easily find the cutoff wave number and the propagation constant:

$$\begin{cases} k_c = \frac{\pi}{a} \\ \beta = \sqrt{k^2 - \left(\frac{\pi}{a}\right)^2} \end{cases} \tag{7.117}$$

When a waveguide for high power transmission purposes is design it is necessary to compute also losses due to dielectric losses (for the effect of high frequency oscillation of the electric field) and conduction losses due to "real" surface resistivity of the external conductors. Attenuation constant as seen in the previous section takes into account losses:

$$\alpha_c = \frac{R_s}{a^3 b\beta k Z_0}\left(2\pi^2 b + a^3 k^2\right) \tag{7.118}$$

where R_s is the surface resistances of boundaries of the waveguide and Z_0 is the vacuum-free characteristic impedance.

7.4.3 Circular Waveguides

A hollow, round metal pipe also supports TE and TM waveguide modes. Figure 7.8 shows the geometry of such a circular waveguide, with its inner radius (a $[m]$). Because

cylindrical geometry is involved, it is appropriate to employ cylindrical coordinates and do a coordination transformation from $[x, y, z]$ to $[\rho, \Phi, z]$ [14] For circular waveguide it is possible

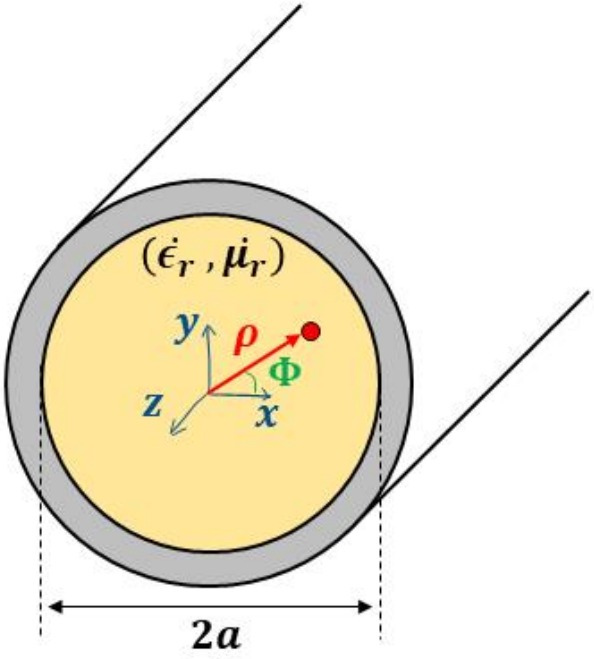

Figure 7.8: Circular waveguide. The propagation direction for the geometry is the z-coordinate. The circular waveguide is characterized uniquely by its radius (a $[m]$).

to derive the cylindrical components of the transverse fields from the longitudinal components as:

$$\begin{cases} E_\rho = -i\frac{1}{k_c^2}\left(\beta\frac{\partial E_z}{\partial \rho} + \omega\mu\frac{1}{\rho}\frac{\partial H_z}{\partial \Phi}\right) \\ E_\Phi = -i\frac{1}{k_c^2}\left(\beta\frac{1}{\rho}\frac{\partial E_z}{\partial \Phi} - \omega\mu\frac{\partial H_z}{\partial \rho}\right) \\ H_\rho = i\frac{1}{k_c^2}\left(\omega\epsilon\frac{1}{\rho}\frac{\partial E_z}{\partial \Phi} - \beta\frac{\partial H_z}{\partial \rho}\right) \\ H_\Phi = -i\frac{1}{k_c^2}\left(\omega\epsilon\frac{\partial E_z}{\partial \rho} + \beta\frac{1}{\rho}\frac{\partial H_z}{\partial \Phi}\right) \end{cases} \tag{7.119}$$

TE modes

For TE modes the z-component of the electric field must be zero, and thus the z-component of the magnetic field is a solution to the wave equation:

$$\nabla^2 H_z + k^2 H_z = 0 \tag{7.120}$$

and in cylindrical coordinates it is possible to obtain the Bessel's differential form of the wave equations:

$$\rho^2\frac{\partial^2 R}{\partial \rho^2} + \rho\frac{\partial R}{\partial \rho} + \left(\rho^2 k_c^2 - n^2\right) R = 0 \tag{7.121}$$

The TE_{nm} modes are thus defined by the cutoff wave number (k_{c-mn}):

$$k_{c-mn} = \frac{p'_{mn}}{a} \tag{7.122}$$

where n represents the number of circumferential variations (Φ $[rad]$) and m represents the number of radial variations (ρ), and then the propagation constant for a circular waveguide can be expresses as:

$$\beta_{mn} = \sqrt{k^2 - \left(\frac{p'_{mn}}{a}\right)^2} \tag{7.123}$$

The cut-off frequency instead is:

$$f_{c-mn} = \frac{1}{2\pi\sqrt{\epsilon\mu}} \frac{p'_{mn}}{a} \tag{7.124}$$

Some values of p'_{mn} are presented in table 7.1 and it highlights that the first TE-mode that propagates is the mode with the smallest p'_{nm}, which is the mode TE_{11}. This mode is therefore the dominant circular waveguide mode and the one most frequently used for RFH processes. For the dominant mode TE_{11} the characteristic impedance is:

Values of p'_{nm} for TE-modes of a Circular Waveguide			
m	1	2	3
n	p'_{nm}		
1	3.832	7.016	10.174
2	1.841	5.331	8.536
3	3.054	6.706	9.970

Table 7.1: Values of p'_{nm} for TE-modes of a Circular Waveguide.

$$Z_{TE-11} = \frac{E_\rho}{H_\Phi} = \frac{-E_\Phi}{H_\rho} = Z_0 \frac{k}{\beta} = Z_0 \frac{k}{\sqrt{k^2 - \left(\frac{3.832}{a}\right)^2}} = Z_0 \frac{1}{1 - \left(\frac{3.832}{ak}\right)^2} \tag{7.125}$$

Attenuation due to dielectric loss is given by equation 7.105. The attenuation due to a real lossy waveguide conductor can be found by computing the power loss per unit length of the circular guide as already done for the rectangular waveguide:

$$\alpha_c = \frac{R_s}{a\beta k Z_0}\left(k_c^2 + \frac{k^2}{14.684 - 1}\right) \tag{7.126}$$

. Circular waveguide may be used for example to properly make a inspect00ion-view-slot in a resonant cavity. If we want for example to measure with a thermal-imaging system the temperature load, it is possible to design a circular waveguide of a certain length to minimize the field leakage but to allow the temperature measure.

7.4.4 Coaxial Waveguide

The coaxial transmission line geometry is shown in figure 7.9, where the inner conductor is at a HV potential (V_0 $[V]$) and the outer conductor is at ground potential ($V_g = 0$ $[V]$) [71]. Coaxial waveguide more generally are designed to admit only TEM-mode propagation. We know that the fields can be derived from a scalar potential function, $V(\rho, \Phi)$, which is a solution to Laplace's equation. In cylindrical the problem that it is necessary to solve is:

$$\begin{cases} \frac{1}{\rho}\frac{\partial}{\partial\rho}\left(\rho\frac{\partial}{\partial\rho}V\right) + \frac{1}{\rho^2}\frac{\partial^2}{\partial\Phi^2}V = 0 \\ V\left(a, \Phi\right) = V_0 \\ V\left(b, \Phi\right) = V_g = 0 \end{cases} \tag{7.127}$$

Solving the equations system of 7.127 it is possible to get the solution of the potential scalar function:

$$V\left(\rho, \Phi\right) = V_0 \frac{\ln\frac{b}{\rho}}{\ln\frac{b}{a}} \tag{7.128}$$

The coaxial line, like the parallel plate waveguide, can also support TE and TM waveguide

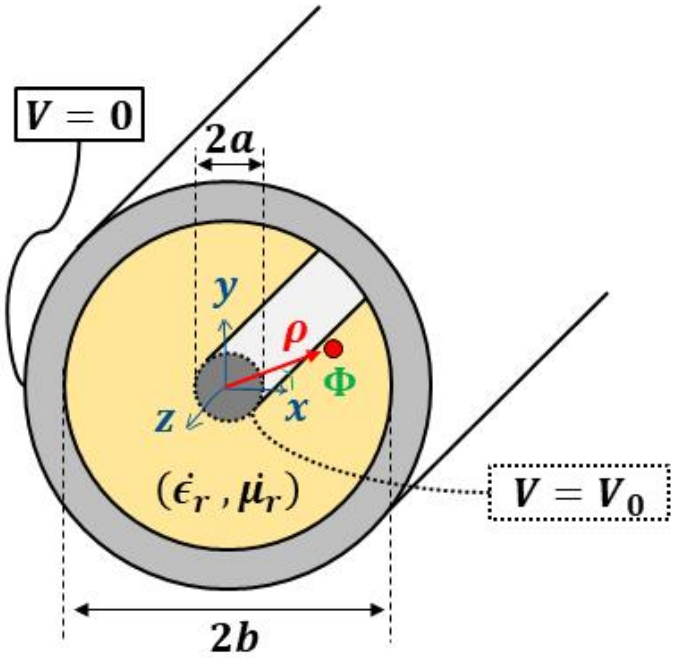

Figure 7.9: Coaxial waveguide. The propagation direction for the geometry is the z-coordinate. The circular waveguide is characterized by its inner radius (a $[m]$) and by its outer radius (b $[m]$). The outer conductor is at ground potential ($V_g = 0$).

modes in addition to the TEM-mode. TE and TM modes are typically evanescent, and that means they only have reactive effects. In coaxial waveguide design it is then necessary to avoid

the propagation of these higher order modes, and that means the design must limit the size of the coaxial waveguide. Now considering the dominant waveguide mode TE_{11} it is possible to get an approximate formulation of the cut-off wave-number (for $n = 1$):

$$k_c = \frac{2}{a+b} = \frac{2}{a\left(1+\frac{b}{a}\right)} \tag{7.129}$$

where $\psi = fracba$ is the ratio between the inner and the outer radius (or equivalently the ratio between the inner and the outer diameter), and we observe that $b/a > 1$ The cut-off frequency of the TE_{11} mode is then:

$$f_{c-11} = \frac{1}{2\pi\sqrt{\epsilon_0\mu_0}}\left(\frac{k_c}{\sqrt{\mu_r\epsilon_r}}\right) = \frac{1}{\pi\sqrt{\epsilon_0\mu_0}}\left(\frac{1}{a\left(1+\frac{b}{a}\right)\sqrt{\mu_r\epsilon_r}}\right) \tag{7.130}$$

7.5 Microwave Network Analysis

Microwave network theory was originally developed in the service of radar system and component development at the MIT Radiation Lab in the 1940s. This work was continued at the Polytechnic Institute of Brooklyn and other locations by researchers such as E. Weber [83], N. Marcuvitz [57] and many other researchers. Field analysis and Maxwell's equations make possible to solve many canonical problems, solving the relation between the magnetic field and the electric field in the domain. Previous sections show how it is possible to get lumped parameters (propagation constant, wave number, reference impedance) for some waveguide geometries. Now it is possible to interconnect various components and use network and/or transmission line theory to analyze the behavior of the entire system of components, including effects such as multiple reflections, loss, impedance transformations, and transitions from one type of transmission medium to another [81].

7.5.1 Impedance and equivalent current and voltage

At microwave frequencies the measurement of voltage or current is difficult and sometimes impossible unless a clearly defined terminal pair is available. The voltage of the B conductor relative to the A conductor can be found integrating the electric field along the path that connect the B conductor to A conductor (V_{AB} $[V]$):

$$V_{BA} = V = \int_B^A \mathbf{E}\cdot d\mathbf{l} \tag{7.131}$$

And the total currents flowing in the two conductors can be computed with the Ampere's law and with any closed loops that "hold" every single conductor alone:

$$\begin{cases} I_A = \oint_{\partial\Omega^A} \mathbf{H} \cdot d\mathbf{l} \\ I_B = \oint_{\partial\Omega^B} \mathbf{H} \cdot d\mathbf{l} \end{cases} \tag{7.132}$$

And then the characteristic impedance (Z_0 [Ω]) is:

$$Z_0 = \frac{V}{I} \tag{7.133}$$

For a waveguide geometry as seen in the previous sections it is possible to relate electric field and magnetic fields to propagation constant, geometrical parameters and material properties. For an arbitrary waveguide mode with both positively (+) and negatively (−) traveling waves it is possible to define transverse electric and magnetic fields as:

$$\mathbf{E}_t = \frac{1}{C_1}\mathbf{e}\left(V^+ e^{-i\beta z} + V^- e^{i\beta z}\right) \tag{7.134}$$

$$\mathbf{H}_t = \frac{1}{C_2}\mathbf{h}\left(I^+ e^{-i\beta z} - I^- e^{i\beta z}\right) \tag{7.135}$$

where the two equations introduce the amplitudes of the traveling waves (A^+ and A^-) and the transverse field variations ($\mathbf{e}$ and $\mathbf{h}$). It is possible to solve the problem considering power and impedance conditions: the complex power flow of the incident wave must be equal to half the product of the incident complex voltage and the conjugated complex of the incident current; the characteristic impedance must be equal instead to specific characteristic impedance of the mode. Finally, for a given waveguide n-mode (n is the number of the mode):

$$\mathbf{E}_t = \sum_{n=1}^{N} \frac{1}{C_{1n}}\left(V_n^+ e^{-i\beta_n z} + V_n^- e^{+i\beta_n z}\right)\mathbf{e}_n \tag{7.136}$$

$$\mathbf{H}_t = \sum_{n=1}^{N} \frac{1}{C_{1n}}\left(I_n^+ e^{-i\beta_n z} - I_n^- e^{+i\beta_n z}\right)\mathbf{h}_n \tag{7.137}$$

and the characteristic impedance is then equal to the wave impedance

$$Z_0 = \frac{V^+}{I^+} = \frac{V^-}{I^-} = \frac{C_1}{C_w} = Z_w = \frac{E_t}{H_t} \tag{7.138}$$

The concept of impedance, then, forms an important link between field theory and transmission line or circuit theory: the impedance is characteristic of the type of field, as well as of the medium. Consider a general waveguide it is possible to consider the arbitrary one-port network to derive a general relation between its impedance properties and electromagnetic energy stored in, and the power dissipated by, the network and the complex power flow:

$$\dot{P} = \frac{1}{2}\oint_{\Sigma} \mathbf{E} \times \mathbf{H}^* \cdot d\mathbf{s} = P_{MWH} + i2\omega\left(W_m - W_e\right) = \frac{1}{2}VI^* \tag{7.139}$$

and then is is possible to obtain the impedance of the system ($\dot{Z}$) as already done in chapter 5 but also considering the magnetic energy stored in the EM-domain:

$$\dot{Z} = R + iX = \frac{V}{I} = \frac{2P_{MWH} + i4\omega\left(W_m - W_e\right)}{|I|^2} \tag{7.140}$$

and so the real part and the imaginary part of the impedance is:

$$\begin{cases} R_{MWH} = 2\frac{P_{MWH}}{|I|^2} \\ X_{MWH} = 4\omega\frac{W_m - W_e}{|I|^2} \end{cases} \tag{7.141}$$

It is useful to understand the that sign of the reactance describe the capacitive-inductive type of the load.

7.6 Impedance matrix

The term port was introduced by H. A. Wheeler in the 1956 [85]. Because of it is possible to define in a microwave network for several "important-points" voltages and currents, it is then possible to use impedances and circuit theory to link these "important-points" or with a better therm: port each other. Considering an arbitrary N-port microwave network as depicted in figure **??**, at a specific point on the n-th port, a terminal plane, t_n, is defined along with equivalent voltages and currents for the incident and reflected waves as already seen in the previous section:

$$\begin{cases} V_n = V_n^+ + V_n^- \\ I_n = I_n^+ - I_n^- \end{cases} \tag{7.142}$$

and the impedance full matrix ($[Z]$ $[\Omega]$) of the microwave-rf network that relates voltages and currents is:

$$[V] = [Z][I] \tag{7.143}$$

where

$$Z_{ij} = \left.\frac{V_i}{I_j}\right|_{I_k=0, i\neq j} \tag{7.144}$$

7.7 The scattering matrix

For RF heating devices it easy to define voltages. It is clear that these devices are characterized by two (or more) electrodes between which an electrical potential difference is

applied, but for MW heating devices it is hard to "find" an unique way to define voltages. A representation more in accord with direct measurements, and with the ideas of incident, reflected, and transmitted waves, is given by the scattering matrix [48]. For an N-port network the scattering matrix ($[S]$ $[-]$) provides a complete description of the network and particularly it links incident ($V^{[}+]$) and reflected (V^{-}) voltages:

$$[V^{-}] = [S][V^{+}] \tag{7.145}$$

where

$$S_{ij} = \left.\frac{V_i-}{V_j+}\right|_{V_k^+=0}, i \neq j \tag{7.146}$$

An important property of the scattering matrix is that if the network is lossless, no real power can be delivered to the network and then the scattering matrix ($[S]$):

$$[S]^* = \left([S]^t\right)^{-1} \tag{7.147}$$

Power Waves and Generalized Scattering Parameters

From the total voltage and current on a transmission line it is possible to explicit the the incident and reflected voltage wave amplitudes:

$$\begin{cases} V_0^+ = \frac{1}{2}\left(V + Z_0 I\right) \\ V_0^- = \frac{1}{2}\left(V - Z_0 I\right) \end{cases} \tag{7.148}$$

And the "active" power dissipated to the load, if the characteristic impedance of the load is purely real (for example with a matching network).

$$P_{MWH} = \frac{1}{2Z_0}\left(|V_0^+|^2 - |V_0^-|^2\right) \tag{7.149}$$

Power waves are defined to solve the problem of 7.149. If we consider the incident power (a $[W]$), the reflected power (b $[W]$) and the reference impedance ($\dot{Z}_R = R_r + iX_R$)

$$\begin{cases} a = \frac{V + \dot{Z}_R I}{2\sqrt{R_R}} \\ b = \frac{V - \dot{Z}_R^* I}{2\sqrt{R_R}} \end{cases} \tag{7.150}$$

and then it is possible to define the active power flow delivered to the load (or dissipated in it):

$$P_{MWH} = \frac{1}{2}\left(|a|^2 - |b|^2\right) \tag{7.151}$$

and the reflection power coefficient (Γ_P) is equal to:

$$\Gamma_p = \frac{b}{a} = \frac{Z_L - Z_R^*}{Z_L + Z_R^*} \tag{7.152}$$

Observing the relation between the power waves and the voltage waves

$$\begin{cases} [a] = [F]\left([V] + [Z_R][I]\right) \\ [b] = [F]\left([V] - [Z_R][I]\right) \end{cases} \tag{7.153}$$

where the matrix $[F]$ is a diagonal matrix with specific elements:

$$F_{ii} = \frac{1}{2}\sqrt{Re\left(Z_{Ri}\right)} \tag{7.154}$$

it is possible also now to define the scattering matrix for the power waves ($[S_P]$) as:

$$[S_p] = [F]\left([Z] - [Z_R]^*\right)\left([Z] + [Z_R]\right)^{-1}[F]^{-1} \tag{7.155}$$

7.8 The transmission matrix

The impedance and the scattering matrix are the base to characterize a certain RF or MW component, but if a series of components are connected together it is necessary to define a transformation that makes possible to analyze the behaviour of the global network, and that for example relates voltages to currents or analyze power transfer efficiency. The ABCD matrix is defined for a general 2-port network:

$$\begin{bmatrix} V_i \\ I_i \end{bmatrix} = \begin{bmatrix} A_i & B_i \\ C_i & D_i \end{bmatrix} \begin{bmatrix} V_{i+1} \\ I_{i+1} \end{bmatrix} \tag{7.156}$$

The cascade of several 2-port components: for example if in the network are present N-components makes possible to relate voltages and currents of all components. The overall matrix $\begin{bmatrix} A_f & B_f \\ C_f & D_f \end{bmatrix}$ is then:

$$\begin{bmatrix} A_f & B_f \\ C_f & D_f \end{bmatrix} = \prod_{i=1}^{N} \begin{bmatrix} A_i & B_i \\ C_i & D_i \end{bmatrix} \tag{7.157}$$

and finally the relation between voltages and current (I_1, V_1) of the Port-1 and voltages and current (I_N, V_N) of the Port-N for a cascade of N-components can be expressed as:

$$\begin{bmatrix} V_i \\ I_i \end{bmatrix} = \begin{bmatrix} A_f & B_f \\ C_f & D_f \end{bmatrix} \begin{bmatrix} V_{n+1} \\ I_{n+1} \end{bmatrix} = \left(\prod_{i=1}^{N} \begin{bmatrix} A_i & B_i \\ C_i & D_i \end{bmatrix} \right) \begin{bmatrix} V_{n+1} \\ I_{n+1} \end{bmatrix} \tag{7.158}$$

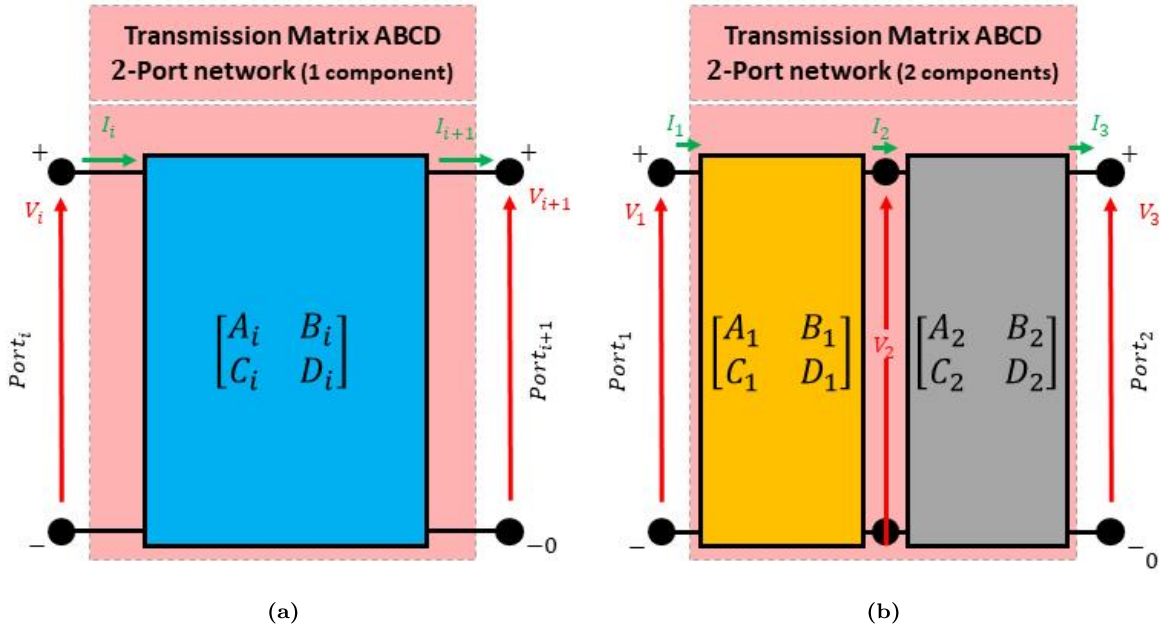

Figure 7.10: Matrix ABCD for 2-port networks. (a) 1 components, (b) 2 components.

7.9 Microwave Resonators

Microwave resonators are used in many applications, such as filters, oscillators, frequency meters, tuned amplifiers and dielectric cavity resonators for microwave heating applications. Because of that last application is the most important in MWH processes that section will analyze it more deeply and particularly how to discuss the excitation of cavity resonators using apertures (slots) and current sheets [15]. Because the operation of microwave resonators is very similar to that of lumped-element resonators of circuit theory, the basic characteristics of series and parallel RLC resonant circuits are extremely important to understand them.

7.9.1 Resonant circuits: Parallel and Series

It is possible to use equivalent *RLC*-equivalent circuit to model MW-resonators for a frequency range close to the resonance condition.

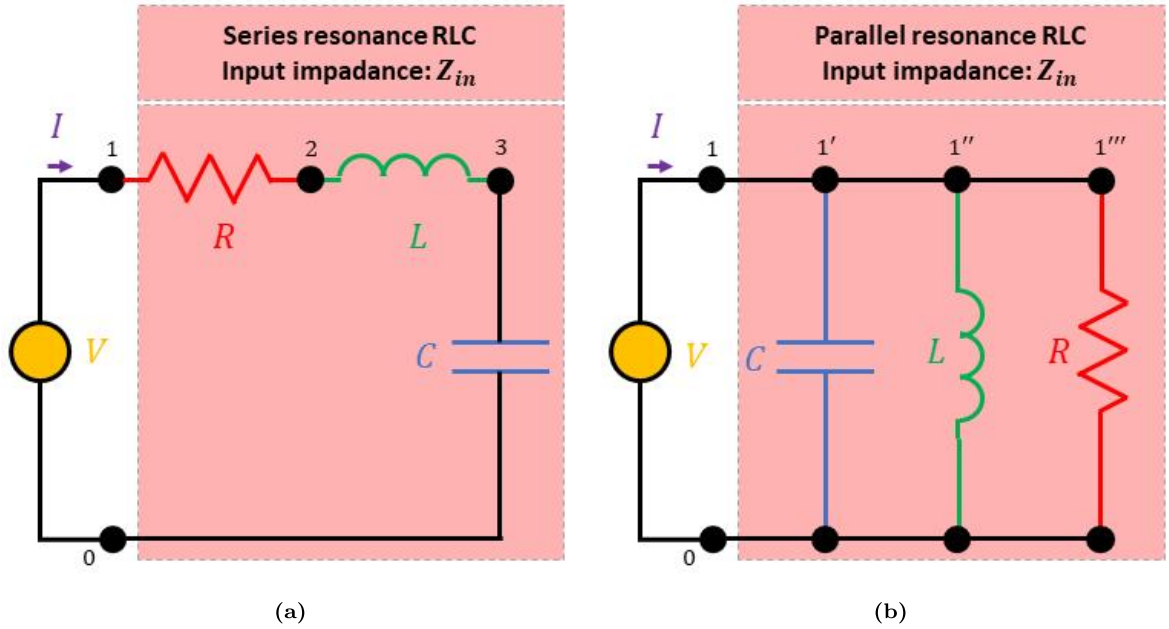

(a) (b)

Figure 7.11: RLC circuit resonators. They are characterized by a resistance (R [Ω]) an inductance (L [H]) and a capacitance (C [F]): (a) A series RLC resonator (b) A parallel RLC resonator.

Series resonant circuit

A series RLC resonant circuit is shown in figure 7.11a. It is possible to describe the input impedance (Z_{in} [Ω]) as:

$$Z_{in} = Z_R + Z_L + Z_C = R_{in} + iX_{in} = R + i\left(\omega L - \frac{1}{\omega C}\right) \tag{7.159}$$

and the complex power ($\dot{P}_{in}$) developed to the MW resonator is then proportional to the square of the current that flow through the circuit (series of the three impedances):

$$\dot{P} = \frac{1}{2}\dot{V}\dot{I}^* = \left[\frac{1}{2}|I|^2\right] R + i\left[\frac{1}{2}|I|^2\right]\left(\omega L - \frac{1}{\omega C}\right) \tag{7.160}$$

For MW heating processes the power dissipated in the resistor is the power delivered to the load that we want to heat (P_{MWH} [W]), the energy stored in the magnetic field (in the inductor) is instead the magnetic energy (W_m [J]) and the energy stored in the electric field (in the capacitor) is instead the electric energy (W_e [J]):

$$\dot{P}_{in} = P_{MWH} + i2\omega\left(W_m - W_e\right) \tag{7.161}$$

It is possible to obtain an explicit form for the input impedance as a function of the power flow:

$$\dot{Z}_{in} = 2\frac{P_{MWH}}{|I|^2} + i4\omega\frac{W_m - We}{|I|^2} \tag{7.162}$$

An important parameter that is useful to analyze resonant circuits is the quality factor (Q $[-]$) that is the ratio of stored energy to dissipated power in dielectrics and conductors:

$$Q = \omega \frac{W_{stored}}{P_dissipated} = \omega \frac{W_m + W_e}{P_{MWH}} \tag{7.163}$$

At series-resonance condition the magnetic energy stored in the inductor is equal to the electric energy stored in the capacitor:

$$W_m = W_e \tag{7.164}$$

and that means the imaginary part of the impedance of equation 7.162 is equal to zero and then:

$$\dot{Z}_{in} = 2\frac{P_{MWH}}{|I|^2} = R = R_{MWH} \tag{7.165}$$

The condition of series resonance also makes possible to obtain the so called resonance frequency (f_0 $[Hz]$):

$$f_0 = \frac{1}{2\pi}\frac{1}{\sqrt{LC}} \tag{7.166}$$

and the quality factor become the unloaded quality factor (Q_0 $[-]$):

$$Q_0 = \omega_0 \frac{W_m + W_e}{P_{MWH}} = \frac{1}{\sqrt{LC}}\frac{2W_m}{P_{MWH}} = \frac{1}{\sqrt{LC}}\frac{2W_e}{P_{MWH}} = \frac{1}{R}\sqrt{\frac{L}{C}} \tag{7.167}$$

At the series-resonance condition the quality factor (Q) assumes its maximum value (Q_0), but in any case it is possible to explicit the form of the quality factor as follows:

$$Q = \omega \frac{W_m + W_e}{P_{MWH}} = \omega \frac{L|I|^2 + C|V|^2}{2R|I|^2} = \omega \frac{L|I|^2 + \frac{1}{C\omega^2}|I|^2}{2R|I|^2} = \frac{1}{2R}\frac{L\omega^2 + \frac{1}{C}}{\omega} = \frac{1}{2R}\frac{LC\omega^2 + 1}{\omega C} \tag{7.168}$$

It is useful to analyze the input impedance ($\dot{Z}_{in}$) in a neighborhood ($\Delta\omega$) of resonance condition (ω_0), then the angular frequency can be expressed as:

$$\omega = \omega_0 + \Delta\omega \tag{7.169}$$

and the input impedance can be rewritten in its form:

$$\dot{Z}_{in} = R + i\omega L \frac{(\omega + \omega_0)(\omega - \omega_0)}{\omega^2} \simeq R\left(1 + i\frac{2Q_0}{\omega_0}\Delta\omega\right) \tag{7.170}$$

Parallel resonant circuit

A parallel RLC resonant circuit is shown in figure 7.11b. The input impedance is then:

$$\dot{Z}_{in} = \left[\frac{1}{R} - i\frac{1}{\omega L} + i\omega C\right]^{-1} \tag{7.171}$$

and it is possible to obtain the complex power delivered to the MW resonator:

$$\dot{P} = \frac{1}{2}\dot{V}\dot{I}^* = \frac{1}{2}|V|^2 \left[\frac{1}{R} + i\frac{1}{\omega L} - i\omega C\right] \tag{7.172}$$

At resonant condition (parallel-resonant condition) as already seen for the series model the electric energy stored in the capacitor and the magnetic energy stored in the inductor are equal and then the resonant frequency (f_0 $[Hz]$) is the same seen for the series resonant cavity:

$$f_0 = f_{0-series} = \frac{1}{2\pi}\frac{1}{\sqrt{LC}} \tag{7.173}$$

Considering now the definition of the quality factor seen in equation 7.163 the quality factor for the parallel circuit at the resonant condition(Q_0 $[-]$) is then:

$$Q_0 = \frac{1}{\omega_0}\frac{R}{L} = \omega_0 RC = R\sqrt{\frac{C}{L}} = Q_{0-series}^{-1} \tag{7.174}$$

The perturbation approach applied to the parallel circuit makes possible to analyze the behaviour of the input impedance ($\dot{Z}_{in}$) near the resonance condition ($\omega = \omega_0 + \delta\omega$):

$$\dot{Z}_{in} \simeq R\left(1 + i\frac{2Q_0}{\omega_0}\Delta\omega\right)^{-1} \tag{7.175}$$

Loaded and unloaded resonant cavity

If we imagine a resonant MW or RF system it is easy to understand that if an external load (Z_{ext}) is considered the behaviour of the global system changes. The unloaded quality factor (Q_0) is an intrinsic characteristic of the resonant system that does not takes into account external load. It is clear that the external load decrease the overall loaded quality factor ($Q^{'}$): If a series model and a parallel model are considered and the external load is purely resistive, then:

$$\begin{cases} R'_{ser} = R + R_{ext} \\ R'_{par} = \frac{R}{R_{ext}}R + R_{ext} \end{cases} \tag{7.176}$$

and in the same way it is possible to define the external quality factor (Q_{ext} $[-]$) that only describes the behaviour of a RF-MW resonant system where the resistor is only the external load, and respectively for the series-model and parallel-model:

$$Q_{ext} = \begin{cases} \omega_0 \frac{L}{R_{ext}} \\ \left(\omega_0 \frac{L}{R_{ext}}\right)^{-1} \end{cases} \tag{7.177}$$

and finally the "global" quality factor for the loaded condition ($Q^{'}$) is then:

$$Q^{'} = \frac{Q_0 Q_{ext}}{Q_0 + Q_{ext}} = \tag{7.178}$$

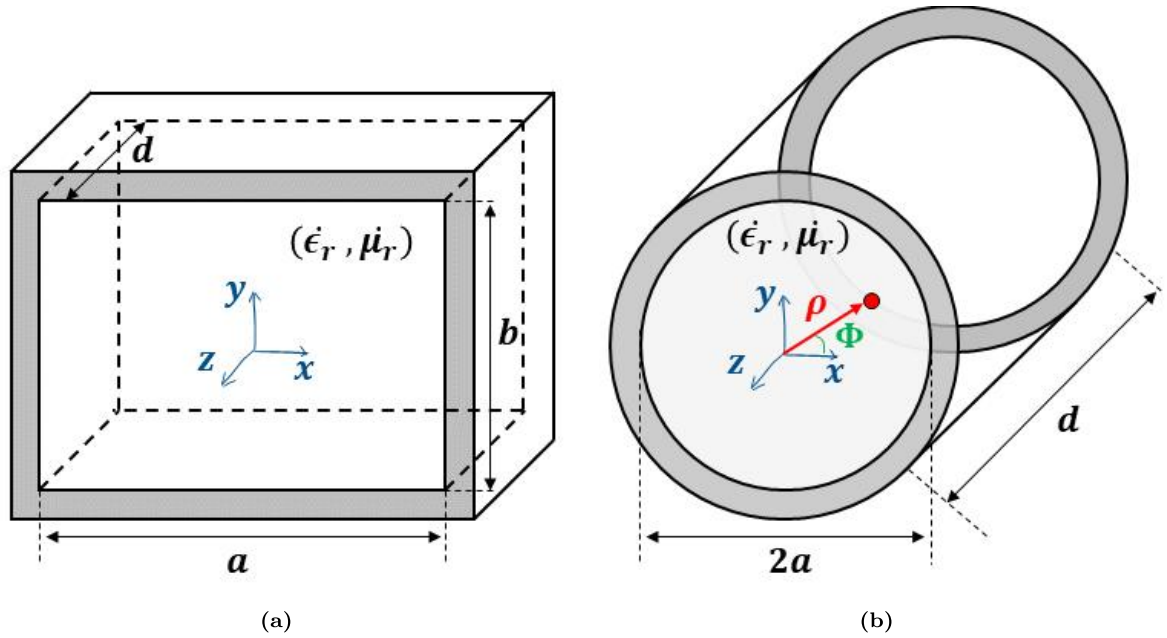

(a) (b)

Figure 7.12: Resonant cavities. (a) Rectangular section resonant cavity. (b)Circular section resonant cavity. The ends of the cavities (z-direction) are short circuited.

7.9.2 Rectangular waveguide resonators

A typical application of what seen in the previous section is the so called microwave resonator cavity. In MW heating processes it is a state of art approach to generate an electromagnetic wave and let is "resonates" in the MW cavity. Microwave resonators can be constructed from closed sections of waveguide, and they represents the easier way to obtain MW resonance in a closed space. A micro-wave oven is a typical example of a resonance cavity. Because of losses from an open-ended waveguide can be significant, waveguide resonators are usually short circuited at both ends, thus forming a closed box. Electric and magnetic energy is stored within the cavity enclosure, and power is dissipated in the metallic walls of the cavity as well as in the dielectric material that may fill the cavity. Coupling to a cavity resonator may be by a small aperture, or a small probe or loop. We will see that there are many possible resonant modes for a cavity resonator, corresponding to field variations along the three dimensions of the structure.

Resonant frequencies

The geometry of a rectangular cavity is shown in figure 7.12a and it is noticeable that a rectangular resonator cavity is characterized by only three parameters: its length (d

$[m]$), its height (b $[m]$) and its width (a $[m]$). The cavity is short-circuited at both ends (if the propagation direction is **z** then the analysis will take into account as short-circuit the two planes: $z = 0$ and $z = d$. As already done in the section of rectangular waveguides, it is possible to easily define the propagation constant (β_{mn}) of the TE_{mn} and TM_{mn} modes:

$$\beta_{mn} = \sqrt{k^2 - \left(\frac{m\pi}{a}\right)^2 + \left(\frac{n\pi}{b}\right)^2} \tag{7.179}$$

and finally applying the short-circuit condition for the two ends of the waveguide the resonance wave number (k_{mnl}) for the rectangular cavity is:

$$k_{mnl} = \sqrt{\left(\frac{m\pi}{a}\right)^2 + \left(\frac{n\pi}{b}\right)^2 + \left(\frac{l\pi}{d}\right)^2} \tag{7.180}$$

And the resonant mode of the cavity (TE_{mnl} or TM_{mnl}) is define by indices m, n and l that indicate the number of variations in standing wave distribution in the space. The resonant frequency is then:

$$f_{mnl} = \frac{c}{2\pi}\frac{k_{mnl}}{\sqrt{\mu_r\epsilon_r}} = \frac{c}{2\pi\sqrt{\mu_r\epsilon_r}}\left(\sqrt{\left(\frac{m\pi}{a}\right)^2 + \left(\frac{n\pi}{b}\right)^2 + \left(\frac{l\pi}{d}\right)^2}\right) \tag{7.181}$$

7.9.3 Circular waveguide cavity resonators

A cylindrical cavity resonator can be obtained extruding along z-direction a circular waveguide and shorting its ends, as done for rectangular cavities [56]. The geometry of a circular cavity is shown in figure 7.12b. Because for a circular waveguide the dominant mode is the TE_{11}, the dominant cylindrical cavity mode is therefore the TE_{111}. The general propagation constant (β_{nm}) for a general mode TE_{nm} is:

$$\beta_{nm} = \sqrt{k^2 - \left(\frac{p'_{nm}}{a}\right)^2} \tag{7.182}$$

where the parameter p'_{nm} is listed in table 7.1 and then the resonant frequency of the mode TE_{nml} is:

$$f_{nml} = \frac{c}{2\pi}\frac{1}{\mu_r\epsilon_r}\sqrt{\left(\frac{p'_{nm}}{a}\right)^2 + \left(\frac{l\pi}{d}\right)^2} \tag{7.183}$$

The unloaded quality factor Q_{0c} of the cavity with lossy walls but an ideal lossless dielectric medium, where the power lost (P_c $[W]$) in the conducting walls is taken into account:

$$Q_{0c} = \omega_0\frac{2W_e}{P_c} \tag{7.184}$$

and instead for a resonant cavity in that is characterized by a real dielectric medium (which permittivity is complex), the unloaded quality factor Q_{0d} can be found taking not account of the power dissipated inside the dielectric (P_d)

$$Q_{0d} = \omega_0 \frac{2W_e}{P_d} = \frac{\epsilon\prime}{\epsilon\prime\prime} = (\tan\delta)^{-1} \tag{7.185}$$

the global unloaded quality factor that takes into account both the phenomena is then:

$$Q_0 = \frac{Q_{0d}Q_{0c}}{Q_{0d} + Q_{0c}} \tag{7.186}$$

7.10 How to excite cavity resonators

In practical applications there is the necessity to couple resonators with RF/MW waveguides or transmission lines. Some of the more common coupling devices are listed in the next lines:

- Micro-strip feed-line [2]
- Coaxial probe
- Apertures (slots)

A good measure of the level of coupling between a resonator and a feed is given by the coupling coefficient. It is important to remember that the maximum power transfer criteria is every time true: remembering the series model for a frequency resonator, near the resonance condition the input impedance of the series resonator, connected to the network (with its characteristic impedance Z_0) must be:

$$\dot{Z}_{in} = R\,(1 + i2L\Delta\omega) = R\left(1 + i\frac{2Q_0}{\omega_0}\Delta\omega\right) \tag{7.187}$$

where the general unloaded quality factor (Q_0) is:

$$Q_0 = \omega_0 \frac{L}{R} \tag{7.188}$$

Considering now the maximum power transfer condition (or the so called perfect matched network) at the resonance point, the input impedance must be equal to the characteristic impedance of the network "at the left" of the connection:

$$\cdot\, Z_{in} = R = Z_0 \tag{7.189}$$

and then the unloaded quality factor at the matched-resonance condition (Q_{0-mr} is:

$$Q_{0-mr} = \frac{\omega_0}{Z_0} L \tag{7.190}$$

Remembering now what seen in the previous section, and particularly equation 7.177 defines the external quality factor due to a general load connected in series with the network:

$$Q_{ext} = \omega_0 \frac{L}{R} = \frac{\omega_0}{Z_0} L = Q_{0-mr} \tag{7.191}$$

Equation 7.191 states that at the critical coupling condition: series resonator perfect matched and at the resonance ($\Delta\omega = 0$), the unloaded quality factor is equal to the external quality factor. It is then possible to define the coupling coefficient (g [−]) that is a measure of how the resonator is coupled to the feeding line and generalize its concept also to a parallel resonator model:

$$g = \frac{Q_0}{Q_e} = \begin{cases} g_{ser} = \frac{Z_0}{R} \\ g_{par} = \frac{R}{Z_0} \end{cases} \tag{7.192}$$

Apertures (slots) for resonant cavities

A good way to couple waveguides (at the moment rectangular) to frequency resonators is to use apertures or slots [52]. Figure 7.13 shows a typical example. Small apertures, in other words their dimensions are small compared with the waveguide wavelength may be considered as shunt inductance (L_s). Considering first resonant mode of the cavity as seen in the waveguide paragraph it is possible to model the cavity as a short circuited TLR and its circuit is shown in figure 7.14. The normalized input admittance seen by the rectangular waveguide may be obtained as function of the frequency:

$$\dot{y}(\omega) = \frac{\pi k_0}{c} \left(\frac{1}{x_L \beta} \right)^2 \left[\frac{1}{2Q_0} \omega_0 + i(\omega - \omega_0) \right] \tag{7.193}$$

From equation 7.193 it is possible to obtain the input resistance seen from the waveguide and impose the coupling-critical condition ($R = Z_0$) and finally the reactance of the apertures (X_L [Ω]) must be:

$$X_L = Z_0 \sqrt{\frac{\pi k_0 \omega_0}{2 Q_0 \beta^2 c}} \tag{7.194}$$

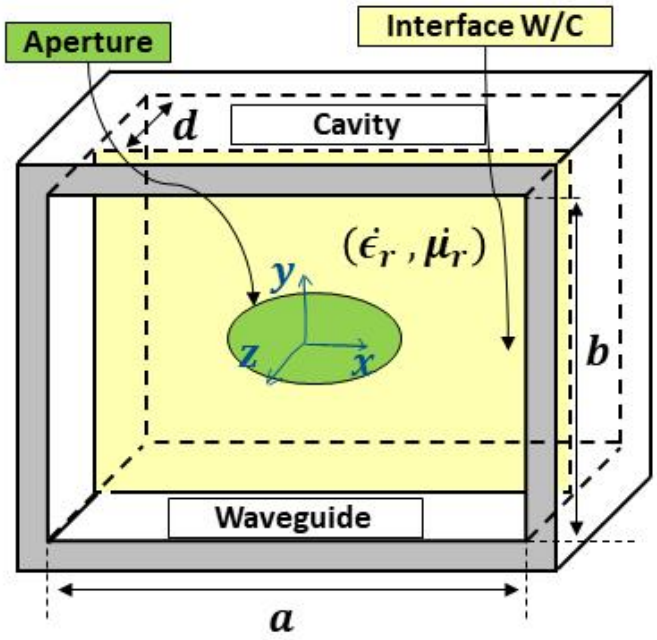

Figure 7.13: Coupling between a rectangular waveguide and a rectangular cavity resonator. The aperture (slot) is highlighted in green. The conductive layer that is the interface between the waveguide region and the resonator is highlighted in yellow

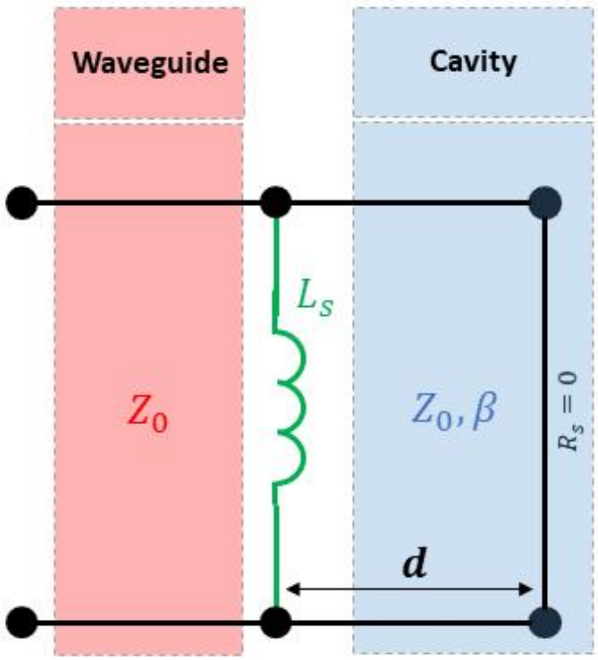

Figure 7.14: Equivalent circuit of an aperture-coupled cavity resonator.

7.10.1 Cavity perturbations

If a MWH cavity applicator, but more generally a MW cavity resonator is well

designed with the approach seen in the previous chapter there could be the necessity to modify the geometry of the cavity by making small changes in their shape for production purposes, or by introducing small pieces of dielectric (for example brackets or insulators) or high-conductive materials (connections and grids) [45]. These variations can be treated as perturbations and their effects can be computed with perturbational methods: material perturbation method and shape perturbation.

Material perturbations

The material filling the cavity may change its permittivity ($\Delta\epsilon$) or its permeability ($\Delta\mu$) and that consequently changes electric fields and magnetic fields [6]. According to Maxwell's equations then it is possible to define initial electromagnetic fields ($\mathbf{E}_0$,$\mathbf{H}_0$) and perturbed electromagnetic fields ($\mathbf{E}_p$,$\mathbf{H}_p$). It is obvious that also resonant frequency changes from ω_0 to ω_p:

$$\begin{cases} \nabla \times \mathbf{E}_0 = -i\omega_0\mu\mathbf{H}_0 \Rightarrow \nabla \times \mathbf{E}_p = -i\omega_p\left(\mu + \Delta\mu\right)\mathbf{H}_p \\ \nabla \times \mathbf{H}_0 = i\omega_0\epsilon\mathbf{E}_0 \Rightarrow \nabla \times \mathbf{H}_p = i\omega_p\left(\epsilon + \Delta\epsilon\right)\mathbf{E}_p \end{cases} \tag{7.195}$$

and finally it is possible to get the equations system that relates the variations of the EM fields to the variation of the material properties:

$$\begin{cases} \nabla \cdot (\mathbf{E}_0^* \times \mathbf{H}_p) = i\omega_0\mu\mathbf{H}_p \cdot \mathbf{H}_0^* - i\omega_p\left(\epsilon + \Delta\epsilon\right)\mathbf{E}_0^* \cdot \mathbf{E}_p \\ \nabla \times (\mathbf{E}_p \times \mathbf{H}_0^*) = -i\omega_p\left(\mu + \Delta_m u\right)\mathbf{H}_0^* \cdot \mathbf{H}_p + i\omega_0\epsilon\mathbf{E}_0^* \cdot \mathbf{E}_p \end{cases} \tag{7.196}$$

Considering the control volume region (Ω) it is possible to sum and integrate the previous equation 7.196 and finally it is possible to get the relationship between the relative change of the resonant frequencies as function of material variations:

$$\Delta\omega_{rel} = \frac{\omega_p - \omega_0}{\omega_p} = -\frac{\int_{\Omega_0}\left(\Delta\epsilon\mathbf{E}_p \cdot \mathbf{E}_0^* + \Delta\mu\mathbf{H}_p \cdot \mathbf{H}_0^*\right)dV}{\int_{\Omega_0}\left(\epsilon\mathbf{E}_p \cdot \mathbf{E}_0^* + \mu\mathbf{H}_p \cdot \mathbf{H}_0^*\right)dV} \tag{7.197}$$

Shape perturbations

As already done in the material perturbation problem it is possible to analyze the case of "small" variations in the shape of the cavity, without varying the materials. It is possible to rewrite Maxwell's equations and we obtain the exact expression for the modified resonant frequency (ω_p) due to a geometry shape variation:

$$\omega_p - \omega_0 = -i\frac{\oint_{\Delta\Sigma}\mathbf{E}_0^* \times \mathbf{H}_p \cdot d\mathbf{s}}{\int_{\Omega}\left(\epsilon\mathbf{E}_p \cdot \mathbf{E}_0 + \mu\mathbf{H} \cdot \mathbf{H}_0^*\right)dV} \tag{7.198}$$

And finally the relative variation of the resonant frequency is function of only stored energies:

$$\Delta\omega_{rel} = \frac{\omega_p - \omega_0}{\omega_p} = \frac{\Delta W_m - \Delta W_e}{W_m + W_e} \tag{7.199}$$

7.11 Microwave Filters

A filter is a two-port network used to control the frequency response at a certain point

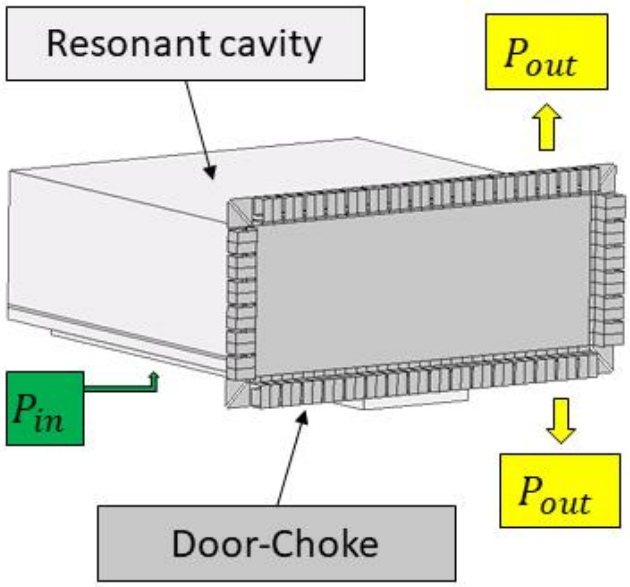

Figure 7.15: A complete microwave system: resonant cavity and door choke.

in an RF or microwave system by providing transmission at frequencies within the pass-band of the filter and attenuation in the stop-band of the filter. Typical frequency responses include low-pass, high-pass, band-pass, and band-reject characteristics. Applications can be found in virtually any type of RF or microwave communication, radar, or test and measurement system. Periodic structures are particularly interesting because of their application as stop-band filters, for example in choke design for MWH cavities.

7.11.1 Microwave door Choke

In microwave applications one of the main problem is the necessity of guarantee low leakage on the frontal part of the system. In home appliance applications we need to guarantee certain electric field value $[V/m]$ (or power density $[W/cm^2]$) that the microwave can't overcome during

a normal working condition [40]. A choke is a particular case of filter that must act as a two-

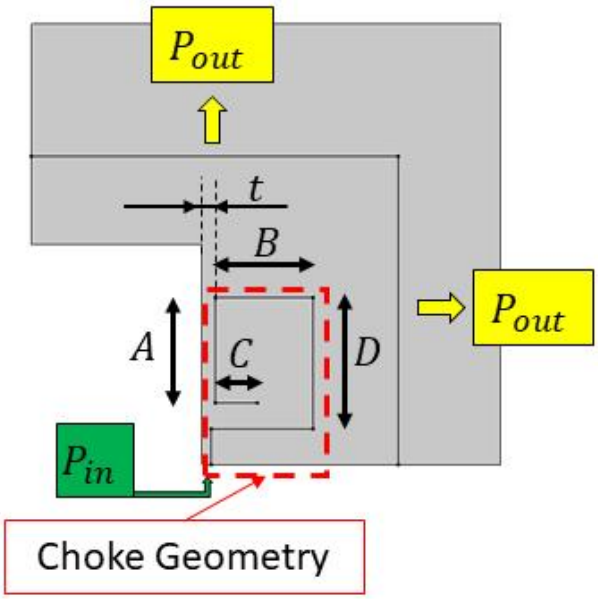

Figure 7.16: A choke geometry for leakage reduction of the front door of the microwave

port network and reduces field emissions due to the non perfect metallic continuity of the door. A developed 2D-geometry of a door-choke is shown in figure 7.16. The necessity of using a choke for the door is the fact that the door is not in electrical continuity with the boundaries of the cavity, in fact a certain air gap of thickness not negligible (t $[mm]$) exists if a door is applied in the front of the cavity. It is possible to solve that problem for example modeling and simulating the EM problem: in figure 7.16 an input power (P_{in} $[W]$) is applied at a TEM-port, the phenomenon of propagation towards the environment is modeled with a port-gate condition (P_{out} $[W]$). The input power surface is modeled with a TEM-port and that means:

$$S = \frac{\int_{S_{in}} (\mathbf{E} - \mathbf{E}_{in}) \cdot \mathbf{E}_{in}}{\int_{S_{in}} \mathbf{E}_{in} \cdot \mathbf{E}_{in}} \tag{7.200}$$

The ouput power surface is modeled with a N-port and that means:

$$S = \frac{\int_{S_{out}} \mathbf{E} \cdot \mathbf{E}_{out}}{\int_{S_{out}} \mathbf{E}_{out} \cdot \mathbf{E}_{out}} \tag{7.201}$$

A door-choke is a $\lambda/4$-filter that wants to minimize the transmission problem from the port-*in* to the port-*out*, and that means in a EM microwave problem that we want to maximize scattering parameters, and particularly we want to minimize S_{21} $[dB]$. For a door-choke design is possible to set an optimization problem that want to solve the transmission problem, studying the system as a 2-port network. In geometry shown in figure 7.16 are listed the main four

parameters that uniquely define the choke shape: A, B, C, D. it is clear that if the air-gap between the cavity and the door varies ($t \Rightarrow t^{'}$), then it is necessary to recalculate the choke geometry and then $A^{'}, B', C', D'$ At the end the mathematical problem is quite simple: we want

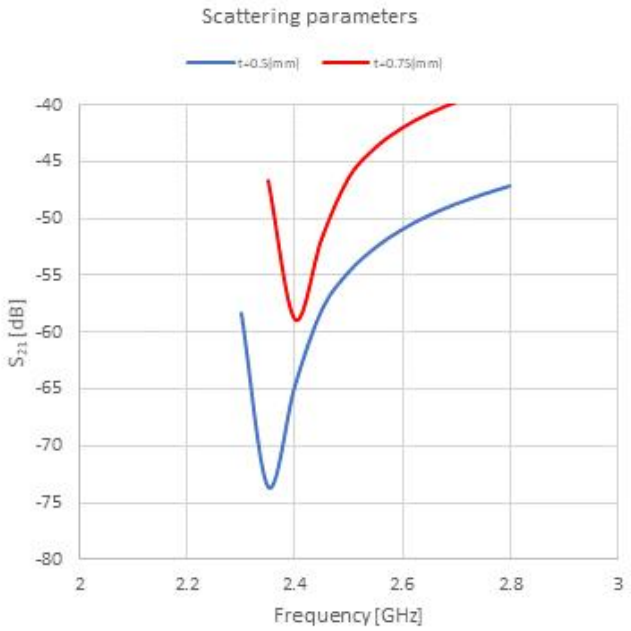

Figure 7.17: S_{21} $[dB]$ vs frequency for the choke shown in figure 7.16. In figure is presented the different in performances varying the air gap cavity-door.

to find teh combination of A, B, C, D that minimizes the scattering parameter seen at the port-*in*. Another important note consists in the fact that a specific choke is guaranteed in therms of electric field reduction only in a certain frequency range, that must be verified. For microwave magnetron-base home-appliance we design choke that are optimised in a narrow frequency range: $2.44[GHz] - 2.48[GHz]$ because of the magnetron may vary its output frequency during its working conditions. For that reasons it is useful to don't minimize the scattering parameter S_{11} $[dB]$ in an unique frequency, but in frequency range $[f_0 - \Delta f, f_0 + \Delta f]$, and then:

$$S^{'}_{21-dB} = \frac{1}{\Delta f} \int_{f_0 - \Delta f} f_0 + \Delta f S_{21-dB} df \tag{7.202}$$

From figure 7.17 it is clear that varying the air gap the performances of the choke varies, both in absolute value of the scattering parameter and in frequency. Results of the optimised geometry are shown in figure 7.18. The final step in the choke design and optimization is to solve the 3D-problem. Because of periodic structures are particularly interesting, after having preliminary studied and 2D-optimized the geometry of the choke teeth it is necessary to study the effect on periodic structure distance and the edge effect at the four corners of the choke.

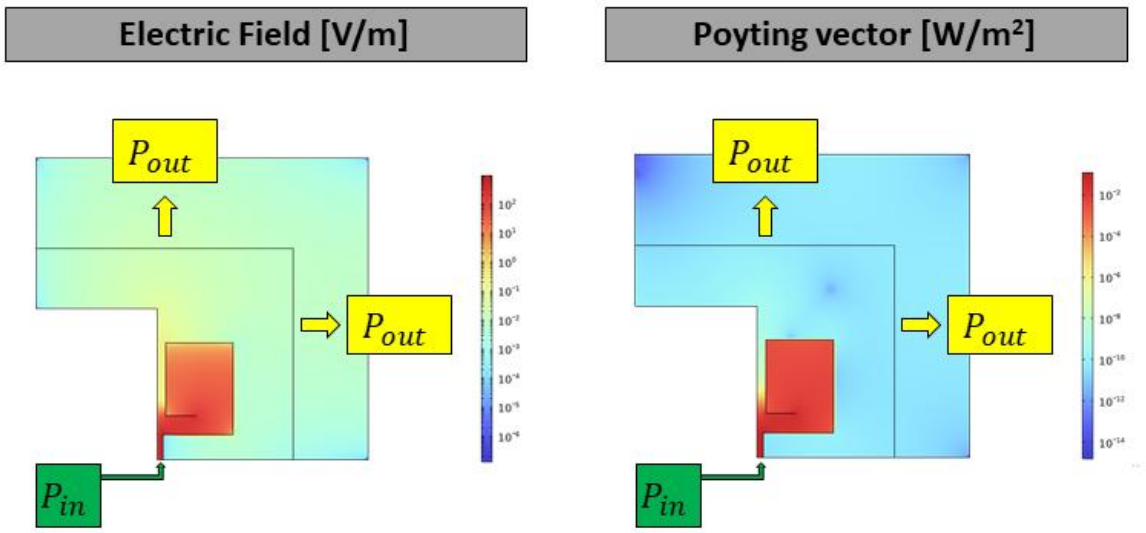

Figure 7.18: Choke performances analysis for 2D FEM simulation, optimised geometry. (a) Electric field distribution $[V/m]$; (b) Poynting vector distribution $[W/m^2]$

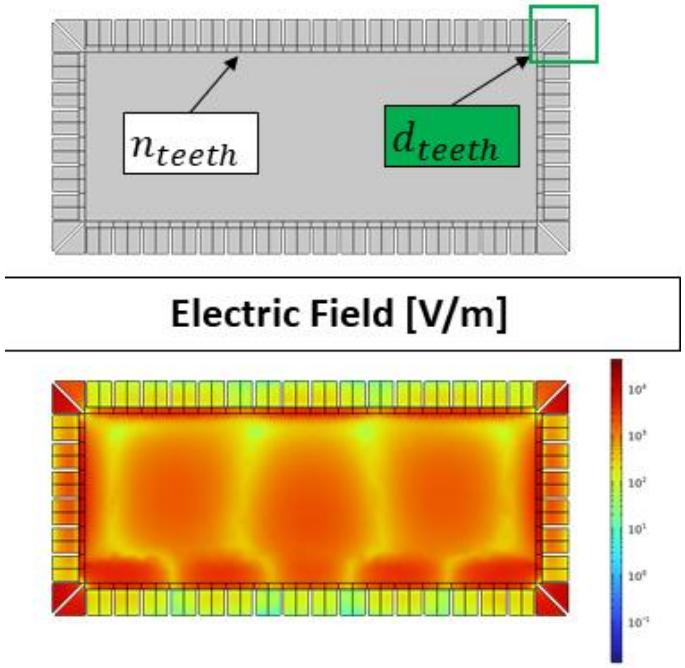

Figure 7.19: 3D choke for a MW oven. Periodic structure optimized with FEM analysis

FEM analysis makes possible to analyse deeply the distribution of the electric field outside the resonant cavity and of the incident power at a certain reference plane. FEM analysis makes possible to minimize maximum electric field where there is the interaction between the user and the device. One of the main problem when we work with resonant cavity is the fact that the no-load condition is typically the worst condition in therms of maximum electric field and

poynting vector. A good optimization should every time takes into account the different working conditions. In our work we developed an optimization for several loads (5 cases):

- Case 01: $m_1 = 1.000[L]$ of water, $k_1 = 1.000$
- Case 02: $m_2 = 0.500[L]$ of water, $k_2 = 2.250$
- Case 03: $m_3 = 0.205[L]$ of water, $k_3 = 3.375$
- Case 04: $m_4 = 0.125[L]$ of water, $k_4 = 5.062$
- Case 05: $m_5 = 0.000[L]$, no load condition, $k_i = 7.592$

The final performance parameter (E'_{max} $[V/m]$) is the average value of the maximum electric field at $5[cm]$ from the cavity weighted for a certain correction coefficient that takes into account the load mass, that is a personal design choice to properly weigh the different possible working conditions during the life of the device.

$$\begin{cases} E^i_{max} = \left[\max |\mathbf{E}^i|\right]_{5[cm]} \\ E'_{max} = \frac{1}{5}\sum_{i=1}^{6} E^i_{max} \cdot k_i \end{cases} \tag{7.203}$$

In figure 7.21 is shown a comparison between an optimized choke, practically varying main choke parameters (in figure the optimization was done finding the best choke-tooth thickness (B $[mm]$) that minimize the poynting vector. Working on the choke geometry it is possible, as the figure highlights, to dramatically improve choke performances. In figure is also introduced an important constraint in choke design: the so called ICNIRP's reference level for exposure, averaged over $30[min]$ and the whole body, to electromagnetic fields from $2[GHz]$ to $300[GHz]$: $20[W/m^2]$ [34].

7.12 Microwave cavity for thawing

As seen in chapter 4 frozen foods are extremely hard to be heated and regenerated. Food regeneration is a process whose purpose is to maintain the quality of the food, trying to bring blast chilled, frozen or packaged foods quickly in the most delicate way to the temperature of consumption [**hinney'thawing**]. In that chapter is presented a new resonant cavity tailored designed for regeneration of frozen-vegetarian-ready meals. As a first step we performed many test in several commercial microwave cavities. We found that "standard" systems are not

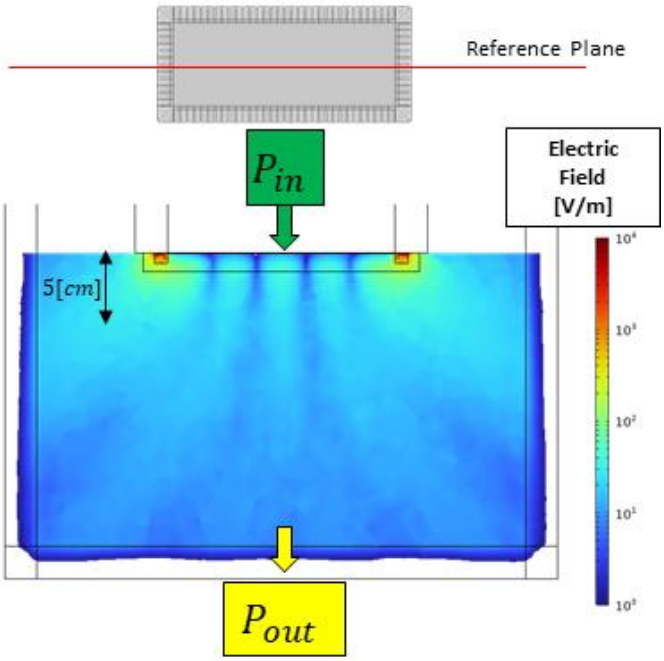

Figure 7.20: Choke performances. Electric field distribution outside the resonant cavity (no load condition)

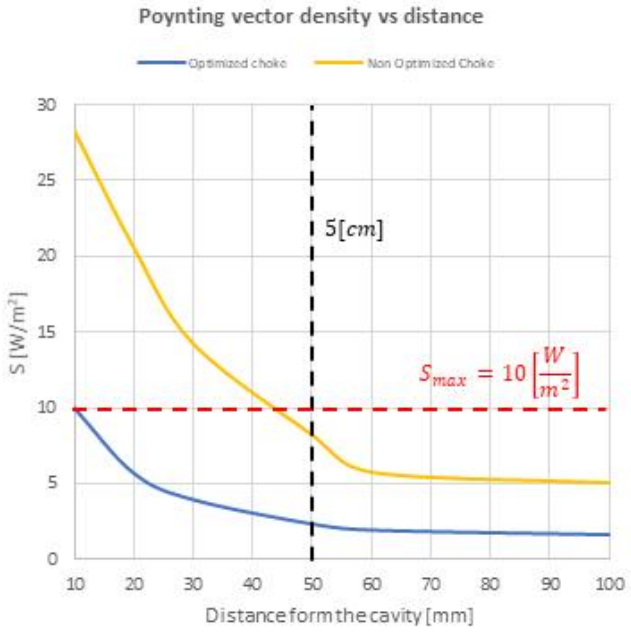

Figure 7.21: Choke performances. Comparison between an optimized choke and a not optimized choke. In figure is highlighted the maximum value of the incident power at 5[cm] fixed by ICNIRP standards.

properly designed for regeneration. Regeneration every-time starts from frozen food (typically $-20[degC]$) and wants to heat food to serving temperature (that is typically above $60[degC]$). Standard microwaves need to work with wide variety of loads. Water is probably the load that may guarantee the best performances in a "standard" commercial microwave. In figure 7.22 are

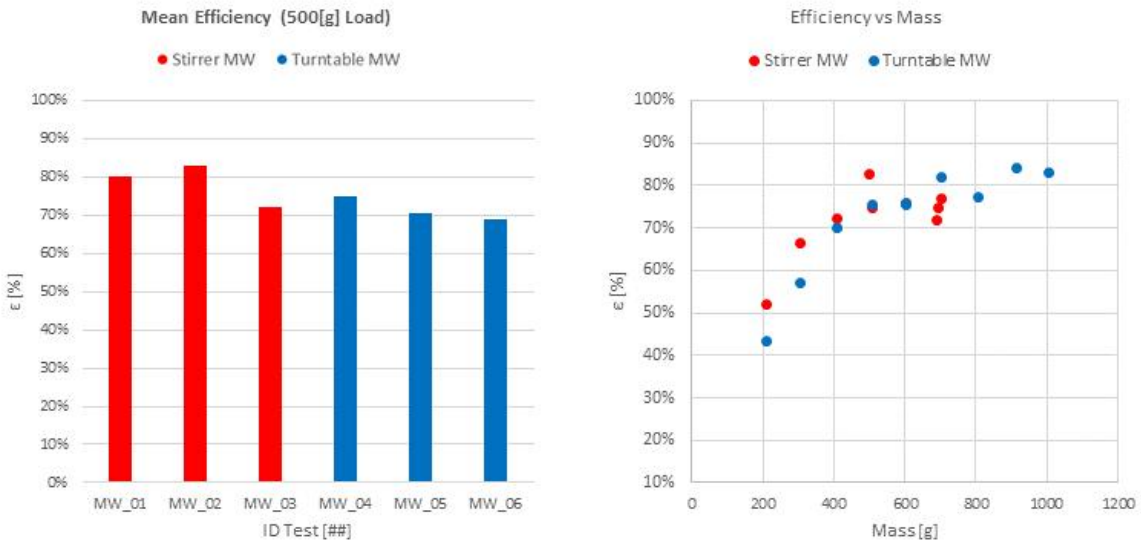

(a) **(b)**

Figure 7.22: MW Efficiency characterization. The considered load is water. (a) Several test performed on different commercial microwaves; (b) Analysis of the effect of the mass of the load to the global efficiency.

shown final results on a experimental characterization on six different commercial microwaves ovens. The mean efficiency, measured with a $500[g]$ water-load was of $70[\%] \pm 3[\%]$. Figure 7.22b shows that the mass of the load is an important parameter on the efficiency of the microwave transmission. When the mass of the load decrease the global efficiency decreases. A single-portion ready meal is typically characterized by weight of about $400[g]$ and that means the efficiency hardly overcomes a value of $70[\%]$. When the dielectric properties are decreased, and for example they are far from the typical value of permittivity of water ($\dot{\epsilon}_{H2O} = 78 - i18$) the efficiency collapses to value of $30[\%]$ as is shown in figure 7.23. To deeply analyze the problem of the thawing we analyzed the performances on fourteen different frozen meals, that are the same presented in chapter 4 on the complex permittivity measure section. All these foods are characterized by a mixture of several ingredients. The meals are cooked and at the end of the process they are blast-chilled to a storage temperature of about $-20[degC]$. An energy-enthalpy analysis was performed as reported in chapter 3 using an enthalpy-concentration relationship. That makes possible to precisely estimate energy needed for thawing processes. In MW thawing-process the energy is directly generated in the food. That means it is possible to relate the energy absorbed by the system (E_{tot} $[J]$) to the energy accumulated in the food. Beacause of the MW system has a certain efficiency (μ_{MW} $[\%]$) due to the transmission problem:

$$E_{tot} = \frac{E_{MW}}{\mu_{MW}} \tag{7.204}$$

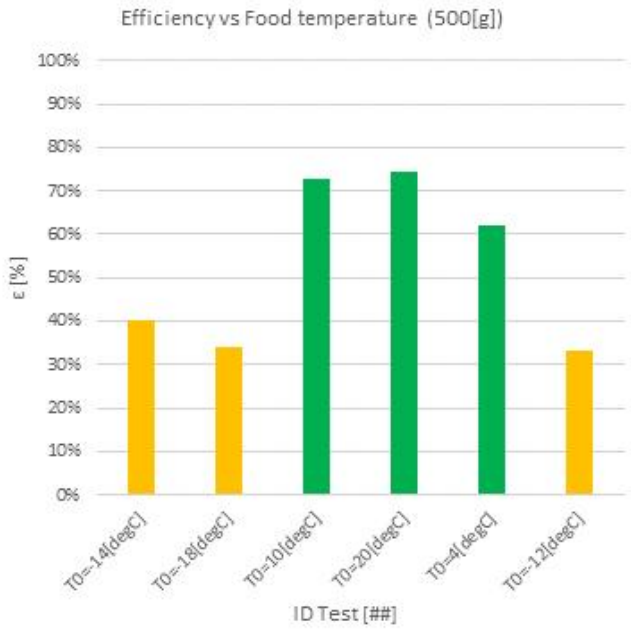

Figure 7.23: MW Efficiency characterization vs initial temperature of the load. The considered load is water and ice.

it is possible to define a simple ratio (k_{reg} $[-]$) between the "microwave-energy" (transfered to the load) and the "food energy", accumulated in the food and that cause the phase change of the ice-solid-phase (H_{food}) and that is function of components concentration.

$$k_{reg} = \frac{E_{MW}}{H_{food}} \tag{7.205}$$

Ready meals are characterize by regeneration recipe that typically the user follows. Because of they are defined for "standard" commercial general-purpose microwaves devices they are limited in power. In commercial microwaves typically is present the so called defrosting function. That particular function practically limits the output radio-frequency power generated by the Magnetron ($P_{MW-nom} \simeq 1000[W]$). A typical limited power considered for defrosting function is $P_{MW-def} \simeq 400[W]$, and that means in a commercial cavity only the 40[%] of the total available power is used. That is due two main effects: the first one is the low efficiency during a thawing process, and that may cause the overheating of the magnetron microwave generator (to avoid that the power is limited), the second one is the runaway phenomena: a frost food is characterized by low imaginary part of complex permittivity, and that means typically low specific microwave heating source in the food. When the ice fraction start to change phase (from solid to liquid) the imaginary part increase a lot, and that practically takes places where edge effects are greater as shown in figure 7.24. In that work we analysed a standard regeneration process that applies for three minutes ($t_{reg} = 180[s]$) the limited regeneration power ($P_{reg} \simeq$

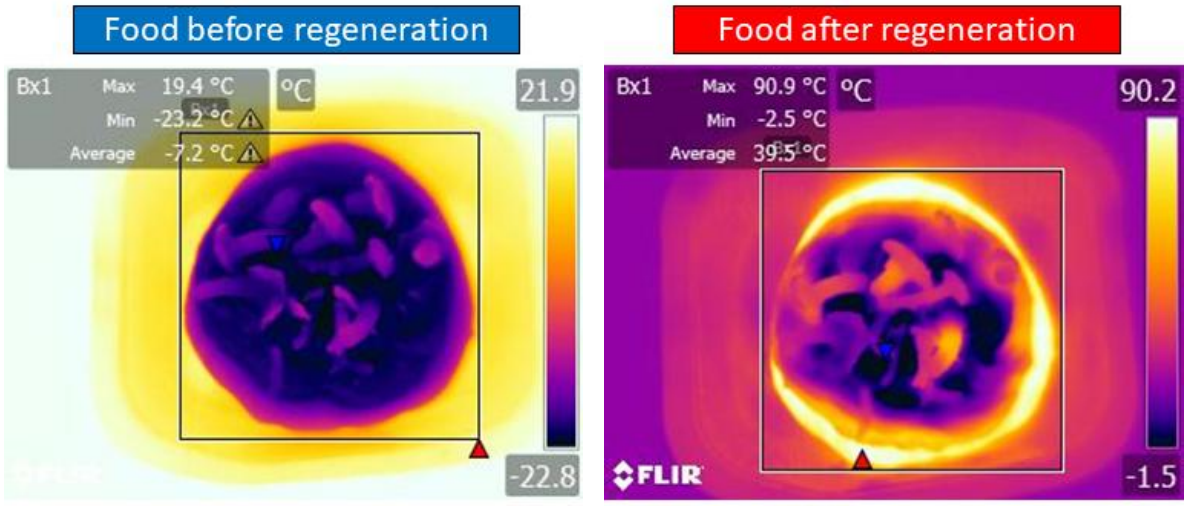

Figure 7.24: Thermal image of a MW regeneration process (food item:$ID009$). (a) is the thermal image before regeneration process; (b) is the thermal image at the end of the regeneration process.

$400[W]$). Runway effects are not accepted in microwave regeneration process because of the quality perceived by the user is dramatically reduced if inside the ready-meal there are hot and cold areas. Figure 7.24b highlights that also if the microwave power is limited ($P_{reg} \simeq 400[W]$) the final product exhibit low temperature uniformity ($T_{max} = 90.9[degC]$ and $T_{min} = -2.5[degC]$) also with areas that are still frozen. For all these reasons we analysed the energy necessary for the process and we computed the microwave-regeneration target that is shown in figure 7.25: green bars represent ready-meals that presented high quality of the final regenerated product (average food temperature close to the target-service temperature ($60[degC]$) and high uniformity of the temperature distribution), blue bars represent ready-meals that presented medium quality of the final regenerated product (average food temperature not far from the acceptance-service temperature ($T^{'} \simeq 40[degC]$) but a medium uniformity of the temperature distribution) and finally red bars represent ready-meals that presented low quality of the final regenerated product (average food temperature far from the acceptance-service temperature ($T^{'} << 40[degC]$) and a low uniformity of the temperature distribution). To guarantee an high quality of the final product it is necessary to properly increase performance of thawing microwave cavities as we will see in the next part of that chapter.

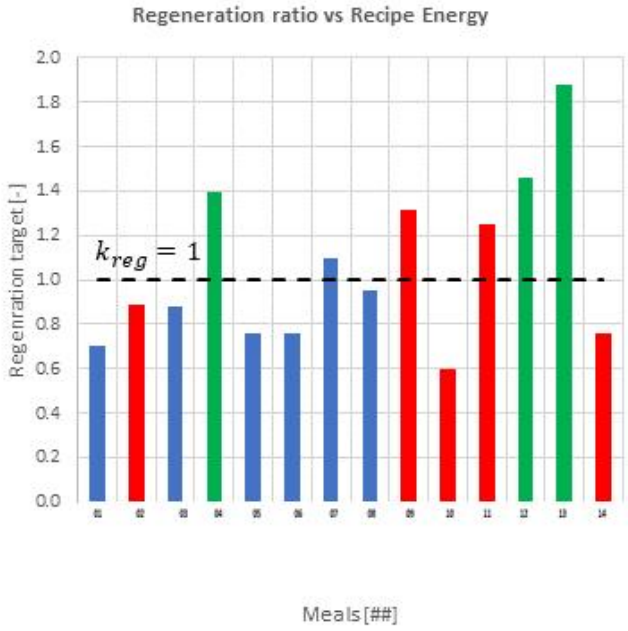

Figure 7.25: Microwave regeneration ratio k_{reg} [−]

7.13 A new tailored microwave cavity for thawing

From the previous section it is clear that it is necessary a new-design that takes into account the real average complex permittivity that characterizes frozen ready meals (low mass and low complex permittivity). The design of the tailored microwave oven for frozen-vegetable-meals wants to solve numerically that technological problem:

- to design a microwave resonant cavity as small as possible but compatible with standard serving dishes, here assumed with a maximum diameter of 280$[mm]$
- to guarantee homogeneous temperature field inside the meal
- to guarantee high efficiency during the defrosting phase

The design phase involves the following parts of the Microwave Oven:

- Resonant cavity
- Waveguide
- Transition Waveguide-Cavity

- Transition Antenna-Waveguide

The initial virtual-design of the cavity wants to optimize the dimensions of the cavity to maximize the transmission efficiency (μ_{MW}) from the rectangular waveguide slot to the load (ready meal), which geometry is defined in figure 7.26.

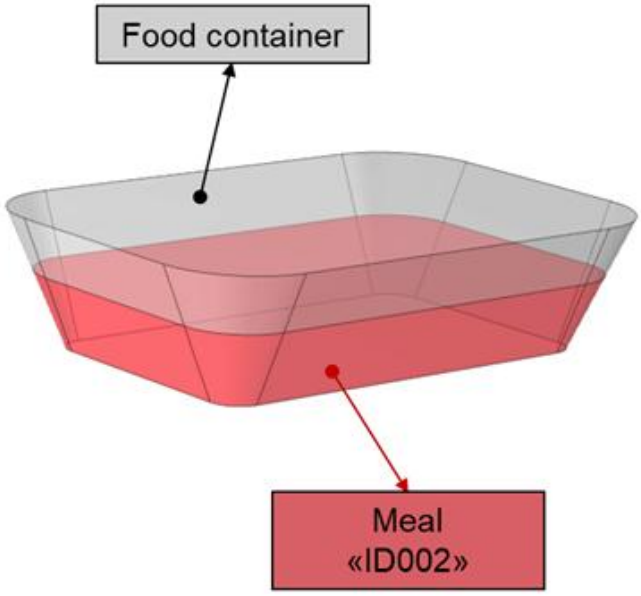

Figure 7.26: Standard load geometry considered for a regeneration process. The volume region of the load (Ω) is characterized by a complex permittivity that was introduced in the chapter 4 ($\dot{\epsilon} = 4.04 - i * 2.57$).

$$\mu_{MW} = \frac{P_{food}}{P_{MW-in}} \tag{7.206}$$

where the total input power in the system is imposed at the feed rectangular port:

$$P_{MW-in} = \int_{S-in} \mathbf{p} d\mathbf{S} \tag{7.207}$$

where the surface of the input port ($S - in$ $[mm^2]$) is function of the geometrical dimension of the slot (as seen in the waveguide-aperture paragraph), the poyinting vector ($\mathbf{p}$) is the vectorial product at the feeding port of the magnetic field and of the electric field and the total power dissipated in the load is the volume integral of microwave power density (w_{MWH} $[W/m^3]$):

$$P_{food} = \int_{\Omega} w_{MWH} dV \tag{7.208}$$

The port condition imposes a strict condition at the port surface ($S - in$):

$$S = \frac{\int_{S-in} (\mathbf{E} - \mathbf{E}_{in}) \cdot \mathbf{E}_{in}}{\int_{S-in} \mathbf{E}_{in} \cdot \mathbf{E}_{in}} \tag{7.209}$$

The first step of the design is to study the effect of the dimensions ($W \times H \times L$) of the resonant cavity on the global efficiency if a rectangular port is applied on the roof of the cavity as shown in figure 7.27. For food applications there is the necessity of separating mechanically the heating cavity to the magnetron, because of during a regeneration process the food releases steam and aromas that may dirty and saturate the wave guide and the magnetron. To avoid that a mica layer was considered in all simulations as barrier between the cavity and the waveguide. Figure

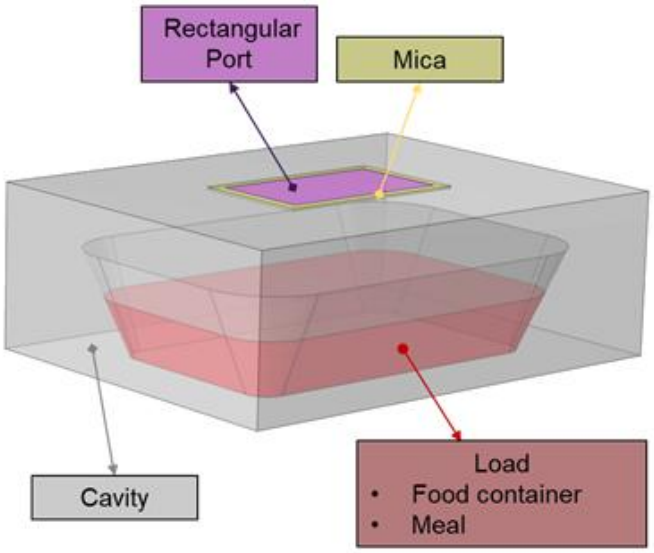

Figure 7.27: Rectangular waveguide resonant cavity with feeding port on the rood of the cavity

7.28 highlights that it is possible to find an optimum configuration that maximize the efficiency of transmission for a specific load (geometry and complex permittivity). in first analysis we assumed a "standard" ready-meal PP dish for microwave regeneration with an height of $25[mm]$ and a top-area of $185[mm] \times 130[mm]$. Figure 7.28a hihglights that the maximum efficiency areas is obtained with cavity height (H_{cavity}) of $100[mm]$. The second problem that we want to solve as seen before is to find the best uniformity conditions that admits good efficiencies. Of coarse that problem is a case of multi (2) objective function optimization. Because of microwave heating power is a space function, due to the electric field distribution, we can define an evaluation grid on the load to estimate the uniformity of the power sources. In that practical case we defined a matrix of 3D-points ($11 \times 11 \times 11$) inside the food load. For each evaluation point is possible to extract the local power density (w_{MWH-i} $[W/m^3]$) due to the electromagnetic heating:

$$w_{MWH-i} = \omega \epsilon_0 \epsilon_r^{''} |\mathbf{E}|^2 \tag{7.210}$$

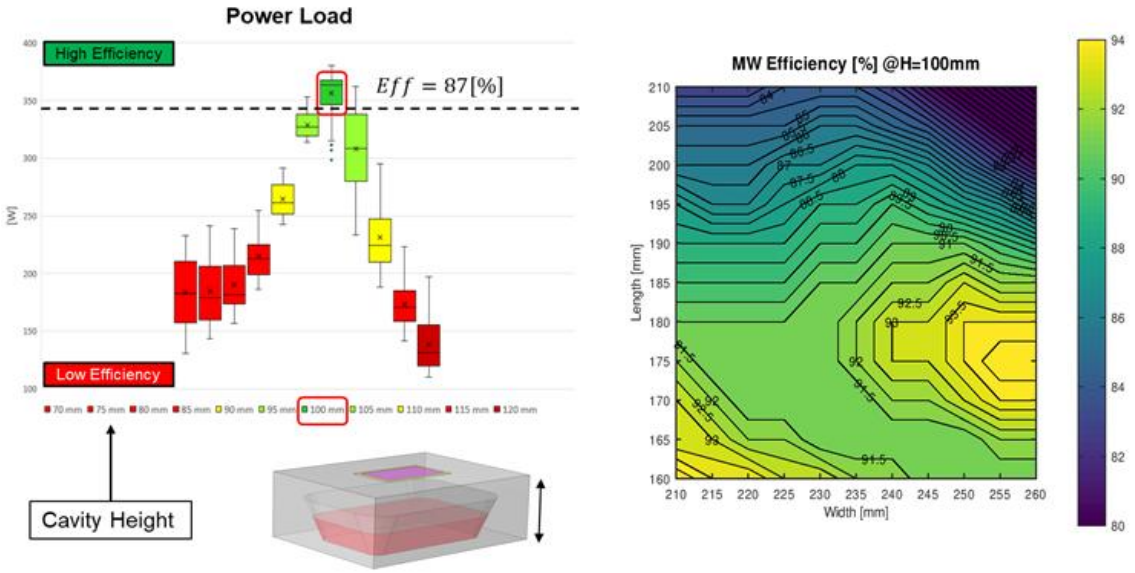

(a) (b)

Figure 7.28: Power load and efficiency analysis for the geometrical layout shown in figure 7.27

where $i = 1, 2, ..., N$ and in that particular case $N = 1331$, and finally a good estimator of uniformity is given by the standard deviation (σ_{MWH}):

$$\sigma_{MWH} = \sqrt{\frac{1}{N}\sum_{i=1}^{N}\left(w_{MWH-i} - w_{MWH-a}\right)^2} \tag{7.211}$$

where the average power density inside the load (w_{MWH-a} $[W/m^3]$) is obtained by the scattering matrix and by the fixed volume of the load (V_{food} $[mm^3]$)

$$w_{MWH-a} = \frac{P_{MW-in}\mu_{MW}}{V_{food}} \tag{7.212}$$

Figure 7.29 shows that is extremely hard to obtain high uniformity on the food load with an only rectangular feeding port in a small cavity. For that reason we though to increase the degree of freedom adding a second feeding port on the roof of the cavity. The use of two rectangular ports on the roof of the cavity increased dramatically the microwave efficiency respect to a single rectangular port from 85[%] to 95[%] and also the uniformity, decreasing the standard deviation of the heating power from 60[%] to 45[%] for the top configuration with two identical ports ($W_{port} = 43[mm]$ and $L_{port} = 76[mm]$). Because of in the optimized 2-ports topology the ports are very close to each other, theoretically a topological configuration with two parallel ports (7.30a) with a certain phase delay between them should guarantee same performances as a configuration with one only wide port, the third step of the cavity design was to exchange the 2-ports condition with 1-wide-port condition (7.30a). A single wide port can be used instead and its dimension are chosen in order to have the propagation of only the TE_{10} mode: That

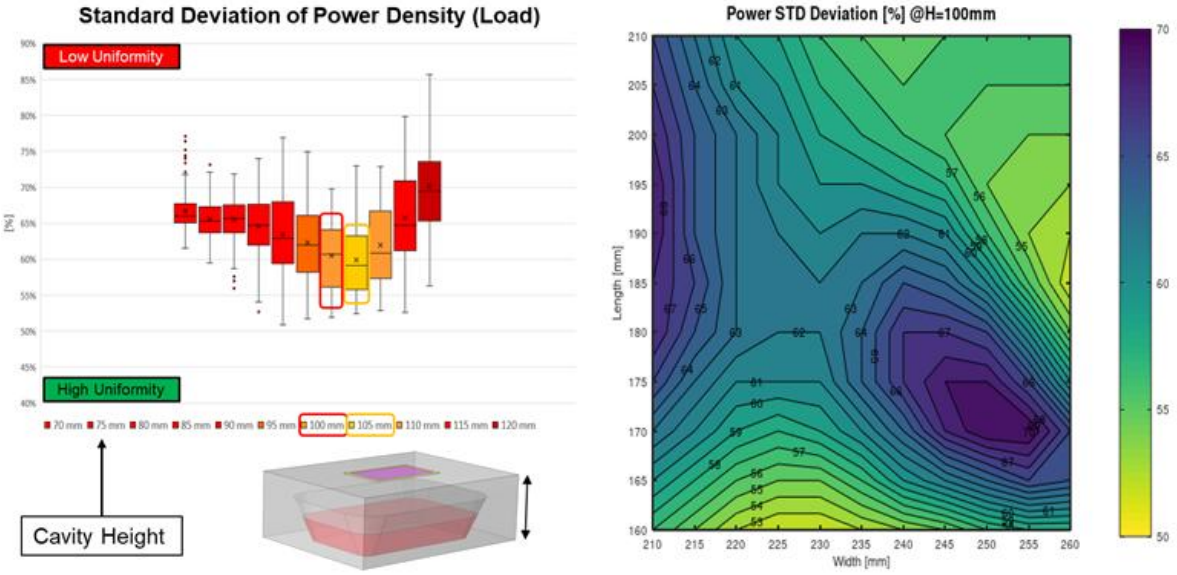

(a) (b)

Figure 7.29: Uniformity problem for the geometrical layout shown in figure 7.27

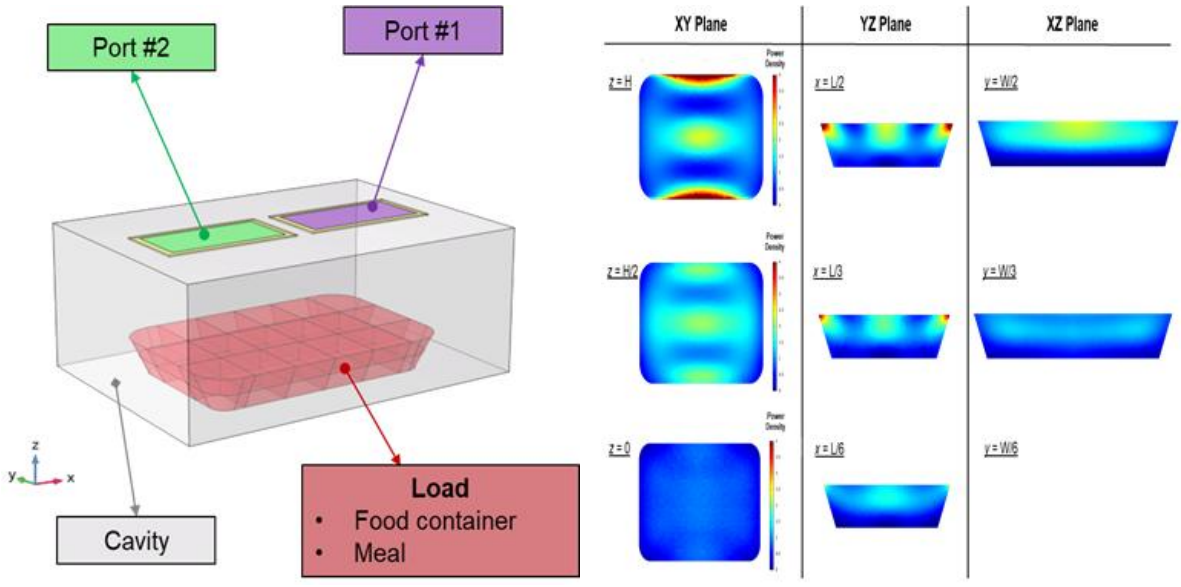

(a) (b)

Figure 7.30: Cavity with two rectangular ports feeding on the roof. (a) Geometry of the system (b) Microwave power heating sources for the best configuration.

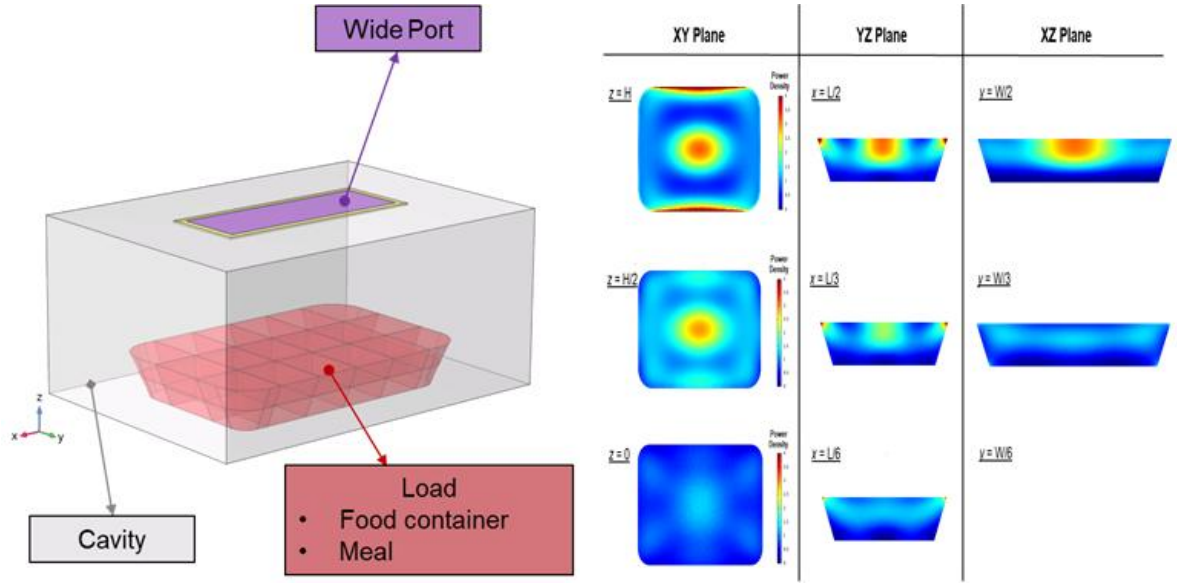

Figure 7.31: Cavity with one wide port on the roof. (a) Geometry of the system (b) Microwave power heating sources for the best configuration.

topology may guarantee in the best configuration ($W_{port} = 40[mm]$ and $L_{port} = 120[mm]$) If we compare these two topological configurations it is clear that edge effects (violet dot lines) due to load corners are reduced and instead the heart heating (red dot lines) is increased in 1-wide port configuration as shown in figure 7.32

Cavity + Waveguide design

The second part of the work consisted on the design of the waveguide that is the transmission line to guarantee a good matching (maximum power transfer between the generator and the cavity) and low scattering parameter (S_{11} $[db]$). For that design a TE_{10} port condition is imposed at the port of the waveguide (violet rectangular surface in figure 7.33). Also in that case we analysed the uniformity of heating as done in the previous part of the work, but we did a different approach, instead of defining a point array we divided the load volume, colored in red in figure 7.33a, in 36 volume regions (V_i) and they are visible in the same figure. For each volume region we computed the mean power dissipated inside it, and then for $i = 1, 2, ...36$

$$P_i = \frac{\int_{V_i} w_{RFH-i}\,(x, y, z)\,dV}{V_i} \tag{7.213}$$

ans as already done, the uniformity is studied through the standard deviation of the mean power of each region. With that practical approach high-power-density local effect are filtered

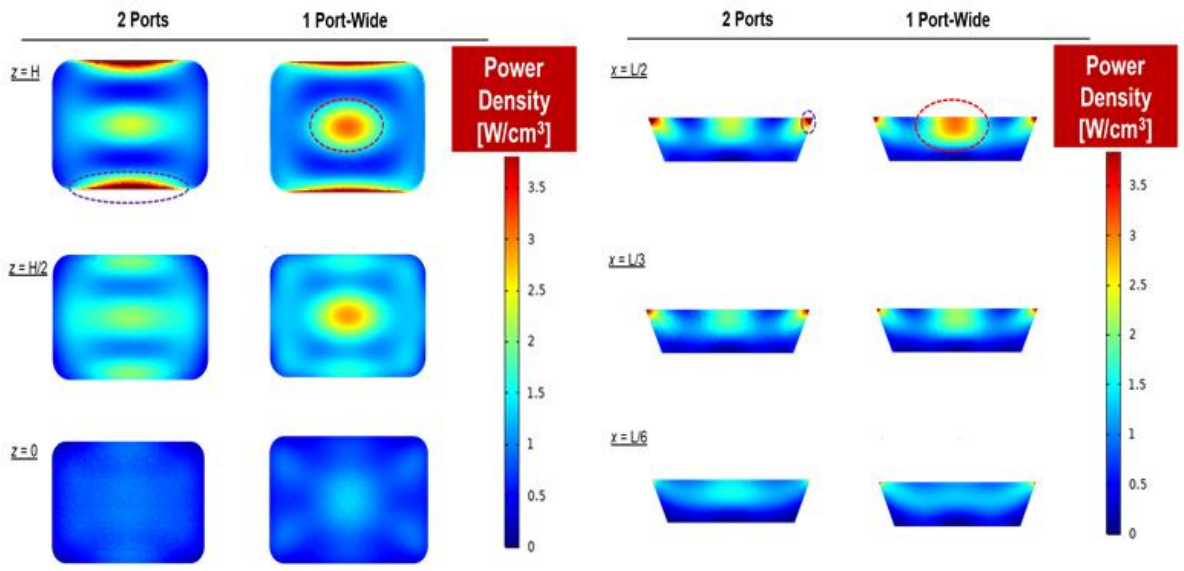

(a) **(b)**

Figure 7.32: Comparison between 2-port topology and 1-wide port topology in therm of heating power density. (a) Geometry of the system (b) Microwave power heating sources for the best configuration.

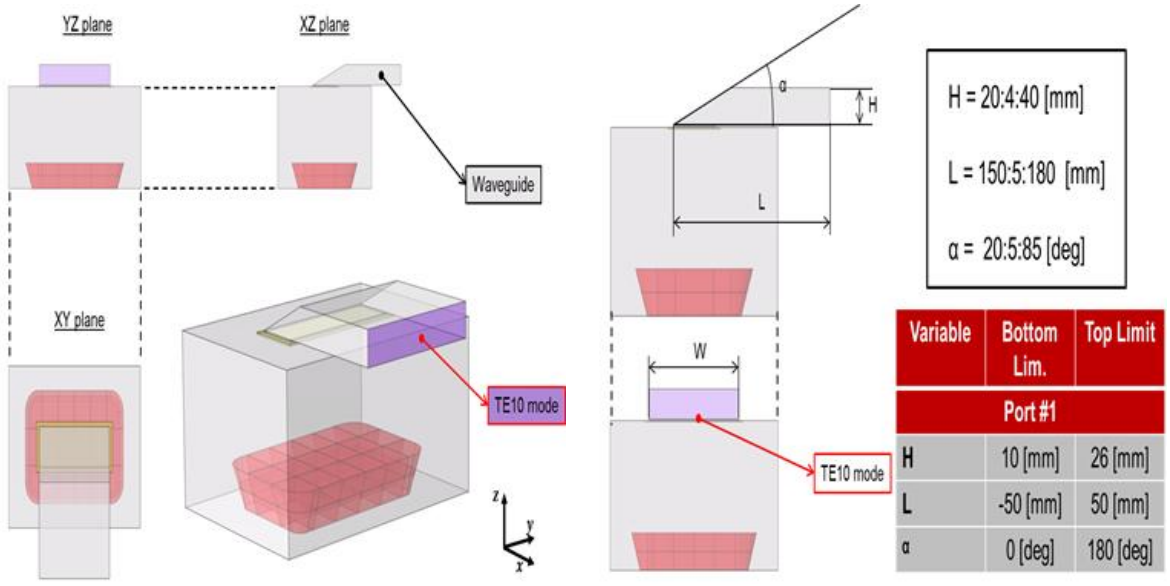

(a) **(b)**

Figure 7.33: Optimization of the waveguide-cavity system (a) MW Cavity and Waveguide geometry; (b) Waveguide main parameters (space of variables) for otpimization of performances.

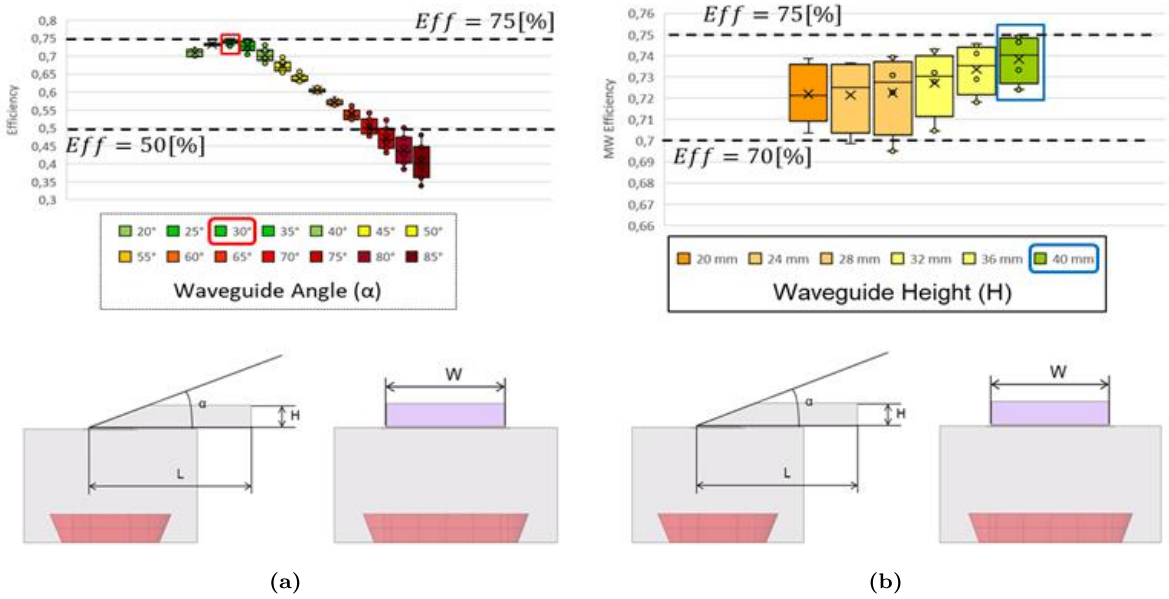

(a) (b)

Figure 7.34: Performances analysis varying main parameters (a) MW Efficiency vs Waveguide Angle (α $[deg]$); (b) MW Efficiency vs Waveguide Height (H $[mm]$)

and neglected. In figure 7.35b is shown the dependence between the uniformity and the position of the aperture of the cavity . That figure highlights that an optimum condition that maximize the microwave performances (in therms of efficiency and standard deviation of heating). The parametric analysis denoted that a theoretic maximum exists for the transition waveguide-cavity. Because of we want to maximize the energy transferred to the load we also analysed the position of the aperture that connects the waveguide to the cavity and guarantee field continuity between the two system. I remember that we impose a dielectric-transition layer of $0.9[mm]$ between the transmission line and the resonant system. The FEM analysis of the system+ demonstrated that it is difficult to improve performances with a standard layout. Also if the electromagnetic transmission was considerably improved, and finally it was close to an acceptable value of $\varepsilon_{MW} \simeq 75[\%]$ the uniformity still shows typical edge effects. To overcome that problem we though to change the topology of the waveguide and we considered a new layout for the transition waveguide-cavity: a three-lobes aperture

Cavity design with special waveguide: three-lobes aperture

During the design process we understood that a typical user need to be free of using its own dished for regeneration. To guarantee flexibility to the user we needed to improve cavity dimension, that practically changed the electric field distribution and needed a new optimization

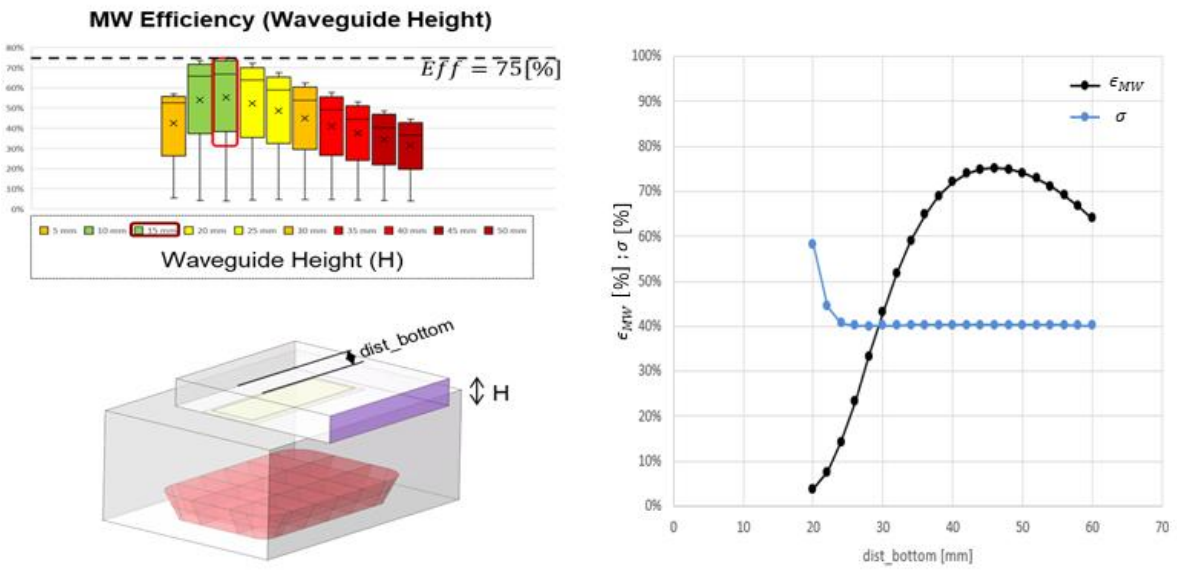

(a) (b)

Figure 7.35: Microwave Efficiency analysis varying waveguide height and aperture (slot) position (a) MW Efficiency vs waveguide height (H $[mm]$); (b) MW Efficiency vs aperture (slot) position ($dist_{bottom}$ $[mm]$)

of the cavity. Because of during the design process we obtained good results with a 1-wide-port configuration we modified the transition between waveguide and cavity and finally found a mathematical good result for a new hybrid slot: the so called three-lobes aperture obtained by a topological optimization of the electromagnetic problem (ε_{MWH} [%]) and of the uniformity problem (σ_{MWH} [%]). Also in that case we considered a meal characterized by a complex permittivity close to $3 - j0.4$. That is a good reasonable value for vegetable-base frozen foods. As seen in the previous part of the work for thawing there is the necessity to increase the power developed to the load, to decrease time required for the regeneration. Home-appliances,a s in that case, a typical used MW generator (Magnetron) is characterized by a reference power $P_{RF-in} \simeq 1000[W]$. In that analysis we designed a system considering a commercial state of art magnetron (with a typical working frequency range of $2.45[GHz] - 2.48[GHz]$). The concept of that oven is to couple the microwave generator (Magnetron) through a rectangular waveguide. With the help of FEM electromagnetic analysis we found a good solution for frozen ready-meals. The optimization workflow consider as space of variables all geometric parameters that characterize the geometry shown in figure 7.37. The only constrain considered during the optimization of the system was the minimum value of the dimension of the cavity, it won't be smaller than $280[mm]$. The three-lobe port optimized topology makes possible to focus electromagnetic waves in the heart of the load as shown in figure 7.38. The global transmission energy, compared with the 1-wide-port on the roof concept was improved from 75[%] to 85[%]

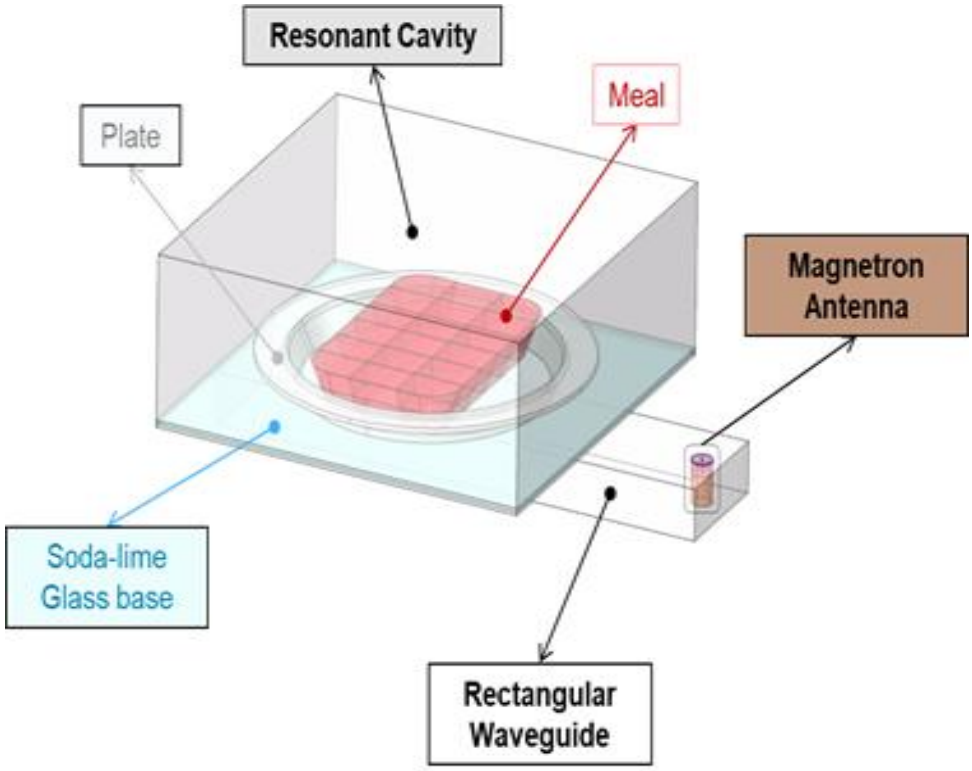

Figure 7.36: New cavity for thawing. Feeding from the bottom with a three-lobe-aperture transition from rectangular waveguide to resonant cavity.

and the standard deviation was reduced from 45[%] to 38[%]. For the optimisation phase a Bound Optimization by Quadratic Approximation method (BOBYQA) method was used [4]. The iterative approximates the objective function by a quadratic model which is valid in a region around the current iterate, the so-called trust region. The quadratic model is updated by minimizing the Frobenius norm of the difference in the Hessians of the two consecutive quadratic. The goal of the method was to maximize efficiency (ε_{MW}) and minimize the relative non uniformity ($sigma'_{MWH}$), the objective function is the sum of these two functions. The relative non uniformity is weighted by average power in the load:

$$\begin{cases} \sigma'_{MWH} = \frac{\sigma_{MWH}}{P_{MW-in}\varepsilon_{MWH}} \\ \varepsilon_{MWH} = \frac{\int_{V_{food}} w_{MWH} dV}{P_{MW-in}} \end{cases} \tag{7.214}$$

The system also showed a very low sensitivity of the transmission efficiency with the frequency variation, instead it showed high sensitivity to the position of the magnetron antenna, and that means during the industrialization phase particular attention must be paid during the coupling between the waveguide and the magnetron antenna: 2[mm] may decrease transmission efficiency of even a 20[%].

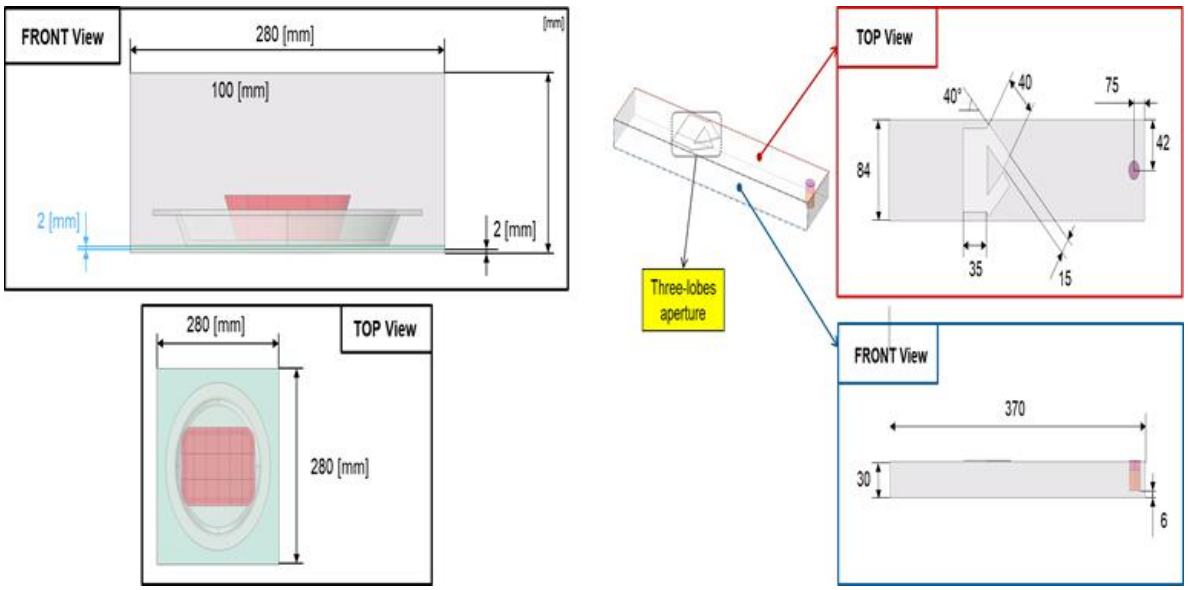

(a) (b)

Figure 7.37: Resonant cavity and waveguide for thawing (a)Resonant cavity (H $[mm]$); (b) Waveguide layout with three-lobe aperture (slot)

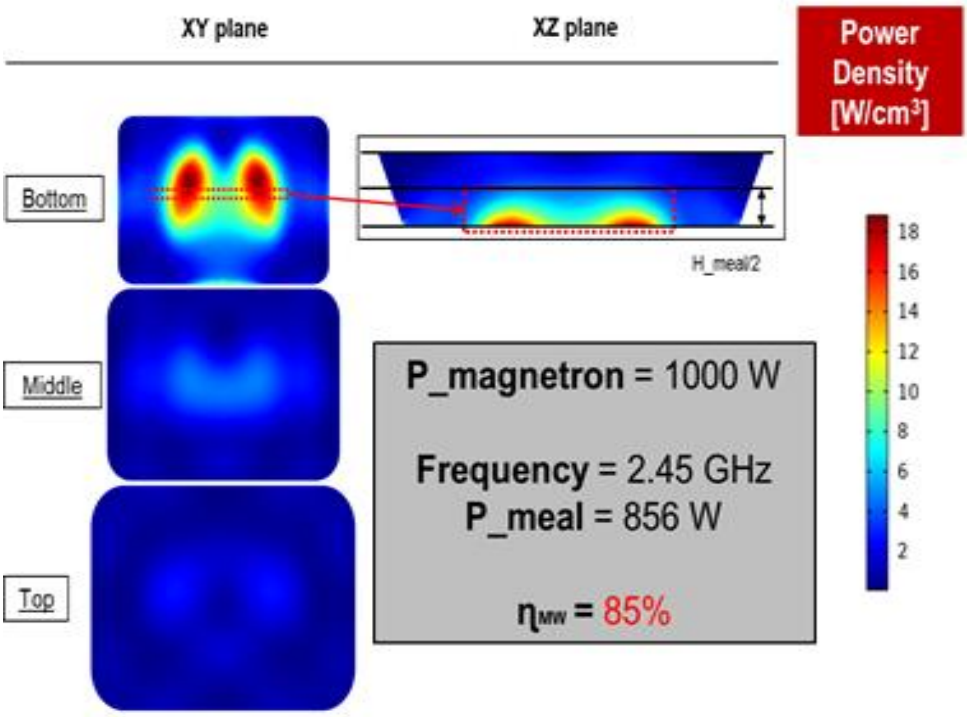

Figure 7.38: Uniformity results for the three-lobe-aperture transition waveguide.

Chapter 8

Conclusions

8.1 Conclusions

The present work studied several heating, thawing and drying processes. Electromagnetic Processing of Materials can guarantee high efficiency and time reduction of high time consuming pre-heating phases. In drying of textiles and paper industry hot rollers are used for evaporation of water vapor. The goal is to reduce the relative humidity of the material by several percentage points and in some cases also to value less than 1[%]. To improve efficiency and production rates high velocities are needed: the main trend imposes to design big-diameter rollers. The main problem of these systems is the high energy requirement due to high mass of heating rollers (that are steel-made work pieces). Because of induction heating may directly generate high density powers directly in the conductive and magnetic material that work presented a new induction heating roller for drying and bossing in paper industry. The design process is introduced and analysed in the present work. A comparison with a state of art (SOA) technology is proposed: diathermic oil. The best results of induction heating hot-rollers for paper (textile) processes are:

- reduction of pre-heating time (from 54[m] of diathermic oil to 30[m] for a low-power application)
- reduction of energy consumption during the preheating phase: $-53[\%]$
- possibility to control the temperature profile (along the length of the roller) controlling the design of the inductor.

In food heating problems and drying of dielectrics, where the main mechanism is vaporization of species Microwave (MW) and Radio-frequency (RF) nowadays represent one of the most interesting technologies because of its capability of generate power losses directly inside the material. Certain biological materials, pharmaceuticals, and foodstuffs are characterized by high values of dielectric permittivity ($\dot{\epsilon}_r \simeq 78 - i18$), low values of thermal conductivity ($\dot{\epsilon}_r < 1[W/(m \cdot K)]$) but high value of specif heat capacity ($C_p \simeq 3000[J/(kg \cdot K)]$). That means practically that energy necessary to increase temperature can be very high. RF and MW heating devices can guarantee strong power sources directly inside the material ($w - RF > 1[MW/M^3]$) but that may cause a localized overheating. In thawing process that problem was observed in several commercial "standard" devices that are designed to work with a wide range of food products. In a regeneration process of frozen food it is necessary to:

- increase final product temperature
- eliminate the frozen fraction (phase change)
- guarantee integrity of food structures (vitamins, proteins, etc.)
- guarantee high uniformity

In chapter 7 is presented a new device that optimize the uniformity and high power transmission to frozen food. A new small cavity with a feeding on the bottom part and a three-lobe-aperture was studied to solve the problem. The cavity geometry and the waveguide geometry are the final result of a numerical optimization of a resonant cavity for low permittivity loads. The optimization was done taking into account two objective functions: uniformity (that must be maximized) and efficiency (that must be maximized). The geometrical details of the the final system are reported in the final part of the chapter. Another interesting point for microwave home appliance ovens is the necessity to properly design the so called door-choke. FEM analysis together with the solution of transmission models for periodic structures made possible to design a specific choke geometry for a small cavity for thawing. Heating and drying with microwave and dielectric energy is distinctly different from conventional means. Whereas conventional methods depend upon the slow march of heat from the surface of the material to the interior as determined by differential in temperature from a hot outside to a cool inside, heating with dielectric and microwave energy is, in effect, bulk heating in which the electromagnetic field interacts with the material as a whole. The heating occurs nearly instantaneously and can be very fast, although it does not have to be. However, the speed of heating can be an

advantage, and it is often possible to accomplish in seconds or minutes what could take minutes, hours, and even days with conventional heating methods. The governing parameters here are the mass of the material, its specific heat, dielectric properties, geometry, heat loss mechanisms, and coupling efficiency, the power generated in the material, and the output power of the microwave–dielectric heating system. If all other things are equal, the speed may be doubled by doubling the output power. Figure 8.1 shows experimental results of evaporation of a fabric

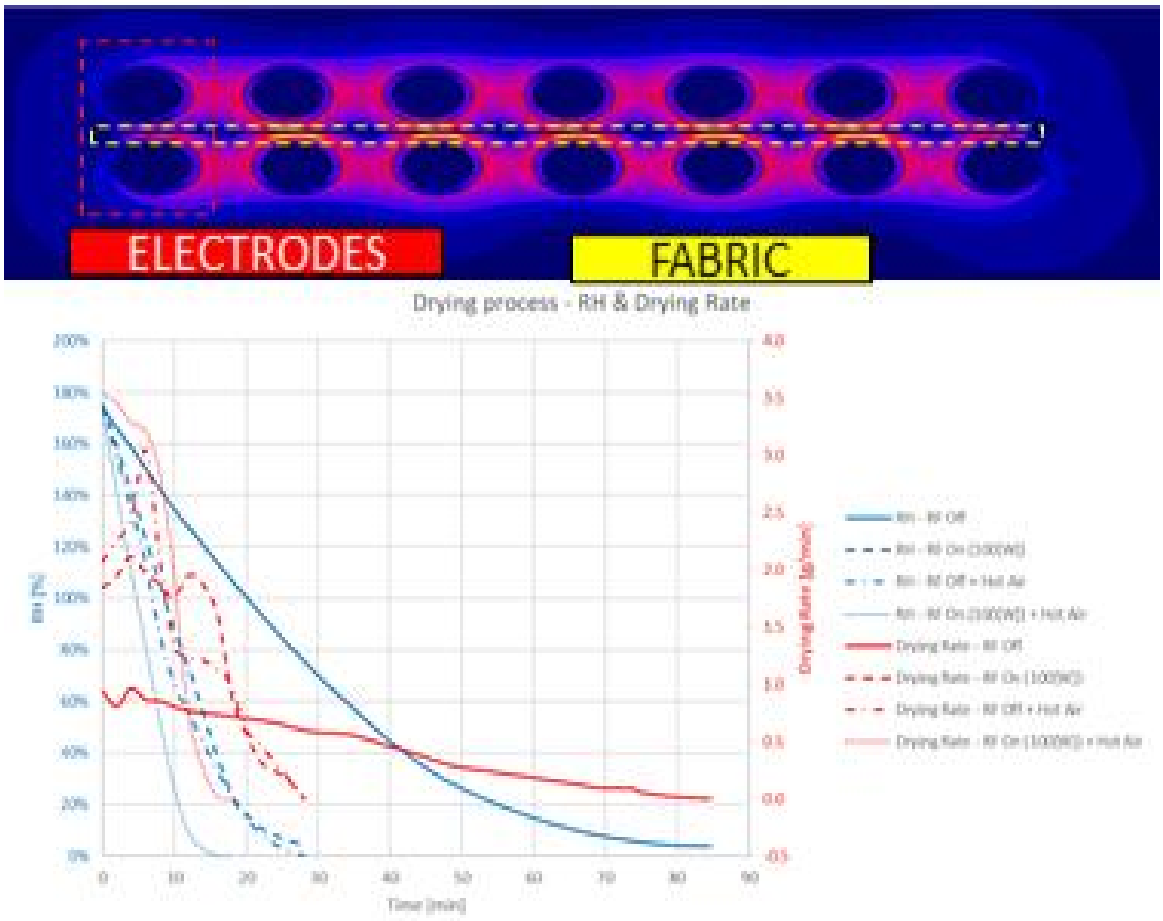

Figure 8.1: Relative Humidity (RH [%]) and Drying rate (δH $[g/min]$) for a fabric product.

(300[μm]) sample where a radio frequency 27[MHz] electric field is applied. A comparison between forced convection system (speed of about 20[m/s]) that may use cold dry air or hot dry air was done and it is clear that the average drying rate is increased by the use of internal heating sources directly on the material matrix. Radio-frequency represents probably the most interesting technology for drying of dielectric foods. Because of typically drying system manufacturers want to maximize drying rates and/or efficiency the design of Radio-Frequency drying systems must be fully optimized around specific products and materials. FEM analysis and simulations made possible to optimize the topology and main geometrical parameters of a

hopper dryer for plastic hygroscopic materials (PET). Inf figure 8.2 are presented final results

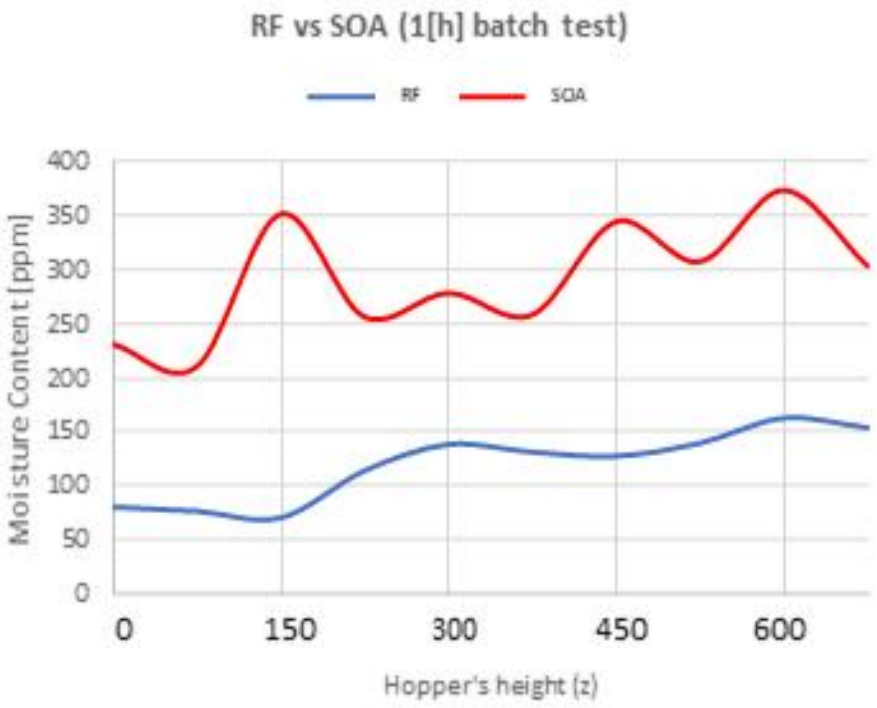

Figure 8.2: Relative Humidity (RH [%]) along the height of the final prototype. State of Art (SOA) hot air drying vs "new" RF-enhanced drying.

in therm of relative humidity. The initial product for the reference test was a raw PET product with a relative humidity of 400[ppm]. A batch process of 1[h] was considered. A SOA process with only dehumidified hot air normally needs 9[kWh] to dry the PET to on average value of 100[ppm] (red line in figure). The RF optimised system with combined effect of RF-heating sources on the material and dehumidified hot air needed 11[kWh] but dries the PET to an average value of 120[ppm] (blue line). Radio-frequency demonstrated an high increasing in drying performances. In chapter **??** are shown the design approach of matching network. Because of for drying process the efficiency is one of the main parameters (together with drying rate, uniformity, drying rate, efficiency) a matching network must properly designed to guarantee high power transmission and low losses in the network line. But matching network represent also a new opportunity on load measurements. Solving the transmission problem for a certain network is possible to directly measure material properties and for example relative humidity. That work is still in progress, but a mathematical resolution of the problem and a relationship between the load impedance and the matching components is proposed. Solid State Generators are characterized by a fix internal impedance and that means transmission varying networks

are required to control reflected/transmitted powers, but at the same time they are smart system to obtain "indirect" measure of thermal state of the system, typically in therms of mean energy and then mean temperature. We obtained a robust method to measure the relationship between the matching measures and the evaporation in a real drying system. A final list of advantages of microwave and dielectric heating is include here:

- Process speed is increased, as described above.
- Uniform heating may occur throughout the material. Although not always true, often the bulk heating effect does produce uniform heating, avoiding the large temperature gradients that occur in conventional heating systems.
- Efficiency of energy conversion: In this type of heating, the energy couples directly to the material that is heated. It is not expended in heating the air, walls of the oven, conveyor, or other parts. This can lead to significant energy savings. Also, the energy source is not hot and plant cooling savings may be realized.
- Better and more rapid process control: The instantaneous on–off nature of the heating and the ability to change the degree of heating by controlling the output power of the generator mean fast, efficient, and accurate control of heating: in that work is presented the capability of RF drying and roasting system that we designed to control the run-away of temperature of roasted coffee beans.
- Floor space requirements are usually less. This is because of more rapid heating.
- Selective heating may occur. The electromagnetic field generally couples into the solvent, not the substrate. Hence, it is the moisture that is heated and removed, whereas the carrier or substrate is heated primarily by conduction.
- Product quality may be improved. Since high surface temperatures are not usually generated, overheating of the surface and case hardening, which are common with conventional heating methods are eliminated. This often leads to less rejected product.

Finally EPM are "smart" technologies that may dramatically improve the intelligence of complex systems. To properly design and control these technologies and devices a deep study of thermal-electromagnetic problem must be carried.

References

[1] U.S. Department of Agriculture. “Food Yields”. In: *Agriculture Handbook* 5 (1975).

[2] D. Anandkumar. “Design and analysis of aperture coupled micro strip patch antenna for radar applications”. In: *International Journal of Intelligent Networks* 1 (2020), pp. 141–147.

[3] S Arslanagić et al. “A review of the scattering-parameter extraction method with clarification of ambiguity issues in relation to metamaterial homogenization”. In: *IEEE Antennas and Propagation Magazine* 55.2 (2013), pp. 91–106.

[4] A.M. Bagirov. “A Method for Minimization of Quasidifferentiable Functions”. In: *Optimization Methods and Software - OPTIM METHOD SOFTW* 17 (Feb. 2002), pp. 31–60.

[5] James Baker-Jarvis, Richard G Geyer, and Paul D Domich. “A nonlinear least-squares solution with causality constraints applied to transmission line permittivity and permeability determination”. In: *IEEE Transactions on Instrumentation and Measurement* 41.5 (1992), pp. 646–652.

[6] S.P. Balmus. “The cavity perturbation method for the measurement of the relative dielectric permitivity in the microwave range”. In: *Journal of optoelectronics and advanced materials* 8.3 (2006), p. 971.

[7] J. Bladel. “On Helmholtz’s theorem in finite regions”. In: *IRE Transactions on Antennas and Propagation* 7.5 (1959), pp. 119–119. DOI: 10.1109/TAP.1959.1144767.

[8] D. A. G. Bruggeman. “Berechnung verschiedener physikalischer Konstanten von heterogenen Substanzen. I. Dielektrizitätskonstanten und Leitfähigkeiten der Mischkörper aus isotropen Substanzen”. In: *Annalen der Physik* 416.7 (1935), pp. 636–664. DOI: https://doi.org/10.1002/andp.19354160705.

[9] A. Cass. “Enhancement of Thermal Water Vapor Diffusion in Soil”. In: *Soil Science Society of America Journal* (1984).

[10] S. Chandrasekhar. Oxford University Press, 1950.

[11] N. Charles. “Mass transfer in heterogeneous catalysis”. In: *Mass.: M.I.T. Press* (1969).

[12] Lin-Feng Chen et al. *Microwave electronics: measurement and materials characterization.* John Wiley & Sons, 2004.

[13] B.K. Chung. “Dielectric constant measurement for thin material at microwave frequencies”. In: *Progress In Electromagnetics Research* (2007), pp. 239–252.

[14] P.J.B. Clarricoats. “Evanescent and propagating modes of dielectric-loaded circular waveguide”. In: *Proceedings of the Institution of Electrical Engineers* 111.12 (1964), pp. 1951–1956.

[15] S.B. Cohn. “Microwave Bandpass Filters Containing High-Q Dielectric Resonators”. In: *IEEE Transactions on Microwave Theory and Techniques* (1968), pp. 218–227.

[16] R.E. Collin. *Field Theory of Guided Waves.* McGraw-Hill, 1960.

[17] F. Costa. “Waveguide Dielectric Permittivity Measurement Technique Based on Resonant FSS Filters”. In: *IEEE Microwave and Wireless Components Letters* 21.5 (2011), pp. 273–275.

[18] Giancoli Douglas. *Physics for Scientists and Engineers with Modern Physics.* 4th ed. Prentice Hall, 1984, pp. 650–680.

[19] M.R. Effendi. “Transmission Phase-Shift Method for Complex Permittivity Determination of Biological Sample Performed Using X-Band Rectangular Waveguide”. In: *2020 IEEE REGION 10 CONFERENCE (TENCON)* (2020), pp. 919–922.

[20] F.T. Erden. “Analytical study of the TE-waveguide modes in time domain”. In: *2017 IEEE International Symposium on Antennas and Propagation and USNC/URSI National Radio Science Meeting* (2017), pp. 45–46.

[21] A. Eucken. “Allgemeine Gesetzmassigkeiten für das Warmeleitvermogen verschiedener Stoffarten und Aggregatzustande”. In: *Forschung auf dem Gebiete des Ingenieurwesens* (1940).

[22] N.D. Farrington. “Development and verification of an accurate FEM electromagnetic model for a complex multi-stage RADAR limiter”. In: *2011 8th European Radar Conference* (2011), pp. 37–40.

[23] T.U. Fawwaz. *Fundamentals of applied electromagnetics*. 5th ed. Pearson, 2007.

[24] R.P. Feynman. *The Feynman Lectures on Physiscs*. Vol. 2. Addison-Wesley, 2005. Chap. 20.

[25] Lau R. W. Gabriel S. and Gabriel C. "The Dielectric Properties of Biological Tissues: Measurements in the Frequency Range 10 Hz to 20 GHz". In: *Phys. Med. Biol* (1996), pp. 2251–2269.

[26] J. C. Maxwell Garnett and Joseph Larmor. "XII. Colours in metal glasses and in metallic films". In: *Philosophical Transactions of the Royal Society of London. Series A, Containing Papers of a Mathematical or Physical Character* 203.359-371 (1904), pp. 385–420. DOI: 10.1098/rsta.1904.0024.

[27] G. Giovannetti. "Radiofrequency coils for magnetic resonance applications: theory, design, and evaluation". In: *Critical Reviews™ in Biomedical Engineering* 42.2 (2014).

[28] E. Grüneisen. "Die Abhängigkeit des elektrischen Widerstandes reiner Metalle von der Temperatur". In: *Annalen der Physik* 408.5 (1933), pp. 530–540. DOI: https://doi.org/10.1002/andp.19334080504.

[29] R.F. Harrington. *Introduction to electromagnetic engineering*. Dover Publications, 2003.

[30] O. Heaviside. *Electromagnetic theory*. The Electrician Printing and Publishing Company Limited, 1893.

[31] I. Hironori. "The characteristic of Powder Oils and Its Application to Food". In: *Japan Oil Chemist's Society* 19.10 (2019), pp. 417–422.

[32] B. Holland. "The Composition of Foods". In: *5th ed. Royal Society of Chemistry* (1991).

[33] J.R. Howell. *Thermal radiation heat transfer*. CRC press, 2020.

[34] ICNIRP. "ICNIRP guidelines for limiting exposure to EM field (100 kHz TO 300 GHz)". In: *HEALTH PHYS* 118(5) (2020).

[35] Allegheny Technologies Inc. *ATI 403 - UNS S40300 - Datasheet*. URL: https://www.atimetals.com/Products/Documents/datasheets/stainless-specialty-steel/martensitic/ati-403_en_tds_v1.pdf (visited on 01/03/2022).

[36] Ferroxcube Inc. *Ferrites 3C90 - Datasheet*. URL: https://elnamagnetics.com/wp-content/uploads/library/Ferroxcube-Materials/3C90_Material_Specification.pdf (visited on 01/04/2022).

[37] Fluxtrol Inc. *Fluxtrol 100 - Datasheet*. URL: https://fluxtrol.com/fluxtrol-50 (visited on 01/03/2022).

[38] Fluxtrol Inc. *Fluxtrol 50 - Datasheet*. URL: https://fluxtrol.com/fluxtrol-50 (visited on 01/03/2022).

[39] Frank A.J.L James. *The Correspondence of Michael Faraday*. Vol. 3. The Institution of Electrical Engineers, 1996, pp. 1841–1848.

[40] M.O. John. "Advances in Choke Design for Microwave Oven Door Seals". In: *Journal of Microwave Power* 8.3 (1973), pp. 296–302.

[41] Raymond A. Serway; John W. Jewett Jr. *Physics for Scientists and Engineers*. Vol. 2. Cengage Learning, 2009, pp. 753–758.

[42] Ruda Kasap S. Koughia C. and Harry E. *Handbook of Electronic and Photonic Materials*. Springer, 2017.

[43] W. Kenneth. *Generalized Thermodynamic Relationships*. 5th ed. McGraw-Hill, 1988.

[44] C. Kittel. *Thermal physiscs*. Freeman, 2000.

[45] O. Klein. "Microwave cavity perturbation technique: Part I: Principles". In: *International Journal of Infrared and Millimeter Waves* 14.12 (1993), pp. 2423–2457.

[46] Y.Y. Kok. "Material characterization Using Microwave Waveguide systems". In: *Microwave Systems and applications* (2016), pp. 341–357.

[47] Jerzy Krupka. "Measurements of the Complex Permittivity of Low Loss Polymers at Frequency Range From 5 GHz to 50 GHz". In: *IEEE Microwave and Wireless Components Letters* 26.6 (2016), pp. 464–466. DOI: 10.1109/LMWC.2016.2562640.

[48] K. Kurokawa. "Power waves and the scattering matrix". In: *IEEE transactions on microwave theory and techniques* 13.2 (1965), pp. 194–202.

[49] T.J. LaFave. "Correspondences between the classical electrostatic Thomson problem and atomic electronic structures". In: *Journal of Electrostatics* 71.6 (2013), pp. 1029–1035.

[50] M. H. Wright Lagarias J. C. J. A. Reeds and P. E. Wright. "Convergence Properties of the Nelder-Mead Simplex Method in Low Dimensions". In: *SIAM Journal of Optimization* 9.1 (1998), pp. 112–147.

[51] Pitaevskii L. P. Landau L. D. Lifshitz E. M. *Electrodynamics of continuous media*. Elsevier Butterworth-Heinemann, 2009.

[52] C.H. Liang. "Electromagnetic fields coupled into a cavity with a slot-aperture under resonant conditions". In: *IEEE Transactions on Antennas and Propagation* 30.4 (1982), pp. 664–672.

[53] L. Lorenz. “On the Identity of the Vibrations of Light with Electrical Currents”. In: *Philosophical Magazine* 4.34 (1867), pp. 287–301.

[54] A.V. Luikov. In: 10 (1970), pp. 599–604.

[55] Olli Luukkonen, Stanislav I Maslovski, and Sergei A Tretyakov. “A stepwise Nicolson–Ross–Weir-based material parameter extraction method”. In: *IEEE antennas and wireless propagation letters* 10 (2011), pp. 1295–1298.

[56] R.H. MacPhie. “Scattering at the junction of a rectangular waveguide and a larger circular waveguide”. In: *IEEE transactions on microwave theory and techniques* 43.9 (1995), pp. 2041–2045.

[57] N. Marcuvitz. “Waveguide Handbook (IEEE Electromagnetic Waves Series)”. In: *The Institution of Engineering and Technology* (1986).

[58] R.A. Matula. “Electrical resistivity of copper, gold, palladium, and silver”. In: *Journal of Physical and Chemical Reference Data* 8.4 (1979), pp. 1147–1298.

[59] J.C Maxwell. “On Physical Lines of Force”. In: *Philosophical Magazine* XXI.XXIII (1959), pp. 451–513.

[60] J.C. Maxwell. *A treatise on electricity and magnetism, Volume I*. Oxford : Clarendon Press, 1873.

[61] J.C. Maxwell. *A treatise on electricity and magnetism, Volume II*. Oxford : Clarendon Press, 1892.

[62] A.S. Mujumdar. *Handbook of Industrial Drying*. 3rd ed. Taylor and Francis, 2006.

[63] V.H. Nguyen. “Measurement of complex permittivity by rectangular waveguide method with simple specimen preparation”. In: *International Conference on Advanced Technologies for Communications* 2015 (Oct. 2014).

[64] P Overbosch, WGM Afterof, and PGM Haring. “Flavor release in the mouth”. In: *Food reviews international* 7.2 (1991), pp. 137–184.

[65] J.N. Paul. *Oliver Heaviside, The Life, Work, and Times of an Electrical Genius of the Victorian Age*. Johns Hopkins University Press, 2002.

[66] N.D. Pavlov and Baloshin Y.A. “Electromagnetic properties of water on GHz frequencies for medicine tasks and metamaterial applications”. In: *Journal of Physics: Conference Series* 643 (2015).

[67] J.H. Perry. *Chemical Engineers’ Handbook*. McGraw-Hill, 1967.

[68] R. Perry. *Perry's Chemical Engineers' Handbook*. McGraw-Hill, 1997.

[69] Dragana Petrović et al. "Mn-Zn ferrite line EMI suppressor for power switching noise in the impulse/high current bias regime". In: *Turkish Journal Of Electrical Engineering and Computer Sciences* 26 (Sept. 2018), pp. 2426–2436. DOI: 10.3906/elk-1710-52.

[70] Lord Rayleigh. "XVIII. On the passage of electric waves through tubes, or the vibrations of dielectric cylinders". In: *The London, Edinburgh, and Dublin Philosophical Magazine and Journal of Science* 43.261 (1897), pp. 125–132.

[71] M. Razmhosseini. "Wideband antennas using coaxial waveguide". In: *IEEE Transactions on Antennas and Propagation* 69.10 (2021), pp. 6273–6283.

[72] W. Schommers. "Structure and Dynamics of Surfaces". In: *Topics in Current Physics* 41 (1986).

[73] R. A. Serwat. *Principles of Physiscs*. 2nd ed. London: Saunders College Pub, 1998.

[74] P. Smith. "Transmission Line Calculator". In: *Electronics* 12.1 (1939), pp. 29–31.

[75] Ecor Steel SpA. *Ferrite 3C90 - Datasheet*. URL: https://elnamagnetics.com/wp-content/uploads/library/Ferroxcube-Materials/3C90_Material_Specification.pdf (visited on 01/03/2022).

[76] Ecor Steel SpA. *Stainless Steels - Datasheet*. URL: https://ecor.com/img/prodotti/pdf/product_catalogue_ECOR_EN.pdf (visited on 01/03/2022).

[77] A.E Stearn. "theory of diffusion in liquids". In: *Journal of Physical Chemistry* 44 (1940), pp. 981–995.

[78] D. Stroud. "The effective medium approximations: Some recent developments". In: *Superlattices and Microstructures* 23 (1998), pp. 567–573.

[79] P. Sulistyaningsih. "Accuracy Analysis of Transmission Phase-Shift Method for Material Characterization". In: *2020 IEEE International Women in Engineering (WIE) Conference on Electrical and Computer Engineering (WIECON-ECE)* (2020), pp. 251–254. DOI: 10.1109/WIECON-ECE52138.2020.9398026.

[80] Aye Tun. "Review of the Thermo-physical properties models of foods". In: (Sept. 2018).

[81] R.A. Waldron. *Theory of guided electromagnetic waves*. Van Nostrand Reinhold, 1970.

[82] M. Wang. "Predictions of effective physical properties of complex multiphase materials". In: *Materials Science and Engineering: Reports* (2008), pp. 1–30.

[83] R.J. Weber. *Introduction to microwave circuits*. Electronic Industry Press, 1991.

[84] C. Wenshan. *Optical Metamaterials: Fundamentals and Applications*. Springer, 2009.

[85] H.A. Wheeler. "H.A. Wheeler [Biography]". In: *IRE Transactions on Microwave Theory and Techniques* 4.2 (1956), pp. 65–65. DOI: 10.1109/TMTT.1956.1125019.

[86] Z. Xu. "Recent developments in radio frequency drying of food and agricultural products: A review". In: *Drying Technology* 37.3 (2019), pp. 271–286.

[87] Zhang. "Trends in microwave-related drying of fruits and vegetables". In: *Trends in Food Science and Technology* 17.10 (2006), pp. 524–534.